



NAVAL FACILITIES ENGINEERING SERVICE CENTER
Port Hueneme, California 93043-4328

DTIC
ELECTR
APR 11 1995
C

Technical Report TR-2038-SHR

MICROSEISM MEASUREMENTS AT THE WATERFRONT - AN AID TO NAVY BASE MICROZONATION

by

John Ferritto

February 1995

Sponsored by:
Office of Naval Research
Arlington, VA 22217-5000

19950410 064

METRIC CONVERSION FACTORS

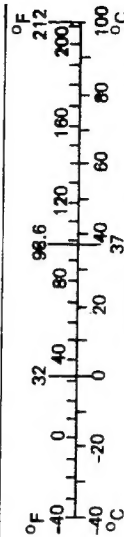
Approximate Conversions to Metric Measures

Symbol	When You Know	Multiply by	To Find	Symbol
in ft yd mi	inches	*2.5 30 0.9 1.6	centimeters	cm
	feet		centimeters	cm
	yards		meters	m
	miles		kilometers	km
in ² ft ² yd ² mi ²	square inches	AREA 6.5 0.09 0.8 2.6 0.4	square centimeters	cm ²
	square feet		square meters	m ²
	square yards		square meters	m ²
	square miles		square kilometers	km ²
oz lb	ounces	MASS (weight) 28 0.45 0.9	grams	g
	pounds		kilograms	kg
	short tons		tonnes	t
	(2,000 lb)			
tsp Tbsp fl oz c pt qt gal ft ³ yd ³	teaspoons	VOLUME 5 15 30 0.24 0.47 0.95 3.8 0.03 0.76	milliliters	ml
	tablespoons		milliliters	ml
	fluid ounces		milliliters	ml
	cups		liters	l
	pints		liters	l
	quarts		liters	l
	gallons		liters	l
	cubic feet		cubic meters	m ³
°F	cubic yards	TEMPERATURE (exact) 5/9 (after subtracting 32)	cubic meters	m ³
	Fahrenheit temperature		Celsius temperature	°C

*1 in = 2.54 (exactly). For other exact conversions and more detailed tables, see NBS Misc. Publ. 286, Units of Weights and Measures, Price \$2.25, SD Catalog No. C13.10-286.

Approximate Conversions from Metric Measures

When You Know	Multiply by	To Find	Symbol
millimeters centimeters meters kilometers	LENGTH 0.04 0.4 3.3 1.1 0.6	inches	in
		inches	in
		feet	ft
		yards	yd
square centimeters square meters square kilometers hectares (10,000 m ²)	AREA 0.16 1.2 0.4 2.5	miles	mi
		square inches	in ²
		square yards	yd ²
		square miles	mi ²
grams kilograms tonnes (1,000 kg)	MASS (weight) 0.035 2.2 1.1	ounces	oz
		pounds	lb
		short tons	
milliliters liters liters cubic meters cubic meters	VOLUME 0.03 2.1 1.06 0.26 35 1.3	fluid ounces	fl oz
		pints	pt
		quarts	qt
		gallons	gal
		cubic feet	ft ³
		cubic yards	yd ³
°C	TEMPERATURE (exact) 9/5 (then add 32)	Fahrenheit temperature	°F
		temperature	



REPORT DOCUMENTATION PAGE			Form Approved OMB No. 0704-018	
Public reporting burden for this collection of information is estimated to average 1 hour per response, including the time for reviewing instructions, searching existing data sources, gathering and maintaining the data needed, and completing and reviewing the collection of information. Send comments regarding this burden estimate or any other aspect of this collection information, including suggestions for reducing this burden, to Washington Headquarters Services, Directorate for Information and Reports, 1215 Jefferson Davis Highway, Suite 1204, Arlington, VA 22202-4302, and to the Office of Management and Budget, Paperwork Reduction Project (0704-0188), Washington, DC 20503.				
1. AGENCY USE ONLY (Leave blank)	2. REPORT DATE Feb 1995	3. REPORT TYPE AND DATES COVERED July 1994 to October 1994		
4. TITLE AND SUBTITLE Microseism Measurements at the Waterfront - An Aid to Navy Base Microzonation		5. FUNDING NUMBERS PR - RM33F60 Task A16 WU - DN387338		
6. AUTHOR(S) John Ferritto				
7. PERFORMING ORGANIZATION NAME(S) AND ADDRESS(ES) Naval Facilities Engineering Service Center Port Hueneme, CA 93043-4328		8. PERFORMING ORGANIZATION REPORT NUMBER TR-2038-SHR		
9. SPONSORING/MONITORING AGENCY NAME(S) AND ADDRESSES Office of Naval Research Arlington, VA 22217-5000		10. SPONSORING/MONITORING AGENCY REPORT NUMBER		
11. SUPPLEMENTARY NOTES				
12a. DISTRIBUTION/AVAILABILITY STATEMENT Approved for public release; distribution is unlimited.		12b. DISTRIBUTION CODE		
13. ABSTRACT (Maximum 200 words) The US Navy has a number of bases in seismically active areas. Mission requirements dictate that these bases be located at the waterfront, often on marginal soils. Since the seismic exposure is high, the Navy has had an active research program to mitigate the risk to waterfront structures. The dynamic response of saturated cohesionless soils results in a loss of strength; liquefaction and the potential for associated damage is a major problem. The 1989 Loma Prieta earthquake caused over \$125 million in damages primarily from liquefaction. In 1993 the Guam earthquake caused an additional \$120 million loss. The Navy has developed automated procedures for conducting site seismicity studies which utilize an epicenter data base and available geologic data to predict the recurrence of seismic events and compute the probability distribution of site acceleration ground motion. A set of response spectra matched to the site conditions can be assembled from a data base of records. To further define local site response, research was conducted on using microseisms as a means of predicting local site amplification. Procedures were developed to measure microseisms on rock and soil sites and computer amplification spectra.				
14. SUBJECT TERMS Earthquake, microseisms, amplification			15. NUMBER OF PAGES 175	16. PRICE CODE
17. SECURITY CLASSIFICATION OF REPORT Unclassified	18. SECURITY CLASSIFICATION OF THIS PAGE Unclassified	19. SECURITY CLASSIFICATION OF ABSTRACT Unclassified	20. LIMITATION OF ABSTRACT UL	

Executive Summary

The Navy has numerous bases situated on marginal soft soils and located in seismically active areas. Ground motion amplification at these sites is high. Recent Navy experience during the 1989 Loma Prieta earthquake and the 1993 Guam earthquake demonstrate that Navy sites sustain high levels of ground shaking which produces damage. For this reason the study of waterfront amplification of motion is of Navy significance.

This report demonstrates the feasibility of using microseism measurements as a tool to gain additional insight into the response of waterfront sites. The report shows that the technique can be used as an extension of analytical techniques to augment geophysical site properties to improve the accuracy of estimating local site response. A typical Navy application would involve soft marginal soils at the waterfront. These sites exhibit significant spatial variation. Existing boring logs may not be available over wide areas and may lack data at depth making it difficult to define bedrock. Often shear wave velocity is not available and must be estimated from standard penetration blowcount data with its associated level of error. Measuring shear wave velocity at a site can be costly and is limited to projects of large enough size to warrant such a detailed investigation. Strain effects on damping and shear modulus require laboratory testing and are usually not performed; several standard type curves for sand and clay are routinely used as substitutes. With these limitations in gathering data for analysis, it can be seen that there is a need for an inexpensive field test to assist in establishing site period and amplification. Microseism measurements seem to offer that potential.

- The report presents microseism measurements which show for soft soil sites high levels of amplification at the low levels of excitation. Data is presented showing such a response is expected and that a relationship exists such that spectral ratio amplification is inversely related to the level of excitation.
- Traditional wave propagation analysis techniques for local site response are seen to be applicable to microseism measurements.
- Because spectral ratio obtained from microseism measurements are higher than those of strong motion shaking, normalized results can be used to provide information on the spatial variation relative to a site of known response.
- Microseism measurements at a soil site can be used to estimate fundamental period and damping of the site and serve as a means for improving the reliability of material property data used in the wave propagation computation. A systems analysis procedure was shown to lend insight to the process.
- Repeatability and reliability of measurements was evaluated and it is shown that averaging of results is essential to characterize site response.
- Use of soil reference sites was studied

It is concluded that microseism measurements can be used on a relative normalized basis to extend the information from a known local response to areas where additional data is lacking. A systems identification procedure applied to the microseism data can be used to extend the knowledge of site material properties such as shear velocity and

Accession For	
NTIS CRA&I	<input checked="checked" type="checkbox"/>
DTIC TAB	<input type="checkbox"/>
Unannounced	<input type="checkbox"/>
Amplification	
ation /	
Availability Codes	
Dist	Avail. and/or Special
A-1	

damping. Long term measurements describe overall site stability and are essential. Microseism measurements can be conducted during windows of stability. A generalized procedure should consist of the following steps:

1. Careful review of site geology
2. Investigation of rock reference site and its variability
3. Selection of a rock reference site
4. Selection of soil reference site having extensive borehole data
5. Long term measurements between rock and soil reference site to establish stability
6. Selection of an array plan to cover region of interest
7. Conducting measurements at rock reference site, soil reference site and at each array site.
8. Reduction of data using appropriate spectral processing.
9. Repeat steps 7 and 8 based on local site variability to obtain best estimate.

It should be noted that it is recommended that closely spaced measurements be made both at the rock and soil reference site throughout the array measurements to monitor overall stability.

CHAPTER 1 EARTHQUAKE MECHANISM

Introduction To Navy Problem

The Navy has numerous bases located in seismically active regions throughout the world. Safe, effective design of waterfront structures requires calculation of the expected site specific earthquake ground motion and effective design of the structural components. The Navy's problem is further complicated by the presence of soft saturated marginal soils which can significantly amplify the levels of seismic shaking as evidenced in the 1989 Loma Prieta earthquake and again in the 1993 Guam earthquake. The Navy began its seismic program in response to the 1977 Earthquake Hazards Reduction Act. Executive Order 12699 reinforces that mandate for earthquake safety. In Fiscal Year 94, the Naval Facilities Engineering Service Center undertook a feasibility study to explore the use of microseisms as a tool for predicting ground motion amplification; Ferritto (1994) presents the results of that effort. Microseism measurements can be used to estimate fundamental period and damping of the site and serve as a means for improving the reliability of material property data used in the wave propagation computation. A systems identification procedure was shown to lend insight to the process. This report will present follow-on research.

The prediction of seismic ground motion amplification at sites with marginal soil properties is of great importance to the Navy since those sites are so prevalent at the waterfront. Most of the naval facilities were constructed on such soils before their earthquake damage potential was recognized. Current procedure for estimating ground motion at a Navy site involve performing a site seismicity study in which historical and geological data are used to estimate seismic ground motion levels for use in design of structures. Site specific spectra are then generated to account for local soil conditions using historical earthquake records. The data base of response records do not account for the response of soft marginal sites. An option for a more detailed analysis of local site response of marginal soils involves wave propagation analysis. This approach requires an insitu shear wave velocity profile to determine the site's shear properties. A one-dimensional wave propagation analysis is usually performed to determine ground motion amplification. This approach is complex, requires field data measurement and may result in significant underestimation of ground motion amplification for sites with marginal soils. This is not surprising since the approach is characterized by several problems.

The geological process of creating the marginal deposits such as bay muds found in harbors and bays involves ocean currents or river erosion. This often results in dipping-layers. Such basin structures violate the assumption of parallel layers assumed in one-dimensional analysis. The problem must be addressed from a two-dimensional or three-dimensional resonance point of view. Two- and three-dimensional resonance characteristics may be significantly different from the one dimensional ones (Bard and Bouchon, 1984; Tiao and Dravinski, 1993). The wave analysis procedures currently in use require material properties from field measurement or laboratory soil tests which are difficult to perform accurately. Further, field tests can be performed only at a limited

number of boreholes since the drilling and testing is expensive. This can significantly limit the understanding of the spatial variation of the soil deposits. There is a need for a new approach for facilitating estimating ground motion amplification at such sites. One such technique involves measurements of long period microtremors.

Even in the absence of earthquakes the ground is continuously vibrating. The amplitude of such vibrations may be less than several microns with periods ranging from tenths of seconds to several seconds, Kanai (1983). The motion of this type is called microtremors. It is common to distinguish two types of microtremors: (i) Long period microtremors or microseisms (with periods $T > 1$ sec) and (ii) short period microtremors ($T < 1$ sec). Usually, microseisms are defined as oscillations of the ground with periods 2 to 20 sec not caused by earthquakes or local causes such as traffic or gusts of wind (Longuet-Higgins, 1950; Hasselman, 1963). In this paper long period microseisms are considered with periods ranging between 0.5 - 10 sec.

To better understand the problem of ground motion amplification, it is important to look at an example of recent Navy experience. The Loma Prieta earthquake occurred when a segment of the San Andreas fault northeast of Santa Cruz, California ruptured over a length of 28 miles producing a Richter local magnitude, M_L , of 7.0 and an average surface wave magnitude, M_S , of 7.1, Seed et. al. 1990. The epicenter was 10 miles (16 km) northeast of Santa Cruz and 20 miles (32 km) south of San Jose. The initial rupture length was estimated to be 24 miles (38 km). The main rupture began at a depth of 11 miles (17.5 km) below the earth's surface and near the center of what would be the rupture plane. Over the next 7 to 10 seconds the rupture spread approximately 12 miles (19 km) to the north and 12 miles (19 km) to the south. The unusual middle location of the hypocenter within the rupture location contributed to the unusually short duration of the event. Approximately 8 to 10 seconds of strong shaking was observed which is considerably less than would be expected from an event of this size. The rupture propagated towards the earth's surface but during the main event appears to have stopped at a depth of 3 to 4 miles (5 to 6 km). Strong ground motion was recorded on the Naval Station, Treasure Island; the peak horizontal ground acceleration components from the main shock were 0.16g and 0.10g, Hryciw et. al. (1991). A significant factor in the Loma Prieta earthquake was the amplification of ground motion in areas underlain by thick deposits of Bay sediments. Treasure Island falls within this observation especially in comparison with recordings on nearby Yerba Buena Island where the peak horizontal accelerations recorded on a rock site were about three times less than those on Treasure Island. Yerba Buena Island, a large rocky outcrop, had horizontal components of motion from this event equal to 0.068g and 0.031g, both significantly less than those on Treasure Island. Of considerable interest is the strain dependent properties for the Bay Mud which have a significantly stiffer modulus with strain. This same phenomenon was observed in Mexico City clays which produced high ground motion amplification. The stiffer soils such as Bay Muds and Mexico City clays respond more elastically and contribute significantly to the observed increases in response.

A one-dimensional soil column analysis using SHAKE, Schnabel 1972, was performed on the site using the actual properties for the Bay Mud as well as properties more typical of a softer clay, Ferritto (1992). Strains in the analysis using the Bay Mud properties are in the range of 0.03 to 0.08 percent in the Bay Mud layers; this results in an effective shear modulus of about 60 percent of maximum with damping in the range of 0.06 to 0.12 of critical. However when typical clay data is used the shear modulus drops to about 10 percent of maximum and damping increases to 0.08 to 0.15 of critical. These material property changes explain the difference in response between the stiffer Bay Mud soil and a typical clay.

The San Francisco site and the Mexico City site both have clays that are substantially stiffer than would be expected. Sharma (1991) shows that the Plasticity Index for Bay Muds is in the range of 20 to 40 between 38 and 75 feet (11.5 and 23 m). The Plasticity Index for Mexico City clays was 30. Vucetic (1991) shows data documenting that the shear modulus is stiffer with shear strain as the Plasticity Index increases. This data indicates that the stiffness of clay under cyclic loading should be increased to account for the Plasticity Ratio. The Plasticity Index is based on the amount of water required to transform a remolded soil from semisolid to a liquid state. It is a function only of the size, shape and mineralogy of the soil particles and the pore water. Engineers should be alert to the presence of high plasticity clay deposits as a potential source of ground motion amplification. The high amplification results in significant damage especially when it is coupled with liquefaction. Amplification of motion at the waterfront where marginal soils are prevalent is a major Navy problem.

To fully understand the amplification problem, we must also look at the frequently occurring associated problem of liquefaction of loose saturated cohesionless deposits which the Navy faces at most of its waterfront sites. Observation of the Naval Station, Treasure Island record from the 1989 Loma Prieta earthquake shows that at about 15 seconds after the start of recording, the ground motion changed indicating the occurrence of subsurface liquefaction. Liquefaction occurred after about 4 or 5 "cycles" of shaking after about 5 seconds of strong motion. Sand boils were observed at numerous locations and bayward lateral spreading occurred with associated settlements. Ground cracking was visible with individual cracks as wide as 6 inches (15 cm). Overall lateral spreading of 1 foot (30 cm) was estimated. Ground survey measurements indicate that settlements of 2 to 6 inches (3 to 15 cm) occurred variably across the island and that some areas had as much as 10 to 12 inches (25 to 30 cm) of settlement. The liquefaction related deformations resulted in damage to several structures and numerous broken underground utility lines, Egan et al. 1991.

The above paragraphs were intended to explain the significance of amplification and liquefaction to Navy facilities. To put this problem in perspective the Navy suffered \$245 million in damages almost entirely from amplification and liquefaction during the 1989 Loma Prieta and 1993 Guam earthquakes. Having identified the Navy problems from marginal soil, there is a strong need for a solution such as microzonation, the identification

mapping of local site response which considers the specific local soil profile at a Navy base.

Earthquake Ground Motion Model

An earthquake occurs when the buildup of stress along a fault exceeds the rupture strength of the rock. This rupture process begins from the weakest location and then propagates for some distance. During the rupture process earthquake induced ground shaking occurs radiating outward. The extent of the rupture and the amount of energy released are proportional to the event magnitude. Earthquake ground shaking is composed of body waves which radiate in three directions and surface waves which radiate in only two directions. Body waves are composed of primary waves, dilational longitudinal vibration compression waves, and secondary waves, distortional transverse vibration shear waves. Surface waves are composed of Love waves, horizontal transverse shear type vibration, and Rayleigh waves, surface vertical longitudinal vibration. There are different wave propagation velocities for each type of wave and each attenuates differently with distance. Since attenuation through the near surface alluvial material is greatest, propagation is generally controlled by bedrock transmission. Waves traveling through bedrock tend to refract toward the vertical because shallower layers have lower propagation velocities. Generally vertically propagating horizontal shear waves are the dominant energy source affecting most structures at sites of interest.

In the 1960's and 1970's seismologists began to analyze the earthquake process in terms of an assemblage of components. This procedure is still in use today as a tool to better understand the elements which affect the response of a structure at a site. The system model consists of :

- Source model of fault mechanism
- Path model of transmission
- Local site model from bedrock to surface
- Structure model

This process allows for the development of component models which can not only be studied in the time domain but also in the frequency domain. Using linear system theory it is possible to establish a series of transfer functions to represent each of the components.

In 1961 Kanai (1961) proposed the idea upon which much recent work is based. In 1972 Lastrico (1972) developed the following model:

$$G = E W X = I X$$

and as

$$|G| = |E| |W| |X| = |I| |X|$$

where all factors are complex functions of frequency and

G	is the surface motion at the site of interest
E	is the equivalent source motion
W	is the crustal bedrock path transfer function
X	is the subsurface site transfer function
I	is the incident motion at bedrock at the site

and are expressed as a Fourier transform. Use of the above model allows the investigator to analyze a series of sites where accelerograms were recorded from a single earthquake event. In this case two sites equally distant from the source can be assumed to have the same source and path functions and local site conditions can be studied. Additionally a single site can be studied for several different earthquakes investigating source and path effects.

The assumptions inherent in this model are that the surface motion is primarily vertically traveling plane shear waves and the subsurface model is composed of elastic horizontal layers overlying bedrock

Fourier analysis will form a main analytical tool. The use of the Fourier spectra provides a measure of the system response. The motion at a given point as a function of time, $g(t)$, may be written as an informationally equivalent Fourier transform, $G(\omega)$, a function of the frequency

$$G(\omega) = \int_{-\infty}^{\infty} g(t) e^{-i\omega t} dt$$

$$G(\omega) = \int_{-\infty}^{\infty} g(t) \cos \omega t dt - i \int_{-\infty}^{\infty} g(t) \sin \omega t dt$$

$$G(\omega) = P(\omega) - i Q(\omega)$$

The Fourier transform can be written in an alternative form which will be used here.

$$G(\omega) = |G(\omega)| e^{i\phi(\omega)}$$

in which

$$|G(\omega)| = [(P(\omega))^2 + (Q(\omega))^2]^{1/2}$$

$$\phi(\omega) = \tan^{-1} [-Q(\omega) / P(\omega)]$$

where the first expression represents the amplitude of the transform and the second expression represents the phase angle. The site amplification can be represented as

$$X = \frac{G(\omega)}{I(\omega)}$$

An alternative measure of site amplification can be represented as the ratio of the cross-spectral density between the reference site and the site of interest to the spectral density of the reference site.

$$H(\omega) = \frac{S_{GI}(\omega)}{S_{II}(\omega)}$$

where

$S_{GI}(\omega)$ cross spectral density of surface to bedrock

$S_{II}(\omega)$ spectral density of bedrock

The coherence function is given by the following

$$\gamma_{GI}(\omega) = \frac{|S_{GI}(\omega)|^2}{S_{II}(\omega) S_{GG}(\omega)}$$

The determination of spectral ratios based on the cross spectral density is fundamentally more exact than the simple division of the soil site spectra divided by the reference site spectra. However, Field et al. (1992) reports some difficulty in using the cross spectrum approach from noise. They also note that the cross-spectrum approach gives an estimation of amplification of about twice the direct ratio method for several sites studied, perhaps from the noise problem. Most papers tend to report results in terms of the direct ratio of the spectra.

Microseism Composition and Source

Microseisms along coastal areas consist of persistent oscillation of seismic waves characterized by long periods which are for the most part generated by ocean wave action. Several studies have shown that the ocean-bottom microseism spectrum is similar to the shape of the continental microseism spectrum but with greater amplitude and can be shown to correlate with known storm activity. Haubrich et al. (1963) identified microseisms as primary and double frequency covering two distinctly different frequency bands .08 Hz (12.5 sec) and .15 Hz (6.66 sec) respectively. The primary microseisms observed on land are between 0.04 and 0.08 Hz and have spectral peaks equal to the wavelength of the dominant ocean waves which appear to form in shallow water by interaction of ocean swells with a shoaling ocean bottom. The double frequency microseisms have a dominant period between 6 to 10 seconds. They are believed to result from an interplay amongst ocean waves of equal frequency traveling in opposite directions resulting in a nonlinear, second-order pressure perturbation on the ocean bottom, Cessaro and Chan (1989).

It is interesting to note that microseisms recorded on land and ocean bottom arrays can be used to track storms by applying frequency wave number analysis. Microseism source azimuths exhibited sufficient stability over periods of one hour to permit determination of reliable source locations by triangulation with two arrays. In these cases the microseism noise source is associated with the near shore process. Cessaro notes that spectral power from primary microseisms associated with major storm activity fluctuates significantly over a matter of minutes. Spectral averaging and moving window analysis are used for azimuth determination. Variation in source with time is not as significant for amplification computation as long as the rock reference site and the soil site are recorded simultaneously since the ratio of the two sites will be used.

Microseisms are generated essentially in three ways (Hasselman, 1963): (i) Action of ocean waves on the coast, (ii) atmospheric pressure variations over the ocean, and (iii) nonlinear interactions between ocean waves. Long period microtremors have been observed for quite some time. However, many of the studies have been limited to their origins and wave characteristics (Longuet-Higgins, 1950; Hasselman, 1963) while only few investigations studied them to explain the ground dynamics of earthquake motion (Ohta et al., 1978). Initially the earthquake problem had been considered only in the short period range (Tanaka et al., 1968). Iida and Ohta (1964) investigated relationships between the amplitude of microtremors and soil structures and proposed correlation for the observations on Nagoya, Japan. Kubotera and Otsuka (1970) observed microtremors in the period range of 1 to 3 sec in Aso Caldera area, Japan. They suggested that the microtremors are mainly Love waves with predominant period which correlates well with the thickness of the soil deposits.

Kagami et al. (1982) observed long period microtremors in deep sedimentary basins of the Niigata Plain and Los Angeles. These locations were selected because strong

ground motion records obtained during the 1964 Niigata earthquake and 1971 San Fernando Earthquake contain large long period amplitudes. Understanding of these predominant long-period motions is very important for evaluation of seismic motion of large scale structures. The results show that the amplitude of long period microtremors increases systematically from basement rock sites compared to deep sediment sites. This coincides with the observations obtained through studies of strong ground motion records. Therefore, Kagami et al. (1982) concluded that simultaneous observation of long period microtremors at multiple stations can provide insight into deep soil amplification effects and therefore, permit an estimate of input motions for large-scale structures.

In another study Kagami et al. (1986) measured long period microtremors in the San Fernando Valley, California. A complete two-dimensional study of the influence of soil deposits on seismic motions was carried out. It was shown that the spectral amplitude of microtremors correlates with the thickness of the sediments and that the site dependency of amplification is consistent with available geological and strong ground motion data.

The Michoacan earthquake of September 19, 1985 which devastated Mexico City prompted Kobayashi et al. (1986) to measure the long period microtremors within the Mexico Valley shortly after the earthquake. The measurements were performed at 95 sites in and around Mexico City. For sites in the downtown area (area of many damaged buildings) microtremor measurements indicate predominant periods from 1 to 2.5 seconds which correspond to the natural periods of the collapsed buildings in this region. (Predominant period is defined as a period of the peak spectral amplitude of the predominant component of motion.) At sites where strong ground motion was measured, the acceleration response spectra of the main shock compare well (with a few notable exceptions) with the Fourier velocity spectra of microtremors at the corresponding locations.

Lermo et al. (1988) extended the microtremor measurements of Kobayashi et al. (1986) to a total of 181 sites. In the transition and the lake bed zones of the Valley of Mexico these measurements show that the period at which peak in microtremor Fourier velocity spectra occurs corresponds to the natural period of the sites. Excellent agreement was obtained between natural period estimates using microtremor spectra and from strong ground motion records.

Cessaro (1992) has performed research using data from three land based long period seismic arrays. Reliable microseism source locations were determined by wide-angle triangulation using azimuths of approach obtained from frequency wave-number analysis of the records of microseisms propagating across these arrays. He found that there were two near shore sources of both primary and secondary microseisms which are persistent and associated with essentially constant locations. Further he noted that secondary microseisms were observed to emanate from wide ranging pelagic locations in addition to the same near shore locations.

In Cessaro's work (Cessaro, 1992) he notes:

" that primary microseisms emanate from persistent near-shore locations that do not correlate well with their associated pelagic storm locations. During the time period sampled for this study, three major storms were active in the North Pacific and Atlantic oceans and two primary microseism source locations are identified: (1) A wide ranging North Pacific storm correlates with a microseism source near the west coast of Queen Charlotte Islands, BC and (2) North Atlantic storms correlate well with a source near the coast of Newfoundland. While the North Pacific storm trajectory subtends an arc greater than 90 degrees from the LASA array, the associated primary microseism source appears to be stable. The microseism near Newfoundland exhibits similar stability"

Cessaro concludes:

Although pelagic storms provide the source of microseismic wave energy, it is the interplay between (1) the pelagic storm parameters, such as tracking velocity, peak wind speed, location, effective area, and the ocean surface pressure variation, (2) the resulting storm waves and their wave number distribution, (3) the direction of the storm wave propagation, and (4) the near-shore and deep-ocean processes that control the production of microseisms. It is apparent that only a fraction of the total storm-related noise field is coherent. from the perspective of a seismic array, at any given moment only the most energetic coherent portion of the noise field is detected by FK analysis, i.e. a peak in the FK power represents the most energetic coherent portion of the microseismic wave field at that instant. ... It is also noted that both primary and secondary microseism source locations do not appear to follow the storm locations directly.

He further notes that there are local areas where near shore locations radiate strong coherent primary and secondary microseisms perhaps as a result of local resonance.

Orcutt (1992) notes that for secondary microseisms with peaks around 0.15 Hz there is no apparent correlation with increases in local wind speed and wave height. He suggests they are controlled by surface gravity waves from large distant storms. Akamatsu (1984) studied the Kyoto basin under different sea conditions noting that the spectra were influenced by the sea waves around Japan in particular during the winter and by typhoons, cold fronts, and monsoons. Although the amplitude and peak frequency varied with meteorological conditions, he noted the spectral ratios were nearly constant in frequency and amplitude. This further emphasizes the fact that microseisms are quite variable and their use is only possible by use of pair of reference site to site of interest response, and not through a single station response.

The Japanese have been using microtremors as a means of site soil classification, Kanai (1961). They note the period distribution curve of microtremors shows a correlation to soil conditions. The presence of a single sharp peak is indicative of a simple stratified layer. The presence of two or more peaks indicates more complex layering. They note the following correlations:

- Mountain peak Sharp peak at period 0.1 to 0.2 sec
- Diluvial soil Peak at 0.2 to 0.4 sec
- Soft alluvial soil Number of peaks 0.4 to 0.8 sec
- Thick soft site Relatively flat curve from 0.05 to 2 sec

They note the period is often influenced by the properties of the first layer of the site. Rock sites tend to have flat curves. When the microtremor spectra exhibits a single peak, that peak correlates well to peaks from earthquake strong ground motion. However when there are more than one peak, the dominant peak can be influenced by the frequency content of the input source motion.

The ability to actually measure microseisms and distinguish the results from local noise is of critical importance to their use in any engineering measurement. Nakamura (1989) made extensive measurements. He reports Fourier amplification for a site during a quiet interval and for an interval having the passage of a train. The spectra have close agreement in the frequency range of 0.1 Hz (10 sec period) to 3 Hz (0.33 sec period). Above 3 Hz (below 0.33 sec period) the effect of the train is noted as substantially higher peaks. It is important to note that for engineering applications to structures the range of interest in period is from 0.5 sec to 5 sec. Most noise is exhibited as low period/high frequency outside the range of engineering interest. Filtering is performed to eliminate these components by high and low pass filters.

In reporting results comparing microseism data to weak or strong motion data, many researchers make comparisons over a wide range of frequency. For engineering applications it is essential to focus on the range of interest. Generally agreement is better for periods greater than 1 sec. When interpreting the conclusions drawn by researchers attention must be paid to the frequency range being reported. It is also critical to understand the frequency range of the instrument being used. Instruments intended for high frequency measurements will be noise sensitive and are not well suited for measurement of long period microseisms.

Earthquake Model System Identification

The system identification process is a powerful tool which can enhance the usage of microseism measurements to confirm fundamental site properties. To illustrate the concept we will focus on representation of a simple system composed of a single degree of freedom oscillator. The Fourier transform can be used to assist in quantification of system properties. The general equation of motion of the system can be expressed as:

$$m \ddot{y}(t) + c \dot{y}(t) + k y(t) = x(t)$$

where

m, c, k scalar coefficients for mass, damping and stiffness
 $x(t)$ excitation
 $y(t)$ response

The transfer function can be shown to be:

$$|H(f)| = \left(\frac{1 + (2\zeta f/f_n)^2}{(1 - (f/f_n)^2)^2 + (2\zeta f/f_n)^2} \right)^{1/2}$$

where

ζ percent critical damping

This for low levels of damping can be approximated by the following at peak response frequency $f = f_n$:

$$|H(f)| = 1/(2\zeta)$$

The system parameters can be estimated from the best fit of the response function as illustrated in Figure 1.1. Figure 1.1 illustrates how the system mass and stiffness control the fundamental period of response and how the peak amplitude of response at the fundamental period is controlled by the system damping. In the specifics of the site response problem, the site is usually analyzed in an engineering analysis using wave propagation techniques. This technique requires a site profile to be modeled by a series of horizontal layers, each having density, shear modulus or shear wave velocity, and damping identified. The simplest boring log data usually reports density data, standard penetration blow counts and soil classification. Often the blow count data is used to estimate shear wave velocity; however the relationship between blowcount and shear wave velocity is imprecise and has a high level of uncertainty. The density is usually more easily defined. The relation of modulus and damping with strain is obtained from laboratory tests and is usually approximated by graphs reported in the literature. Depending on the depth of the boring log, the depth to firm ground or bedrock may or may not be well

wave propagation techniques, we are often limited by lack of data. The systems identification process allows us to use the measured microseism data such as fundamental period of response and amplification to quantify the possible range of parameters. For example, if the computed period differs from the measured consideration can be given to adjusting either the depth to bedrock or the initial modulus of the soil which affects the stiffness. If for example the depth to bedrock were well established by the boring log, emphasis could be placed on the shear modulus, since density is usually defined. The amount of damping can be adjusted to converge on the appropriate level of amplification. In this way the measured response to microseisms can be used to confirm low level site response and associated material properties. This allows us to converge on an acceptable site model especially when site response strong motion data are lacking. The process helps reduce the levels of uncertainty and establishes the bounds of material properties and site response.

Figure 1.2 illustrates how the coherence function can be used as a measure of statistical confidence in a spectral transfer function estimate. The imaginary part of the transfer function can give an indication of the system damping. Figure 1.3 illustrates two cases (after Palo 1994). The first case indicates a frequency independent damping while the second illustrates frequency dependent damping. The case of frequency dependent damping results in an integro-differential equation in the form of:

$$m \ddot{y}(t) + \int c(\tau) \dot{y}(t - \tau) d\tau + k y(t) = x(t)$$

Application of Earthquake Ground Motion Model to Study Site Amplification

A specific application of the general earthquake ground motion system model can be made to study site amplification. For the case where the source and path are shown to be the same, two sites may be directly compared. One of those sites is chosen as a *reference* rock outcrop site such that that site has a transfer function from surface to bedrock of essentially unity. The accelerogram recordings made on the reference rock outcrop can then be directly used as the bedrock motion at the second site, the site of interest. It is important to note that the procedures for doing this involve measurement of ground motion but do not require quantification of the material properties.

There are several elements to the problem which must be noted:

- Acceptability of linear transfer function concept using rock outcrop and soil site;
- Use of ocean induced microseism as excitation;
- Establishing a frequency range of interest for building structure response.

The general concept of combination of source path and site effects has been widely used by seismologists. Hutchings (1991) demonstrated that empirical Green's function method can be used to capture the propagation and linear site response effects for frequencies from 0.02 to 0.5 Hz (periods from 2 to 50 sec). He predicted actual recorded

ground motion from the Loma Prieta earthquake at 5 San Francisco sites using recordings of Loma Prieta aftershocks. He presented 25 source models that spanned the range of uncertainty. Nonlinear material properties such as the variation of shear modulus and damping with strain level are widely accepted, and use of equivalent linear strain dependent material properties for transient wave propagation analysis in the frequency domain is common. Program SHAKE for example has been in use for twenty years and has been shown to accurately predict site amplification. It is recognized that as the level of ground shaking increases there is a reduction in shear modulus and an increase in damping. Jarpe et al. (1993) shows that although there is evidence that some soft sites respond nonlinearly, linear predictions do a surprisingly good job of estimating earthquake level site response. Aki (1988) notes that nonlinearities were evident only in the case of liquefaction such as in the Niigata 1964 earthquake records. He states "As a matter of fact, seismologists tend to find a good correlation between weak and strong motions at a given site, namely similar amplification factors for both, implying that non-linearities are not important as the first order effect in most cases." However he also notes that for the SMART-1 ground motion array in Taiwan that the standard deviation of ground motion acceleration is less for large events than small indicating a magnitude dependence which may be attributed to non-linear soil effects.

The process of using microseisms as a predictor of amplification seems viable. The mechanism of combination of source, path and site models is feasible since the first two components, source and path are fundamentally appropriate for linearization. The site transfer function may incorporate nonlinearities, but these nonlinearities do not preclude the use of microseisms as long as they are recognized. If this is done the fundamental concept of microseisms usage requires linearity only in source and path. The subject of nonlinearity of site transfer function is a main topic of this research and will be discussed in detail in following chapters. It is most important to note that *long period microseisms* will be used for this study. High frequency noise such as traffic and other man made signals are minimized by this selection. For this study the frequency band of 0.1 to 2 Hz (0.5 to 10 second period) is used and is a region chosen because it is applicable to building response. While it may have academic interest, ground response at 50 Hz does not affect building response significantly. It is important to keep this fact in mind, since in reading research papers by others many elements of system response are reported. In sorting out data it is essential to consider the frequency range of the data, the source of the excitation and the applicability to structures. The microseism research area has not progressed to a state where there is common acceptance of results and development of standardized procedures. There are reported papers showing unsuccessful results. These are important as a learning tool.

Udwadia and Trifunac (1973) report 15 events recorded in El Centro, California and compare results to microtremor excitations. They conclude that local soil conditions are overshadowed by source mechanism and transmission path. They found that the microtremor and earthquake processes vary widely in character and have little correlation in ground response. On first appearance the results seem to negate the feasibility of use of microseisms. The paper presents a study based only on spectra not spectral ratio. It does

not use a rock reference site but simply analyzes response at the site of interest. It presents results over a wide range of frequency. The microtremors were high frequency short period measurements. *The procedures suggested as part of this study will use lower frequency long period measurements at both a rock reference site and a soil site to eliminate source and path effects. Further this study will use the systems identification process to tie measured microseism data to computations for earthquake response.*

Gutierrez and Singh (1992) report on another study where microtremor and earthquake response agreement was only fair. They studied a location in Accapulco, Mexico using a rock reference site and several sites on sand and clay deposits, alluvium, and a sand, lime and clay bar. They use an seismometer with a period of 5 seconds and report results from 0.5 Hz to 50 Hz. Measurements were made during high traffic times and at night. They found that the traffic noise affected both the shape and amplitude of the spectra. For structural response applications the region of interest would be much narrower than the high frequency reported and would cover only the lower end of 0.5 to 2 Hz. To better cover the long period - lower frequency segment, this study obtained wide band seismometers with a 20 second period and flat bandwidth from 0.05 to 20 Hz to give better response in the region most affecting structures.

Amplification As A Function Of Level Of Excitation

The ground motion reaching a site is a function of the causative rupture. There are differences in the frequency content of two ground motion records both at the same nominal peak acceleration, one caused by a distant large event, the other caused by a local small event. Site response depends in part on the frequency content of the driving ground motion. Rogers et al. (1983) present an interesting discussion of nonlinear site effects. "Although laboratory data suggest that soils behave in a nonlinear fashion when strain exceeds 10^{-5} ... field data have been collected suggesting that high- and low-amplitude soil response are perhaps linear for strains up to 10^{-3} ." They report experience using distant nuclear explosions and the data from the 1971 San Fernando earthquake to illustrate that transfer functions from both are similar over a wide range of strain. They postulate that nonlinear soil behavior may be limited to a small area around the fault. "For instance, a magnitude 7-7.5 earthquake develops velocities on soil sites exceeding 100 cm/sec at distances less than 7-13 km.... For soil sites with 200 m/sec shear velocities, strains of 5×10^{-3} will be developed within this zone. Based on the observations discussed above, this strain level may still be below the level of significant non-linear behavior. Because damaging motions on soils (with intensity) $III > VI$ occur to distances of 60-100 km (50 percentile) for a 30 km rupture, the area of damage susceptible to non-linear soil response is about 2-9 percent of the total area of damage." They note that the zone of nonlinear behavior may produce the greatest life loss but also note that a high percentage of total damage occurs outside this zone. Murphy (1983) also confirms that over a wide range of strain consistency has been observed for spectral ratios from earthquakes and nuclear explosions. Boore et al. (1983) reports on measurements

taken in a sediment valley in the Garm region of what was the Soviet Union. The measurements covered a range of ground motion from 10^{-5} to 0.2 g with high agreement of the amplification ratio over the wide range in levels of motion supporting linearity of response. Table 1.1 summarizes some of the observations which support the concept that response is independent of the level of excitation and linear theories are adequate.

Darragh and Shakal (1991) measured the site response at Treasure Island, California to weak and strong ground motion using the Yerba Buena Island site as a rock reference. The data included strong shaking from Loma Prieta and its aftershocks. They note that the amplitude, shape and frequency distribution of the spectral ratios for the soft Treasure Island site on Bay Mud varies with local magnitude. Figure 1.4 shows peak ground velocity and amplification. Figure 1.5 shows event magnitude and amplification. These results may be interpreted to show a clear trend that amplification increases as the size of the event decreases giving the implication of a nonlinear process. They conclude "that weak ground motion may be amplified to a greater extent than strong ground motion especially at sites similar to Treasure Island where nonlinear effects are observed at peak acceleration and velocity levels as low as 0.16g and 33 cm/sec, respectively. The corresponding rock motion near this soft site is only 0.07g and 15 cm/sec." It is important to note that the Treasure Island site liquefied during the Loma Prieta event and significantly affected at least part of the response record. The liquefaction occurrence obviously introduced nonlinearities into the site. Absent the occurrence of liquefaction it is not clear whether the site response would have been higher and of an amplification level comparable to that measured by aftershocks which did not liquefy the site. Darragh and Shakal (1991) also report on another site at Gilroy with a stiff site response. They report that the stiff site had an amplification of 2 for the 7.1 Loma Prieta earthquake, and an amplification of 4 for the 6.1 Morgan Hill and 5.6 Coyote Lake earthquakes. The same data is presented by Jarpe et al. (1989) suggesting the nonlinear response at high strain. They report additional data for two sites (one composed of thin alluvium over sandstone, the other thick dry alluvium) in Livermore, California where weak ground motion spectral ratios are essentially at the same levels as main shock data and they cite similar observations from the Coalinga California earthquake from a dry site having strong motion accelerations of up to 0.7g where weak motion spectral ratios were of the same levels. Field et al (1990) reports on a microtremor evaluation of a site in Flushing Meadows, New York where significant amplification over 50 was observed in the spectral ratios. The site had a 10 to 15 meter layer of soft Holocene organic clay and a thin layer of man made fill to cover the previous marsh environment.

Kameda et al (1991) reports on six sets of sites using Loma Prieta data and microtremor data. Four of the sites on bay mud exhibited much larger microtremor spectral ratio amplification than corresponding strong motion data. Two sites of thick Quaternary deposits exhibited the same order of magnitude for both Loma Prieta and microtremor data. Akamatsu (1991) presents similar data in a very constructive manner. Spectral amplification ratios increase with proximity to the San Francisco Bay and Holocene estuarine Bay Mud soils. Clearly waterfront deposits are affecting response. Okada et al. (1991) studied the Sapparo region conducting microtremor readings from the

Ishikara Bay inland. They noted that microtremor spectral ratio data increased from 10 to 25 with proximity to the coastline. Celebi (1987) notes in his study of the 1985 Chile earthquake that spectral ratio amplification transfer functions (on the order of 40 to 60 at 2 Hz) computed from weak ground motion aftershocks substantially exceeded transfer functions computed from strong-ground motion of the main shock. The sites were coastal areas composed of estuarine terrace deposits, sands, and alluvial deposits. The fact that the same phenomenon occurs with weak ground motion from earthquakes suggest process is controlled by the geology rather than the excitation source.

Sato (1991) measured microtremors at Ashigara Field, a site a few kilometers from Sagami Bay having upper layer shear wave velocities of 110 m/sec. This site produced peak spectral ratios of 50 at a frequency of 2 Hz. Sato notes that the site response is controlled by the upper 10 m soft surface layer. This implies that saturated waterfront marginal site would be expected to have amplification from microseisms greater than that from main shocks of large earthquakes, but dry alluvial sites may not exhibit these differences. The Table 1.2 summarizes some cases which indicate marginal waterfront soils experience a nonlinear amplification effect as a inverse function of level of excitation.

Tazoh et al. (1988) reports on two sites in Japan where the site period based on transfer functions of depth to surface varied from 0.25 sec for small local earthquakes to 1.35 for a large event. This phenomenon may depend on the frequency content of the source and also represent the effect of site properties with level of strain. It is well known that local events producing the same site acceleration as distant large events have lower energy in the 1 to 10 second period range.

References

Abrahamson N. A. (1993) in publication

Akamatsu J. (1984) "Seismic amplification by soil deposits inferred from vibrational characteristics of microseisms" Bulletin Disaster Prevention Research Institute, Kyoto University, Vol. 34 Part 3 No 306 Sept. 1984

Akamatsu et al (1991) "Long period (1-10s) microtremor measurement in the areas affected by the 1989 Loma Prieta earthquake", Fourth International Conference on Seismic Zonation, Stanford California

Aki, Keliti (1988) "Local site effects on strong ground motion" Earthquake Engineering and Soil Dynamics - Recent Advances in Ground-Motion Evaluation, ASCE Geotechnical Special Publication 20, New York NY

Archuleta R. J. et al (1992) Garner Valley Downhole array of accelerometers: Instrumentation and preliminary data analysis." Bulletin of the Seismological Society of America, Vol. 82 No 4, pp 1592-1621, August 1987

Bard, P-Y., and Bouchon, M., 1985. The two-dimensional resonance of sediment-filled valleys, Bulletin Seismological Society of America,, No 75, 519-541.

Bard, P (1983) " Site effects: Two dimensional modeling and earthquake engineering", Proceedings of Conference XXII, A Workshop on "Site-specific Effects of Soil and Rock on Ground Motion and the Implications for Earthquake-resistant Design" USGS, Reston VA

Bard, P. and J. C. Gabriel (1986) "The seismic response of two-dimensional sedimentary deposits with large vertical velocity gradients." Bulletin of the Seismological Society of America, No 76, pp 343-346

Blakeslee S. and Peter Malin. (1991) "High frequency site effects at two Parkfield downhole and surface stations." University of California, Institute for Crustal Studies, Santa Barbara CA July 1991

Boore D. (1983) "Some studies concerning site response." Proceedings of Conference XXII, A Workshop on "Site-specific Effects of Soil and Rock on Ground Motion and the Implications for Earthquake-resistant Design" USGS, Reston VA

Campbell K. (1983) "The effects of site characteristics on near-source recordings of strong ground motion", Proceedings of Conference XXII, A Workshop on "Site-specific Effects of Soil and Rock on Ground Motion and the Implications for Earthquake-resistant Design" USGS, Reston VA

Celebi, M. (1987) "Topographical and geological amplifications determined from strong-motion and aftershock records of the 3 March 1985 Chile earthquake", Bulletin of the Seismological Society of America, Vol. 77 No 4, pp 1147-1167, August 1987

Cessaro R and W. Chan, (1989) " Wide-angle triangulation array study of simultaneous primary microseism sources." Journal of Geophysical Research, Vol. 94, No B11 pp. 15.555-15.563 Nov. 1989.

Cessaro R. (1992) TGAL 92-13 " Land-based seismic array studies of low frequency ambient oceanic noise." Teledyne Geotech, Alexandria VA., Feb. 1992

Darragh R and A. Shakal (1991) " The site response of two rock and soil station pairs to strong and weak ground motion." Bulletin of Seismological Society of America Vol. 81 pp 1885-1899

Donovan, N. (1983) " A practitioner's view of site effects on strong ground motion" Proceedings of Conference XXII, A Workshop on "Site-specific Effects of Soil and Rock on Ground Motion and the Implications for Earthquake-resistant Design" USGS, Reston VA

Egan, John A. and Zhi-Liang Wang, (1991) " Liquefaction Related Ground Deformation And Effects On Facilities At Treasure Island, San Francisco, During the 17 October 1989 Loma Prieta Earthquake", Proceedings from the Third Japan-US. Workshop on Earthquake Resistant Design of Lifeline facilities and Countermeasures for Soil liquefaction, National Center for Earthquake Engineering Research, State University of New York at Buffalo Feb. 1991

Ferritto, J. M. (1992) N-1844 "Ground Motion Amplification and Seismic Liquefaction: A Study of treasure Island and the Loma Prieta Earthquake", Naval Civil Engineering Laboratory, Port Hueneme, CA June 1992

Ferritto J. M. (1994) NFESC TR-2020-SHR "Feasibility For Use Of Microseisms As An Aid to Navy Base Microzonation" Port Hueneme CA August 1994

Field E. H. et al. (1990)" Using microtremors to assess potential earthquake site response: A case study in Flushing Meadows, New York City" Bulletin of the Seismological Society of America, Vol. 80 No 6 pp 1456-1480 DEC 1990

Field E. H. et al. (1992)" Earthquake site response estimation: a weak-motion case study" Bulletin of the Seismological Society of America, Vol. 82 No 6 pp. 2283-2307 Dec. 1992

Gutierrez, G and S. K. Singh, (1992) "Site Effects in Acapulco, Mexico" Bulletin of the Seismological Society of America, Vol. 82 No 2 pp. 642-659 April 1992

Haubrich R. et al. (1963) "Comparative spectra of microseisms and swells", Bulletin of Seismological Society of America, 53 , pp 27-37

Hasselman, K., 1963. A statistical analysis of the generation of microseisms, Review Geophysics, 1, No. 2, 177-210.

Hryciw, Roman D. et al. (1991) "Soil Amplification at treasure Island During The Loma Prieta Earthquake", Proceedings Second International Conference on Recent Advances in Geotechnical Earthquake Engineering and Soil Dynamics, March 11-15 1991, St. Louis, Missouri

Hutchings, L J. (1991) "Prediction of strong ground motion for the 1989 Loma Prieta earthquake using empirical Green's functions", Bulletin Seismological Society of America, 81, 1813-1837

Iida, K., and Ohta, Y., (1964) "A study of microtremors observed in Nagoya and its vicinity", Journal Earth. Sciences, Nagoya University, Vol. 12, 192-221.

Jarpe S. P. et al. (1989) " Selected strong and weak motion data from the Loma Prieta earthquake sequence." Seismological Research Letters, Vol. 60, No 4 Oct-Dec 1989

Jarpe, S. and P. Kasameyer, (1993) "Validation of a methodology for predicting broadband kinematic strong motion time histories from empirical Green's functions", UCRL-JC-102465 Lawrence Livermore National Laboratory, Livermore CA May 1993

Jibson, R. (1987) "Summary of research on the effects of topographic amplification of earthquake shaking on slope stability" US Geological Survey Open File Report 87-268 Meno Park CA

Kagami, H., Duke, C. M., Liang, G. C. and Ohta, Y., (1982) "Observation of 1- to 5-second microtremors and their application to earthquake engineering. Part II. Evaluation of site effect upon seismic wave amplification due to extremely deep soil deposits", Bulletin Seismological Society of America b.f. 72, pp. 987-998 (1982).

Kagami, H., Okada, S., Shiono, K., Oner, M., Dravinski, M., and Mal, A.K., (1986) Observation of 1- to 5-second microtremors and their application to earthquake engineering. Part III. A two dimensional study of site effect in the San Fernando valley, Bulletin Seismological Society of America, b.f. 76, 1801-1812.

Kameda H. et al (1991) "Comparative observation of soil amplification from long period microtremor and earthquake recordings for seismic microzonation.", Fourth International Conference on Seismic Zonation, Stanford California

Kamiyama, M et al (1992) Technical Report NCEER-92-0023 "A semi-empirical analysis of strong motion peaks in terms of seismic source, propagation path and local site

conditions." National Center for Earthquake Engineering Research, State University of New York at Buffalo, NY Sept. 1992

Kanai, K. (1961) "On Microtremors. VIII", Bulletin of Earthquake Research Institute, 39: 97-114

Kanai, K. (1961) An empirical formula for the spectrum of strong earthquake motions, Bulletin Earthquake Research Institute, Tokyo University, 39 pp. 85-96

Kanai, K., 1983. "Engineering Seismology", University Tokyo Press, Tokyo.

Kanai K and T. Tanaka, (1961) On Microtremors, VIII" Bulletin of the Earthquake Research Institute, University of Tokyo, Vol. 39 1961

Kubotera, A., and Otsuka, M., (1970) "Nature of non-volcanic microtremor observed in Aso-caldera", Journal of Physical Earth, 115-124.

Lastrico, R. et al. (1972) Effects of site and propagation path on recorded strong earthquake motions. Bulletin of the Seismological Society of America, Vol. 62 No 4 pp. 933-954 Aug. 1972.

Lermo, J., Singh, S. K., Dominguez, T., Ordaz, M., Espinoza, J.M., Mena, E. and Quaas, R., (1988) "A study of amplification of seismic waves in the Valley of Mexico with respect to a hill zone site", Earthquake Spectra, No. 4, 653-674.

Lindley and Archuleta (1993) "Variation of seismic site effect in the Santa Cruz Mountains, California" in publication

Lodde, P.F. (1992) Dynamic Response of San Francisco Bay Mud" MS Thesis, University of Texas at Austin 1982.

Longuet-Higgins, M.S., 1950. "A theory of the origin of microseisms," Philosophical Transactions Royal Society London A 243, 1-35.

Murphy J. (1983) "Site effects on strong ground motion observed from underground nuclear explosions." Proceedings of Conference XXII, A Workshop on "Site-specific Effects of Soil and Rock on Ground Motion and the Implications for Earthquake-resistant Design" USGS, Reston VA

Nakamura, Y (1989) "A method for dynamic characteristics estimation of subsurface using microtremor on the ground surface" QR or RTR1, Vol. 30, No 1, February 1989

Nogoshi, M. "Site Characterization by detailed seismic intensities, aftershocks, and microtremors." Seismological Laboratory, California Institute of Technology, Pasadena

Ohta, Y., Kagami, H., Goto, N., and Kudo, K., (1978) "Observation of 1- to 5-second microtremors and their application to earthquake engineering. Part I: comparison with long-period accelerations at the Tokachi-oki earthquake of 1968, Bulletin Seismological Society of America, b.f. 68, pp. 767-779.

Ohta, Y., and Nogouchi, S., (1972) Observation of 1- to 5-sec microtremors and their application to earthquake engineering, (in Japanese), Proceedings Symposium Disaster Science, b.f. 9, 247-248.

Okada S. et al " Two dimensional analysis on site effects in the Sapparo urban region, Japan, based on observation of 1 to 10 second microtremors." Fourth International Conference on Seismic Zonation, Stanford California

Orcutt John A.(1992) "Seafloor pressure array studies at ultra low frequencies." California University, San Diego AD A247663

Palo, P. (1994) Oral communication

Rogers A. et al, (1983) "The issues surrounding the effects of geologic conditions on the intensity of ground shaking", Proceedings of Conference XXII, A Workshop on "Site-specific Effects of Soil and Rock on Ground Motion and the Implications for Earthquake-resistant Design" USGS, Reston VA

Sato K., et al (1991) " Estimation of Surface Ground Motion at Ashigara Field using microtremors." Fourth International Conference on Seismic Zonation, Stanford California

Seekins (1994) Oral communication

Seo K., et. al (1991) "Microtremor measurements in the San Francisco Bay Area." Fourth International Conference on Seismic Zonation, Stanford California

Rollins, Kyle et al. "Soil Amplification at Treasure Island During The Loma Prieta Earthquake" in publication

Schnabel Per B., et. al. (1972) "SHAKE, A Computer Program For Earthquake Response Analysis Of Horizontally Layered Sites", EERC 72-12 University of California, Berkeley, Ca Dec. 1972.

Seed H. B. et al. (1987) Relationships Between Soil Conditions and earthquake Ground Motions in Mexico City In The Earthquake of Sept. 19, 1985" EERC 87-15 University of California, Berkeley Ca Oct. 1987

Seed R. B. et. al. (1990) EERC 90-05 "Preliminary Report On The Principal Geotechnical Aspects Of The October 17, 1989 Loma Prieta Earthquake" College of Engineering University of California, Berkeley, California April 1990

Sharma H. D. (1991) "Performance of a hazardous Waste and Sanitary Landfill subjected to Loma Prieta Earthquake", Proceedings Second International Conference on Recent Advances in Geotechnical Earthquake Engineering and Soil Dynamics, March 1991, St. Louis Missouri

Tanaka, T., Kanai, K., and Osada, K., (1968) Observation of Microtremors. XII, Bulletin Earthquake Research Institute, b.f. 46, 1127-1147.

Tanaka A and K Migata (1988) "Estimation of shear wave velocity based on the results of microtremor observation" Geophysical Exploration Vol. 41 No.1 Feb. 1988

Tiao, Z., and Dravinski, M., 1993. "Resonance of sediment valleys and its prediction through an eigenvalue method", Geophysical Journal International, submitted. for publication.

Toriumi, I., Takeuchi, I., and Ohba, S., (1972) Observation of microtremors with a 10 sec. pickup in Nagoya (in Japanese), Proceedings. Symposium Disaster Science, b.f. 9, 249-252.

Udwadia, F.E. and M.D. Trifunac (1973), " Comparison of earthquake and Microtremor Ground Motions in El Centro, California" Bulletin of the Seismological Society of America, Vol. 63 No 4 pp. 1227-1263 August 1973

Vucetic M. et al. (1991) " Effect of Soil Plasticity on Cyclic Response" Journal of Geotechnical Engineering Vol. 117 No. 1. January 1991.

Table 1.1
Cases showing response independent of level of excitation.

Site	Soil	Effect	Reference
various Japan	various Alluvium - rock	Period same eq and microtremor	Kanai & Tanaka (1961)
San Francisco, CA	Various sites at distances from Bay	Normal amplification Peninsula sites (AP6,MTR,SVL etc.) Santa Clara Valley ARP, PAH rock Santa Cruz (BAR, KPL, SHE,etc)	Akamatsu (1991)
San Francisco, CA	Alluvium	Period same earthquake & microtremor	Seo(1987)
McGee Creek, CA	Glacial moraine over hornfels	linear response range magnitudes M 6.4, 5.8	Seale and Archuleta (1989)
Garm, Chusal & Yasman	sediment valley	Acceleration range 10^{-5} to 0.2 g no difference in site response	Tucker and King (1984)

Table 1.2
Cases showing high amplification of microtremors or weak motion
compared with strong ground motion

Site	Soil	Amplification	Reference
Ashigara Field near Sagami Bay Japan	$V_s = 110$ m/sec thick sediment deposit S7/R7	50 at 2 Hz	Sato (1991)
San Francisco, CA	Various sites at different distances from Bay	6 to 18 waterfront Holocene Bay Mud 1 to 2 at distance from waterfront on Quaternary alluvium	Akamatsu (1991)
Canal Beagle, Vina del Mar Chile	CBA estuarine terrace TRA sand EAC sand MUN alluvial REN sand	40 to 60 for weak ground motion	Celebi (1987)
San Francisco, CA	Treasure Island Bay Mud	Loma Prieta peak amp. 1-4 Hz = 4 Aftershocks peak amp. 1-4 Hz = 12	Jarpe (1989)
San Francisco, CA	Treasure island AP2 Bay Mud RSH/RWS Bay Mud MAL Bay Mud SVL/SH4 alluvium ASH/AOH alluvium	L P* - Microtremor 3.35 4.62 4.32 17.93 2.42 13.59 3.43 5.34 1.81 5.04 *LP - Loma Prieta	Kameda (1991)

• = numerical | H(f) | estimate

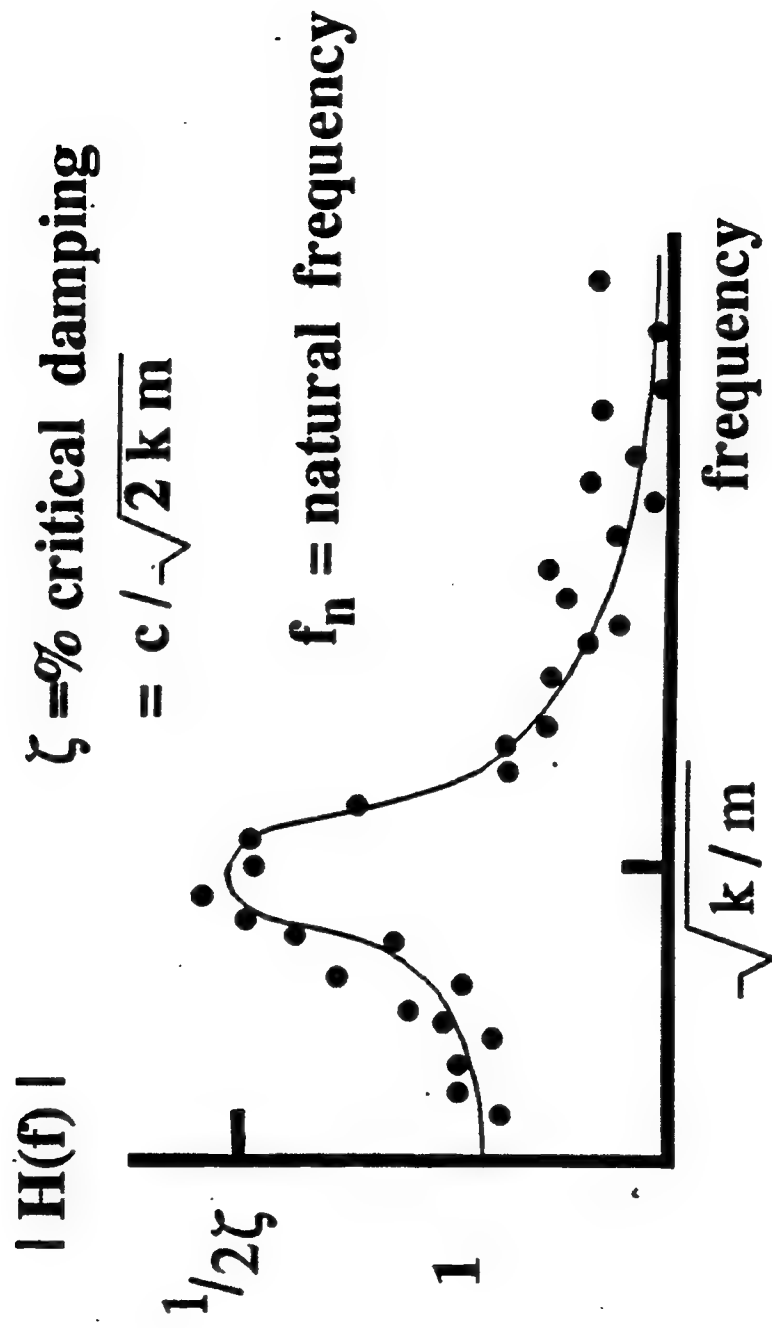


Figure 1.1 System identification, after Palo, 1994

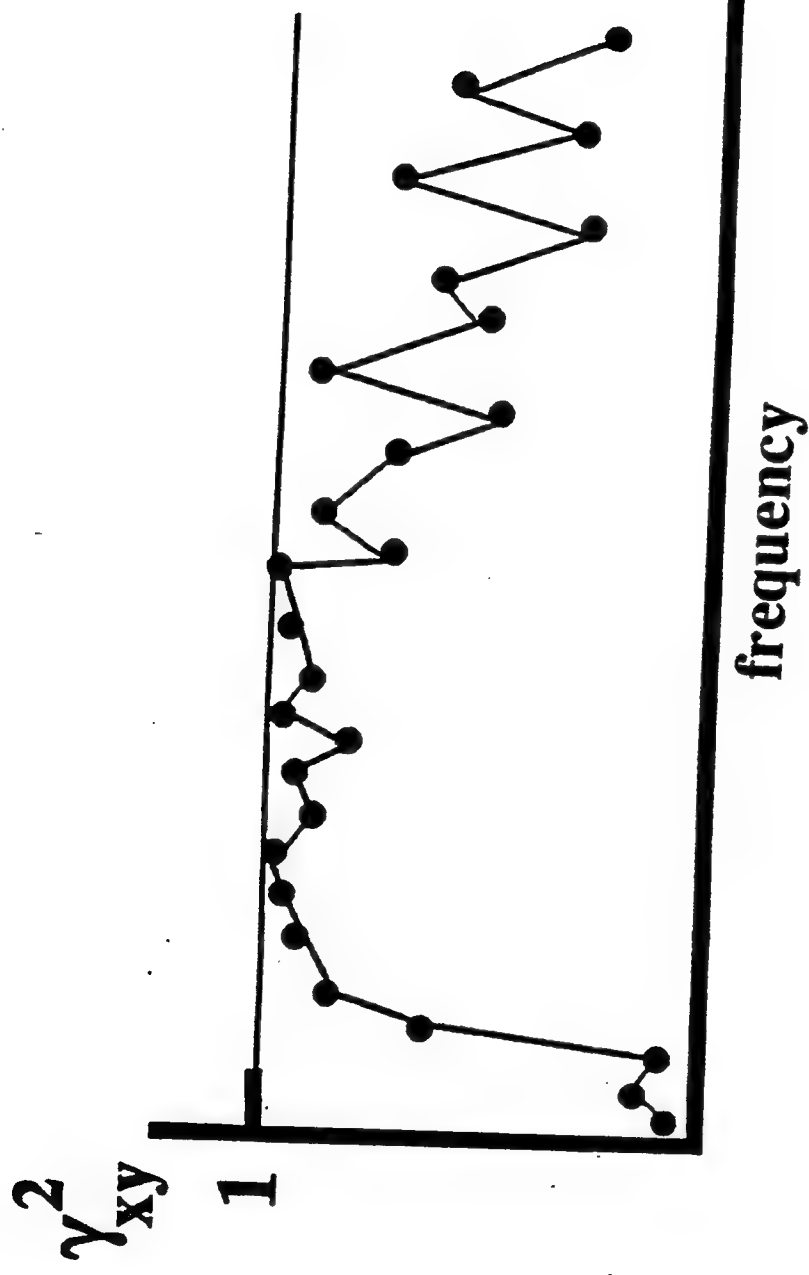


Figure 1.2 Coherence function, after Palo, 1994

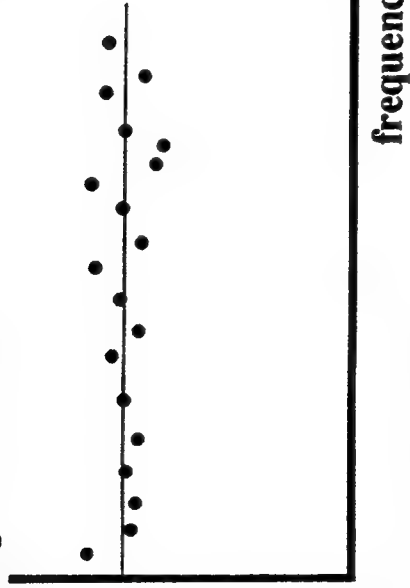
• = numerical | $H(f)$ | estimate

— = best analytical fit

$H_{Imag}(f) / (2\pi f)$

Case #1: estimated damping is independent of frequency, so:

- $c = \text{constant}$,
- equation of motion is *differential*.



$H_{Imag}(f) / (2\pi f)$

Case #2: estimated damping is NOT constant versus frequency, so:

- equation of motion is integro-differential;

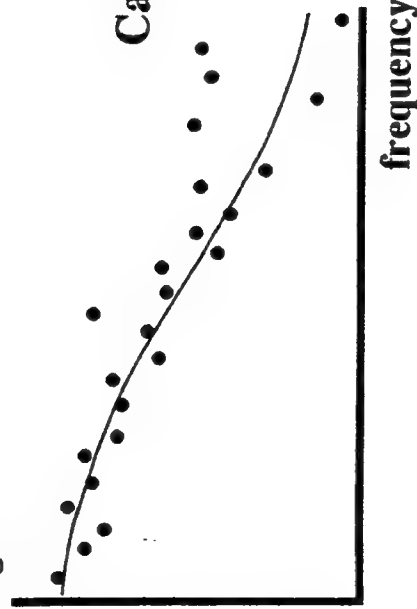


Figure 1.3 Imaginary part of transfer function,
after Palo 1994

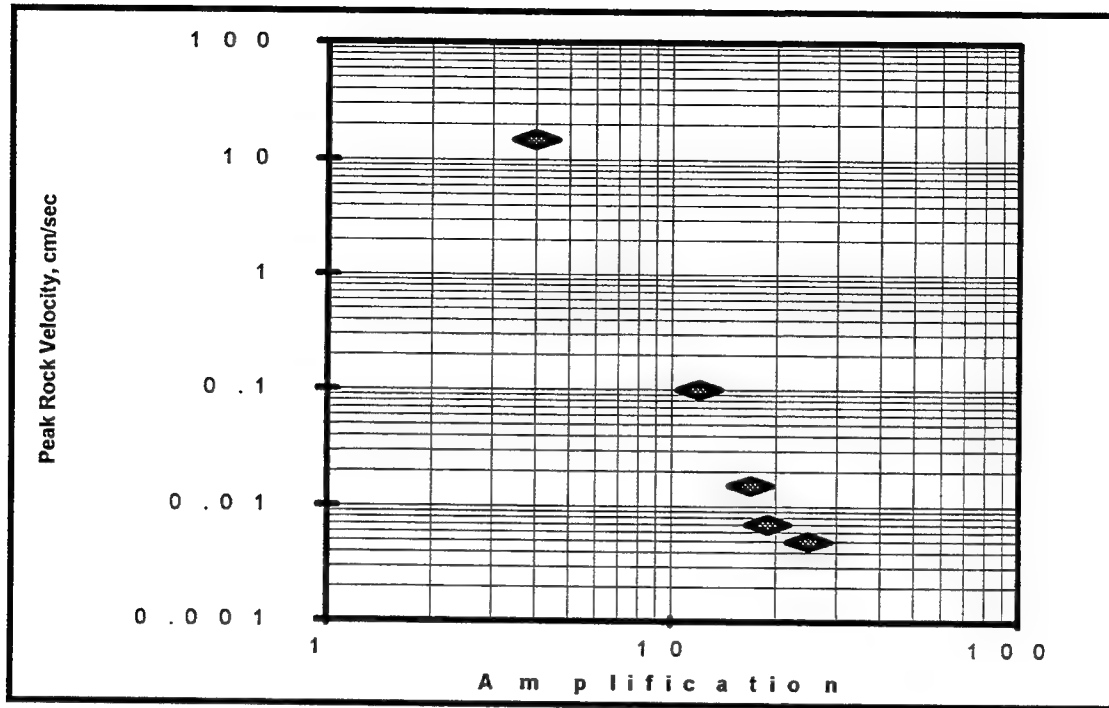


Figure 1.4 Amplification as function of peak velocity
For Treasure Island Site

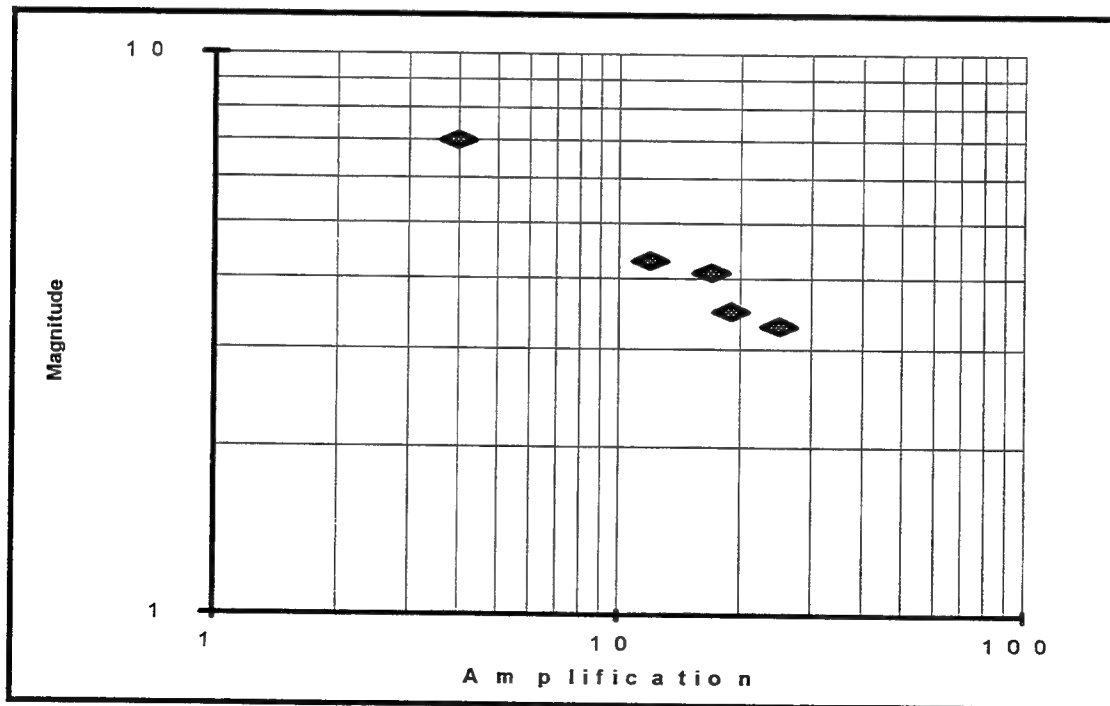


Figure 1.5 Amplification as function of magnitude
for Treasure island Site.

CHAPTER 2 MICROSEISM RECORDING

Introduction

Previous work explored the feasibility of using microseism recordings in conjunction with analysis as a means of determining site ground motion amplifications. It is now important to evaluate some of the proposed techniques for data recording.

Nature of Microseism Motion

Figure 2.1a is a typical portion of a microseism recording made at the Naval Facilities Engineering Service Center. Three orthogonal seismometers were used to make the measurement. The velocity records were integrated to obtain displacement, Figure 2.1b. Two and three component displacement plots were made to show the nature of the motion, Figures 2.1c and 2.1d. The time period shown is for 1 minute. To better illustrate the nature of the motion a random 5 second portion of the record was selected for enlargement and is shown in Figure 2.2a. Displacement traces are shown in Figures 2.2b and 2.2c. The motion is elliptical moving horizontally and vertically. Figure 2.3a is a randomly selected earthquake record from the October 17, 1989 Loma Prieta set of recordings. A section of the record was randomly selected and is shown in Figure 2.3b Figure 2.3c and 2.3d to show the displacement traces of two- and three-dimensional movement. There is some similarity of movement between the microseism record and the earthquake record; both exhibit a "looping movement" elliptical in form. This illustration is not intended to be an extensive statistical presentation but rather a representation of loose similarity between two randomly selected events.

Microseism Variation

A series of microseism measurements were made with seismometers oriented in the same direction and located in close proximity to each other. (They were spaced 2 feet apart to avoid magnetic cross interference between instruments.) Recordings were made for 35 minute duration and then the record broken down into 5 minute segments. Each 5 minute segment was analyzed and its variance determined. During the period measured, each segment record had essentially a 0 mean value. Figure 2.4 shows the change in 5 minute time history variance. There is relative stability for the interval examined and approximate stationarity may be claimed. Figure 2.5 presents the Fourier spectra for each of the seven recordings and the mean and mean plus one standard deviation. One of the records has a higher region of energy in the 10 to 20 second period; but, the ensemble gives a reasonably narrow band of variation indicating minor variation in the recordings.

Figure 2.6 give three of the seven normalized autocorrelation plots for a full 300 second delay time, τ , and then only for the first portion of the delay time to 25 seconds. The autocorrelation functions exhibit the same general type of behavior in that the sharp drop off is indicative of wide band random signal without the presence of a sinusoidal or deterministic component.

As stated above, two seismometers closely located simultaneously recorded data for 35 minutes; the two instrument data records were subdivided into 5 minute segments and each analyzed. Figure 2.7 shows the transfer function from the first 5 minutes of record of each seismometer. For this computation, there was zero time delay between records. The transfer function is essentially 1.0 over the period range of interest (0.5 sec to 10 sec). The coherence between the records is above 95 percent over the range of interest. Various delay times between the records were created by selecting a portion of the record from seismometer number 1 and a time delayed portion of the record from seismometer number 2. A number of recordings were evaluated. Figure 2.8 shows results for one recording pair with a 5 minute delay time. The transfer function on average remains near 1.0 but has much larger variation. The coherence drops significantly. Figure 2.9 shows the change in transfer function for various delay times.

From the above, it is concluded that it is essential to have simultaneously recorded signals to be able to compute a transfer function with high reliability even though there is a measure of stability of measurements over a larger band of time.

Proximity of Reference Site

It was of interest to evaluate the variation in microseism recordings as a function of the separation distance between the rock reference site and various soil sites. We expected to see some change in the coherence of signal pairs. The Mugu Rock site was selected as the rock reference site. This site is a sea level site on the coast having lower Miocene Vaqueros Formation sandstone, claystone and siltstone overlain by a very thin layer of fill and a concrete slab. The soil sites were selected on alluvium. Figure 2.10 shows the location of the sites with the furthest site, Site 5, being 2.2 miles from the reference site. One seismometer was setup at the reference site; a second made sequential measurements at each site with the rock and soil recordings being made simultaneously. The first recording location was at Mugu Rock itself about 25 feet from the reference measurement seismometer. Figure 2.11 shows the coherence for the sites. The coherence between all the sites is not very high but at the same levels for all locations. High coherence could only be achieved with the instruments essentially side by side as shown above. This is interpreted as showing substantial local site response variability. The two signals do not have a direct cause and effect relationship such that one signal is the driving function and the other is the response and thus are directly related. Rather both signals are response signals to a distant driving source. The local site conditions have marked effected on the composition of the surface measured response. Each of the signals is produced by a bedrock motion exciting separate unrelated dynamic systems.

Measurement Noise

Moderate/Strong Winds Occasionally the coastal site experienced gusty winds. To evaluate the effect of these winds one seismometer was shielded from the wind by a large box and a second adjacent instrument left exposed. Figure 2.12 shows a 5-minute time history of the seismometer exposed to the moderate gusting wind having a sustained speed

of 10 knots with gusts to 13 knots. The exposed seismometer had a peak velocity of .00164 cm/sec. The shielded seismometer 5-minute record is shown in Figure 2.13 and had a peak velocity of 0.000172 cm/sec. Figure 2.14 shows the transfer amplification function of the wind exposed instrument compared to the shielded instrument. As can be seen moderate gusting winds do have an effect on the measurements. For this reason measurements in shielded locations or in small light weight buildings such as sheds having concrete slabs are probably preferable to exposed areas subject to high winds. The majority of the times winds are not a factor.

Vehicle Noise A Navy base is often subject to traffic generating local vibrations which are a source of signal noise. Surprisingly many areas can be found which are quiet and free of both industrial and traffic noise. The most common problem is the passing of large tractor-trailer trucks which produce high frequency noise even at separation distances in excess of 50 feet. Cars however were noted to have little effect when separated by at least 20 feet from the measuring location. Figure 2.15 illustrates a site with high truck traffic. Figure 2.16 shows the Fourier spectra for the signal in Figure 2.15. Note the traffic noise is centered about 5 Hz and is higher in frequency than our range of interest in use of long period microseisms (0.1 to 2 Hz or 0.5 to 10 sec). The high frequency noise is quite discernible in the microseism recording and can be eliminated either by repeating the measurement or by excluding of a portion of the record.

Ocean Waves Breaking On Rocks Ocean waves often impact sea walls or shoreline rock boulders during periods of high tide. Sites in close proximity to shoreline will see the effect of local wave impact such as noted in Figure 2.17a. Figure 2.17b shows a 20 sample overlapping average Fourier spectra; note the increase at 0.6 seconds. Figure 2.17c is the spectral ratio with respect to a rock reference site and shows a high peak at 0.6 seconds. Figure 2.17d is the same spectral ratio with the omission of the segments containing local wave noise; the high peak noted previously has been eliminated. Generally for most sites not in close proximity to a sea wall this effect is not observed. The problem can be avoided by measuring at times other than high tide, by not getting within 50 feet of the coastline, or by removal of the anomalous portion of the record.

Nakamura Method

Nakamura (1989) performed a series of microtremor studies in Japan, recording data hourly for 30 hours at several sites. In this study he proposed a procedure for removing source effects from microtremor records based on a modification of the transfer function. He assumes that the surface source of microtremors generates Rayleigh waves which affect both horizontal and vertical motions in the surface layer. Under these conditions:

$$E_S = S_{vs} / S_{vb}$$

where

E_s	Amplitude effect of source
S_{vs}	Spectral vertical motion at surface
S_{vb}	Spectral vertical motion of base

The transfer function of a site is defined by

$$S_T = S_{HS} / S_{HB}$$

where

S_T	Site transfer function
S_{HS}	Spectral horizontal motion at surface
S_{HB}	Spectral horizontal motion at base

The source effects are compensated for by dividing S_T by E_s as follows:

$$S_{TT} = S_T / E_s$$

This can be written as

$$S_{TT} = R_s / R_B$$

where

R_s	is defined by	S_{HS} / S_{VS}
R_B	is defined by	S_{HB} / S_{VB}

Nakamura assumes that $R_B = 1.0$ over the range of engineering interest based on his extensive studies and field experience. Thus the transfer function is given by R_s alone, the ratio of horizontal to vertical surface motions. This approach replaces the traditional rock reference site response with the vertical response. The base or bedrock motion fluctuates over a much narrower range than surface motions. This approach has been tried by several researchers and results support the premise of similarity of spectral ratios from microtremors and strong motion at least in the long period range. Seekins (1994) applied this technique to sites in San Francisco at which the 1989 Loma Prieta event was measured with good results over a narrow frequency band at two stations.

The Nakamura Method was extensively evaluated. Figure 2.18 gives a typical East-West microseism and Figure 2.19 gives a simultaneously recorded vertical microseism. Figures 2.20 and 2.21 show the Fourier spectra and Figure 2.22 give the spectral ratio. As noted in Figure 2.22 there is a high peak at the 5 to 7 second period indicative of the ocean wave activity. The procedure fails to cancel the ocean components as does use of rock reference sites. The level of spectral ratio is about 1 at period from

0.5 to 2 seconds. This value is not correlatable to the values obtained from a site analysis, Ferritto (1994).

Petrolia Earthquake

On September 1, 1994 a moment magnitude 7.2 earthquake occurred about 90 miles offshore of Eureka, California starting at about 8:15:40. It occurred along the Mendicino Transform Fault, an undersea strike-slip fissure that separates the Pacific and North American plates. The shaking consisted of three earthquakes a minute apart and was felt from Grants Pass, Oregon to Palo Alto California. Microseism recordings were underway at Laguna Peak, a rock site at elevation 1457 feet having middle Miocene Topanga Formation sandstone siltstone and conglomerates overlain by a thin layer of alluvial deposit. The Laguna Peak site is about 600 miles from the epicenter. Figure 2.23 shows a map of the epicenter and the recording site at Laguna Peak. Figure 2.24 give time histories and spectra for portions of the microseism recording starting at 07:00 AM. Note the quiet signal in Figures 2.24a and 2.24b. At about 07:42 AM the signal exhibited higher amplitude motion which may have been a precursor to the event. At about 08:17 AM the event was observed with a peak velocity of 0.0016 cm/sec before the instrument went offscale. The reader is cautioned that the reported times are approximate since the computer clock was not synchronized with absolute time and was off by 52 sec. It remained offscale until about 09:00 AM when strong sinusoidal oscillations were noted. The signal remained elevated until 12:00 PM.

No local effects of the earthquake were noted including the absence of any unusual tidal or wave action near the recording site. The strong microseism propagated rapidly to the site with an approximate velocity of 24,000 ft/sec. To achieve that propagation velocity, it is concluded that the earthquake travelled through competent bedrock. This again confirms the premise that distant sources are capable of propagating through bedrock and reaching local sites.

Discussion

Previous Navy microseism research was published, Ferritto (1994), and we were fortunate to have a number of outside reviewers of the work who made comments, suggestions and raised questions for discussion. In this section we will discuss those issues.

Reviewer comment:

"Microseism energy is centered around a 6 second period. At 1 second microseism energy is very low and the 1 Hz 'noise' is from other sources. I would expect the longer period microseism comparison between reference site and soil site to work well. At 1 Hz and above the noise field between the reference site and soil site may be different due to the noise sources and depending on the relative distance between

reference and soil site. I would expect the method to not work as well. Strong motion from earthquakes is centered around 4-6 Hz, well above microseism frequency."

It is true microseism energy is centered at 6 seconds. However the energy should be looked upon as wide band random excitation. A typical soil power spectral density is shown in Figure 2.25 and shows peaks at 5 to 6 seconds and about 12 seconds. It also shows a lower but significant peak at 1 second. By viewing the ocean induced excitation as a random vibration source capable of vibrating the site it is possible to calculate the site fundamental period much in the same way as a large structure is excited by a small vibrator. The large component of energy at 6 seconds is effectively eliminated in the division which occurs in forming a transfer function. It is very true that noise can be a significant factor in influencing site response. We observed this in measurements at Yerba Buena Island for one site location near one of the columns of the Oakland Bay Bridge. This column was a direct feed of the heavy bridge traffic and affected the area around the column foundation, Ferritto (1994). The sites on Navy bases we have thus far investigated have been relatively low traffic quiet sites. Noise such as from a passing truck has been of high frequency and readily visible as a transient during signal recording. The comment made is true; however it is believed that Figure 2.25 indicates that there is sufficient energy in the 1 Hz region for the concept to work.

Review comment:

"In data acquisition is a "huddle test" between reference and site seismometers done to determine the difference in calibration of the instruments"

This was done but not reported. The concept of testing the instruments in close proximity was performed and expanded upon earlier in this chapter. It is a very useful tool which showed us the time variation of the signals.

Review Comment:

"There is no doubt that microtremors tell you something about local site conditions and local geology and, thus are informative for earthquake purposes, particularly, for comparing two sites. There is, however, a difficulty in extrapolating from microtremors to strong ground shaking which involve stress that are 5,000 or more times greater."

We fully concur in the comment. Chapter 7 of the previous report, Ferritto (1994) discussed the nonlinear amplification effect. Figures 1.4 and 1.5 illustrate the increased amplification with reduction in excitation level. For this reason we proposed using microseism measurements in conjunction with an analytical site model to define site period. We proposed a systems identification process to define site properties of damping and period. The measured values are used to validate the site model; then the site model is used to predict the response under a large earthquake. We agree that we can not at this time predict earthquake levels of amplification from microseism response.

Review comment:

"There are some articles by Gutierrez and Singh, 1992, Borchardt, 1970 and Udwadia and Trifunac, 1973 which show evidence that microtremors are unreliable predictors of earthquake ground motion amplification. "

Gutierrez and Singh installed instruments in Acapulco, Mexico on both rock and soil sites. They recorded the 25 April 1989 magnitude 6.9 event and also 7 lesser events of magnitude 4.2 to 5.0. They present spectral ratio amplification functions of soil to rock for 4 soil sites. They conclude that spectral ratio for the magnitude 6.9 event falls within the band of the lower magnitude events. While this is true for the response taken as a whole, it is not true for the frequency range 0.2 to 1 Hz where there is a difference. Unfortunately they present data over a range of 0.1 to 100 Hz which makes it difficult to focus on the 0.1 to 2 Hz range of interest in structural response. They conducted microseism measurements and present data comparing spectral ratios for the same 4 sites. They used a 20 second segment of a 1 minute recording to obtain Fourier spectra and spectral ratios. The microseism data begins at 0.5 Hz. and extends to a range of 100 Hz. They are presenting high frequency response, Figure 2.26. Note that while overall agreement is poor, agreement in the low frequency end is perhaps better. Our work here is focusing on long period low frequency response; We are using different procedures to obtain data. Perhaps if they used longer samples with repeated averaging a better trend might be observed. From our research, we would not expect agreement; rather, we would expect the microseism data to be higher in spectral ratio having peaks at approximately the same locations.

Udwadia and Trifunac (1973) used 15 strong motion records recorded at El Centro to compile a series of Fourier spectra. They show that source mechanism and site path are significant. They also investigated the use of microtremors. They indicate that:

"there is a diversity of prevalent opinion on the basic nature of microtremors. The source of microtremors has been tacitly considered by many investigators to be a process analogous to white noise input into "bed rock". The validity of such a point of view is questionable in view of the strong possibility that the other source comprises close-in surface excitations. As the nature of these ground inputs is usually unknown, deductions from microtremor ground measurements need to be made with caution"

Their measurements were made with 1 second 70 percent damped seismometers over a 3 minute duration; 40 seconds of data were used. Microtremor Fourier spectra were directly compared with earthquake Fourier spectra. They note over short periods of time the microtremor signals are stationary however there is variation with longer intervals. The frequency content of microtremors is shown to be different than earthquakes. The approach used in the paper is significantly different from that used in the

Navy research. The paper directly compared Fourier spectra and did not use rock reference sites to compute relative amplification. It is thus not possible to make any further comparisons.

Borcherdt (1970) made measurements of nuclear explosions at 37 locations and microseisms at 4 sites near San Francisco and compared the results to the 1906 earthquake intensities. "The recordings showed marked amplitude variations which are related consistently to the geologic setting of the recording site" They conclude the general shape and amplitude of the nuclear explosion spectra and the microseism spectra agree. "Considering the entirely different nature of the sources and that different kinds of recording instruments were used for each event (earthquake, microseism and nuclear explosion), the similarity of the respective curves suggest that the spectral amplification curves are mainly dependent on the conditions at the recording site and are independent of the source characteristics and instrument response. ... The spectral amplification curves differ in detail, but their gross features are similar."

Review comment:

"Contour maps make me a little nervous. Some of the data shows a lot of scatter. The data should be plotted to scale."

We concur in the comment. Recent experience has shown the need for repetition of measurements to reduce the standard deviation. A contour plot is a simple tool to present a data base in graphical form. It must be realized that it is intended to give an approximate picture variation of response rather than a detailed numerical index. Its main purpose is to spatially show "soft spots" of high response.

Review comment:

"I suppose that the approach taken by the author represents a reasonable attempt to make use of the spectral ratio data obtained from the microseism recordings. Correlating the data with the results of standard ground response calculations does have the effect of bringing the number more in line with reality and in that sense the approach has merit. On the negative side, however, the approach supposes that the ratio of response for one damping level is the same as that for another level of damping."

This is not the case. We propose to obtain the damping from the microseism data and use that level of damping only for microseism response calculations. For earthquake calculations we propose to establish the low level of strain damping as that equal to the microseism measured damping and use higher damping at the earthquake levels. The microseism data does not directly provide us with information about damping at higher levels. Soil test data or existing damping-shear strain attenuation curves will have to be used. The improvement of the proposed procedure is that it attempts to validate the model response to microseisms. This gives insight on parameters such as depth to bedrock etc. which affect the fundamental period of response and the amplitude of

response. After one does the best to identify a site model using all available data, a quick microseism measurement is seen as a model validation at low levels of excitation.

Review comment:

"I do not believe that microseism measurements should be used directly for microzonation"

We concur. Microseism measurements are used to validate parameters for a site model. They are useful for giving a picture of variation of fundamental period over a region. Normalized spectral ratios are used to give a picture of spatial variation of response; however, earthquake response amplification is obtained by performing a site response analysis.

Review comment:

"The issue of spatial sampling and aliasing needs to be addressed in the design of a (microseism measurement) array. For example, ... the array extends over roughly 300 m in the x direction. There are about 3 samples in this direction. In this case, the sampling interval (d) is 100 m. The spatial Nyquist frequency ($1/2d$) is 0.005 cycles/m. Thus only wavelengths longer than 200 m in the x direction have been sampled by the array without spatial aliasing. This corresponds to a velocity of 200 m/sec for a wave with a period of 1 second. Denser array spacing, and perhaps oversampling is needed at some sites to avoid spatial aliasing."

While the above is true for an array of strong motion measurements, it is thought not necessary for the microseism measurements. Measurements are made during a period of general stationarity. The measurements are thus made sequentially and are effectively assuming a static sequence. It is recognized that this is an assumption and approximation. Since a reference rock site is used the time varying effects are normalized out. Figure 2.27 shows the time variation for a soil site and rock reference site.

References

Ferritto J. M. (1994) NFESC TR-2020-SHR "Feasibility For Use Of Microseisms As An Aid to Navy Base Microzonation" Port Hueneme CA August 1994

Borcherdt Rd (1970) "Effects of Local Geology On Ground Motion Near San Francisco Bay" Bulletin Seismological Society of America, Vol. 60, No 1 February 1970

Gutierrez, G and S. K. Singh, (1992) "Site Effects in Acapulco, Mexico"
Bulletin of the Seismological Society of America, Vol. 82 No 2 pp. 642-659 April 1992

Nakamura, Y (1989) " A method for dynamic characteristics estimation of subsurface using microtremor on the ground surface" QR. or RTR1, Vol. 30, No 1, February 1989

Udiwadia F.E. and M.D. Trifunac (1973) "Comparison of Earthquake and Microtremor Ground Motions in El Centro, California" Bulletin Seismological Society of America, Vol. 63, No 4 August 1973

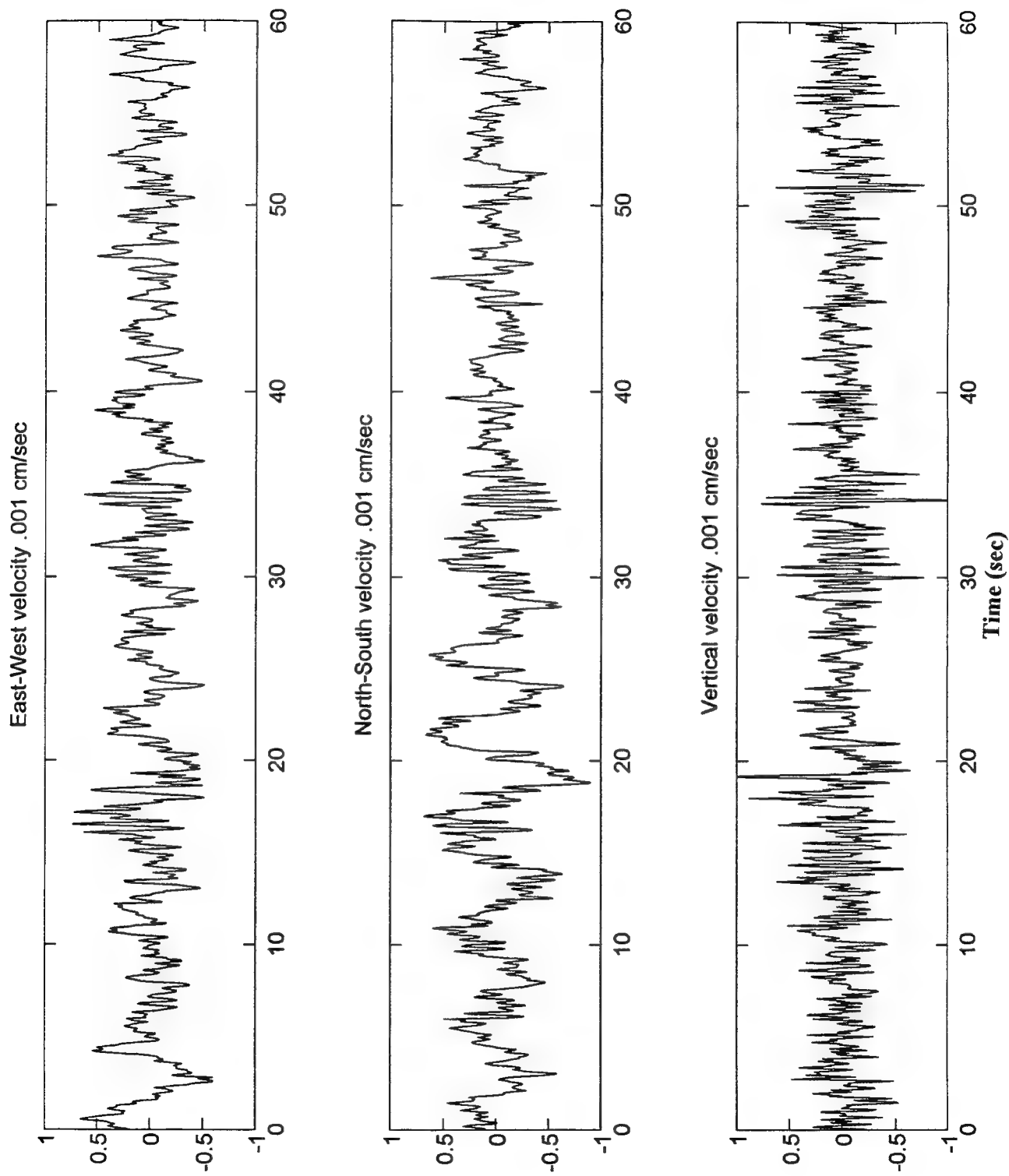


Figure 2.1a. Microseism velocity timehistory.

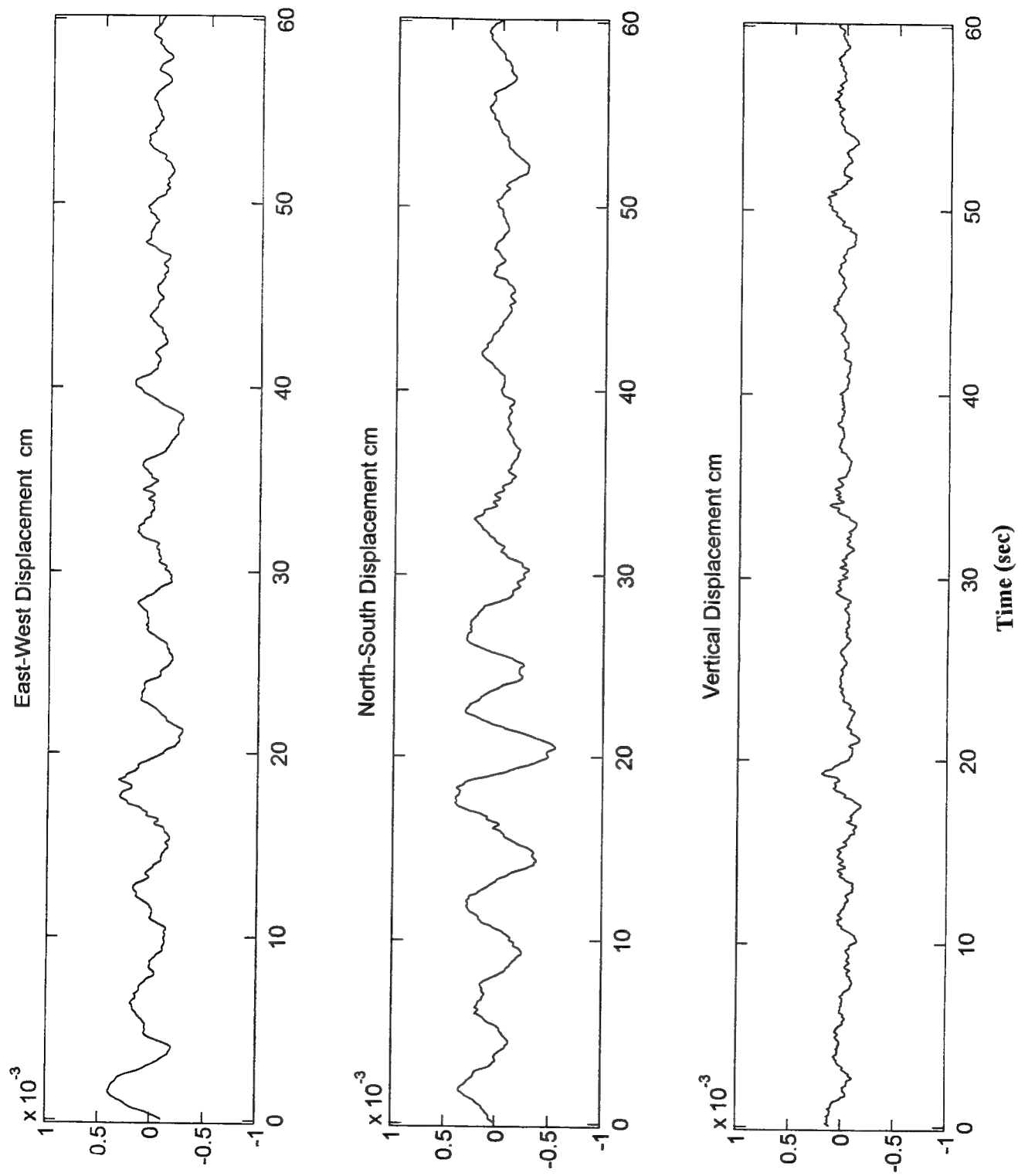


Figure 2.1b. Microseism displacement timehistory.

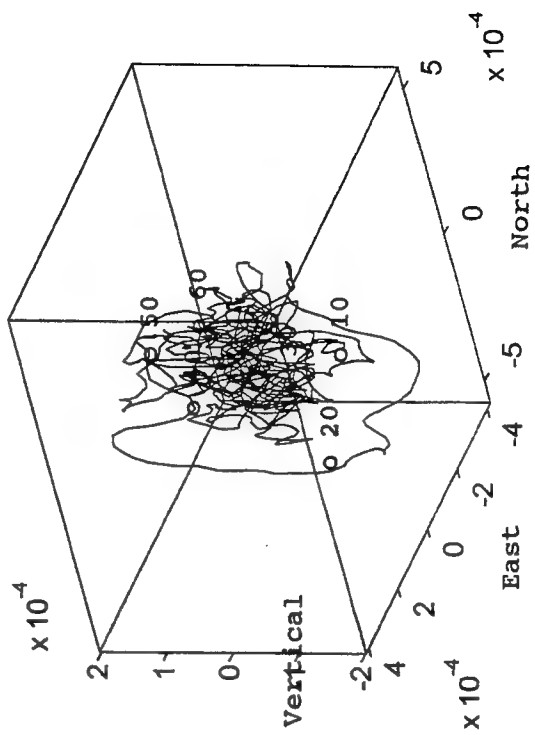
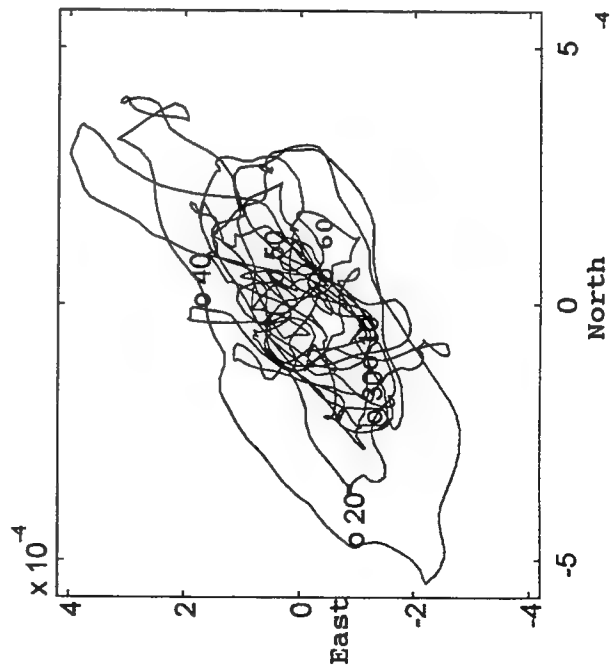
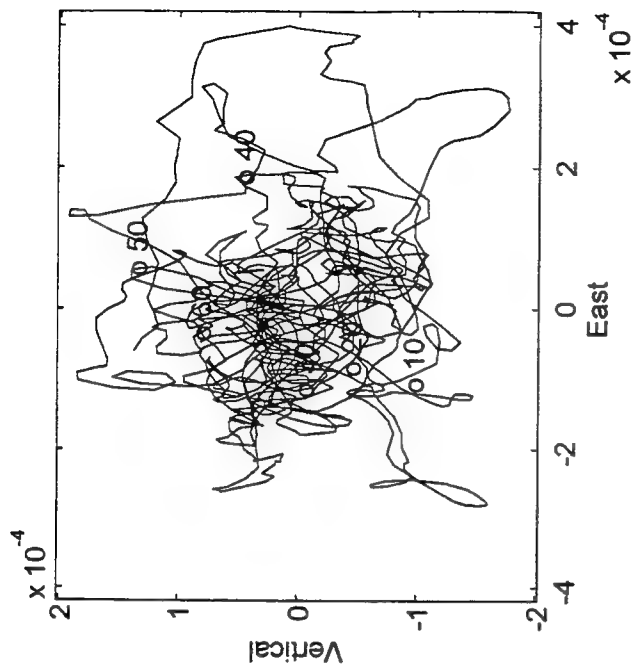
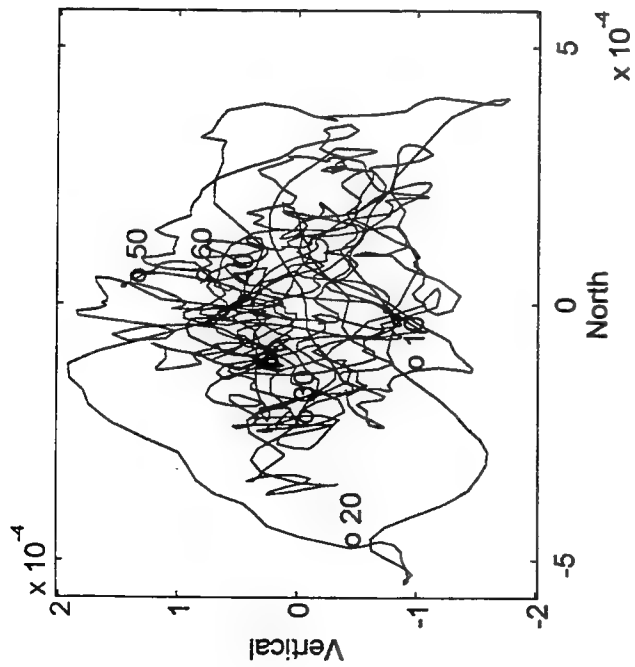


Figure 2.1c. Displacement traces.

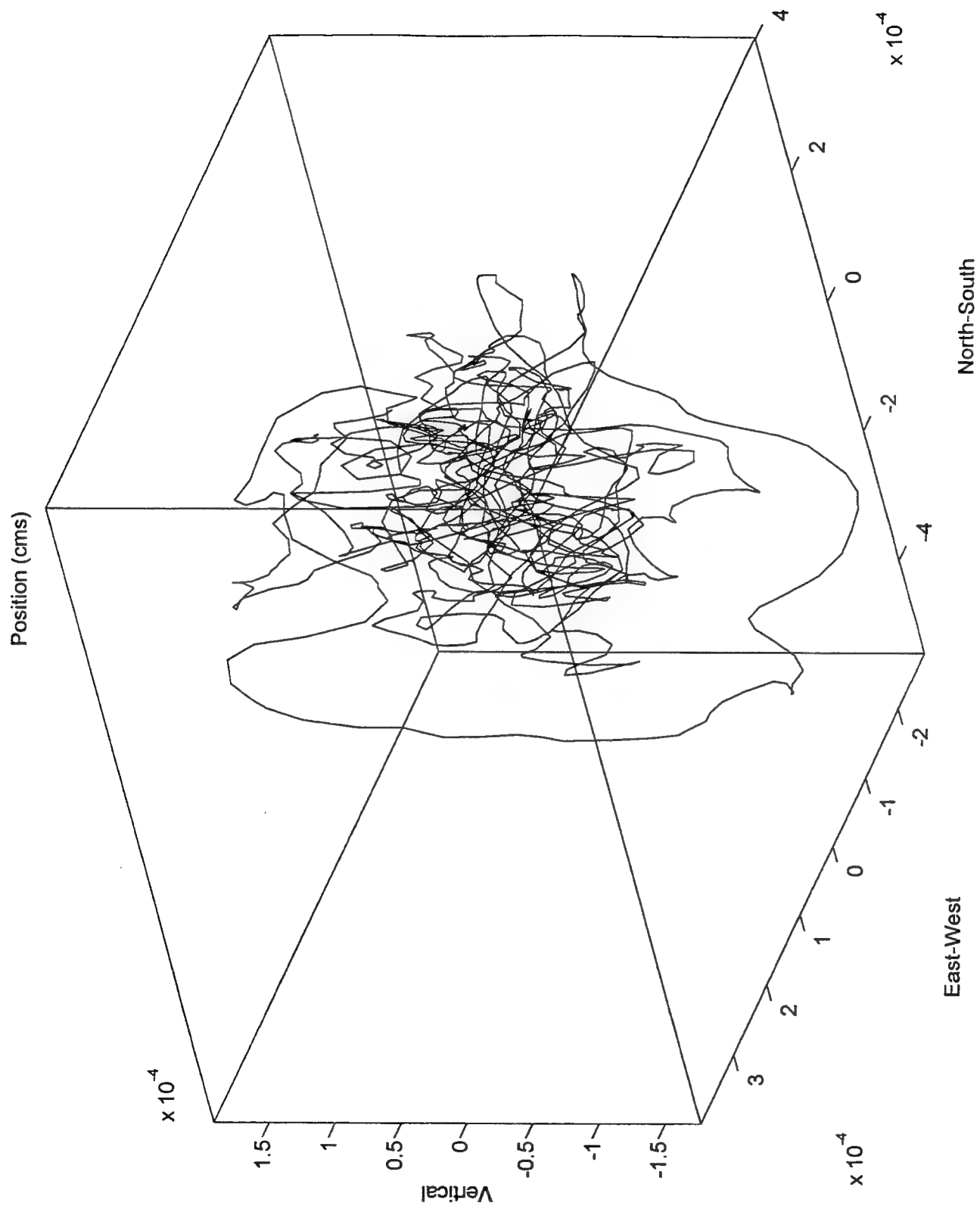


Figure 2.1d. Three-dimensional displacement history.

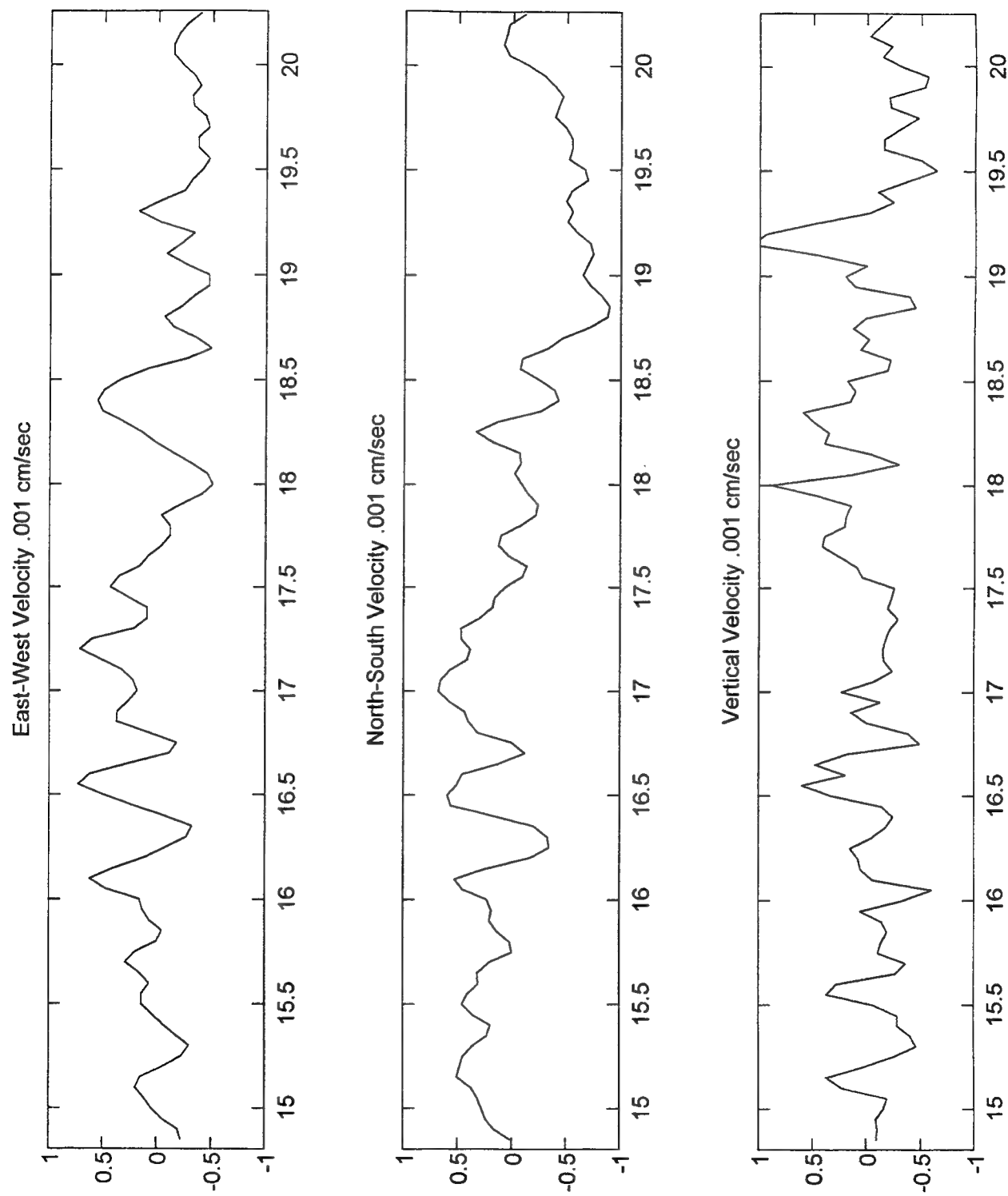


Figure 2.2a. Portion of microseism velocity timehistory from Figure 1.

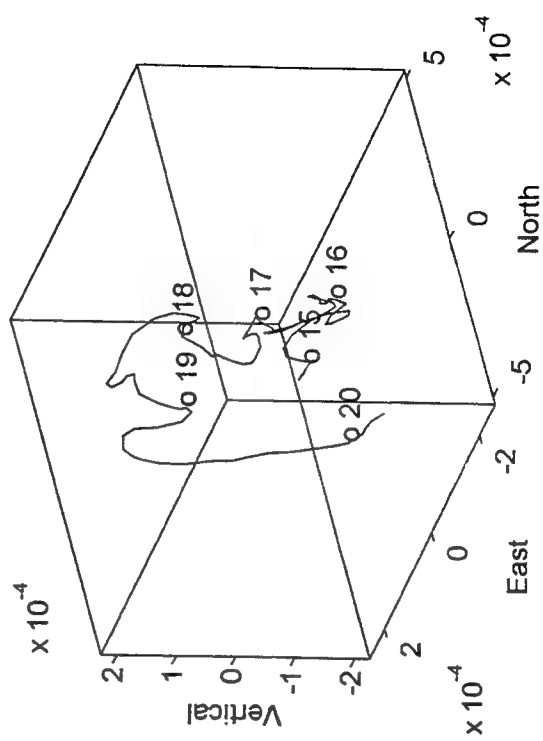
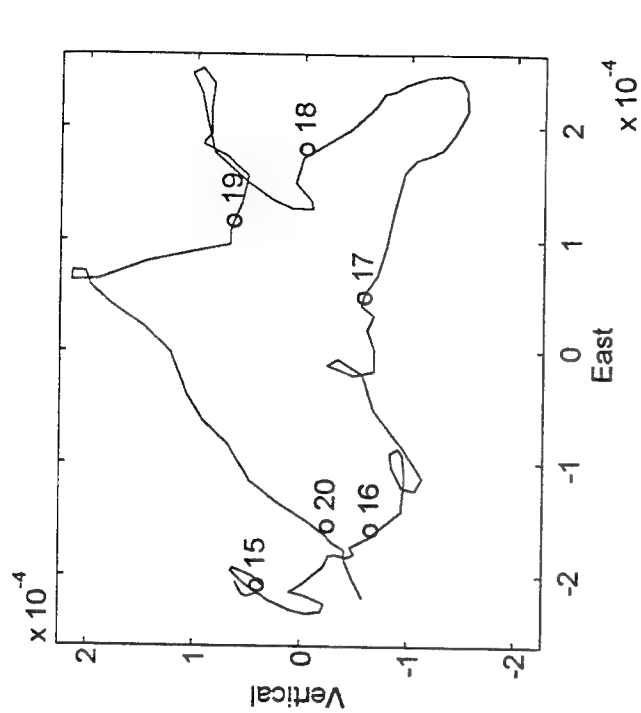
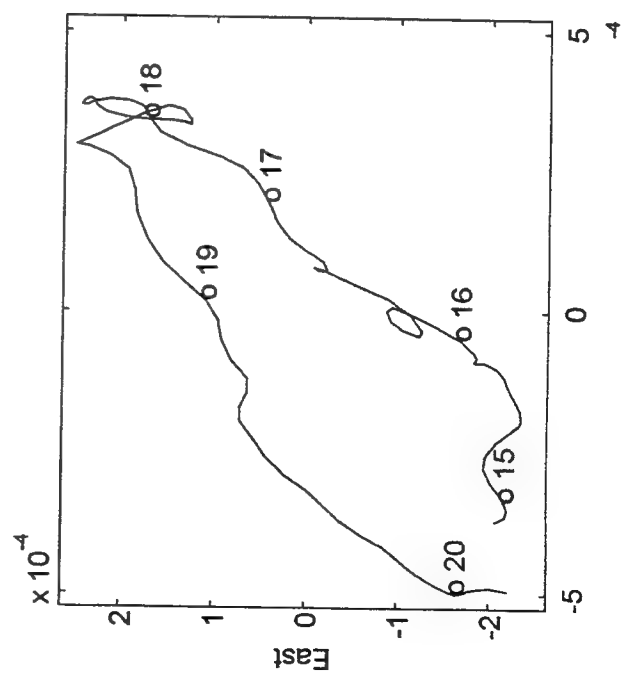
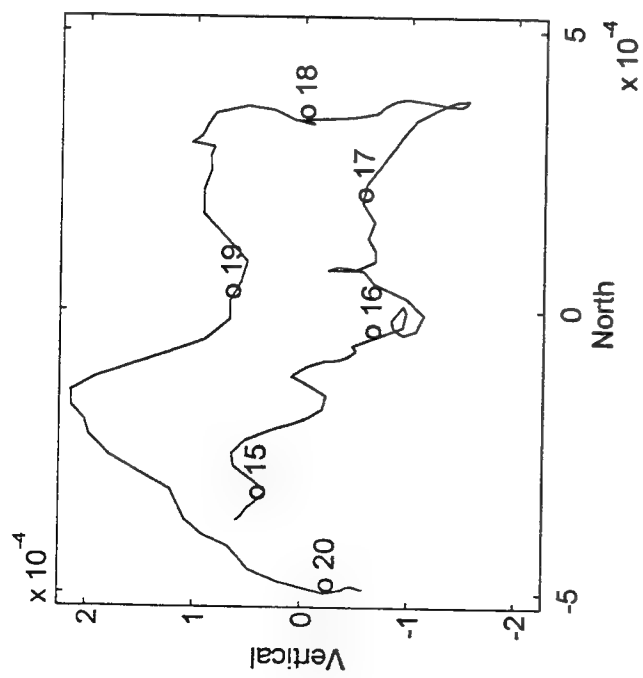


Figure 2.2b. Displacement traces.

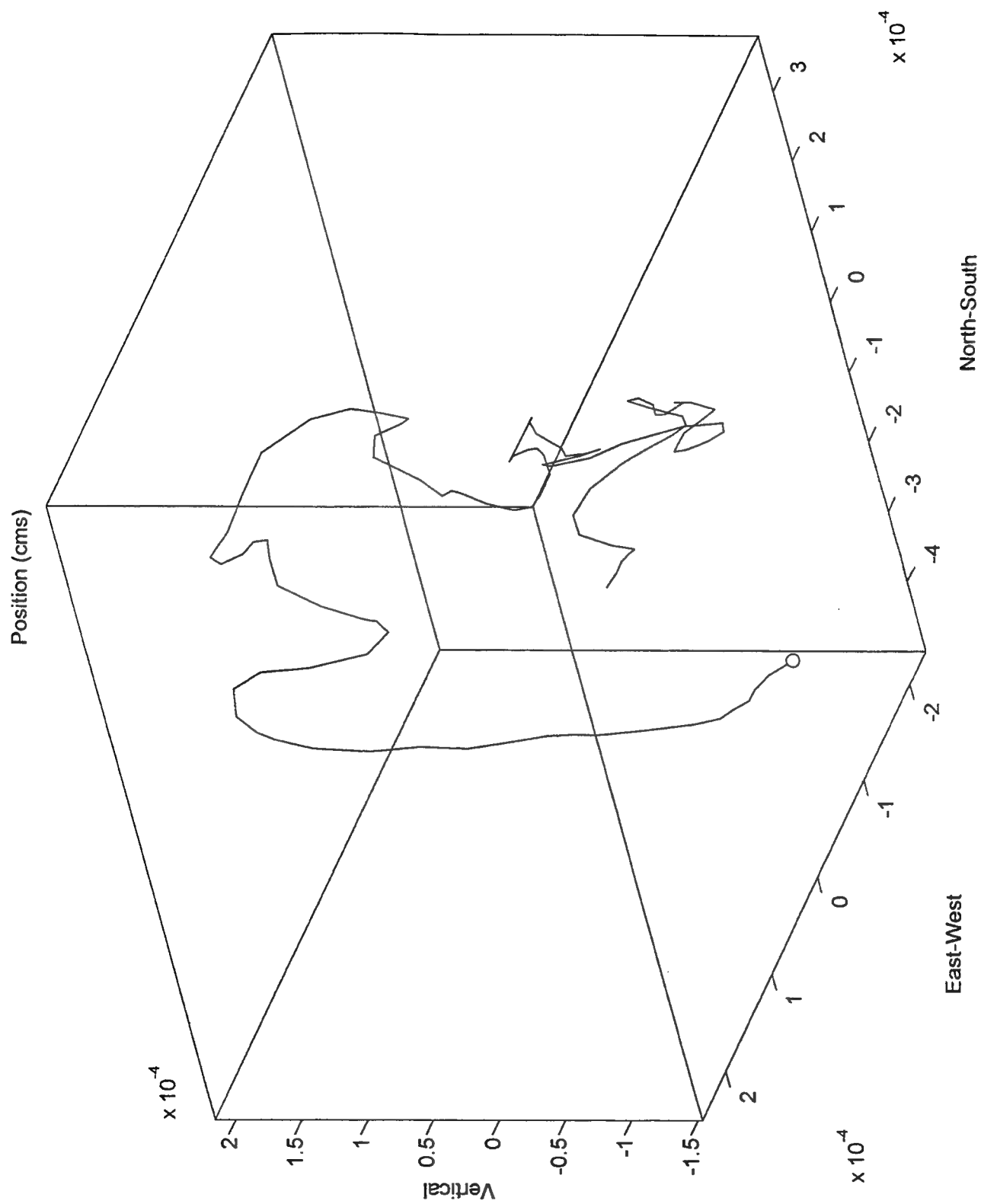


Figure 2.2c. Three-dimensional displacement history.

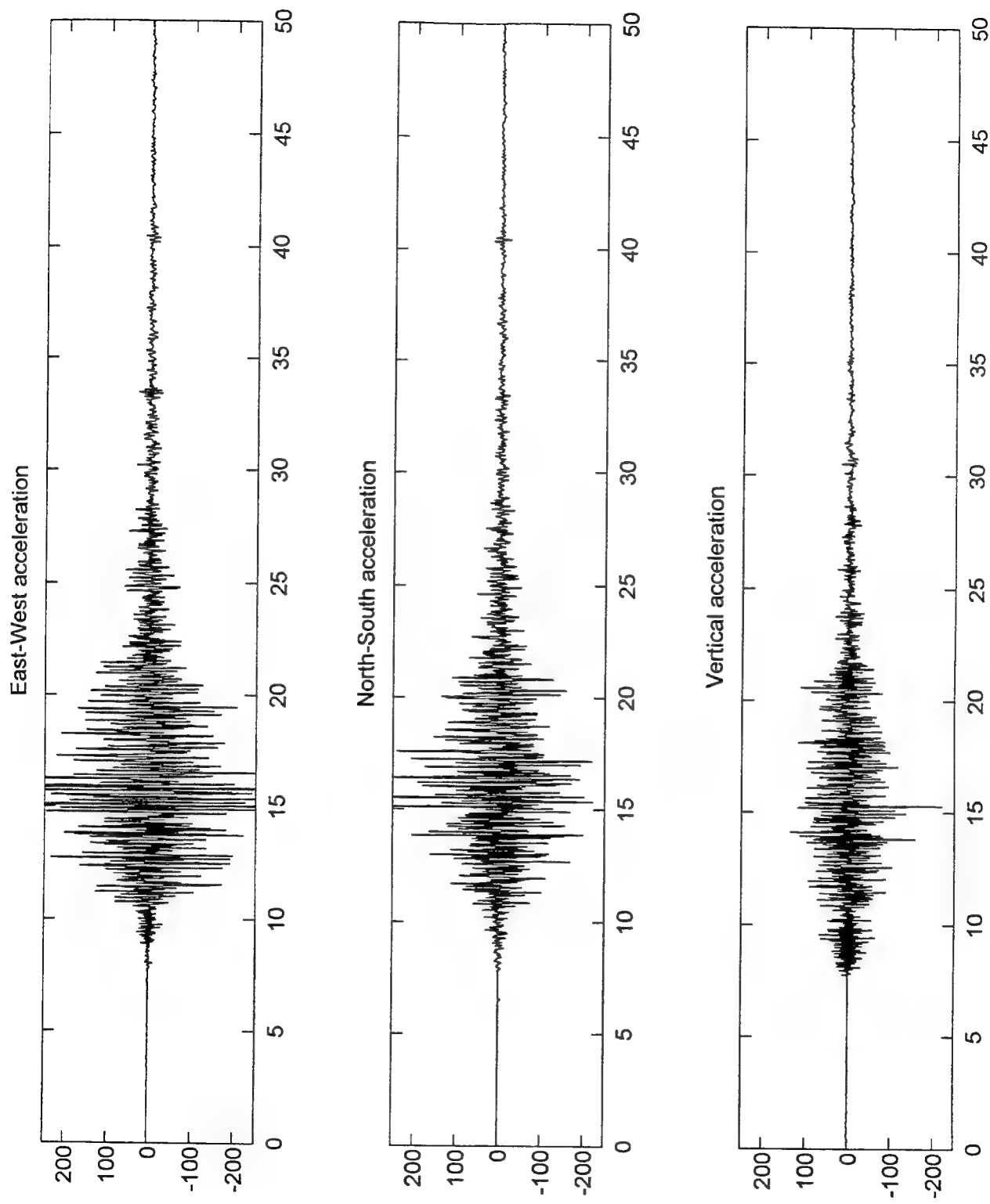


Figure 2.3a. Earthquake acceleration timehistory, Loma Prieta Oct. 17, 1989, UC Santa Cruz station.

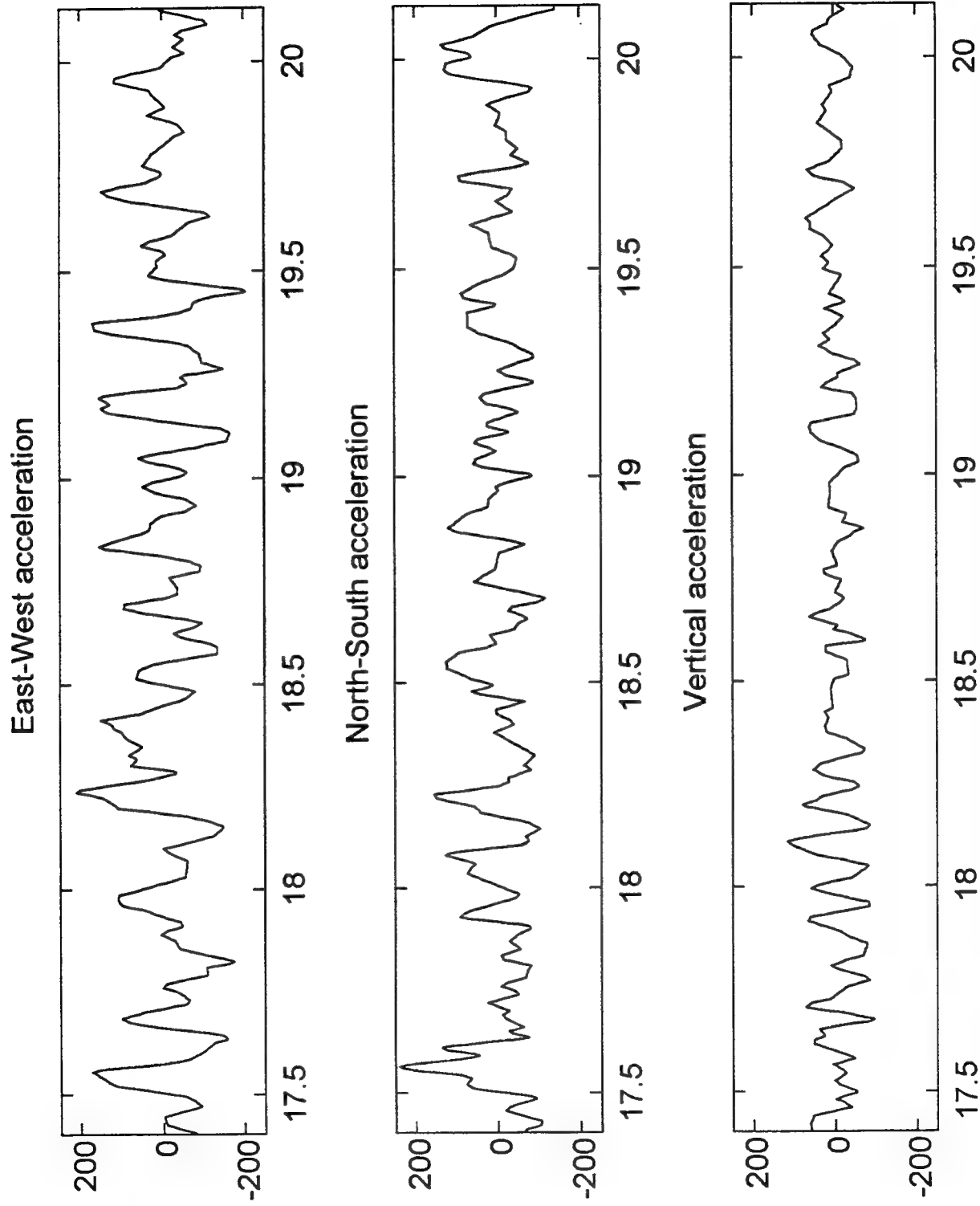


Figure 2.3b. Portion earthquake acceleration timehistory.

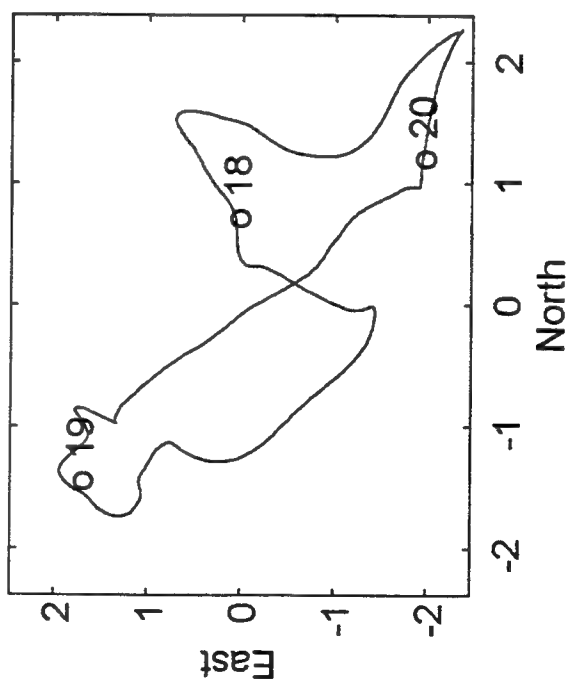
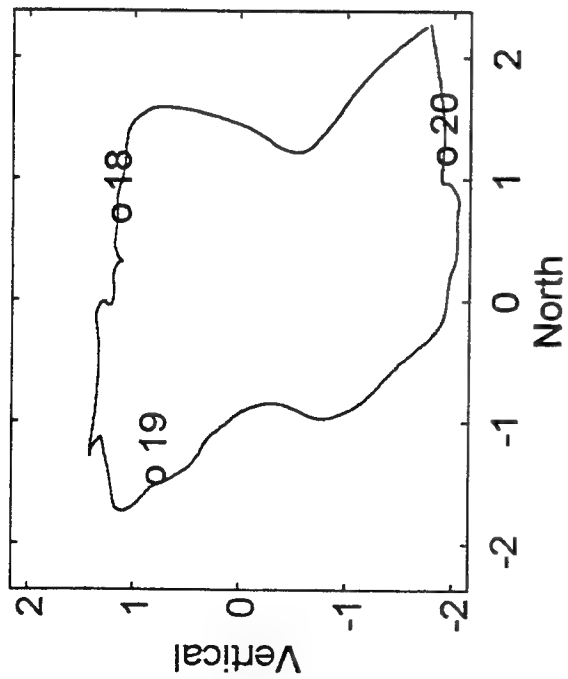
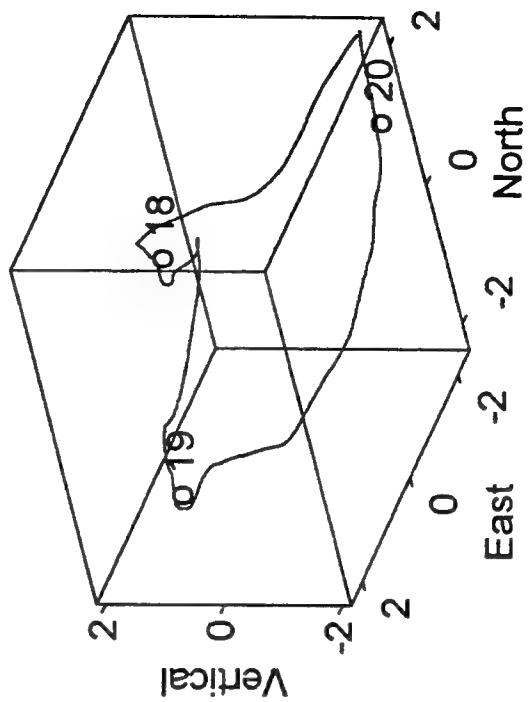
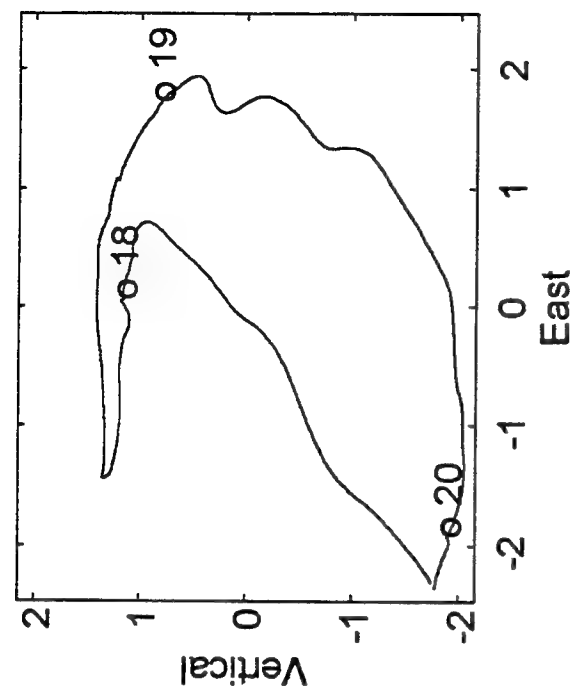


Figure 2.3c. Displacement traces.

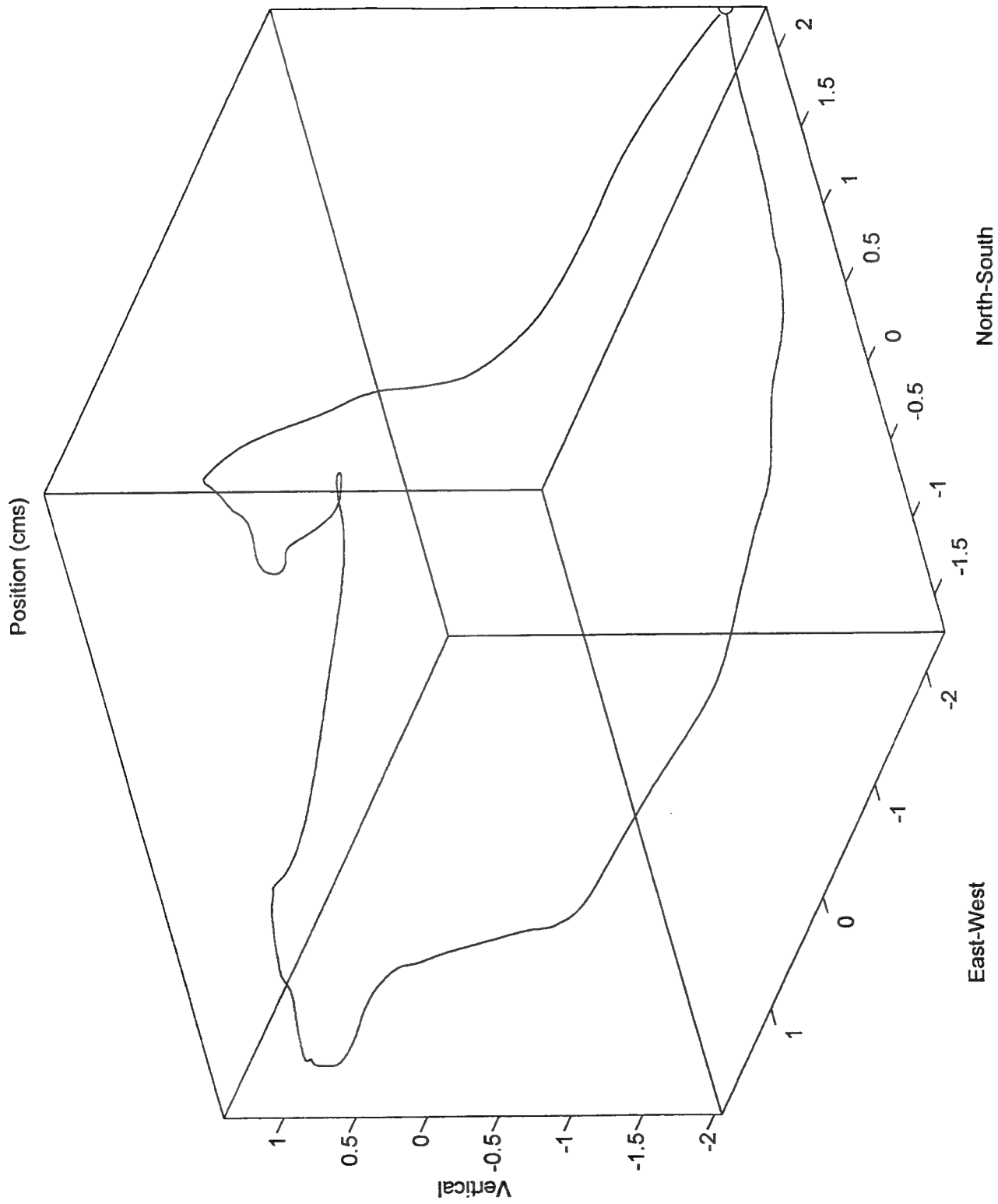


Figure 2.3d. Three-dimensional displacement history.

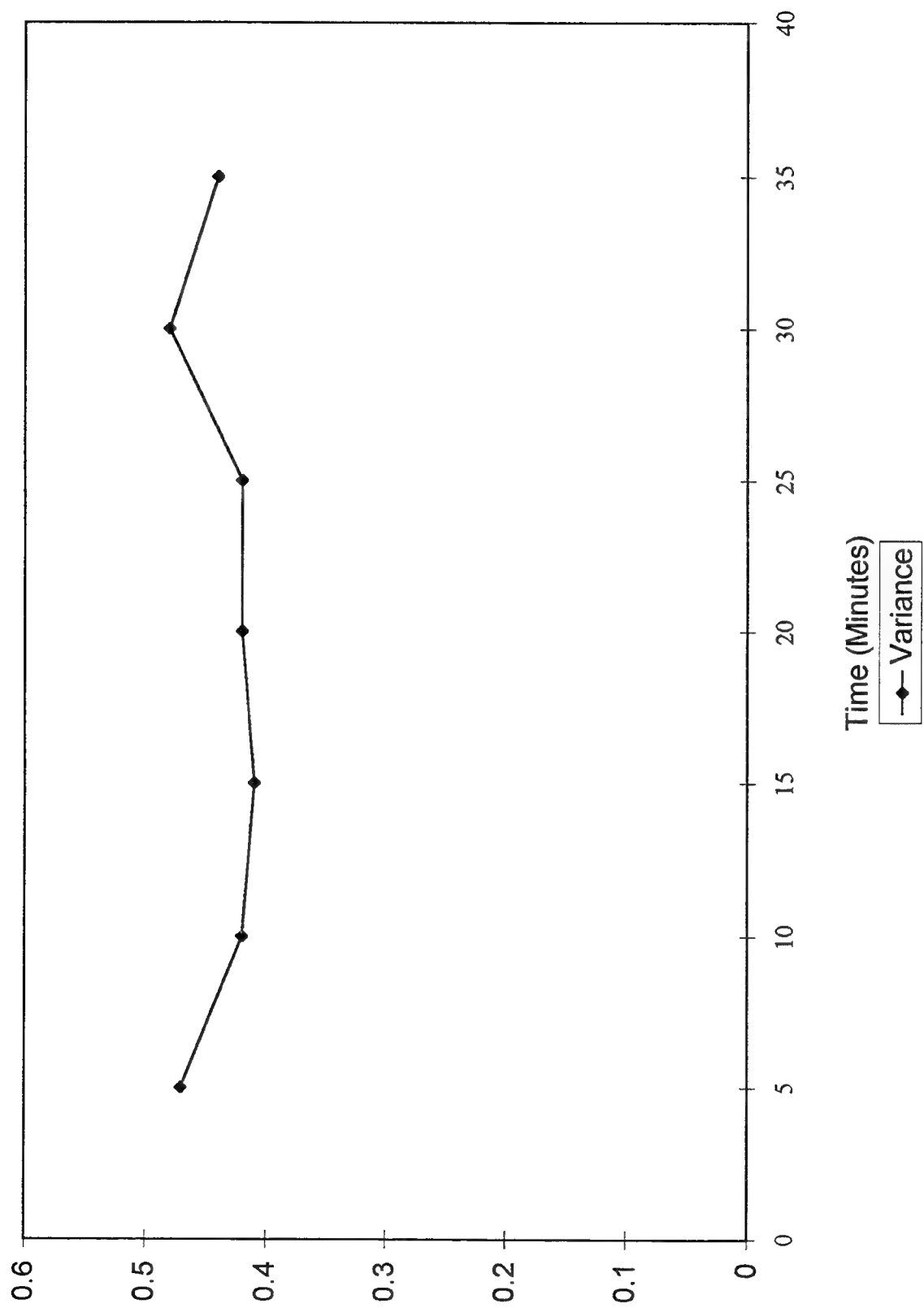


Figure 2.4. Change in microseism variance with time.

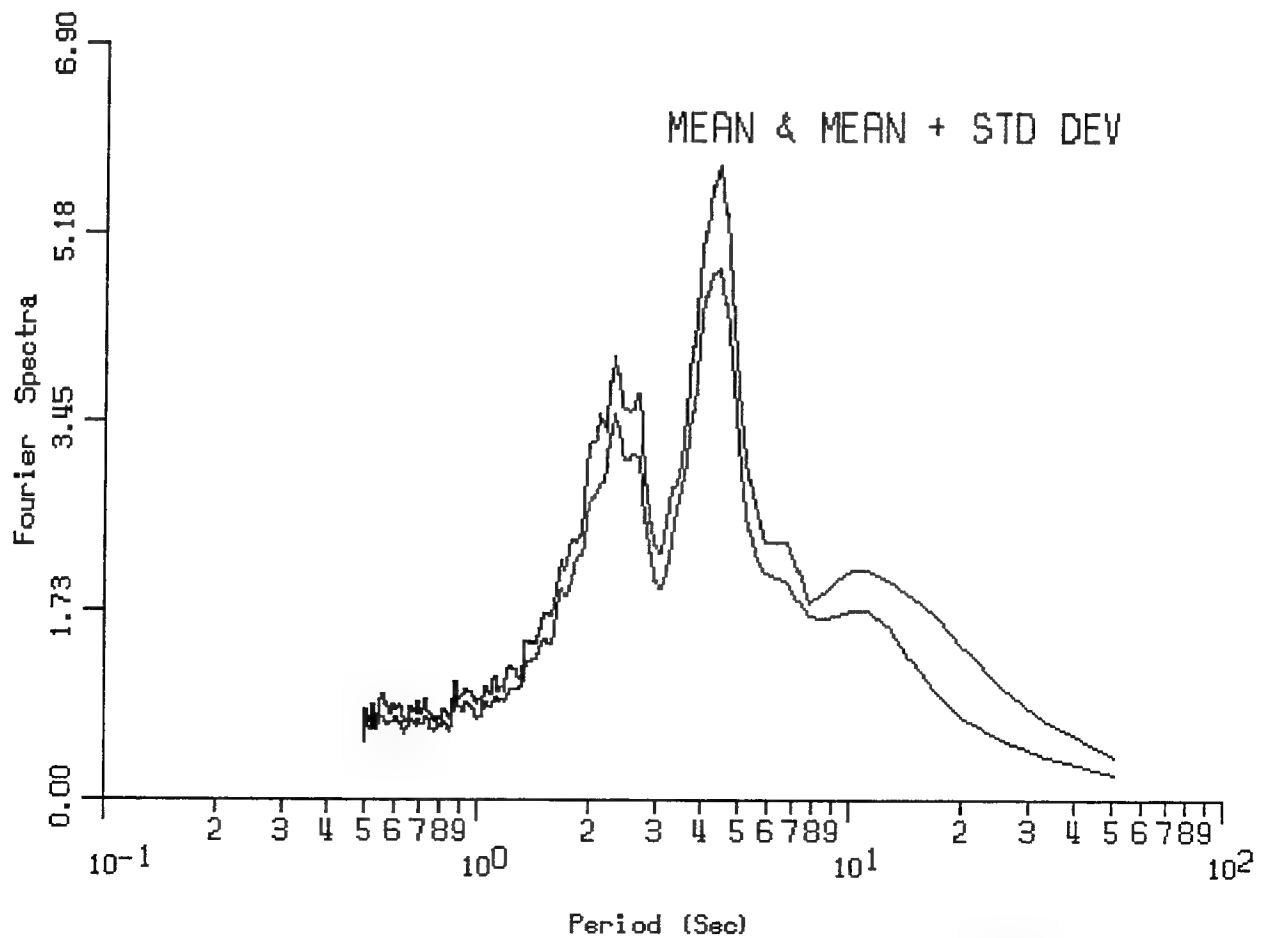
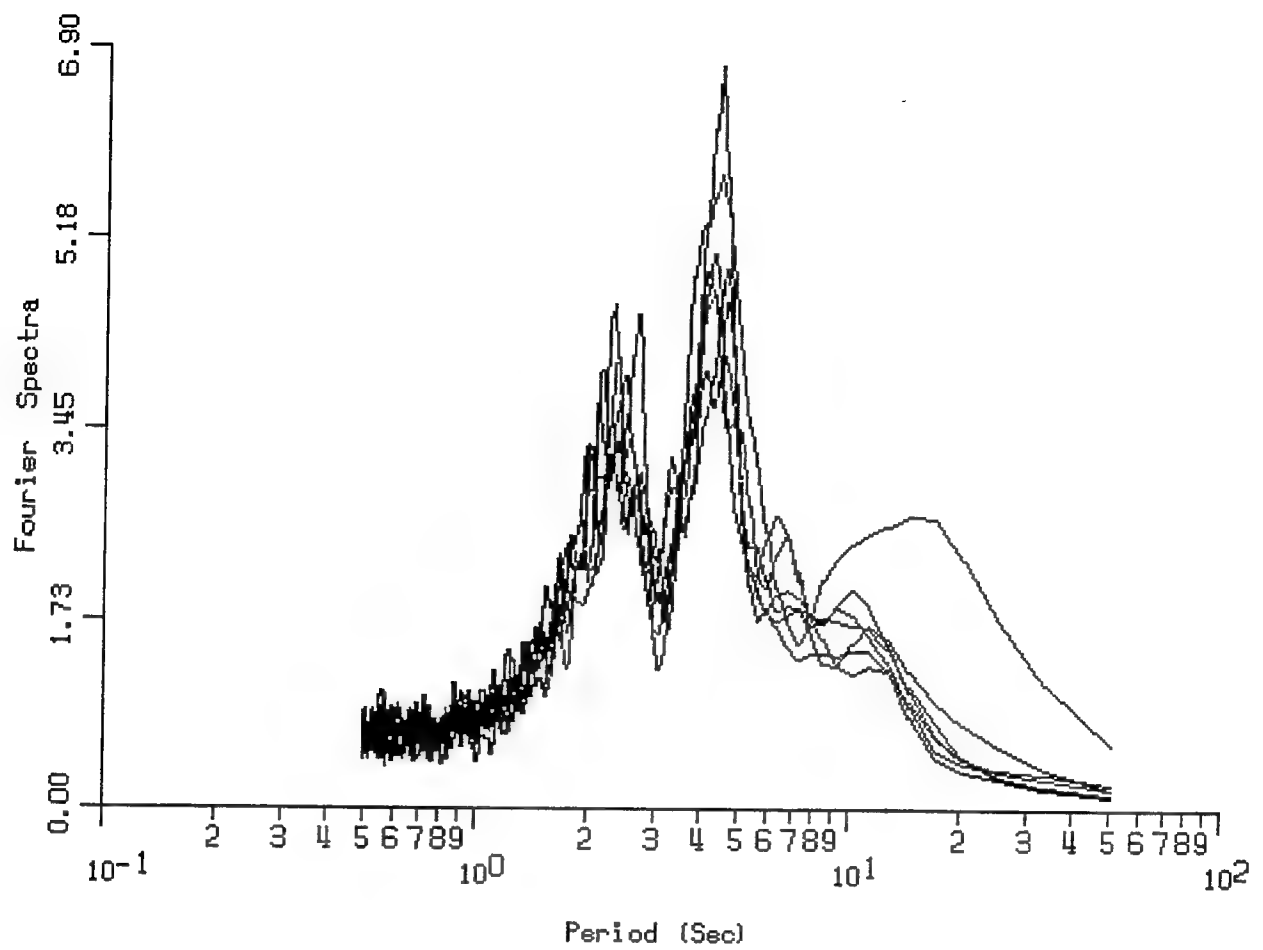


Figure 2.5. Fourier spectra of seven sequential 5-minute microseism recordings.

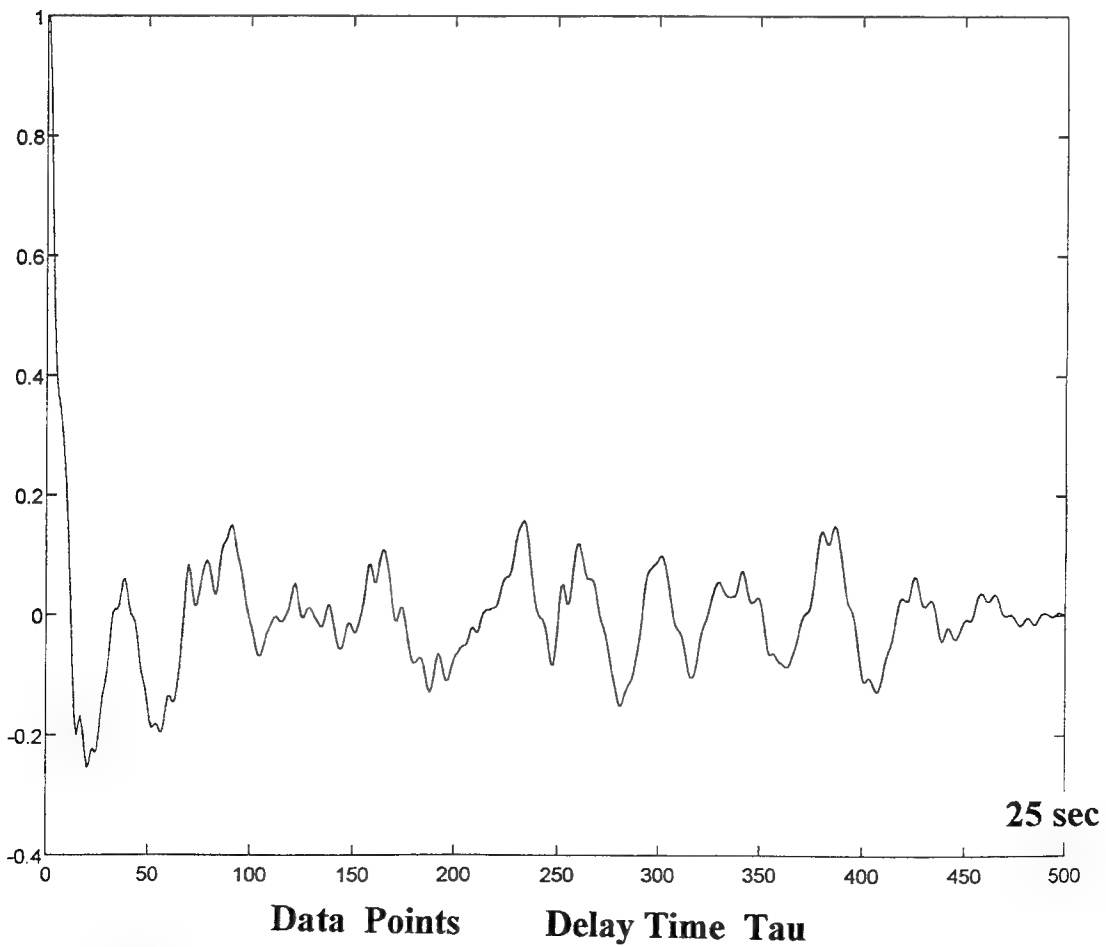
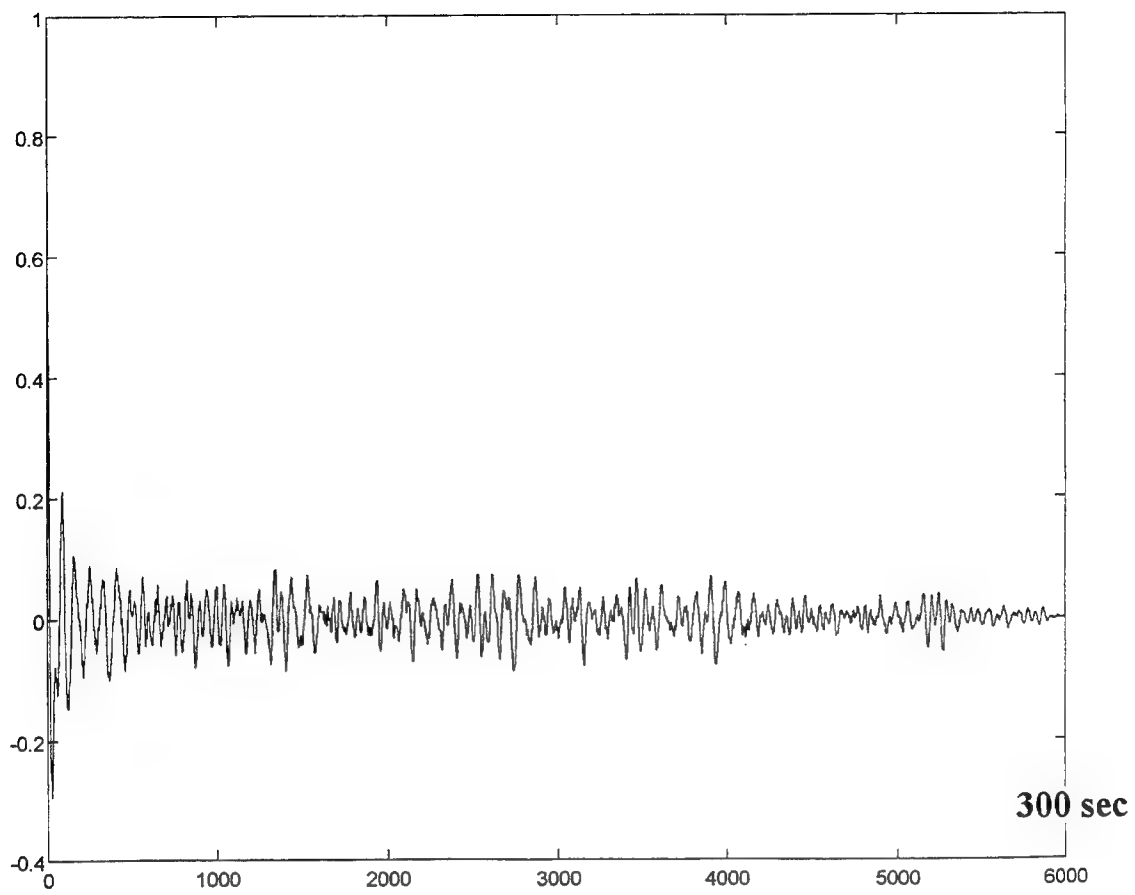


Figure 2.6a. Autocorrelation function 1st microseism recording.

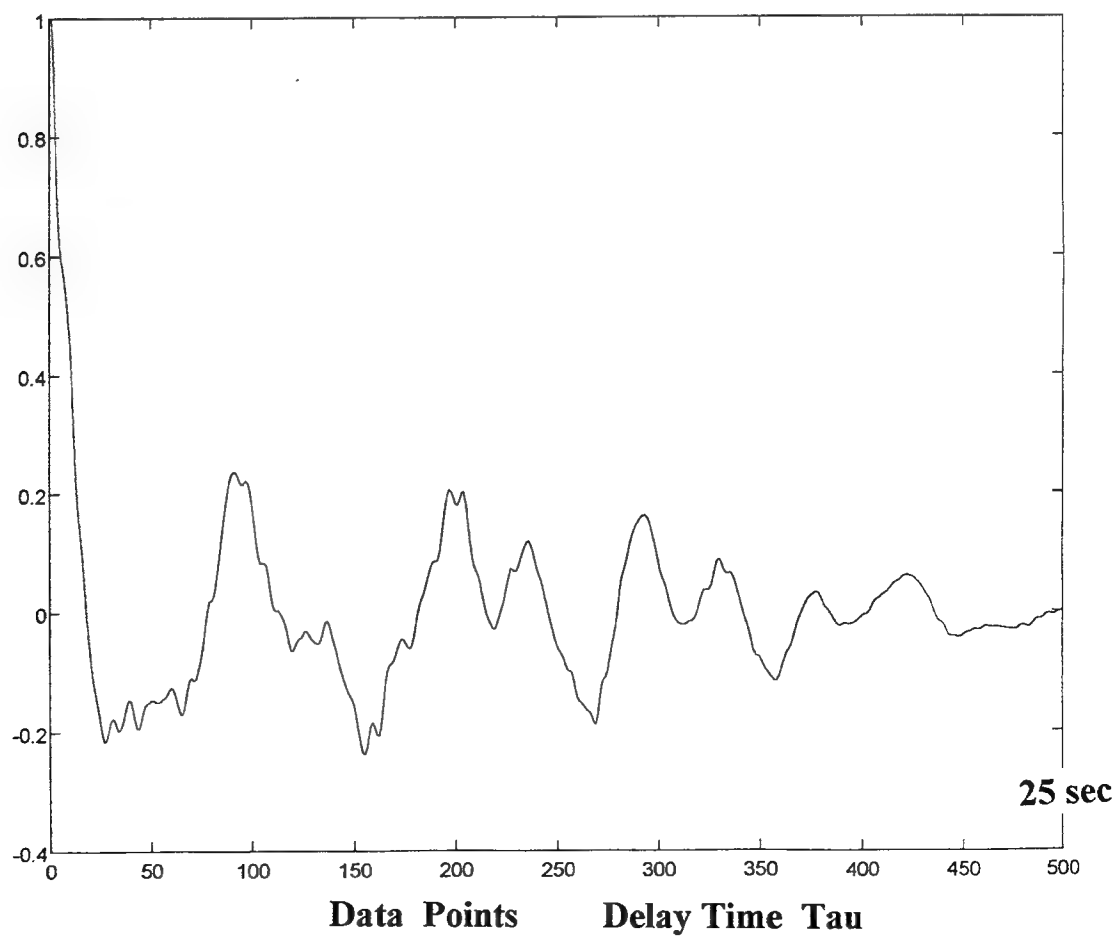
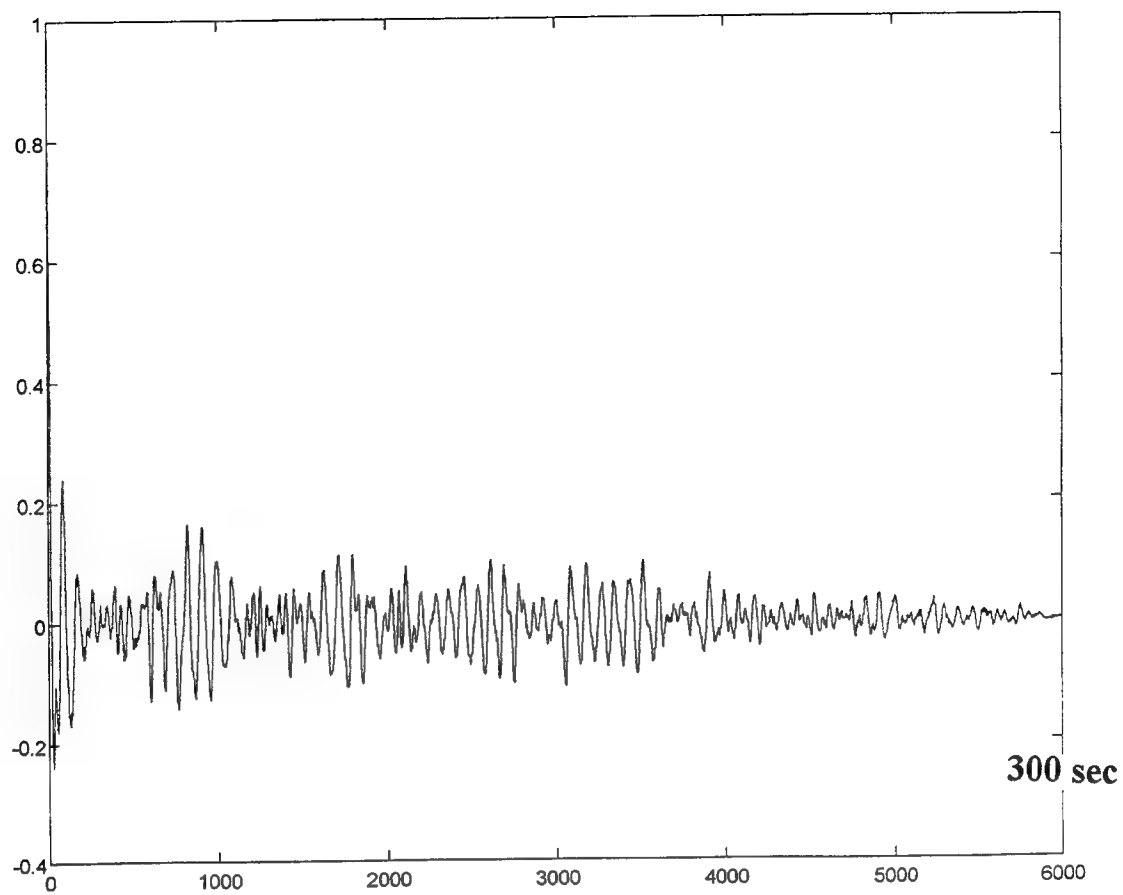


Figure 2.6b. Autocorrelation funtion 2nd microseism recording.

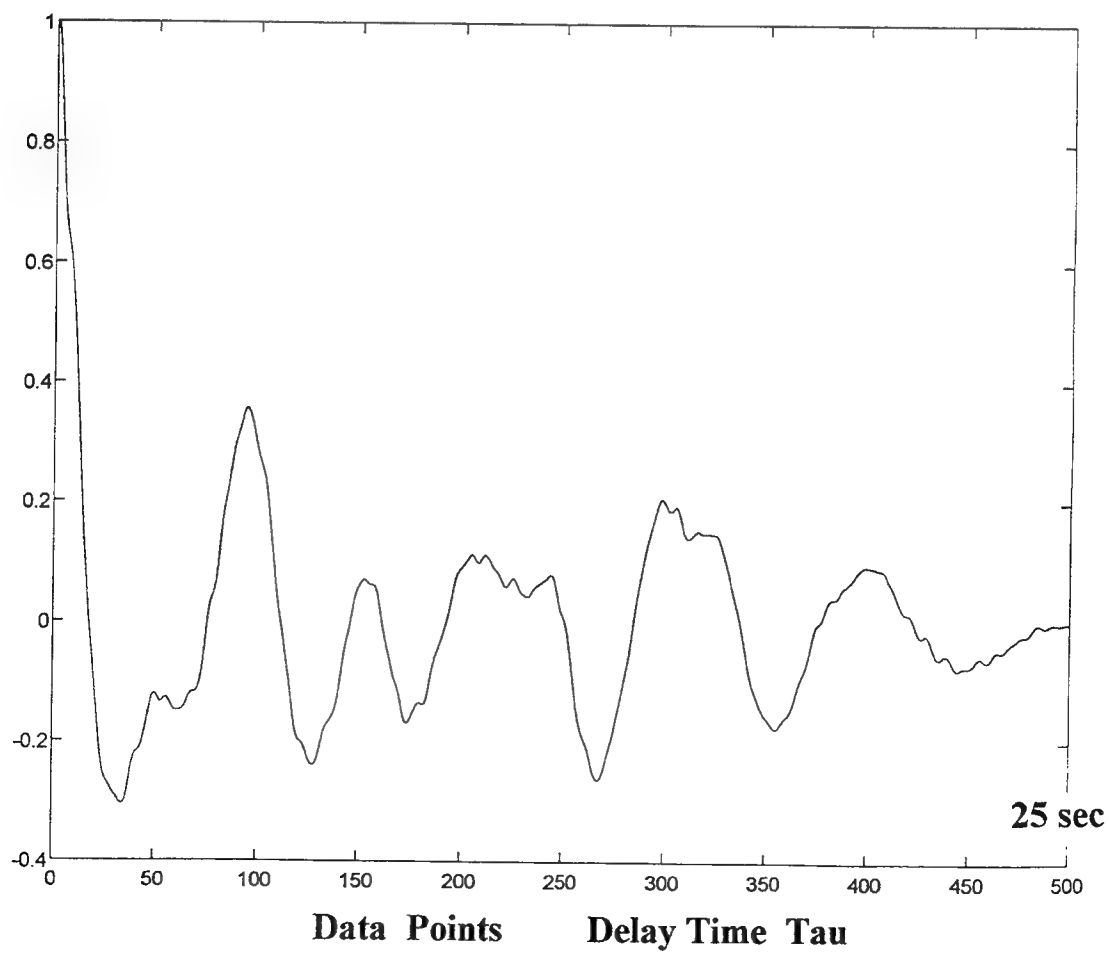
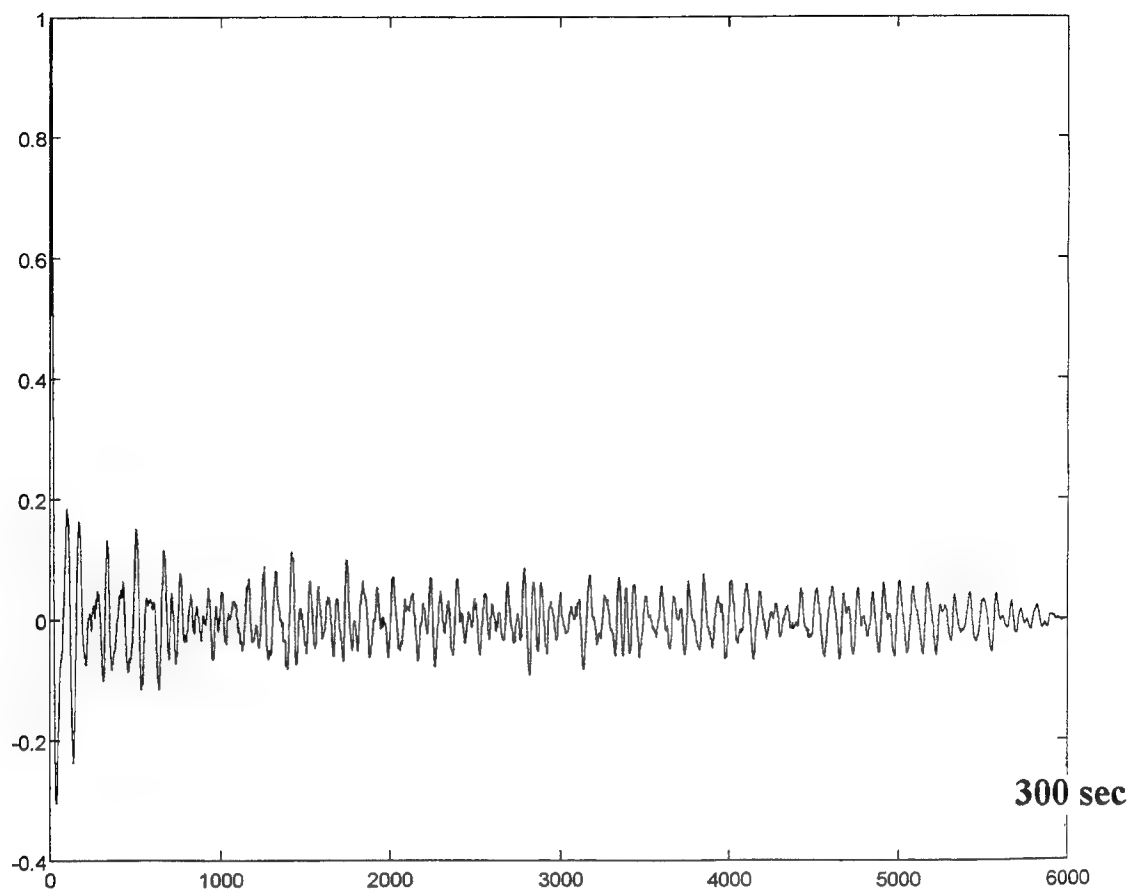


Figure 2.6c. Autocorrelation funtion 3rd microseism recording.

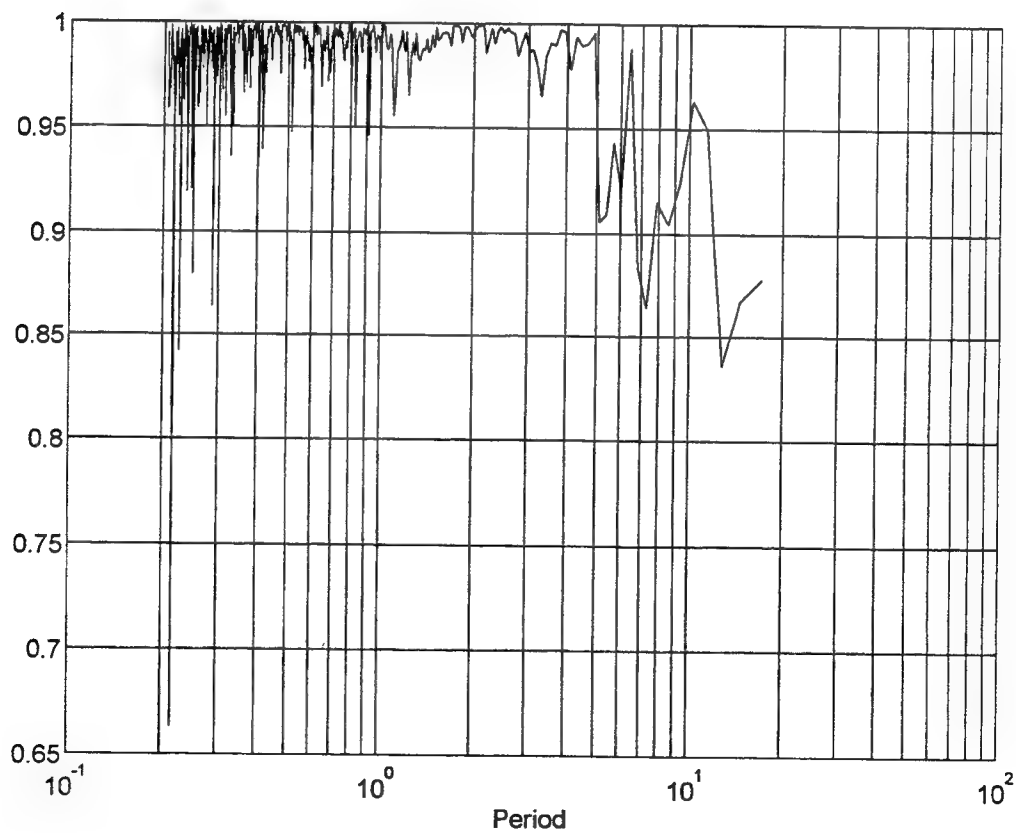
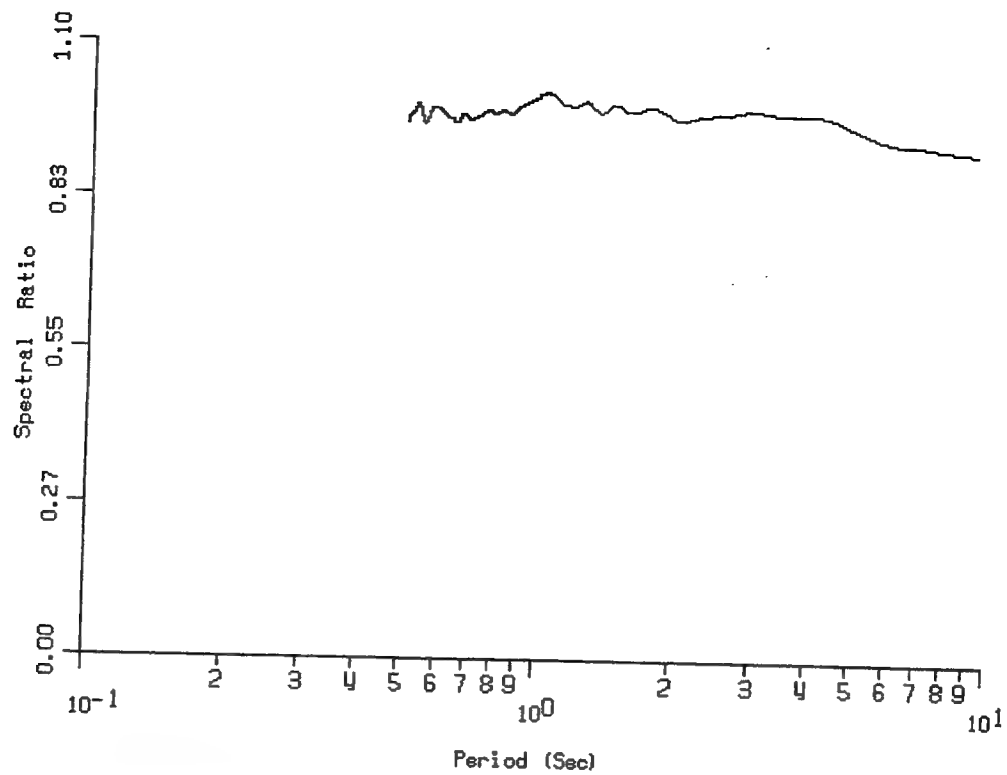


Figure 2.7 Transfer function (above) and coherence (below) for two microseism recordings with zero delay between signals.

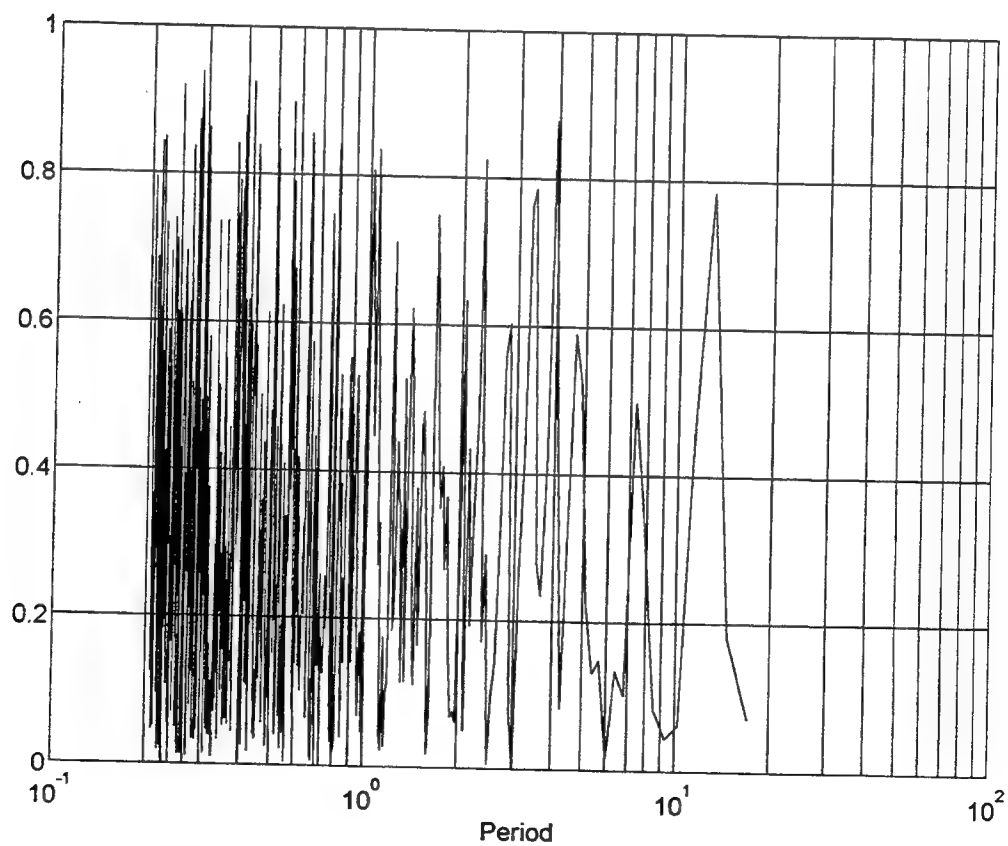
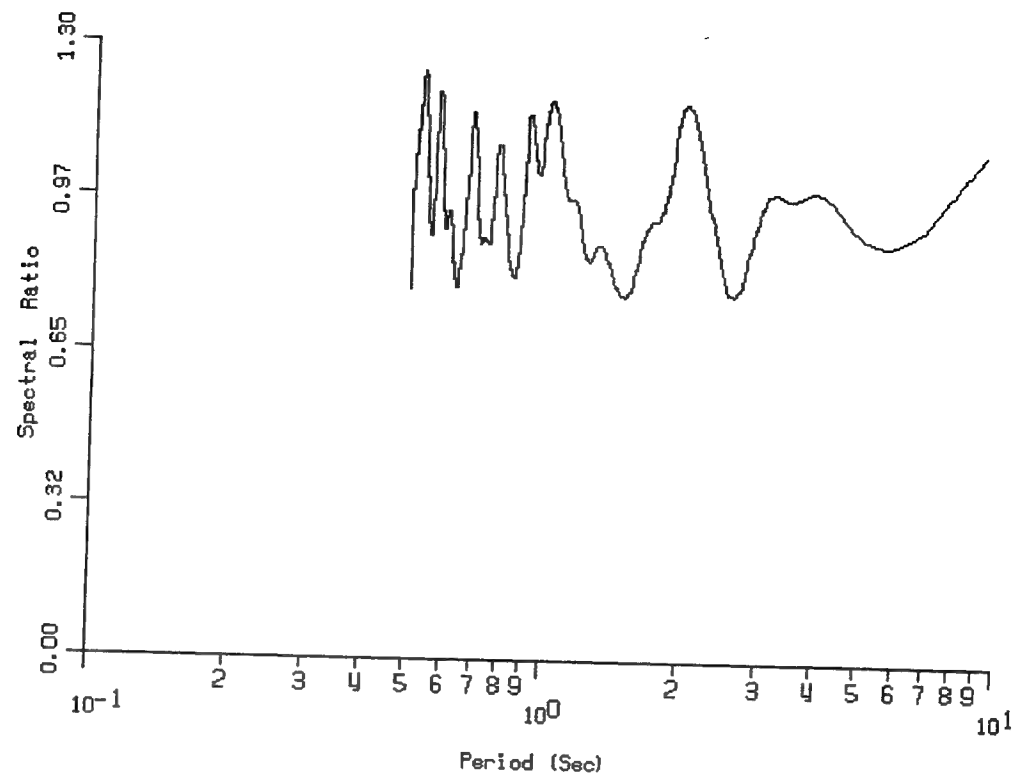


Figure 2.8 Transfer function (above) and coherence (below) for two microseism recordings with 5 minute delay between signals.

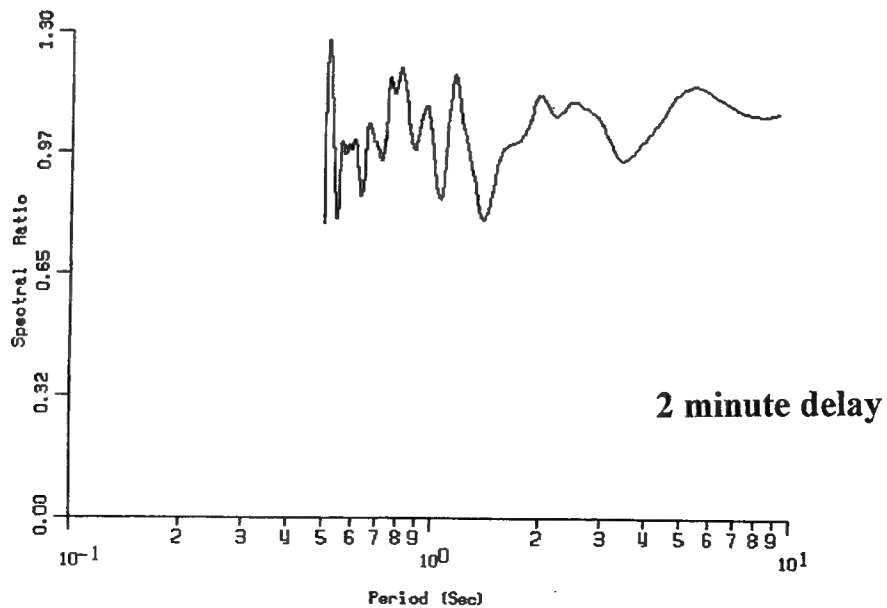
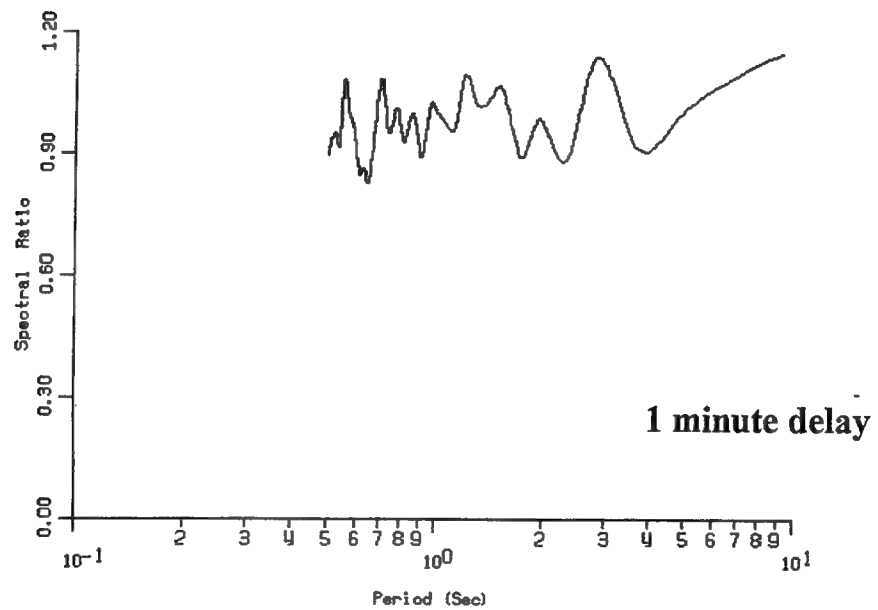
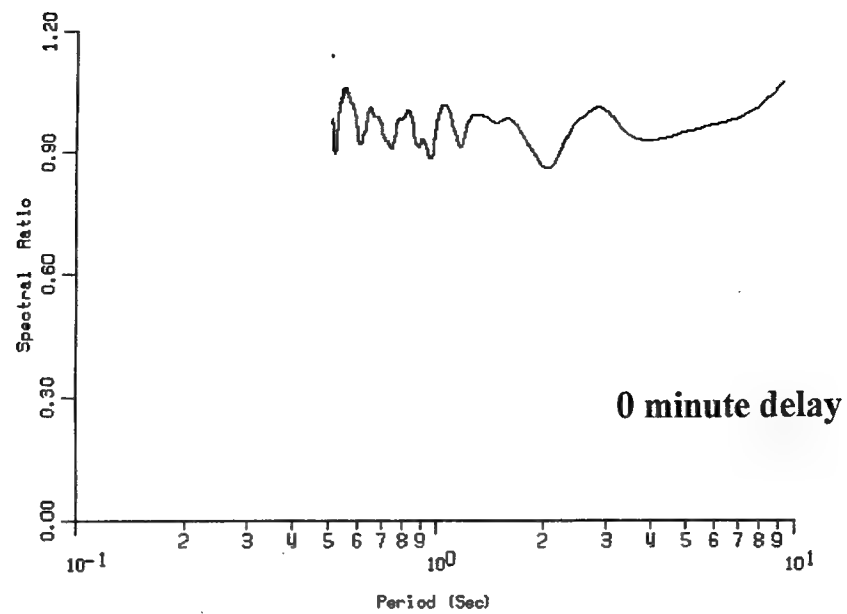


Figure 2.9 Transfer function for two microseism recordings with various delay times between signals.

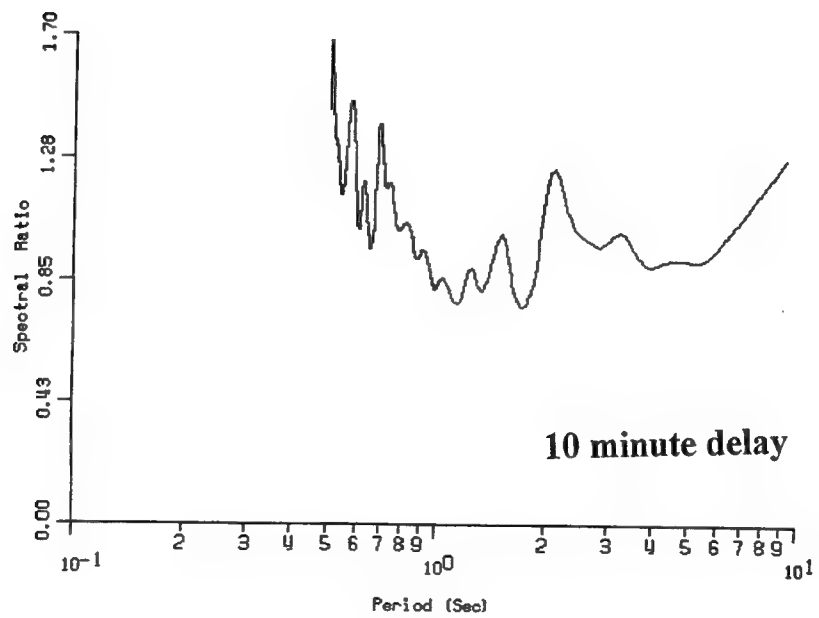
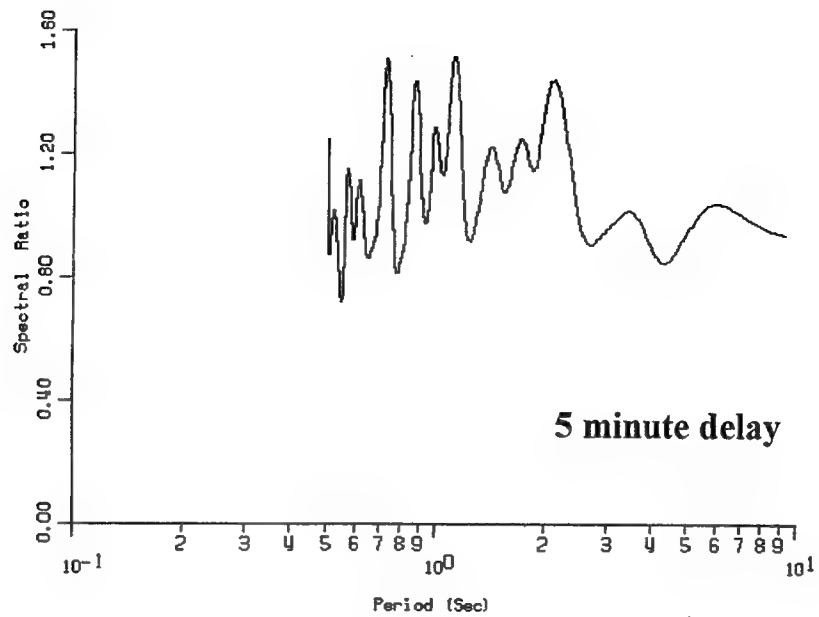


Figure 2.9 Continued

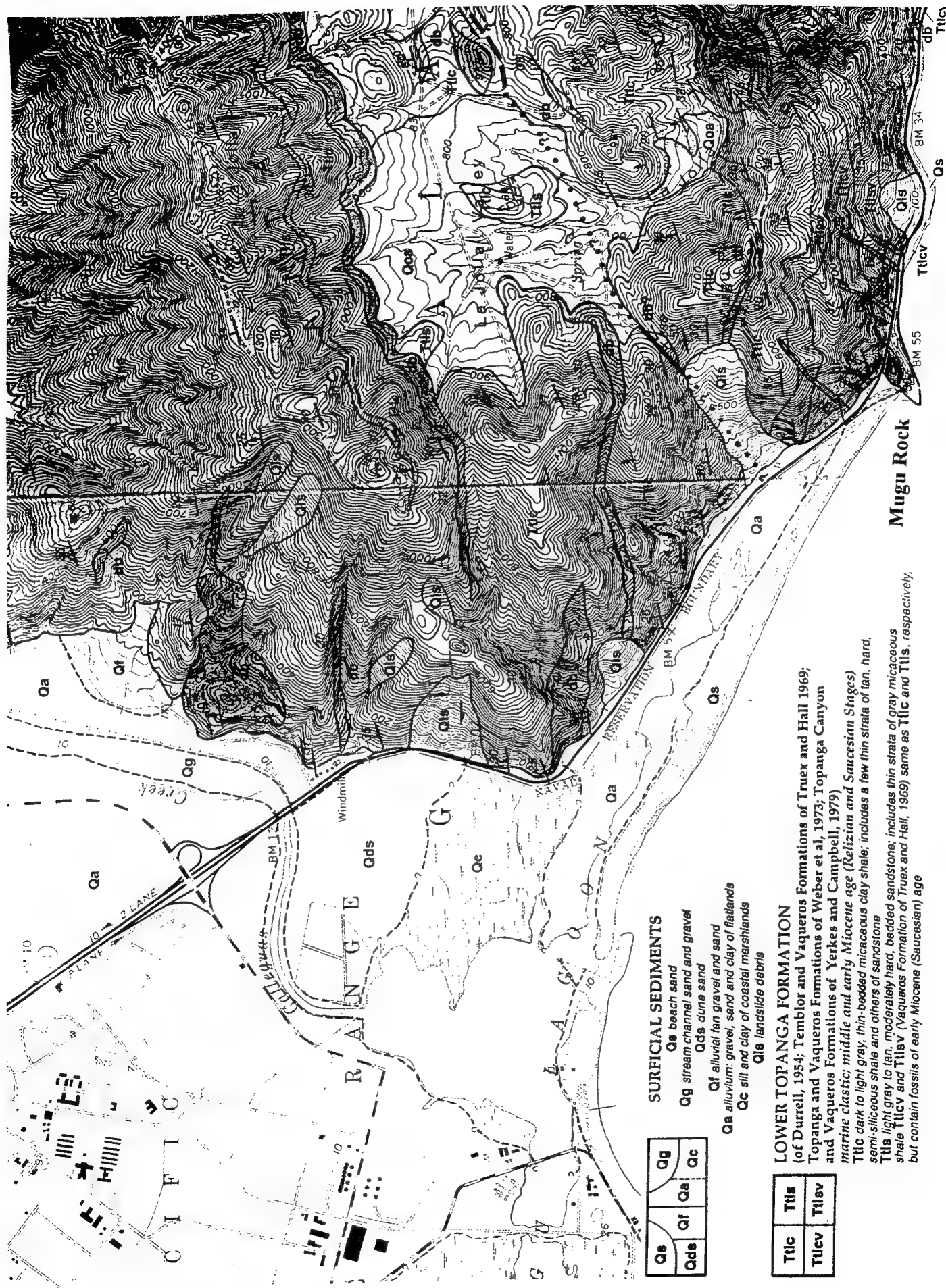


Figure 2.10 Map showing Mugu Rock geology and sites

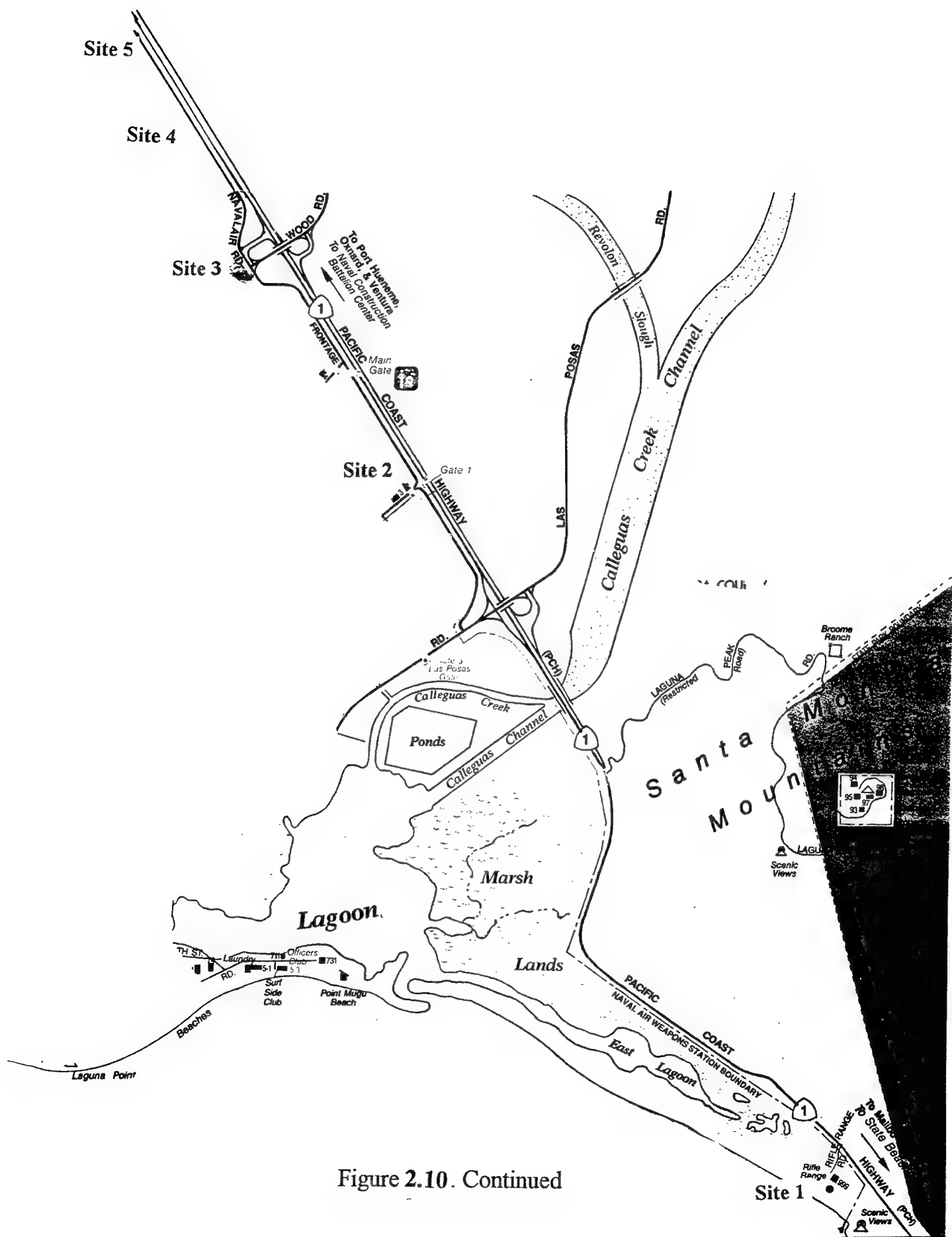


Figure 2.10. Continued

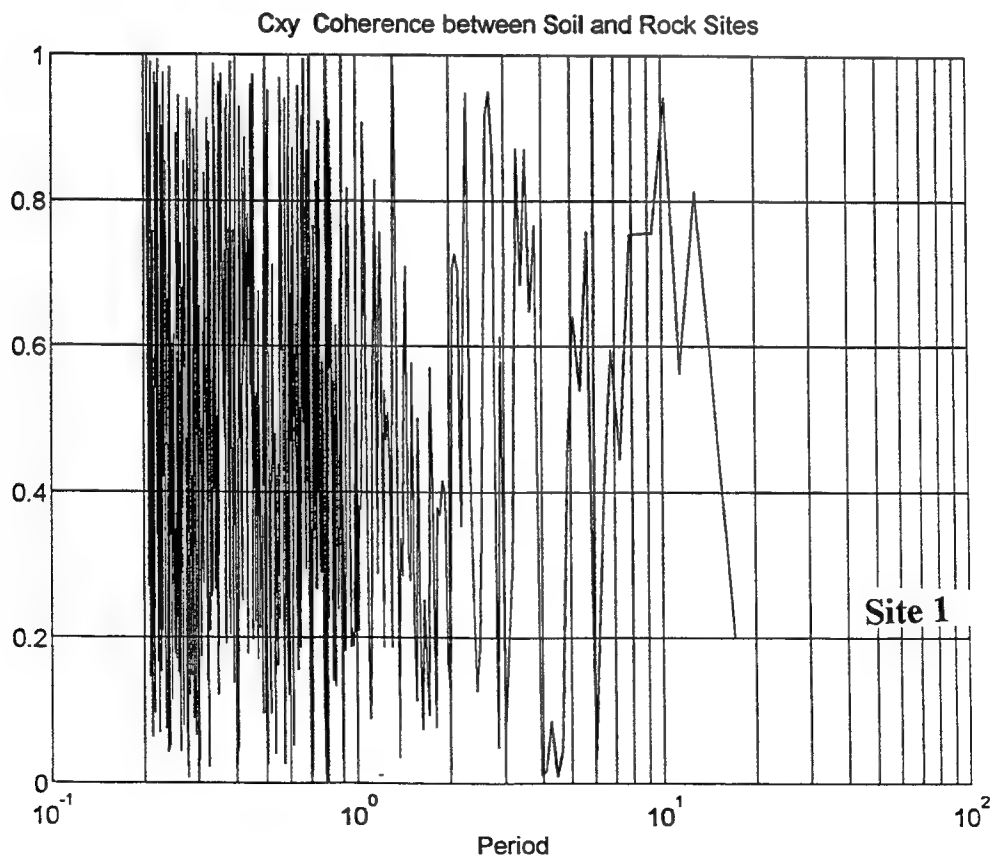
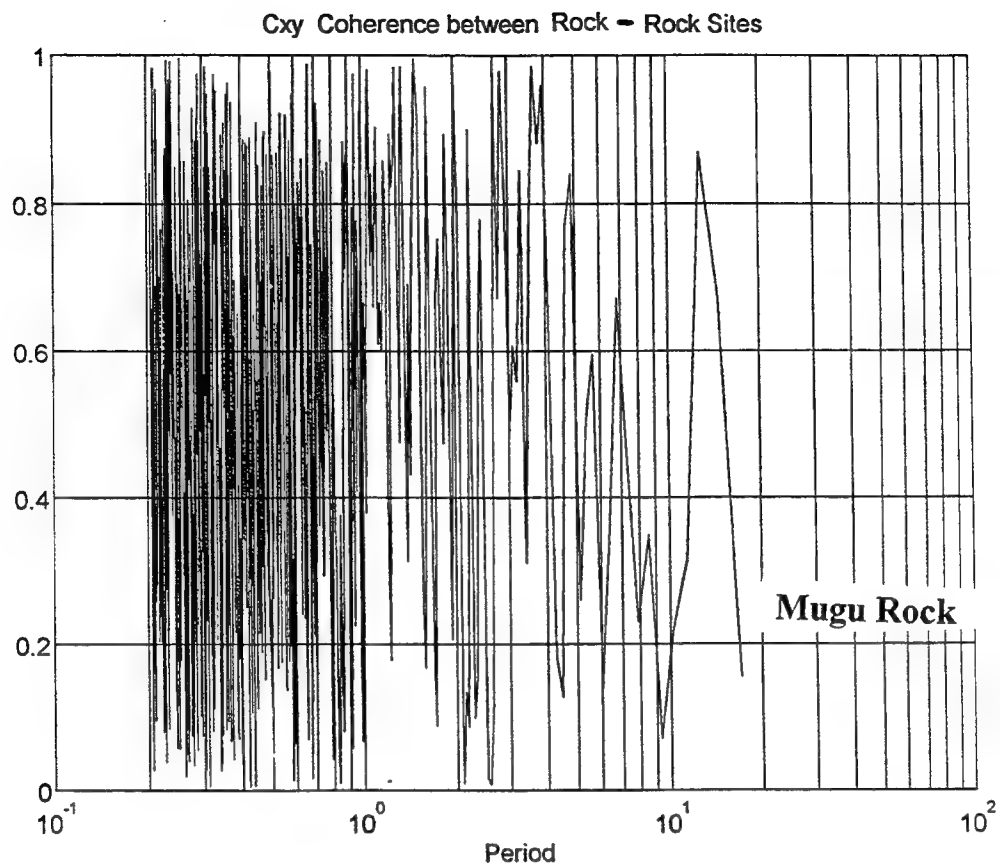


Figure 2.11 Coherence between rock and soil sites.

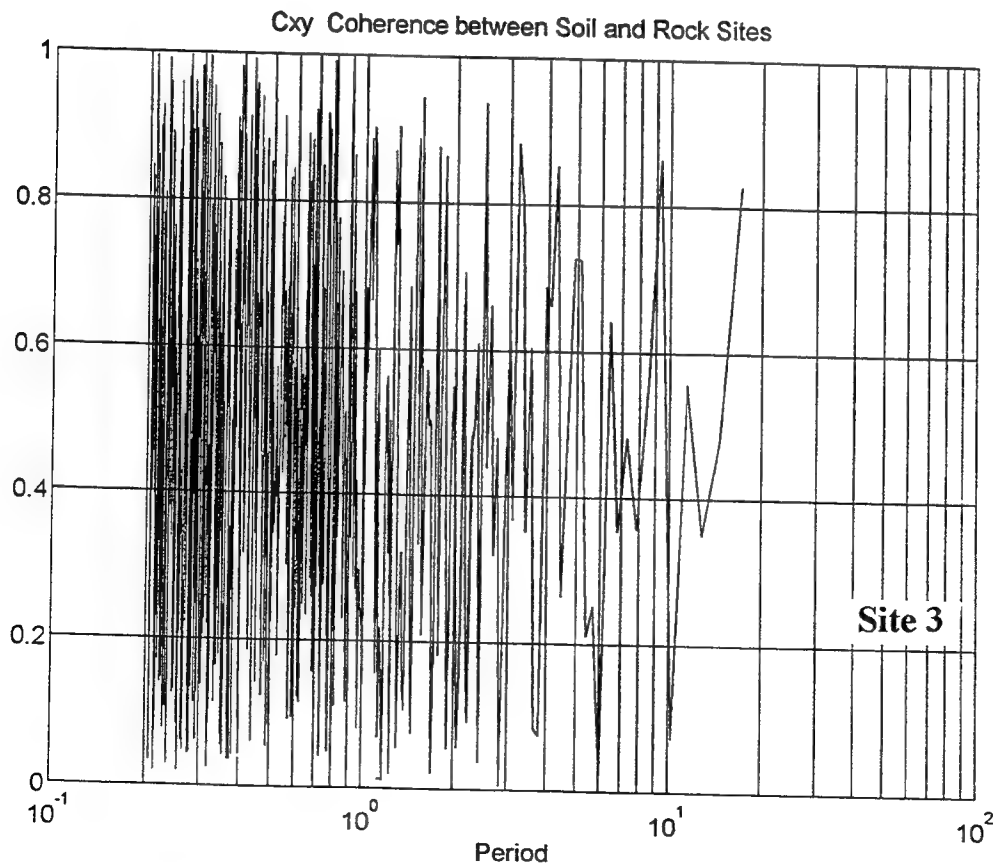
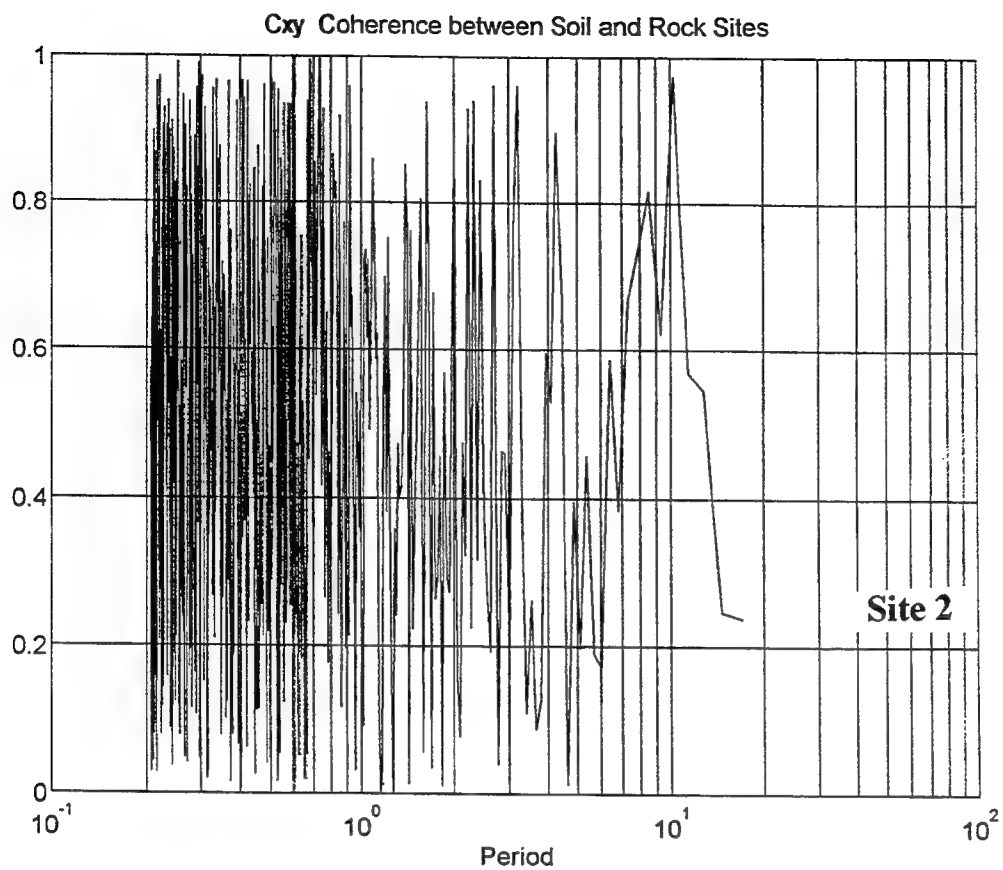


Figure 2.11 . Continued

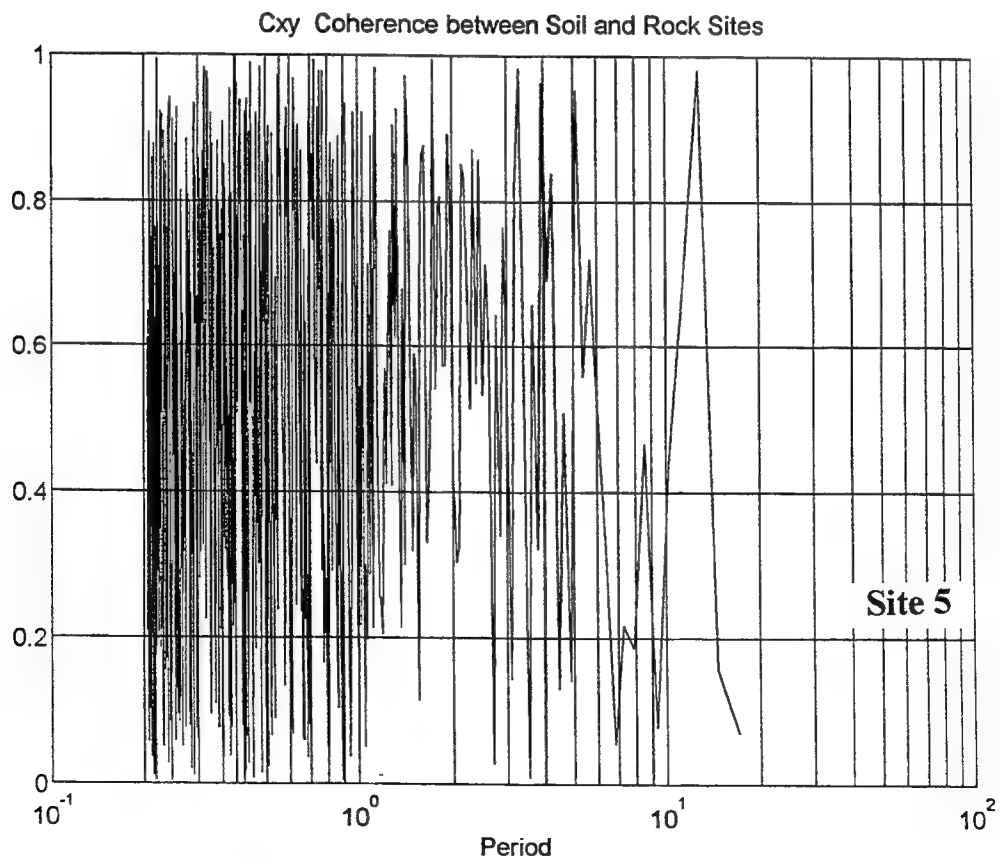
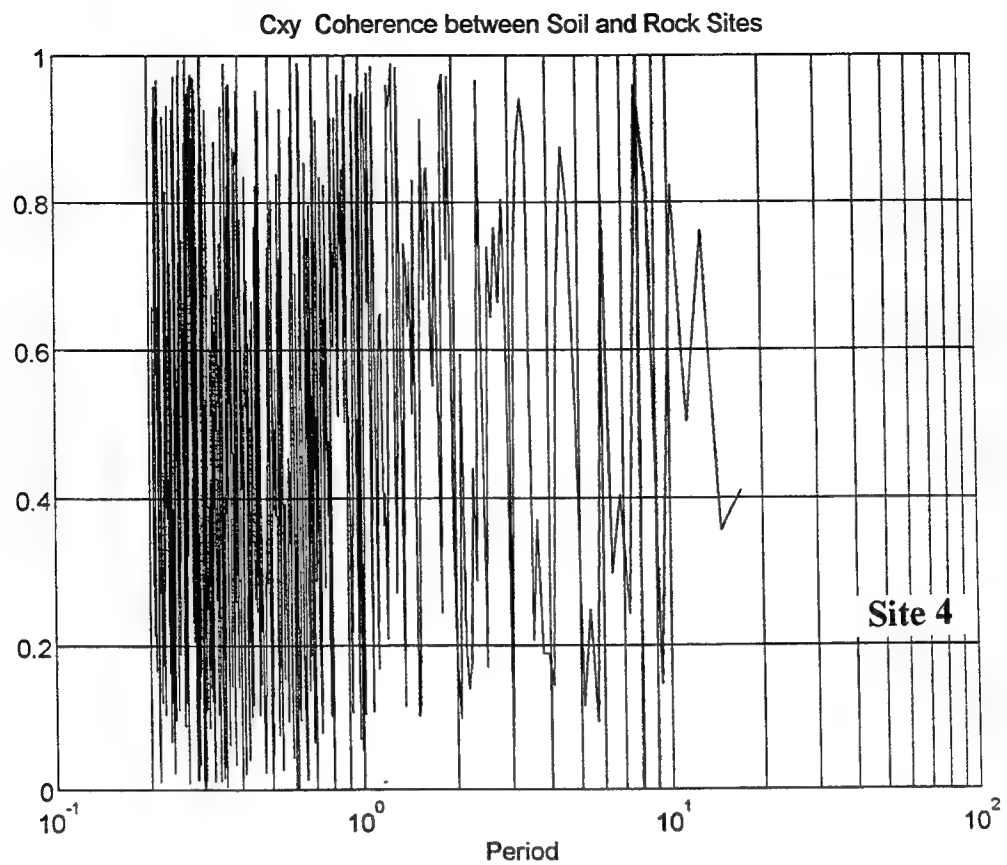


Figure 2.11. Continued

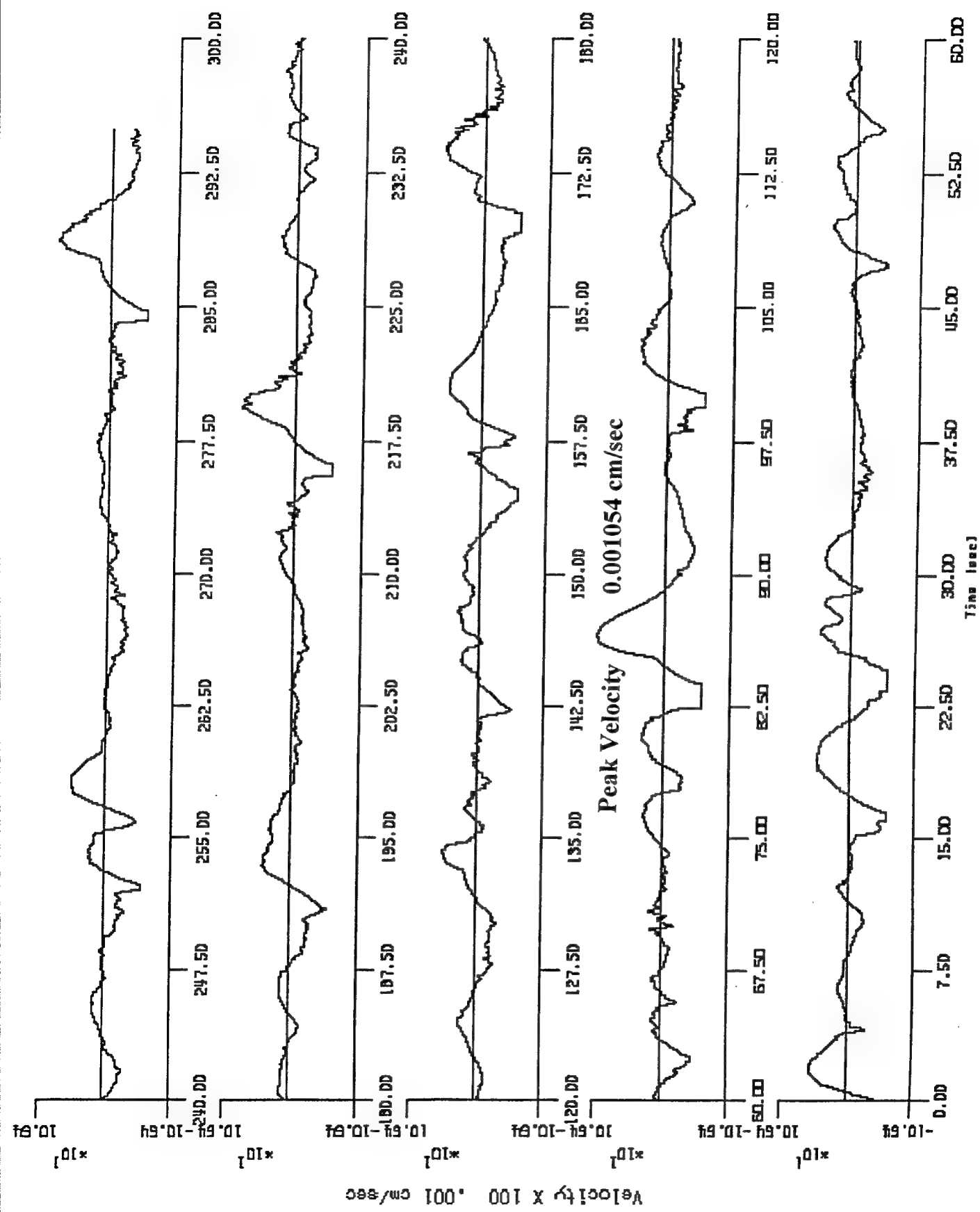


Figure 2.12. Time history of instrument exposed to gusting winds.

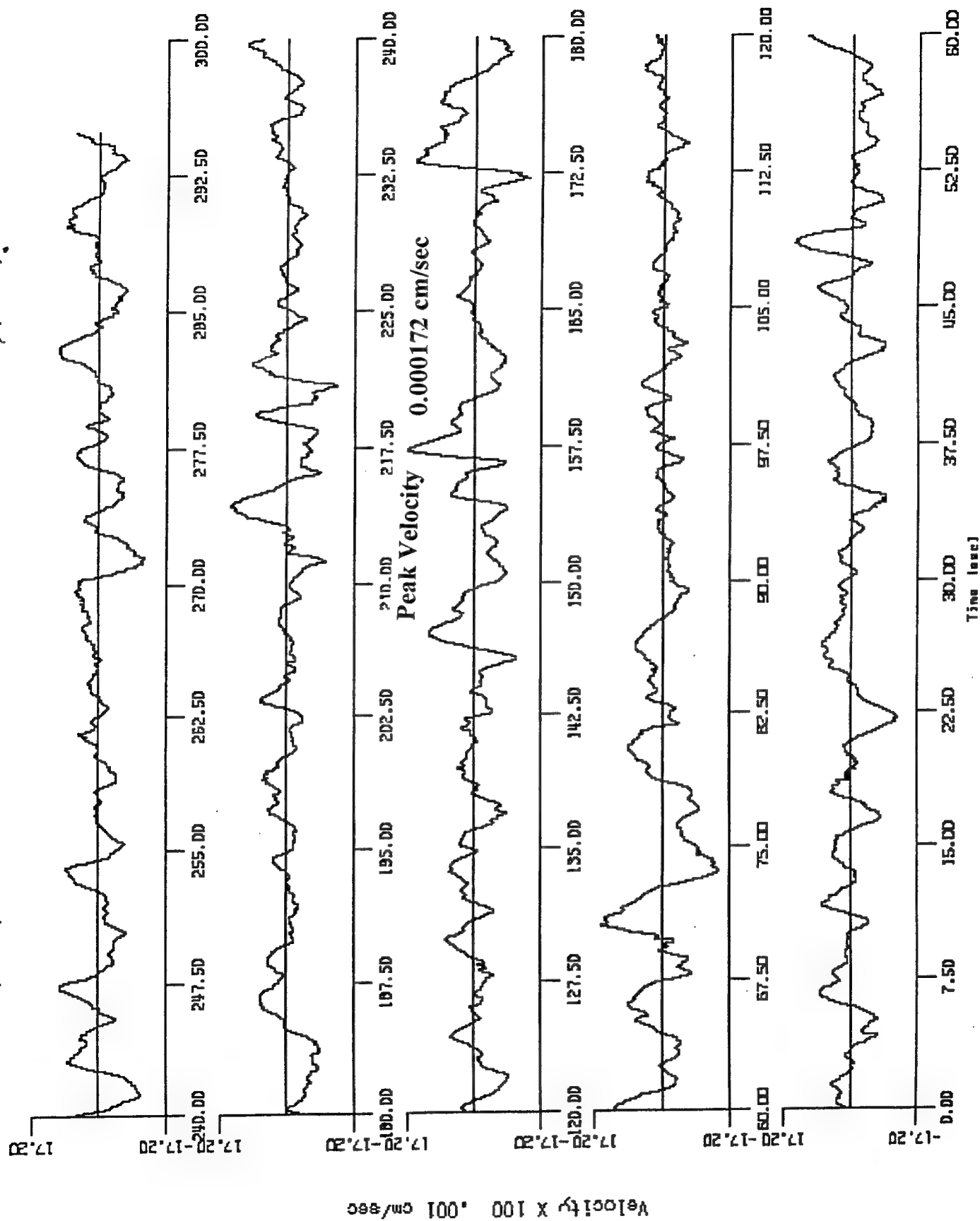


Figure 2.13. Time history of shielded instrument.

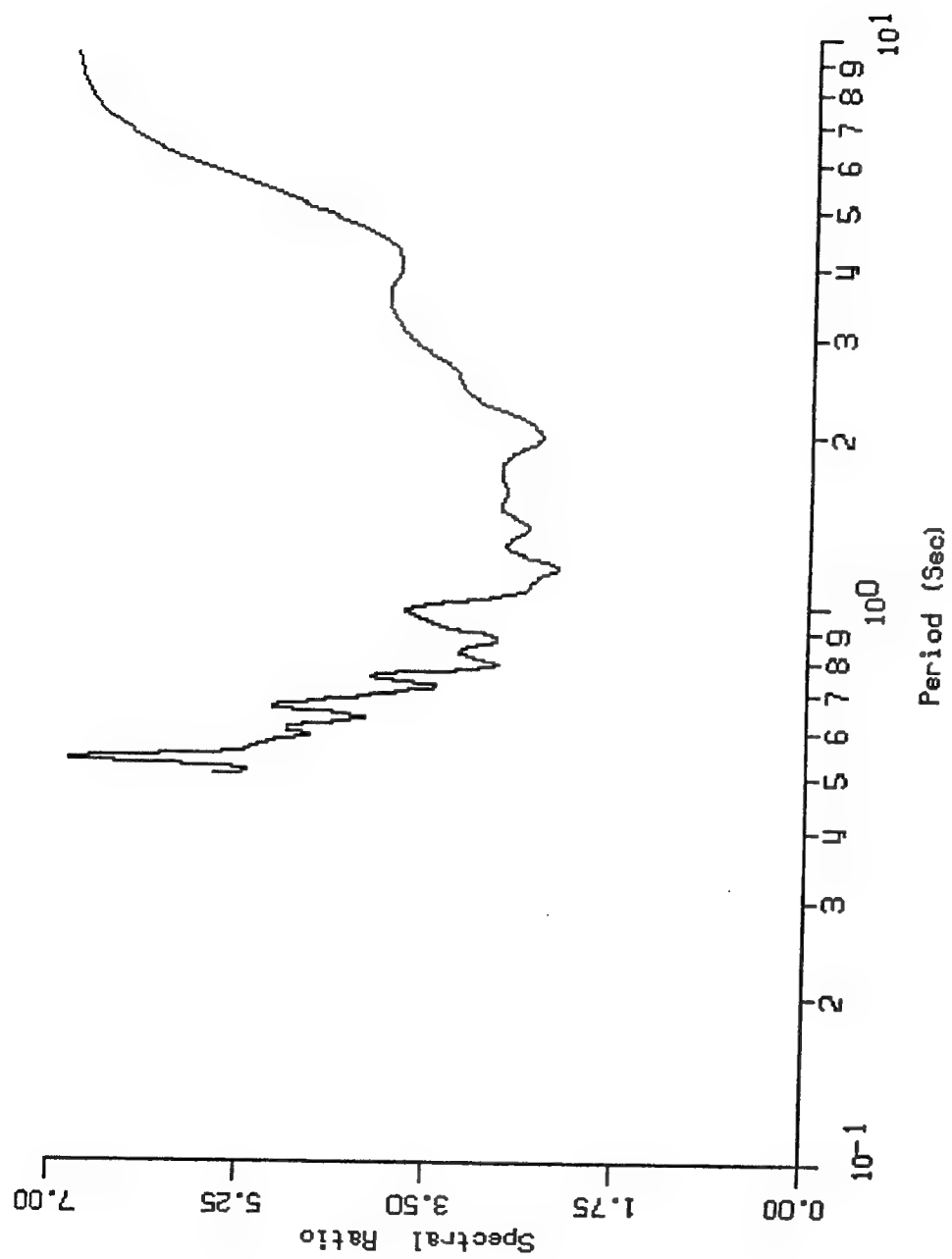


Figure 2.14. Transfer function exposed instrument/shielded instrument.

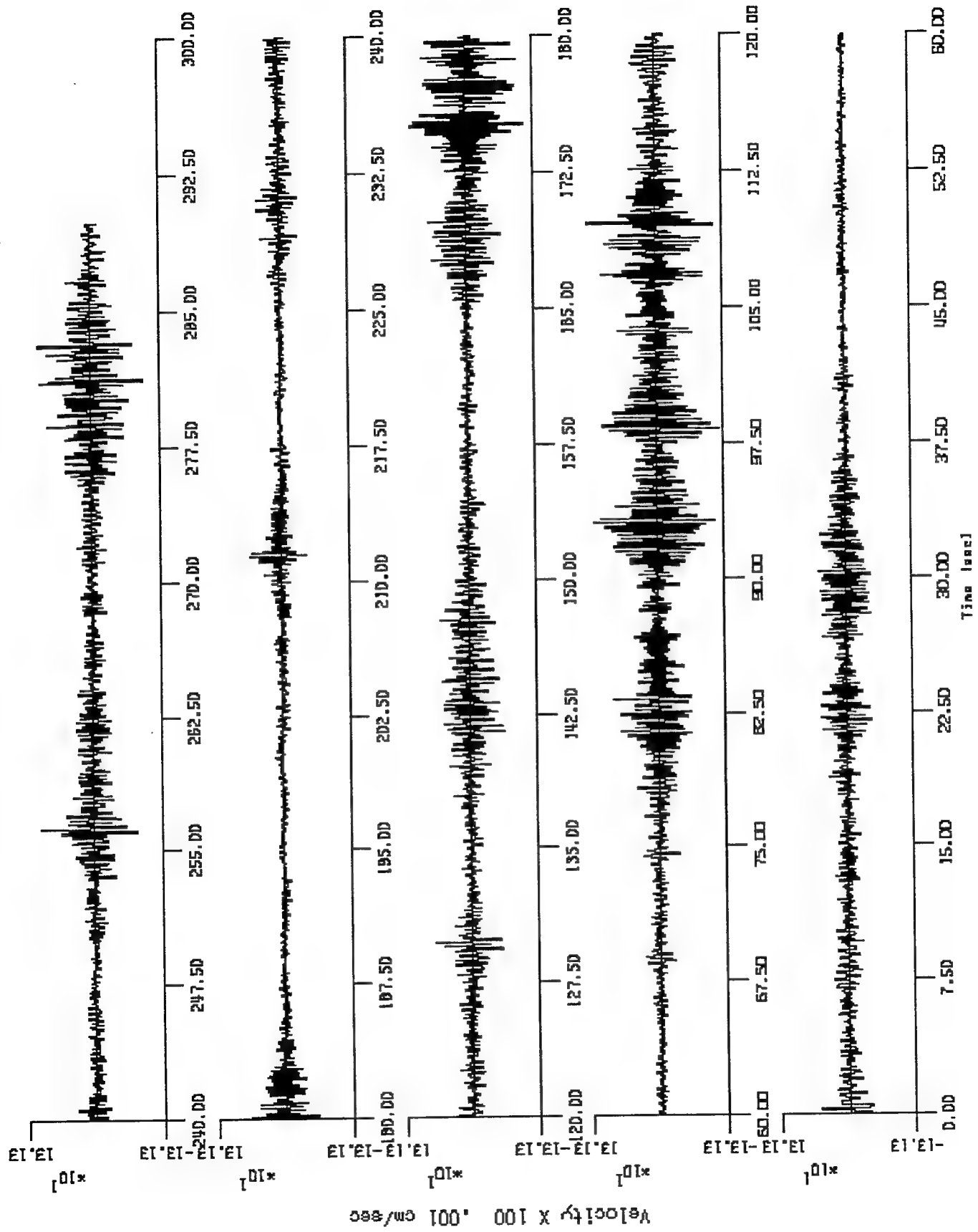


Figure 2.15. Time history of site with high traffic noise.

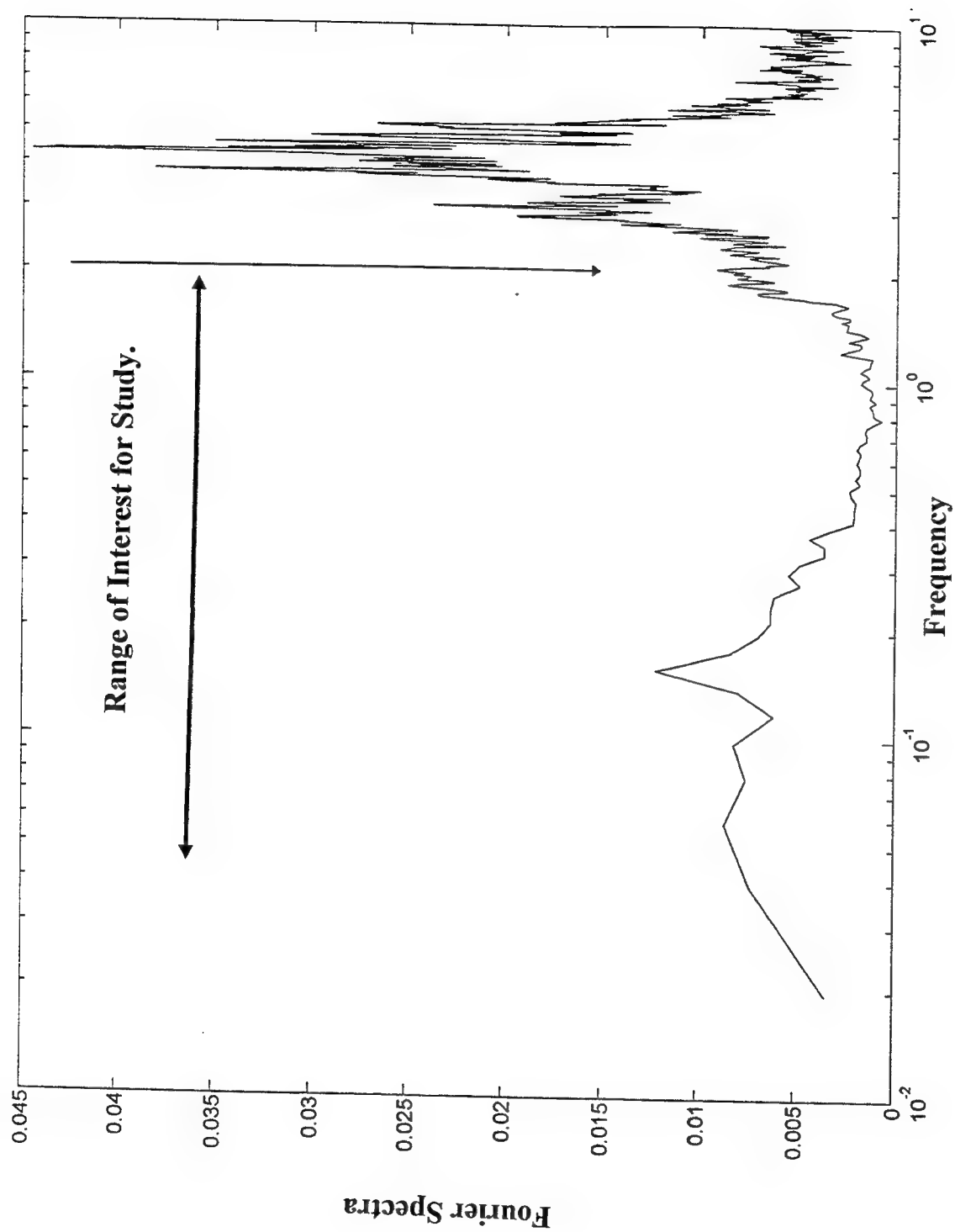


Figure 2.16 . Fourier spectra of record containing traffic noise.

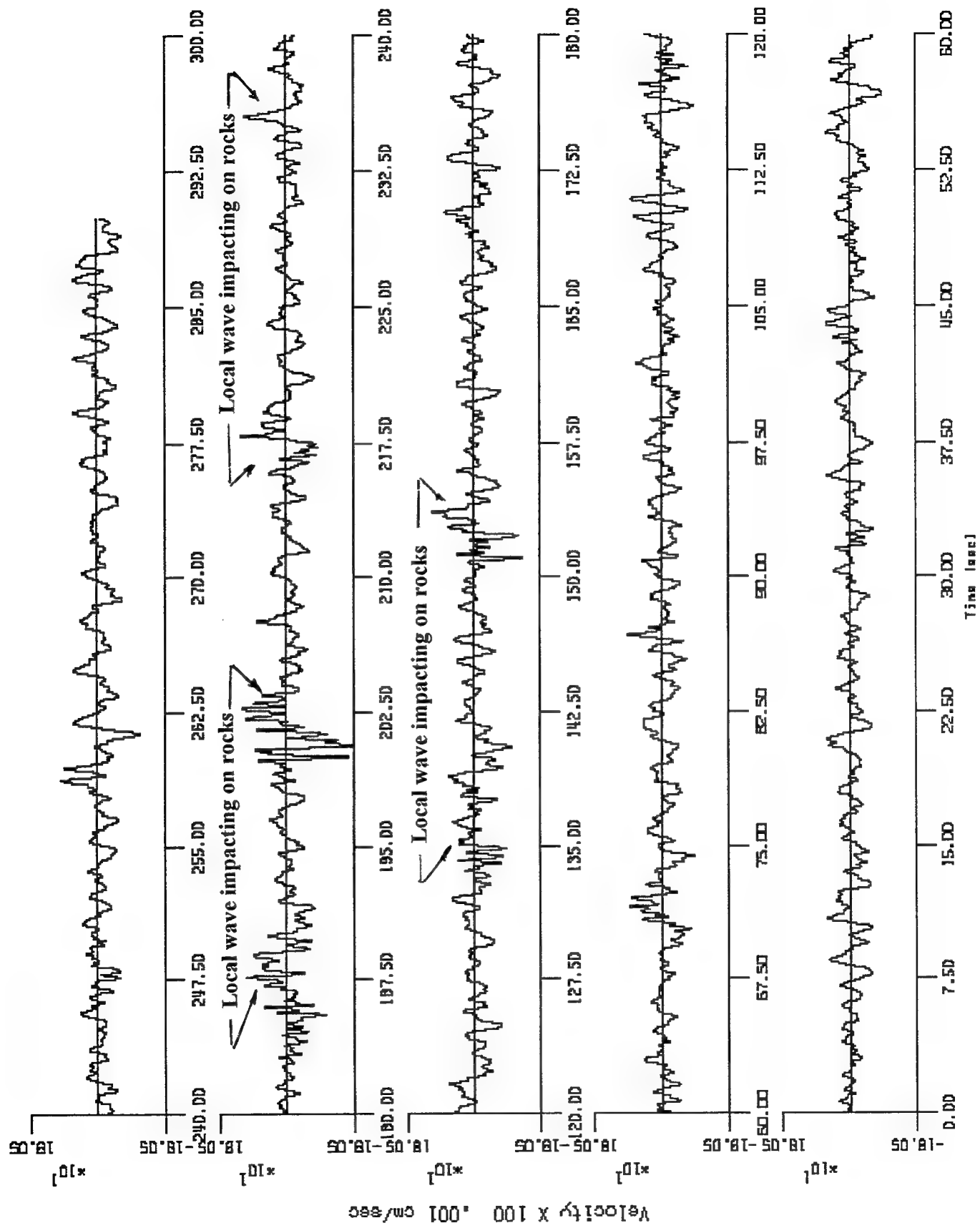


Figure 2.17a. Time history of record with impacting ocean waves.

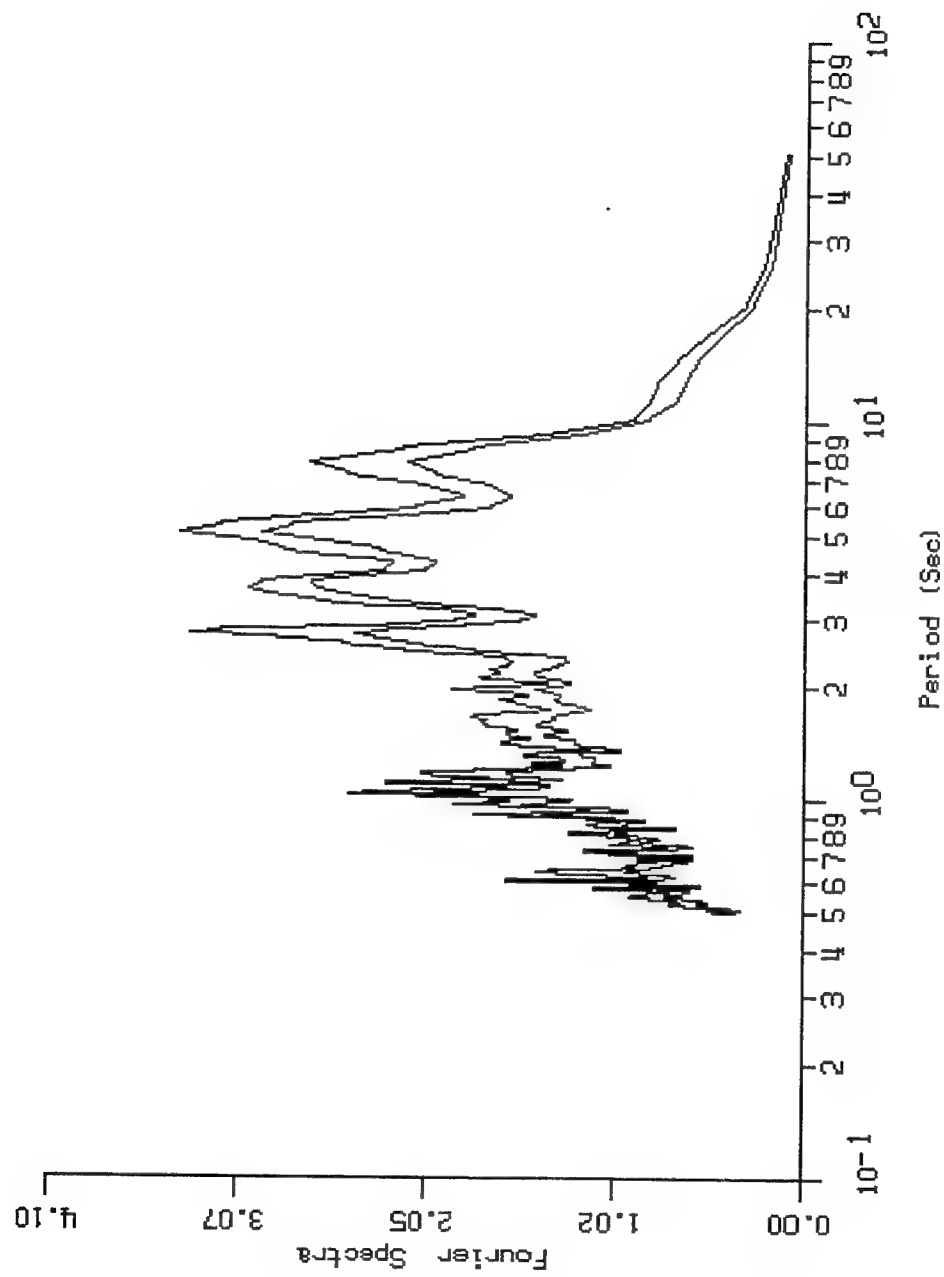
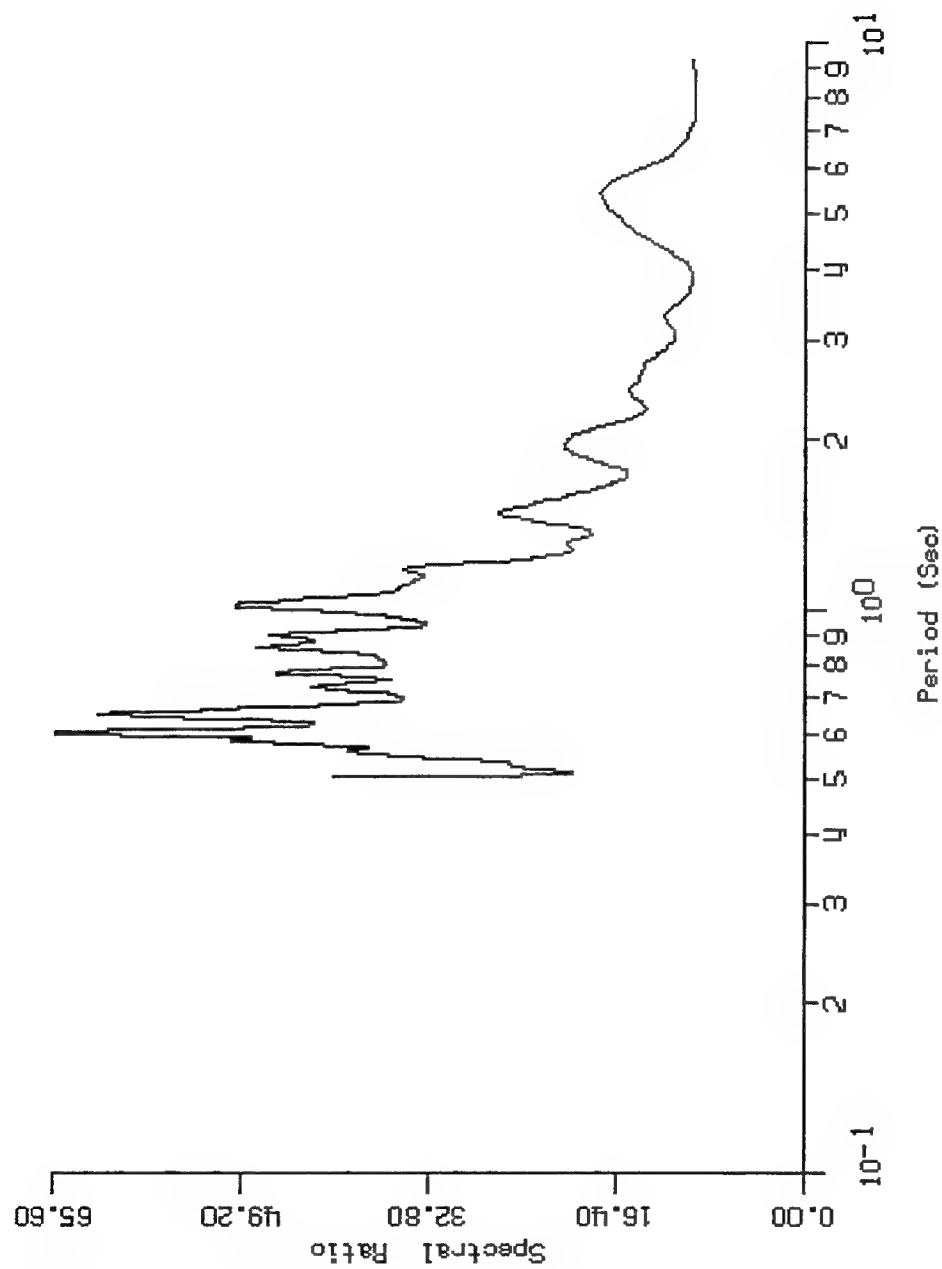
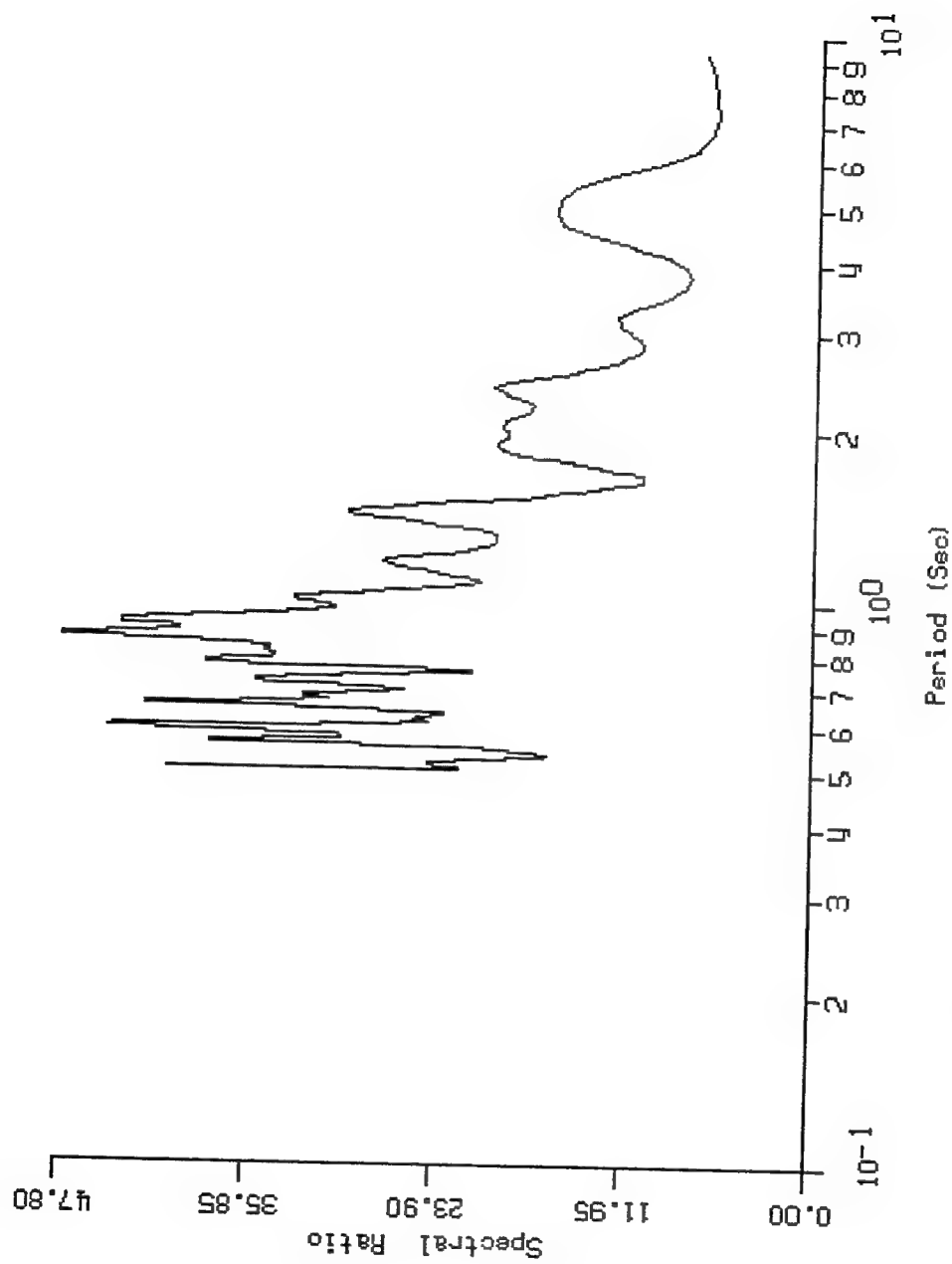


Figure 2.17b. Fourier spectra of time history in Figure 2.17a.



**Figure 2.17c. Spectral ratio with respect to rock site
showing effects of local waves.**



**Figure 2.17d. Spectral ratio with respect to rock site
with elimination of local wave noise.**

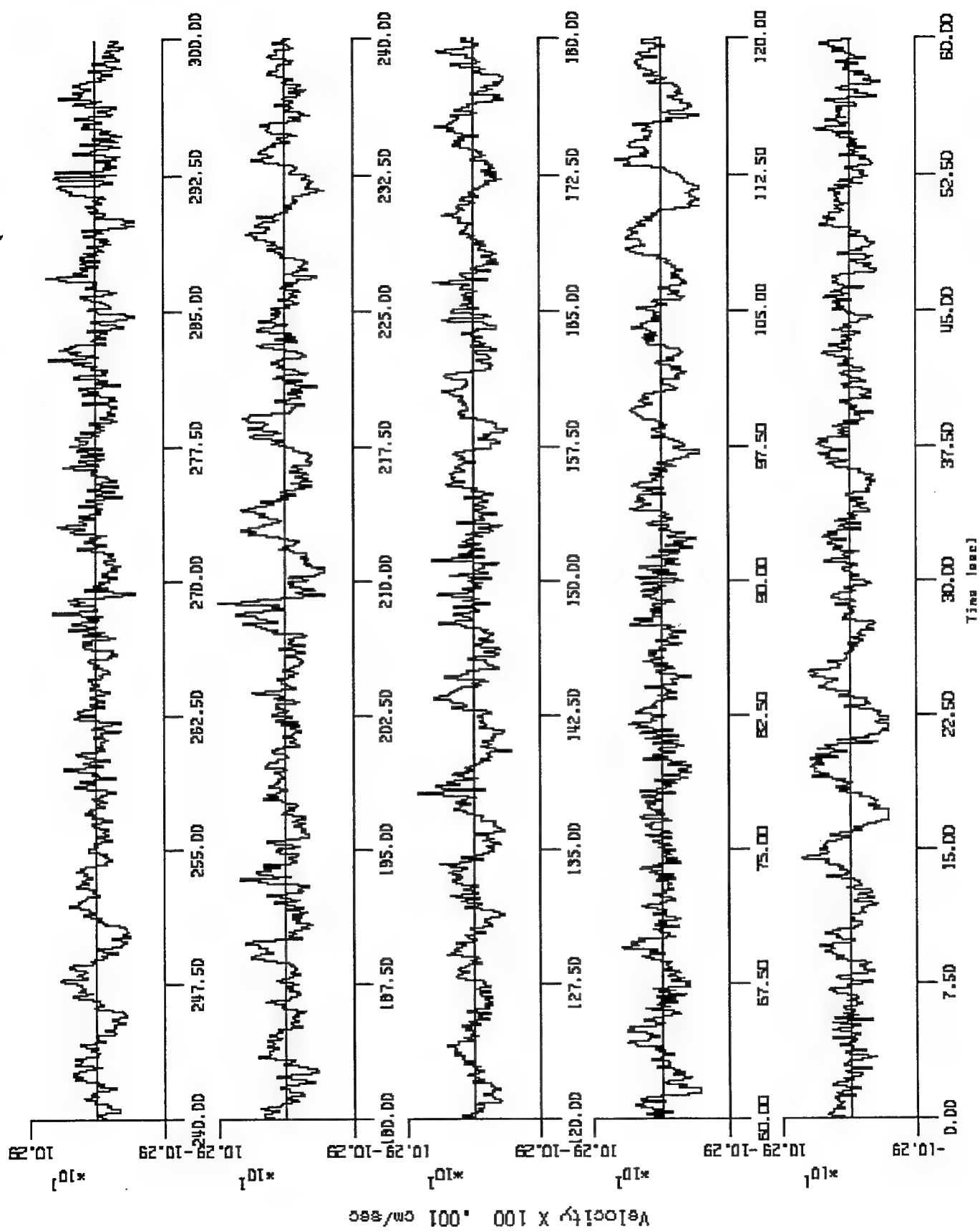


Figure 2.18. East-West microseism recording.

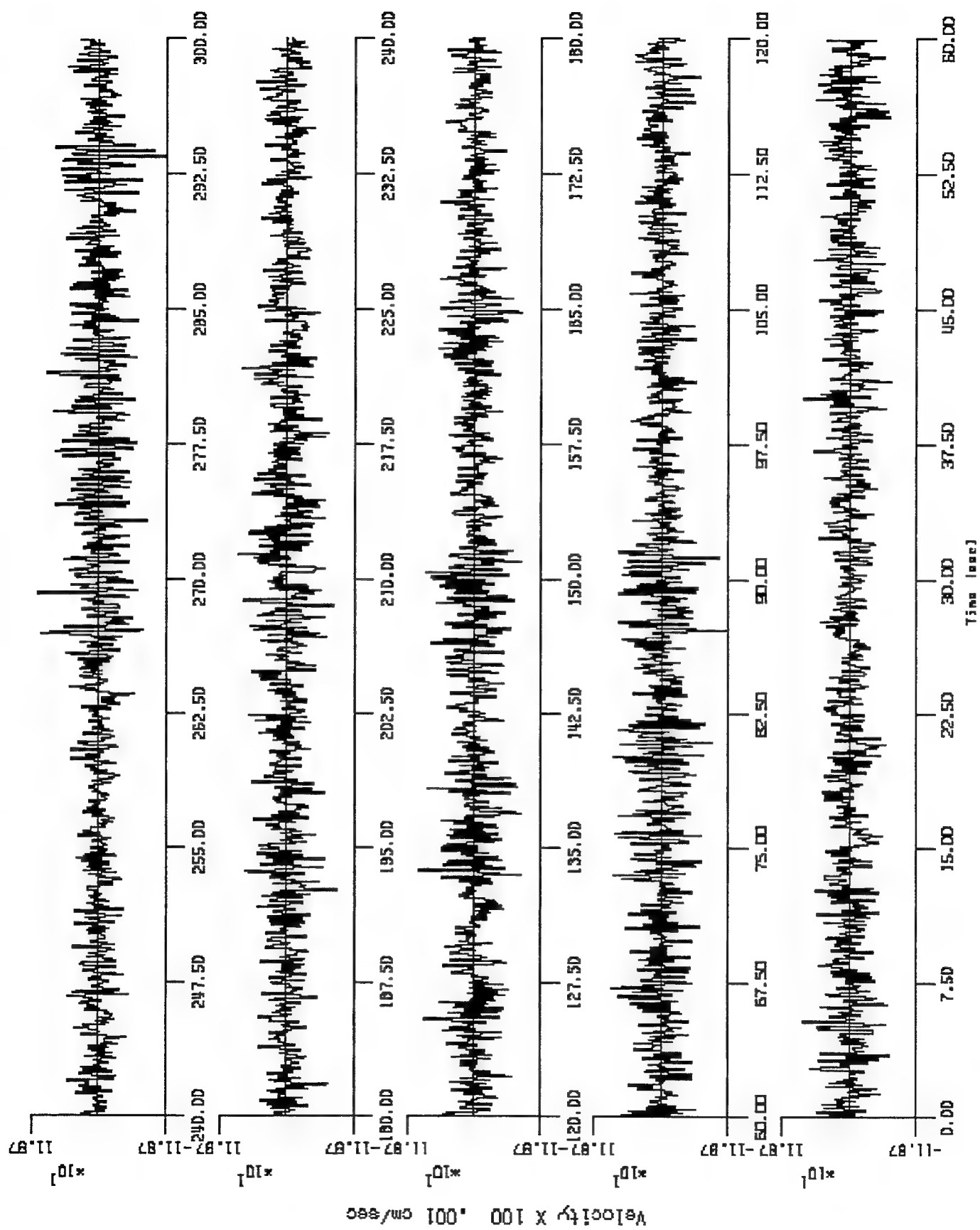


Figure 2.19. Vertical microseism recording.

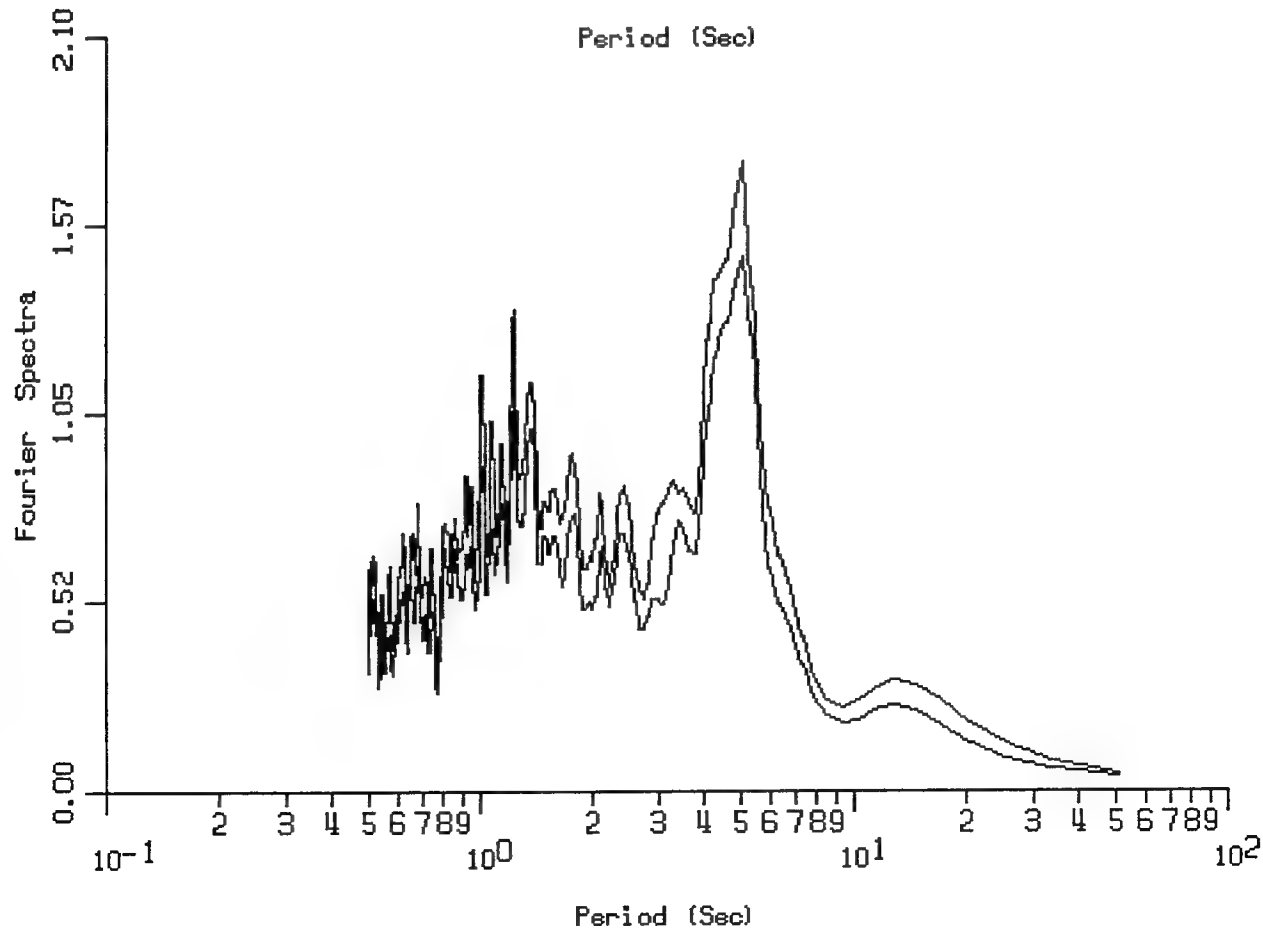
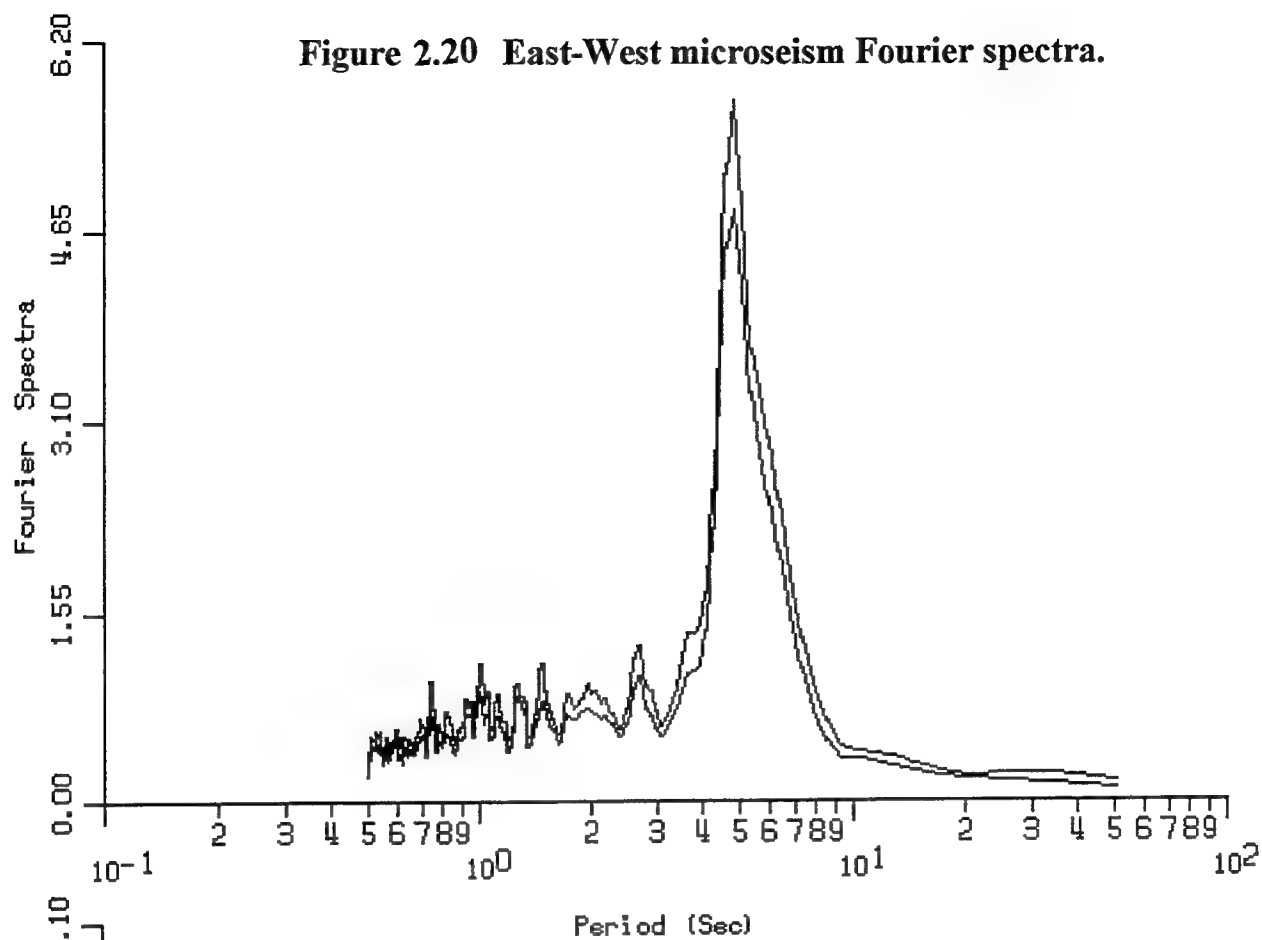


Figure 2.21. Vertical microseism Fourier spectra.

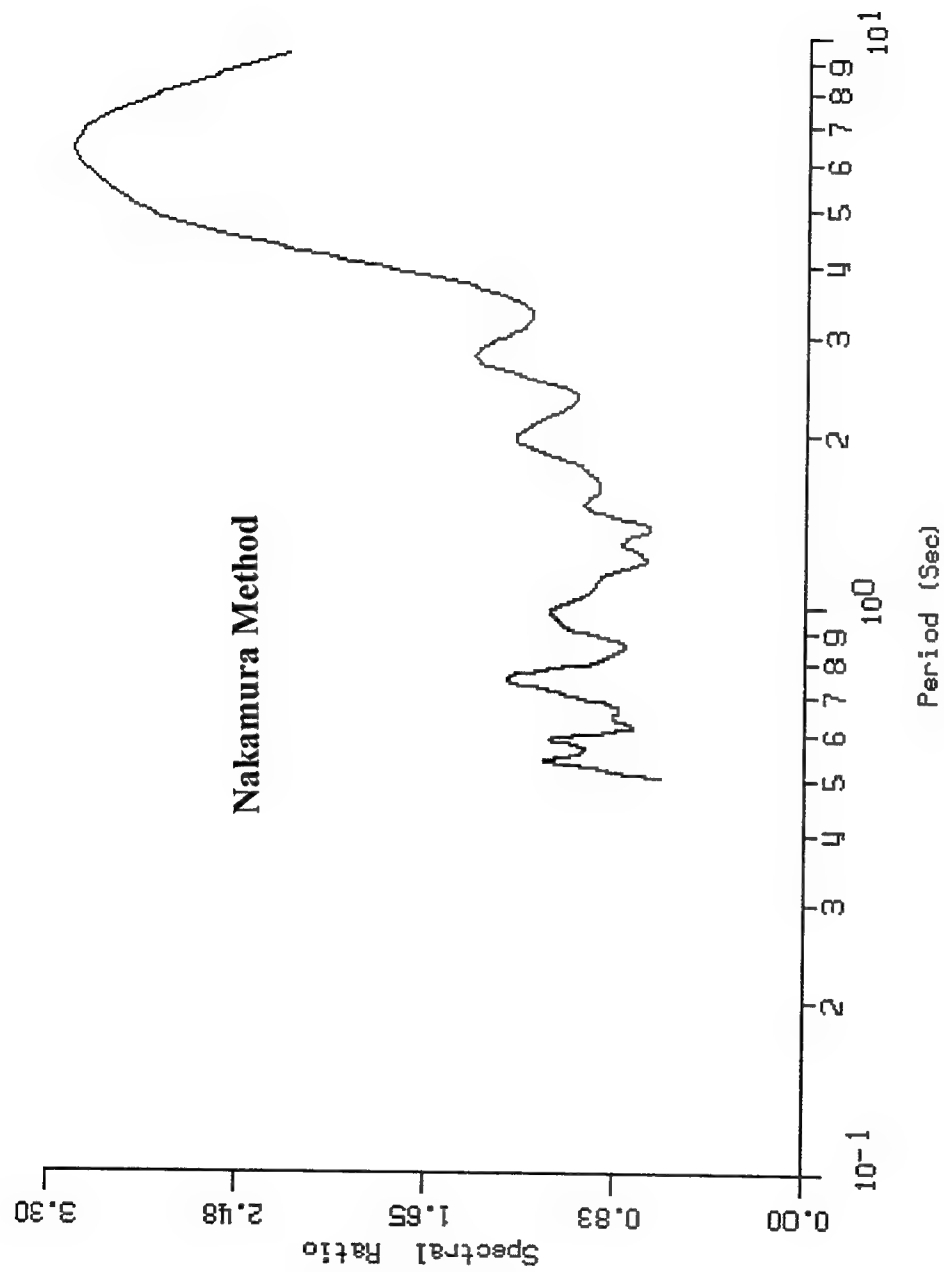


Figure 2.22. Spectral ratio (East-West/Vertical).

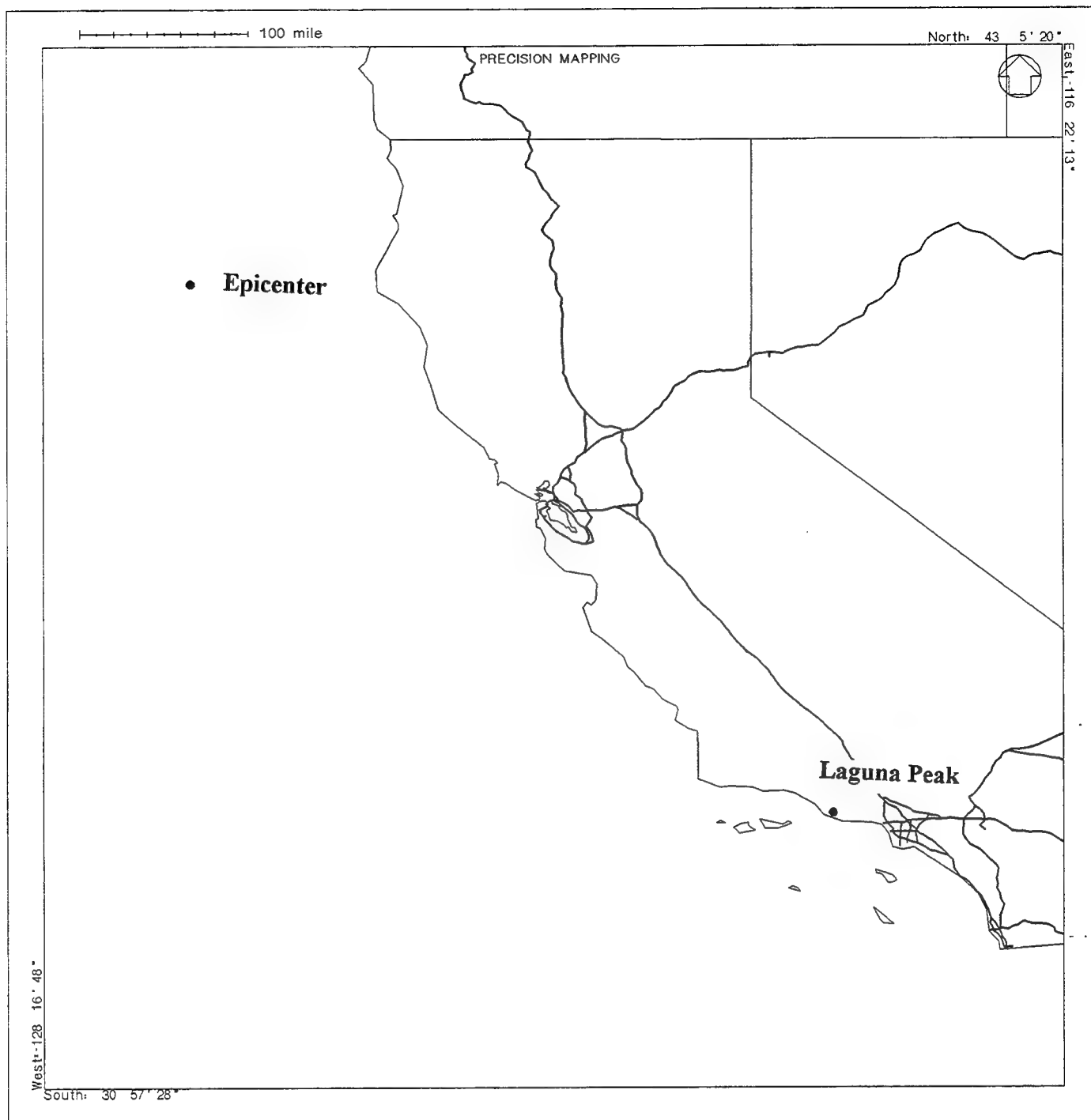
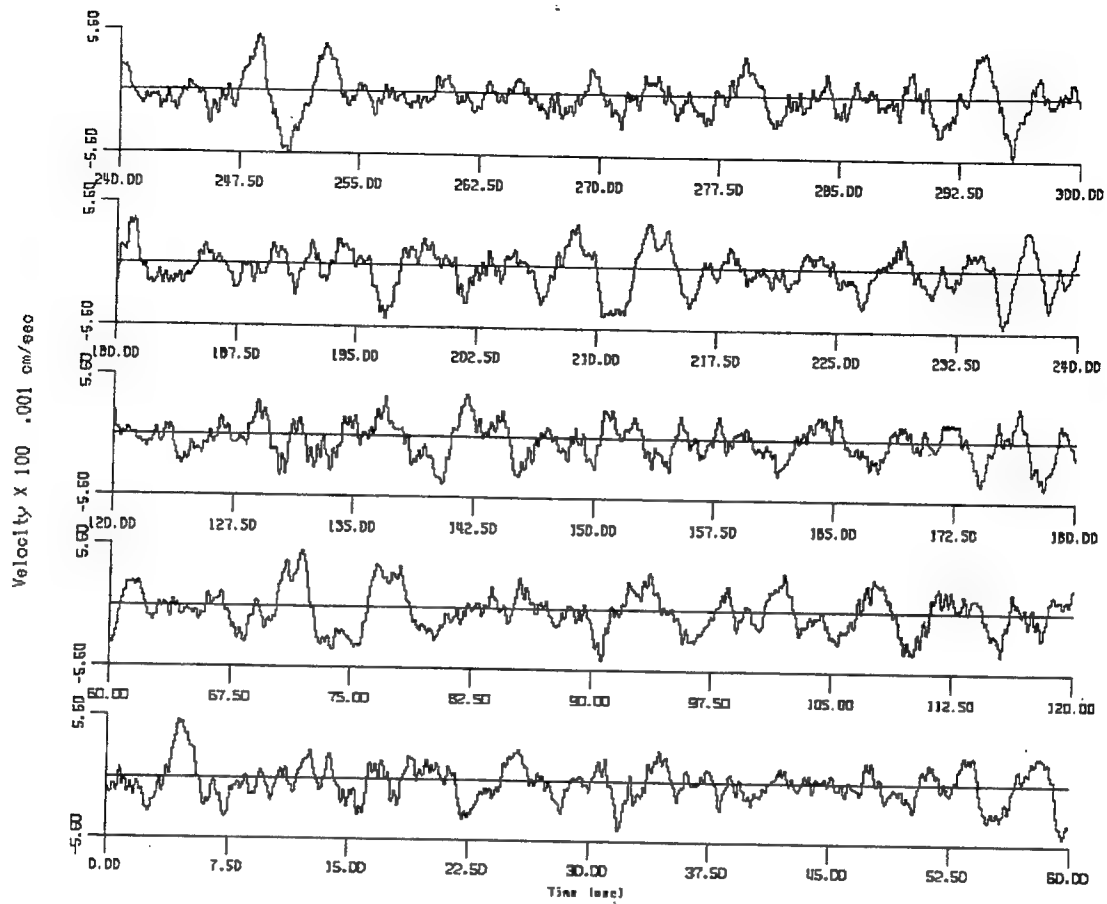


Figure 2.23. Map showing epicenter for Sept 1 1994 Magnitude 7.2 event (N40.45 W 126.36) and Laguna Peak recording station.

LP901E 66 07:00:00 07:05:02 09-01-1994



Peak Velocity 0.000055 cm/sec

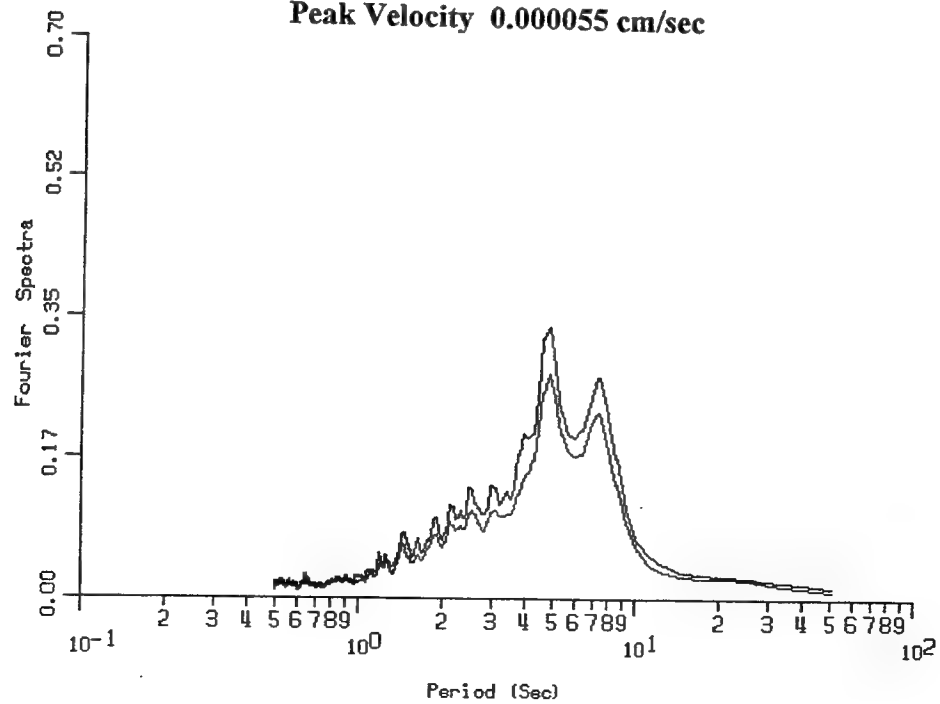
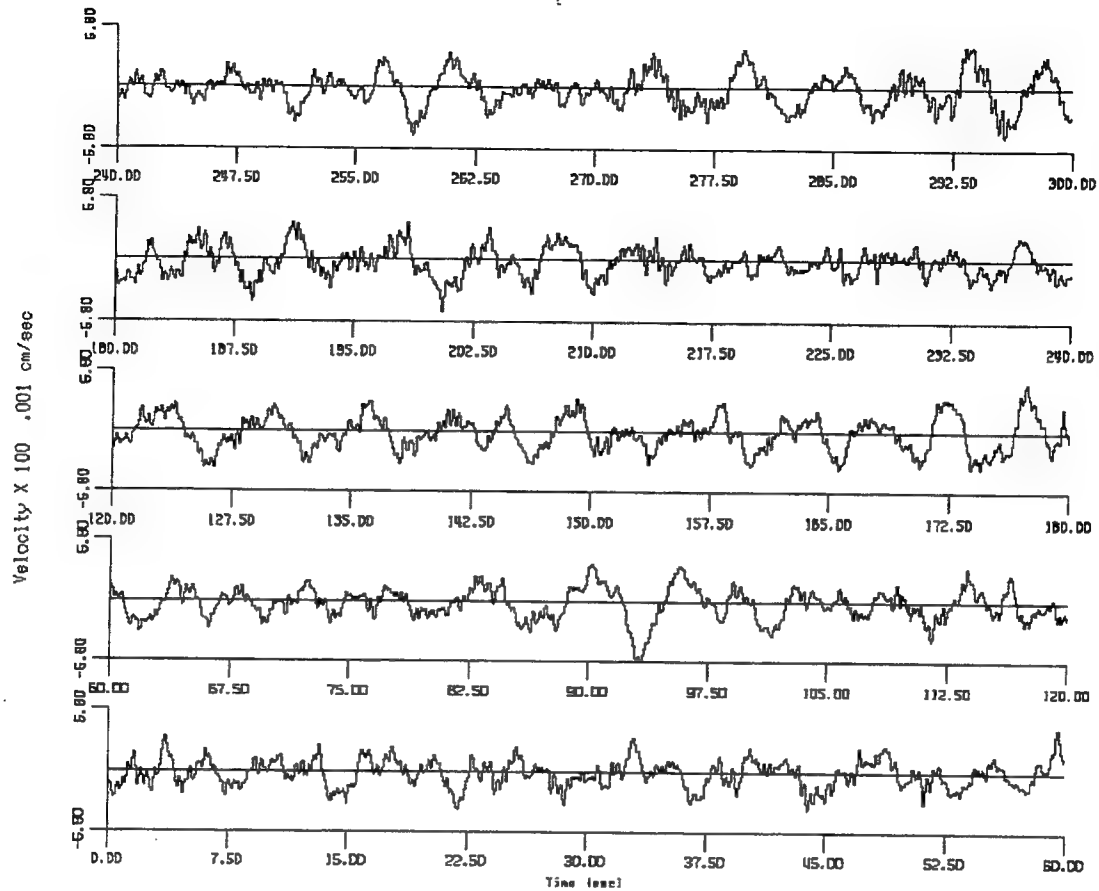


Figure 2.24a. Microseism recording Sept. 1, 1994, Time 07:00.

LP901E 66 07:30:00 07:35:02 09-01-1994



Peak Velocity 0.000068 cm/sec

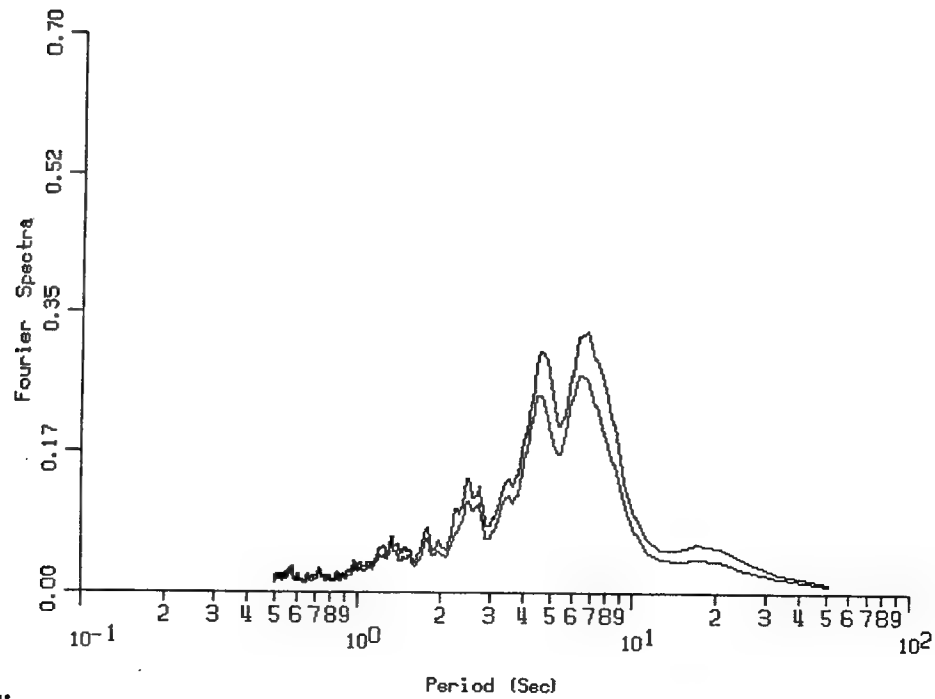
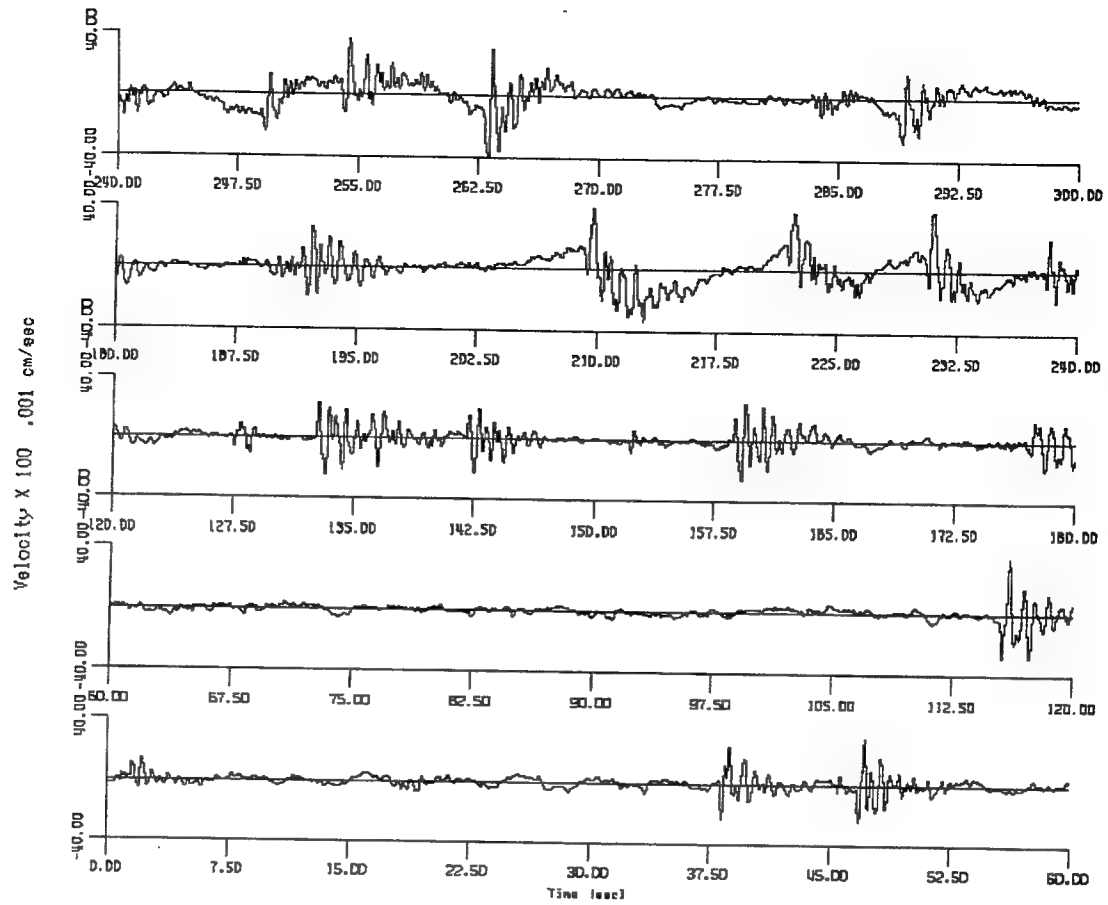


Figure 2.24b. Microseism recording Sept. 1, 1994, Time 07:30.

LP901E 66 07:42:00 07:47:02 09-01-1994



Peak Velocity 0.000400 cm/sec

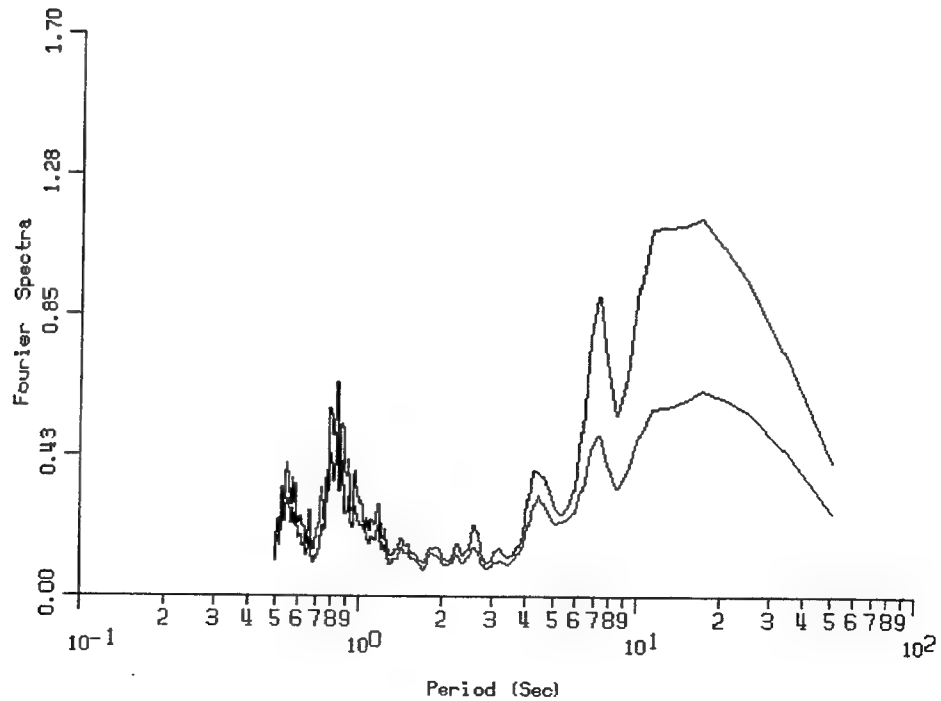
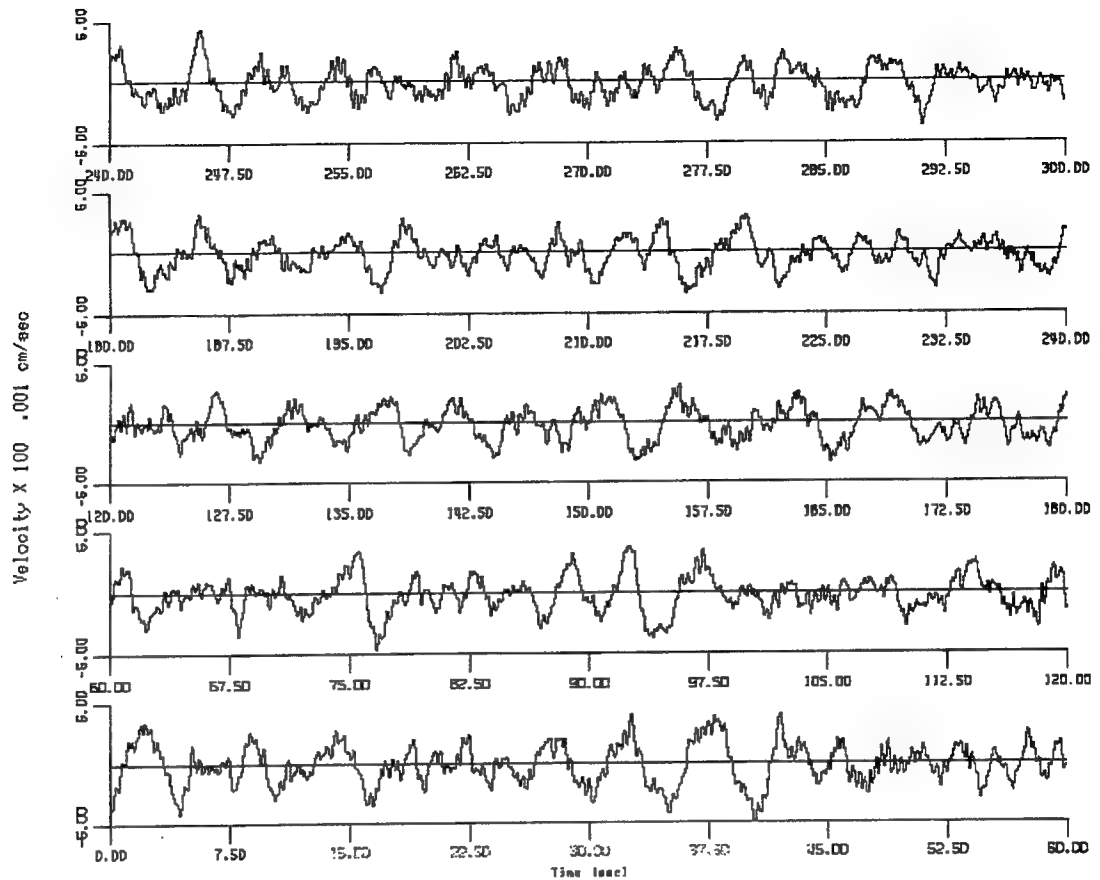


Figure 2.24c. Microseism recording Sept. 1, 1994, Time 07:42.

LP901E 66 08:00:00 08:05:02 09-01-1994



Peak Velocity 0.000060 cm/sec

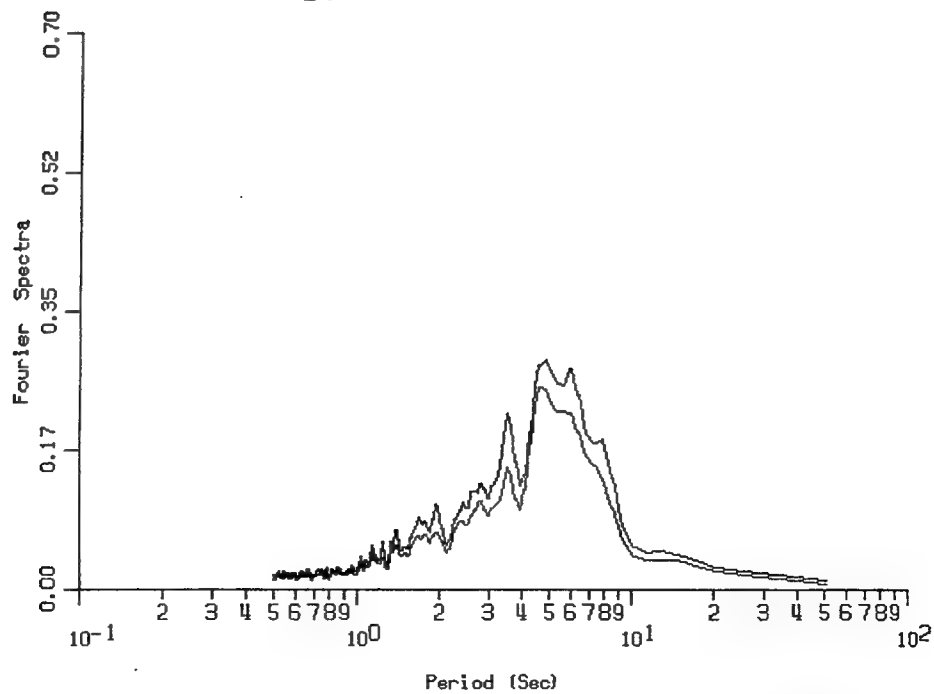
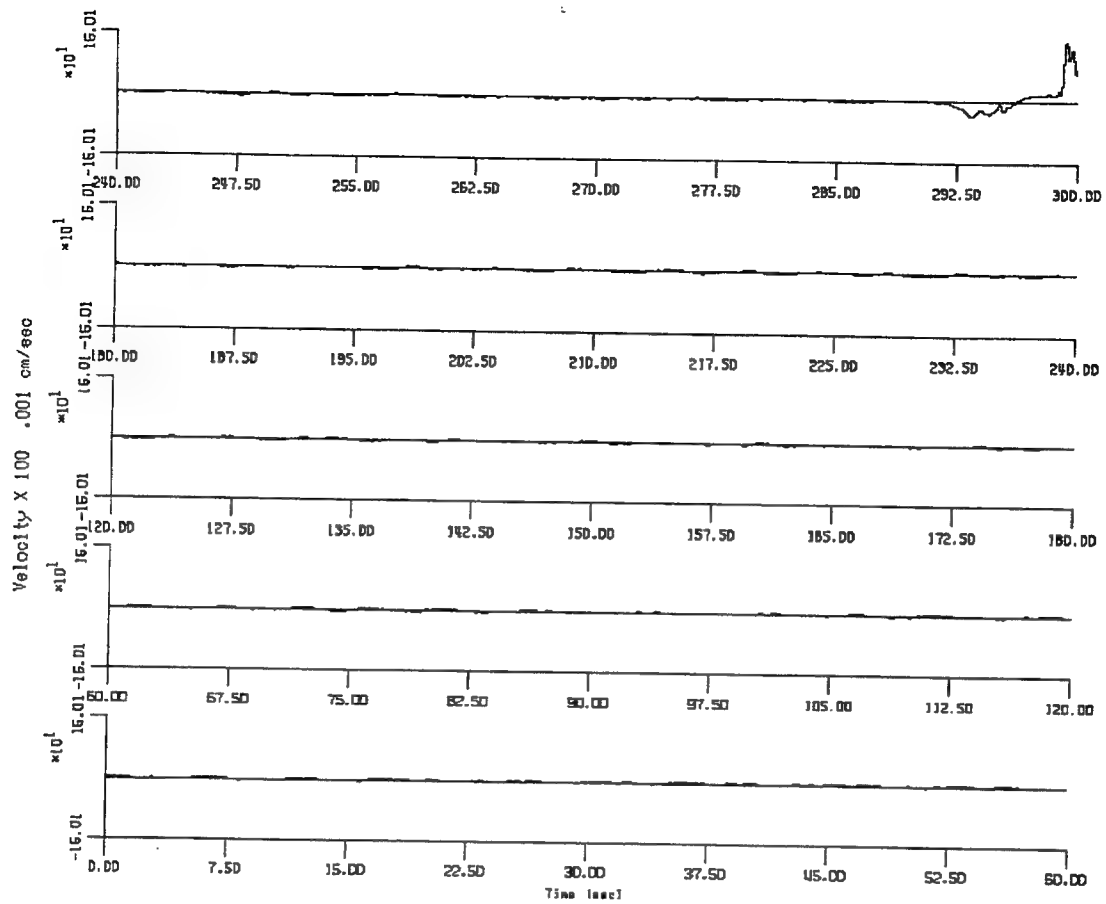


Figure 2.24d. Microseism recording Sept. 1, 1994, Time 08:00.

LP901E 66 08:12:00 08:17:02 09-01-1994



Peak Velocity 0.001601 cm/sec

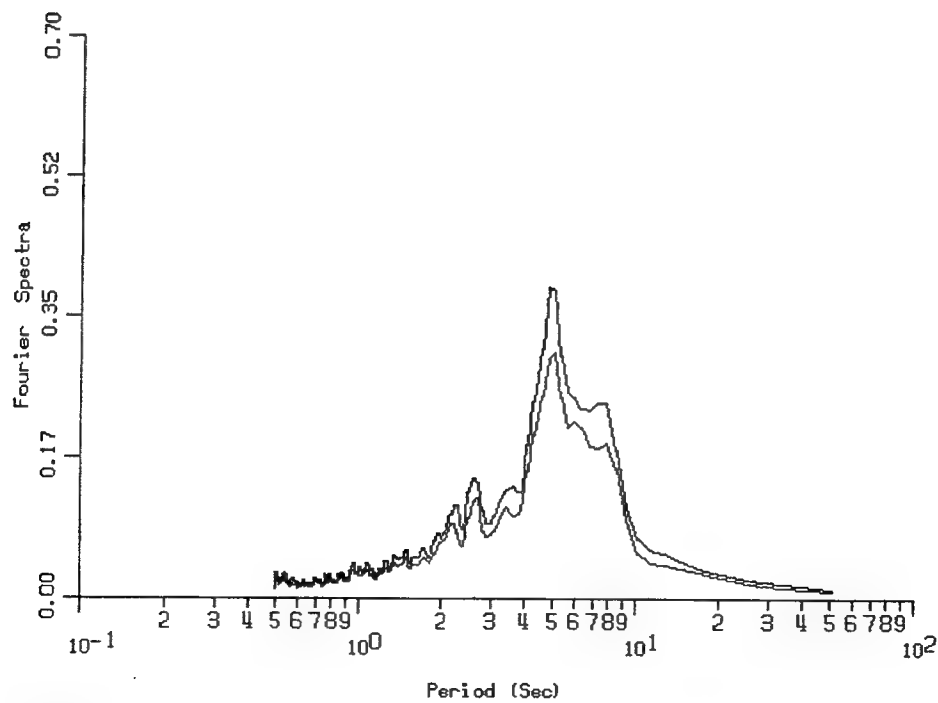
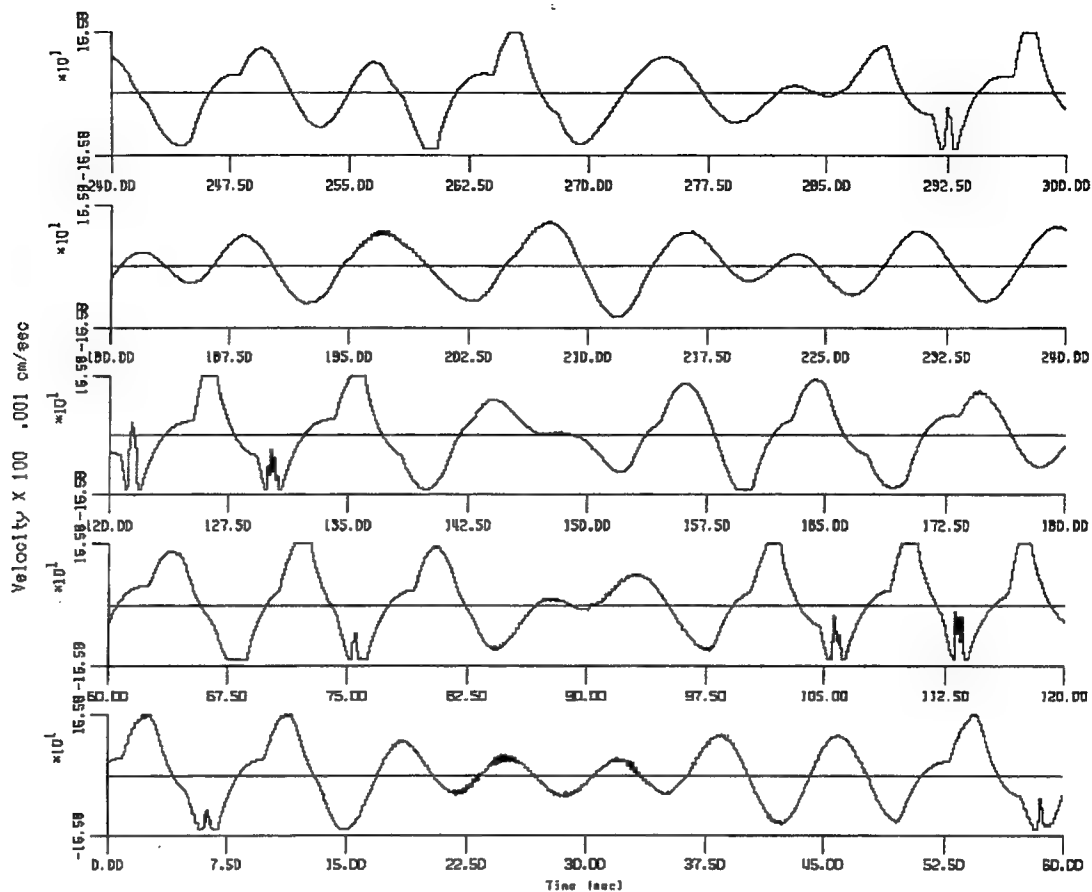


Figure 2.24e. Microseism recording Sept. 1, 1994, Time 08:12.

LP901E 66 09:00:00 09:05:02 09-01-1994



Peak Velocity 0.001658 cm/sec

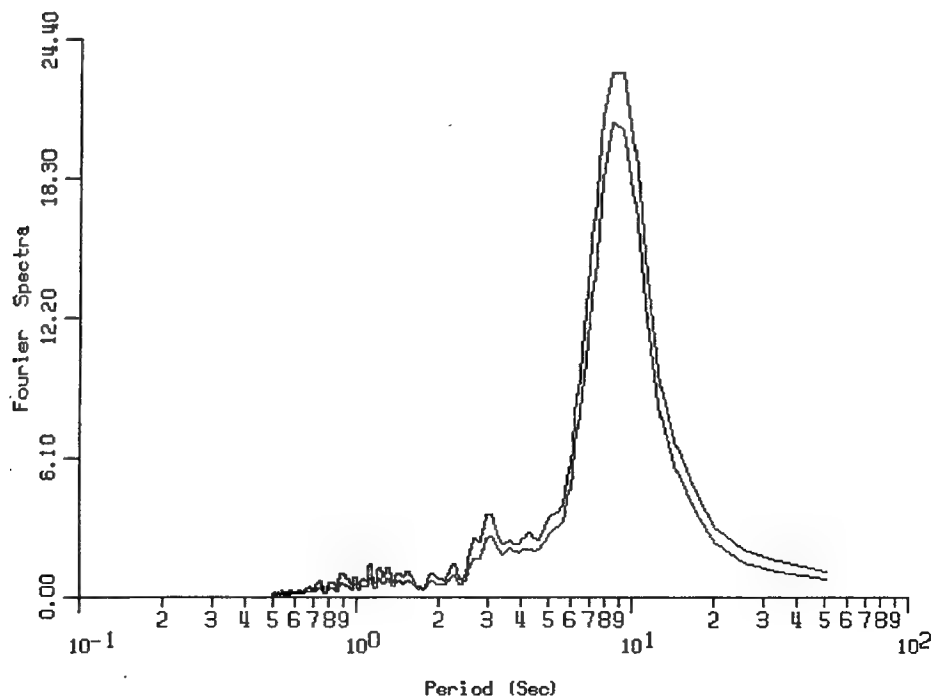
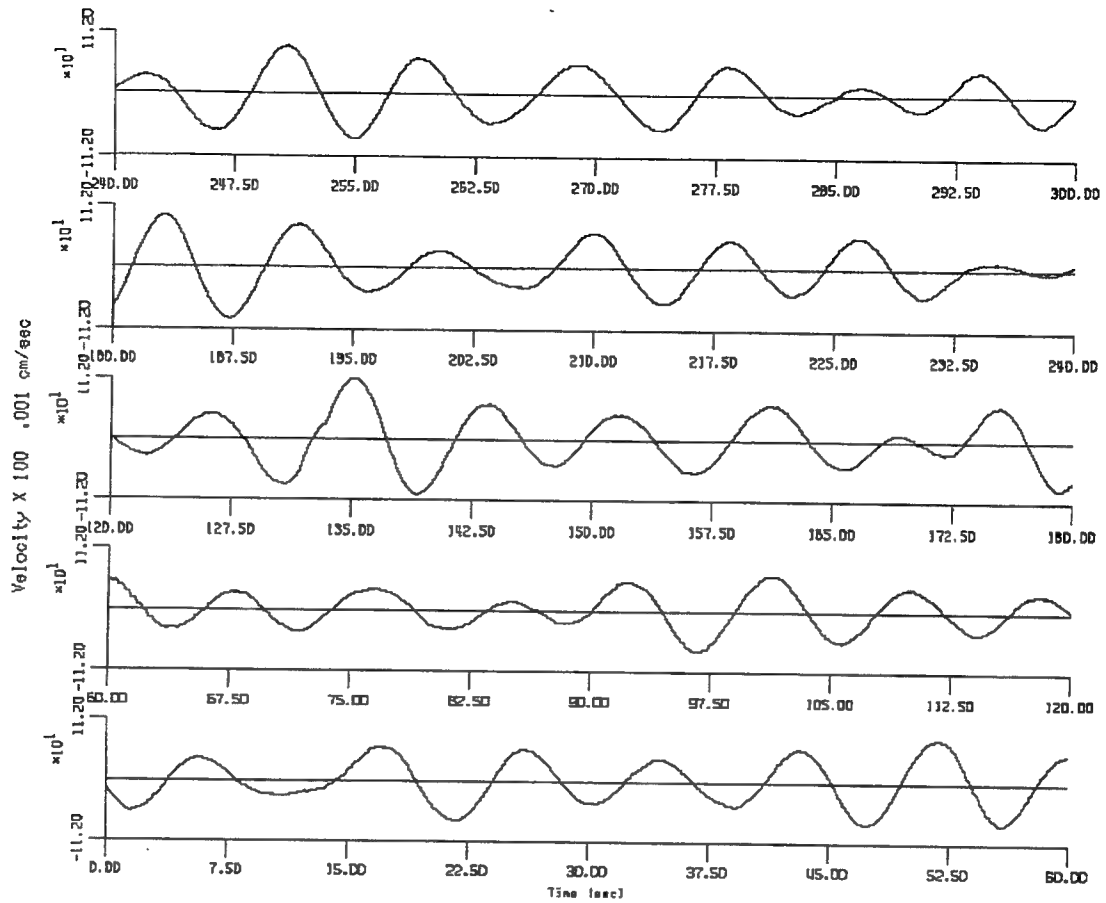


Figure 2.24f. Microseism recording Sept. 1, 1994, Time 09:00.

LP901E 66 09:30:00 09:35:02 09-01-1994



Peak Velocity 0.001120 cm/sec

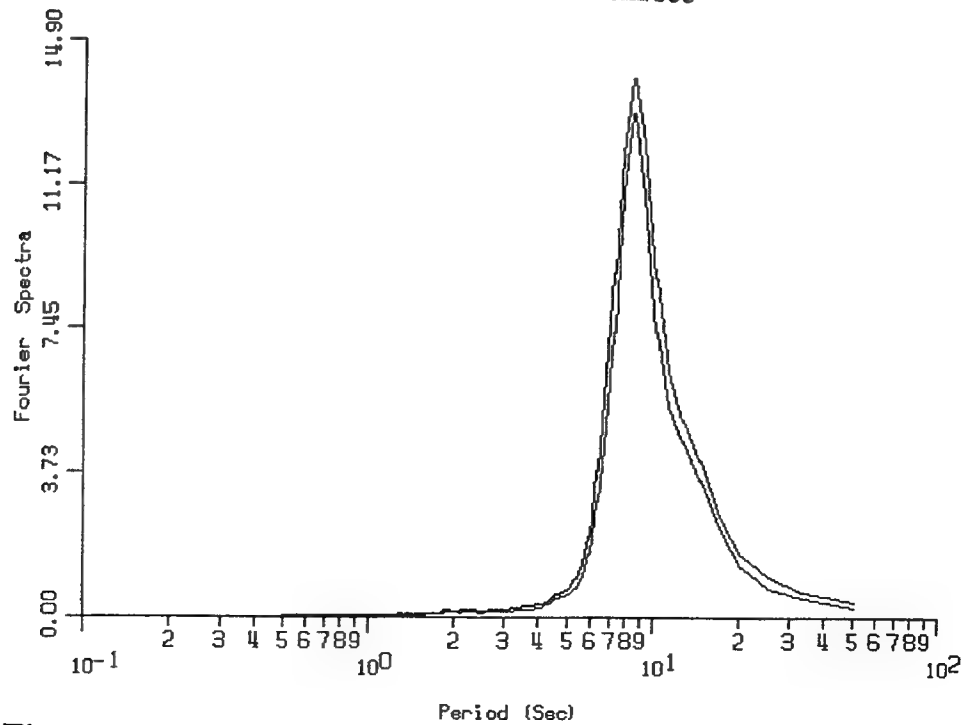
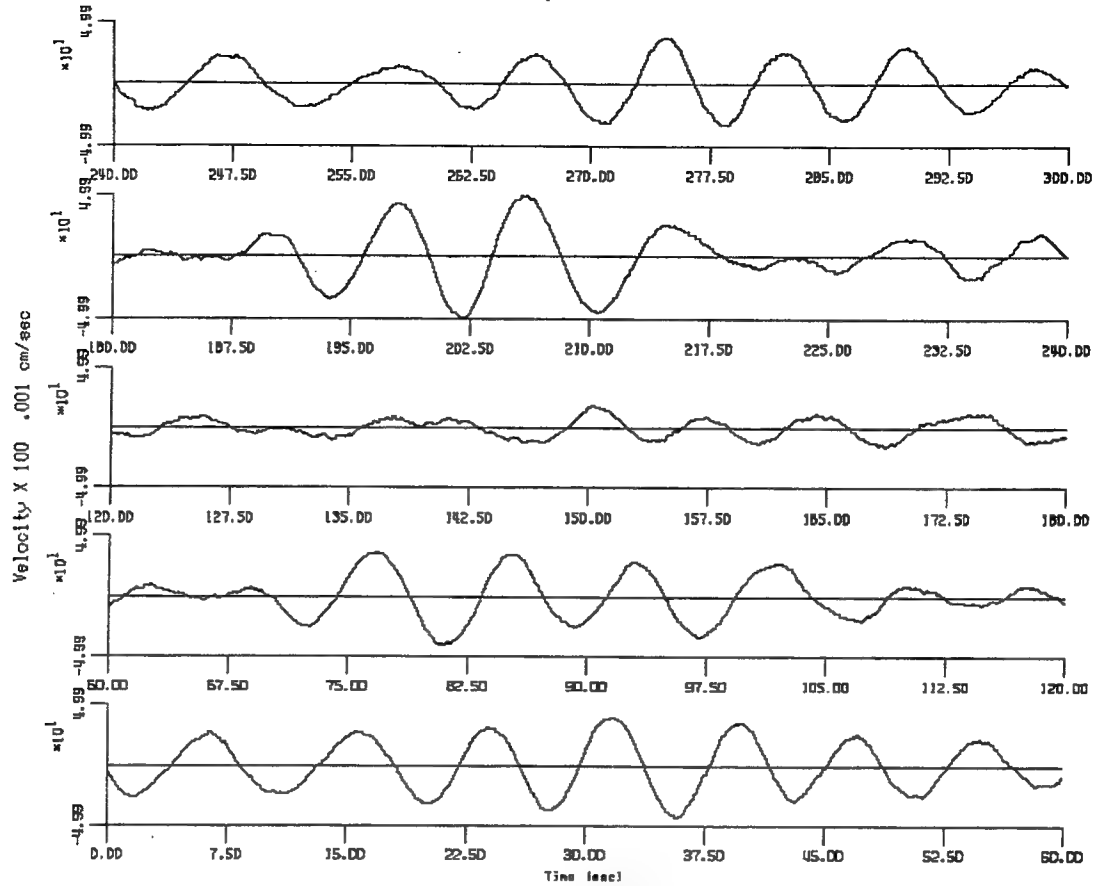


Figure 2.24g. Microseism recording Sept. 1, 1994, Time 09:30.

LP901E 66 10:00:00 10:05:02 09-01-1994



Peak Velocity 0.000499 cm/sec

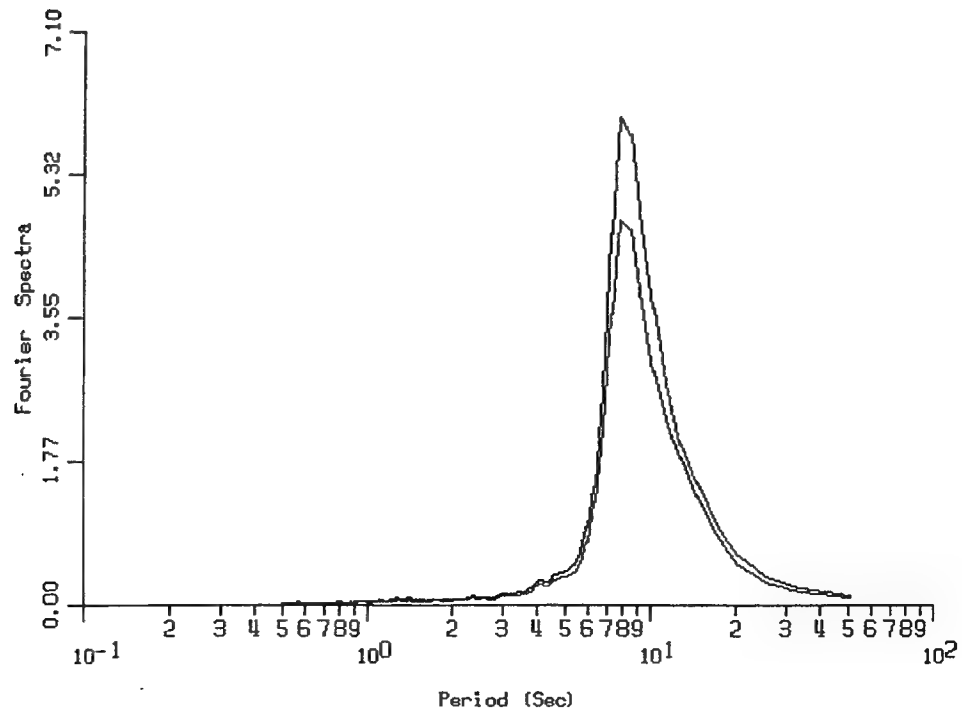
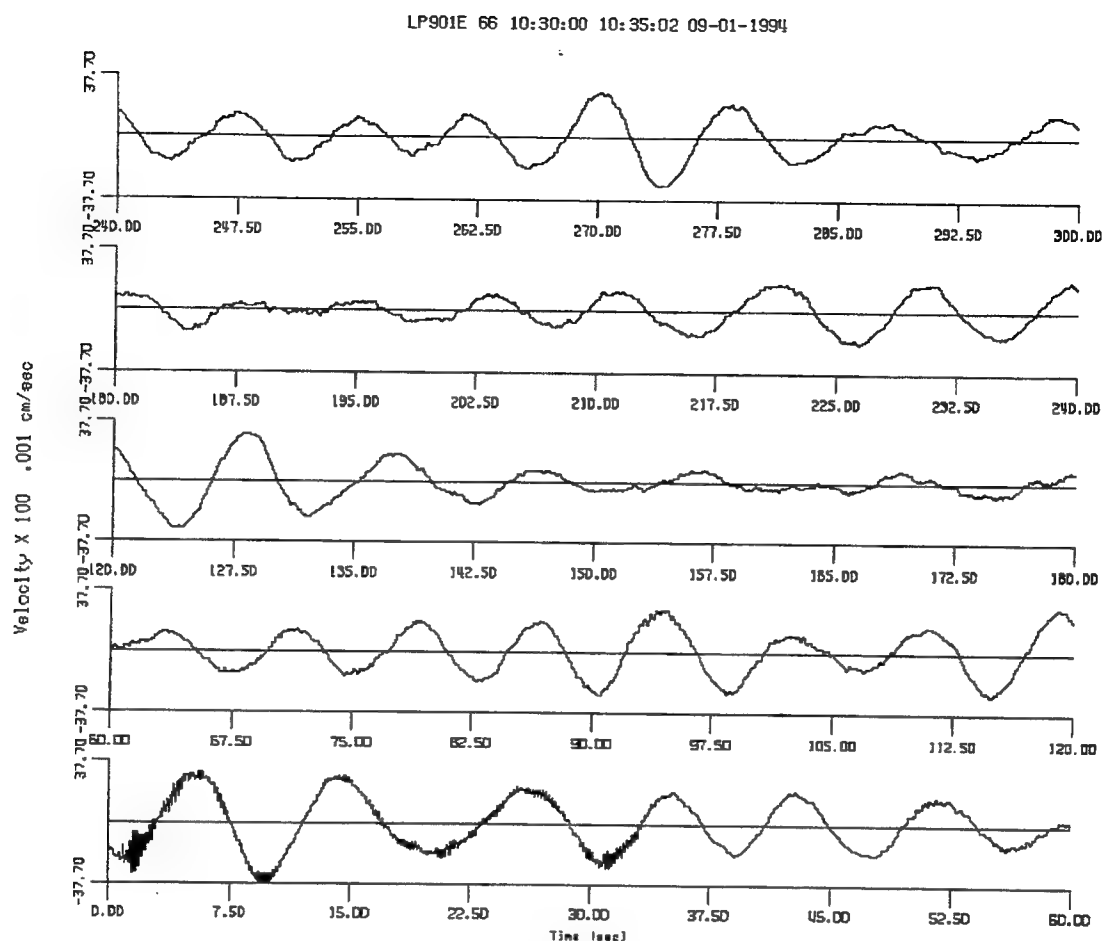


Figure 2.24h. Microseism recording Sept. 1, 1994, Time 10:00.



Peak Velocity 0.000377 cm/sec

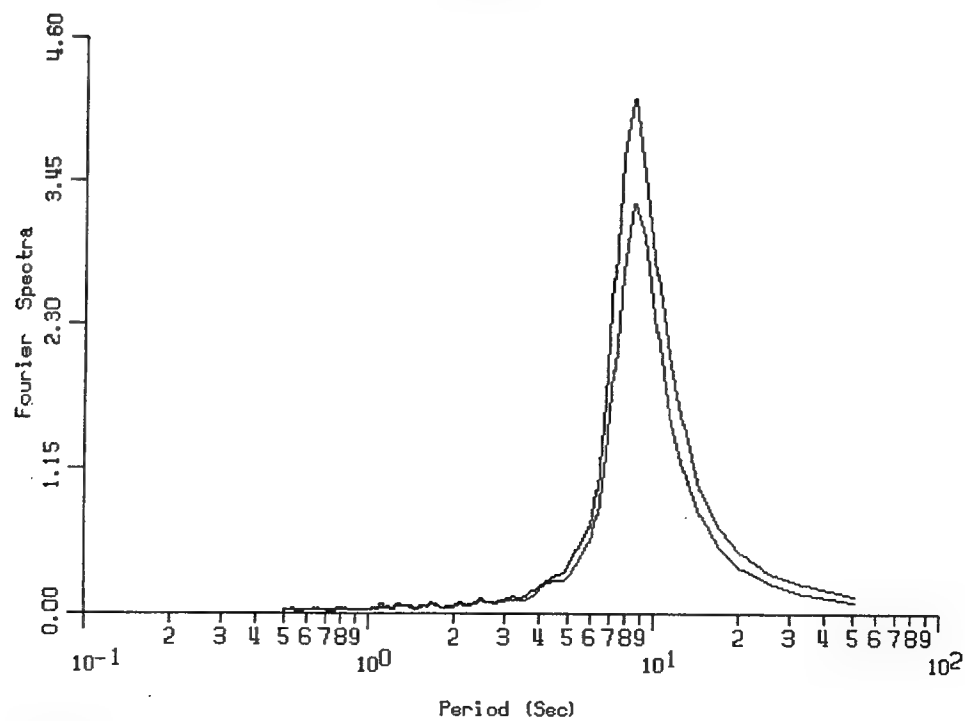
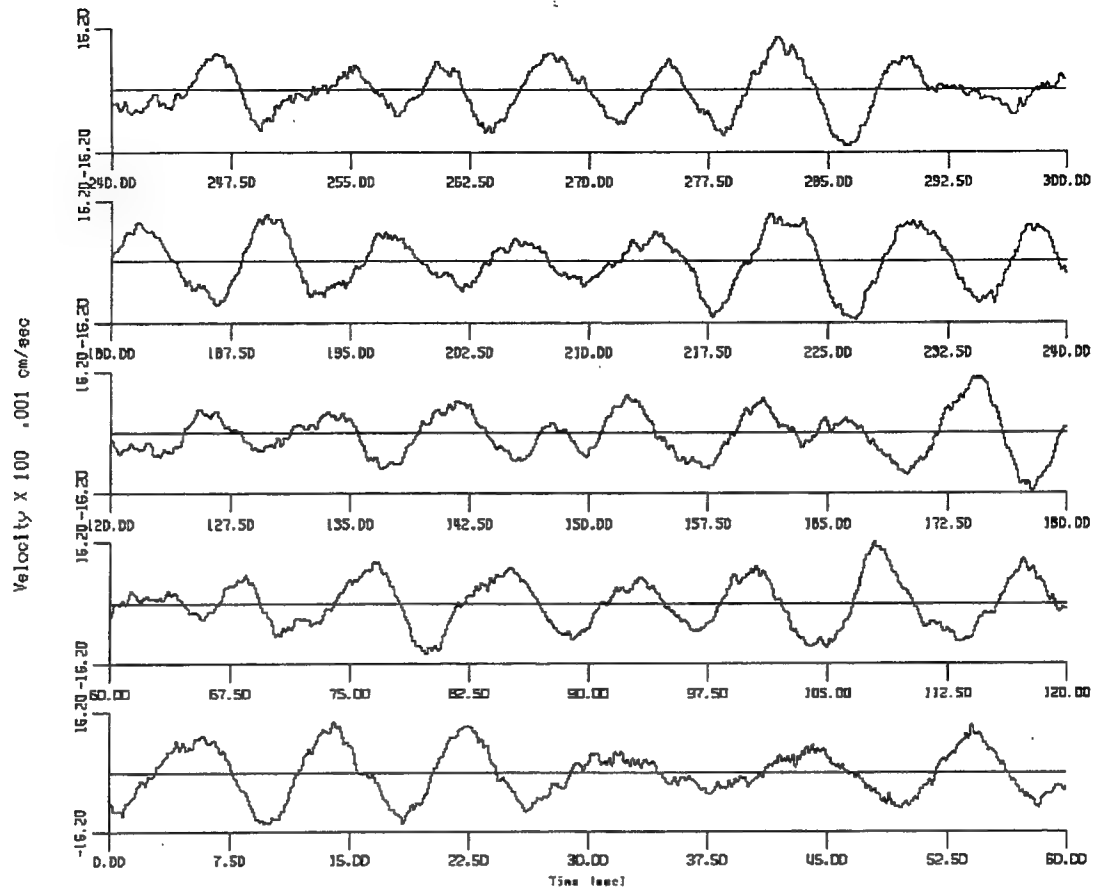


Figure 2.24i. Microseism recording Sept. 1, 1994, Time 10:30.

LP901E 66 11:00:00 11:05:02 09-01-1994



Peak Velocity 0.000162 cm/sec

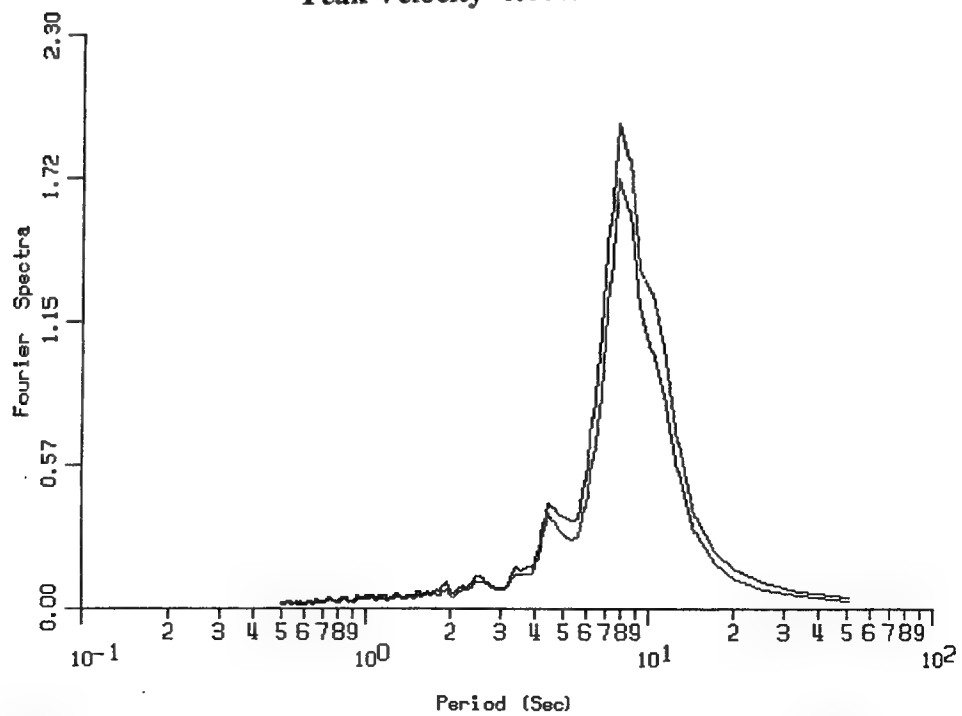
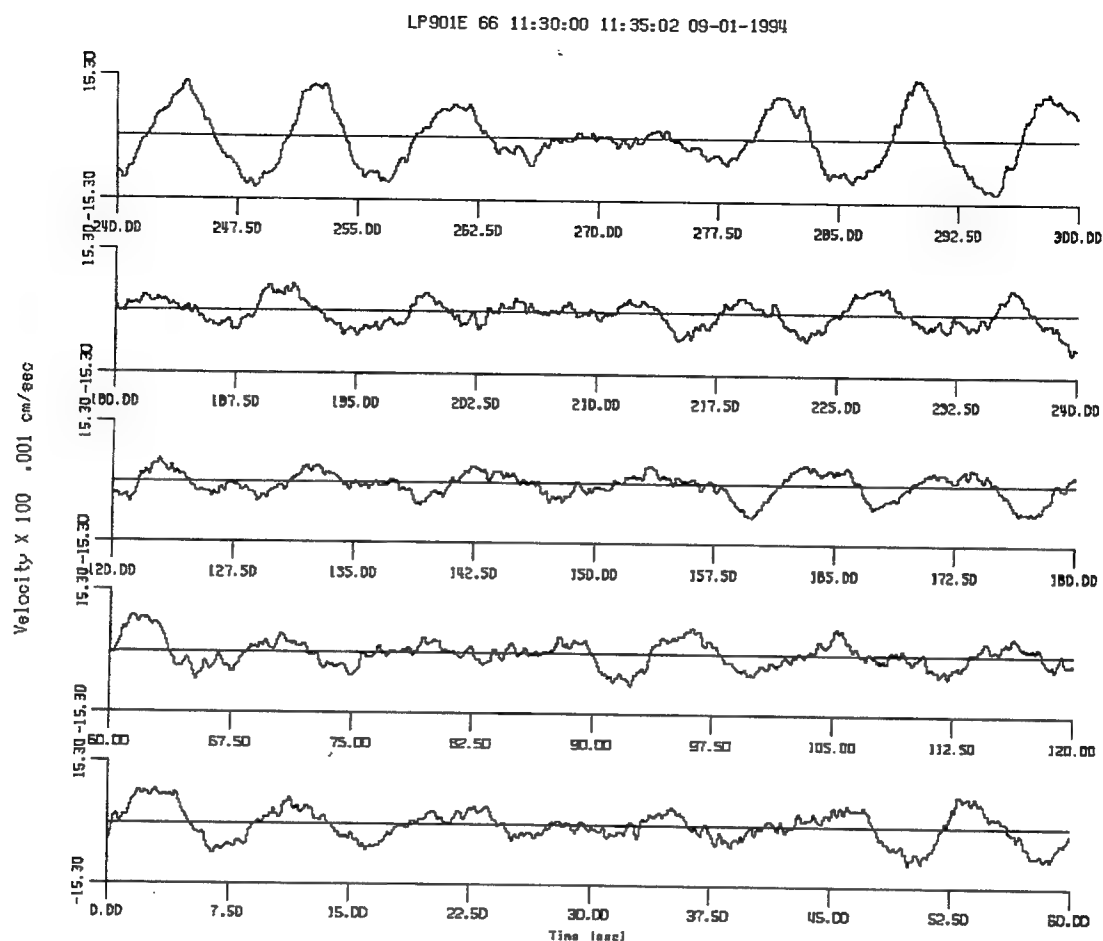


Figure 2.24j. Microseism recording Sept. 1, 1994, Time 11:00.



Peak Velocity 0.000163 cm/sec

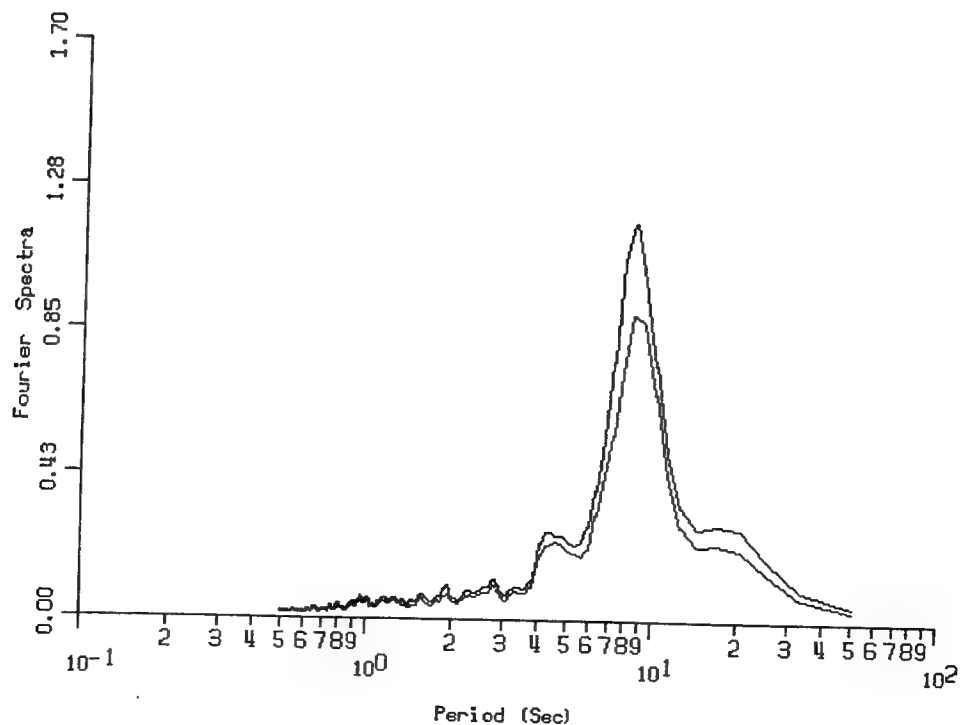
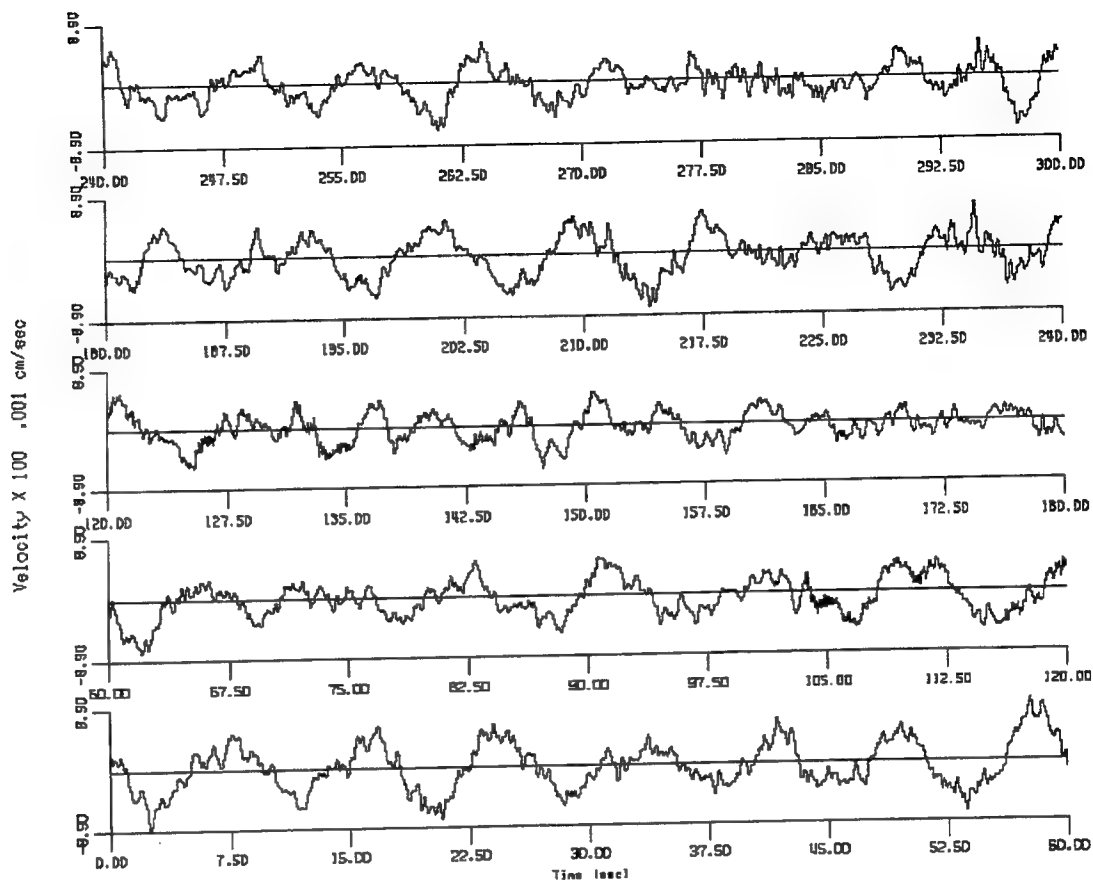


Figure 2.24k. Microseism recording Sept. 1, 1994, Time 11:30.

LP901E 66 12:00:00 12:05:02 09-01-1994



Peak Velocity 0.000083 cm/sec

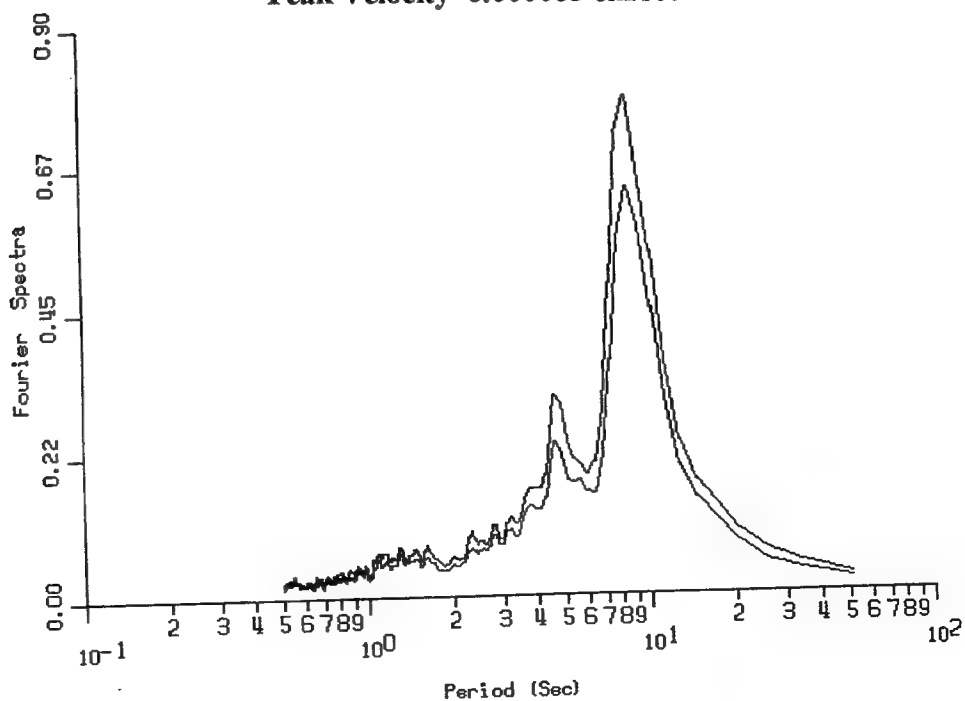


Figure 2.241. Microseism recording Sept. 1, 1994, Time 12:00.

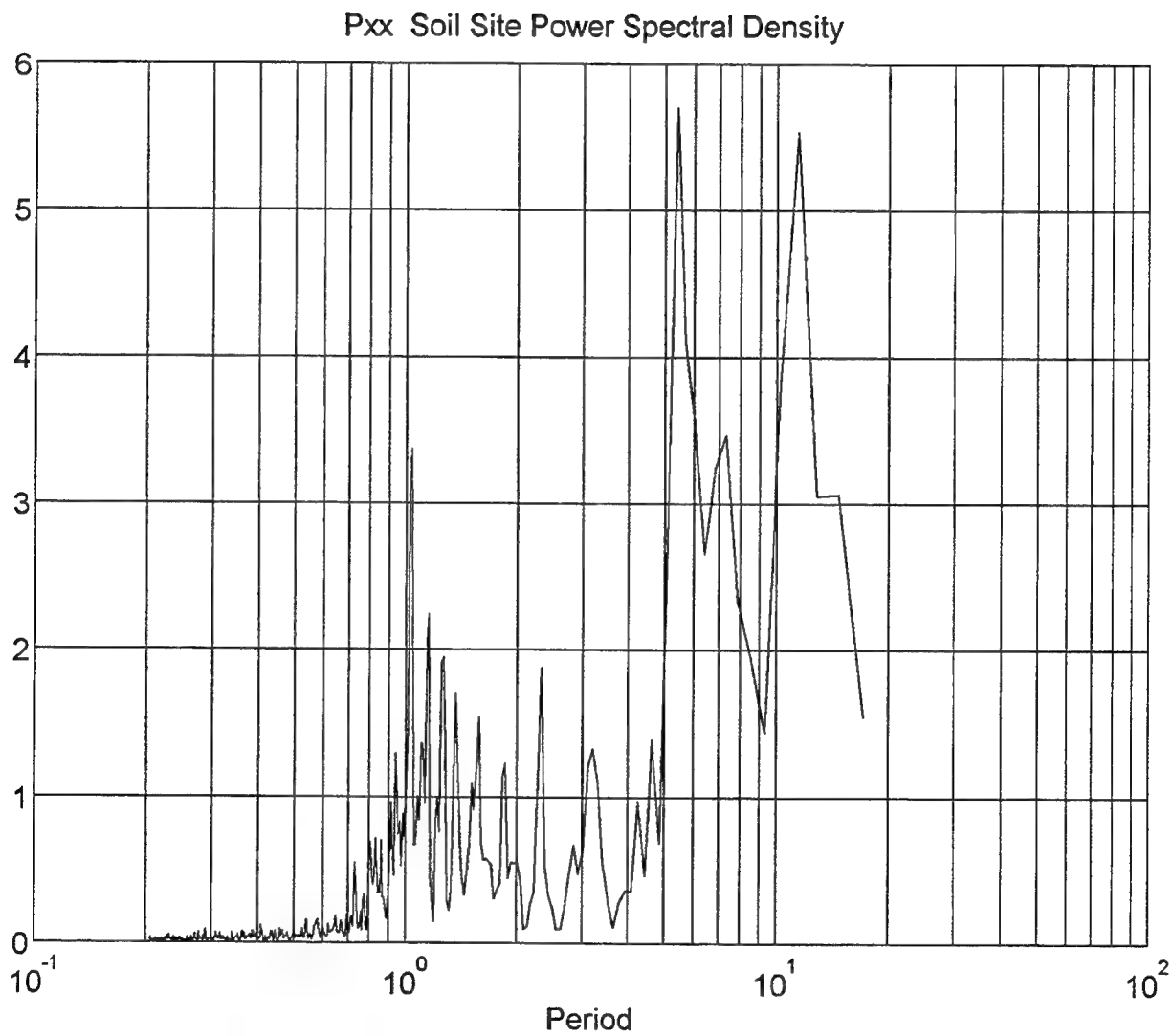


Figure 2.25. Power spectral density.

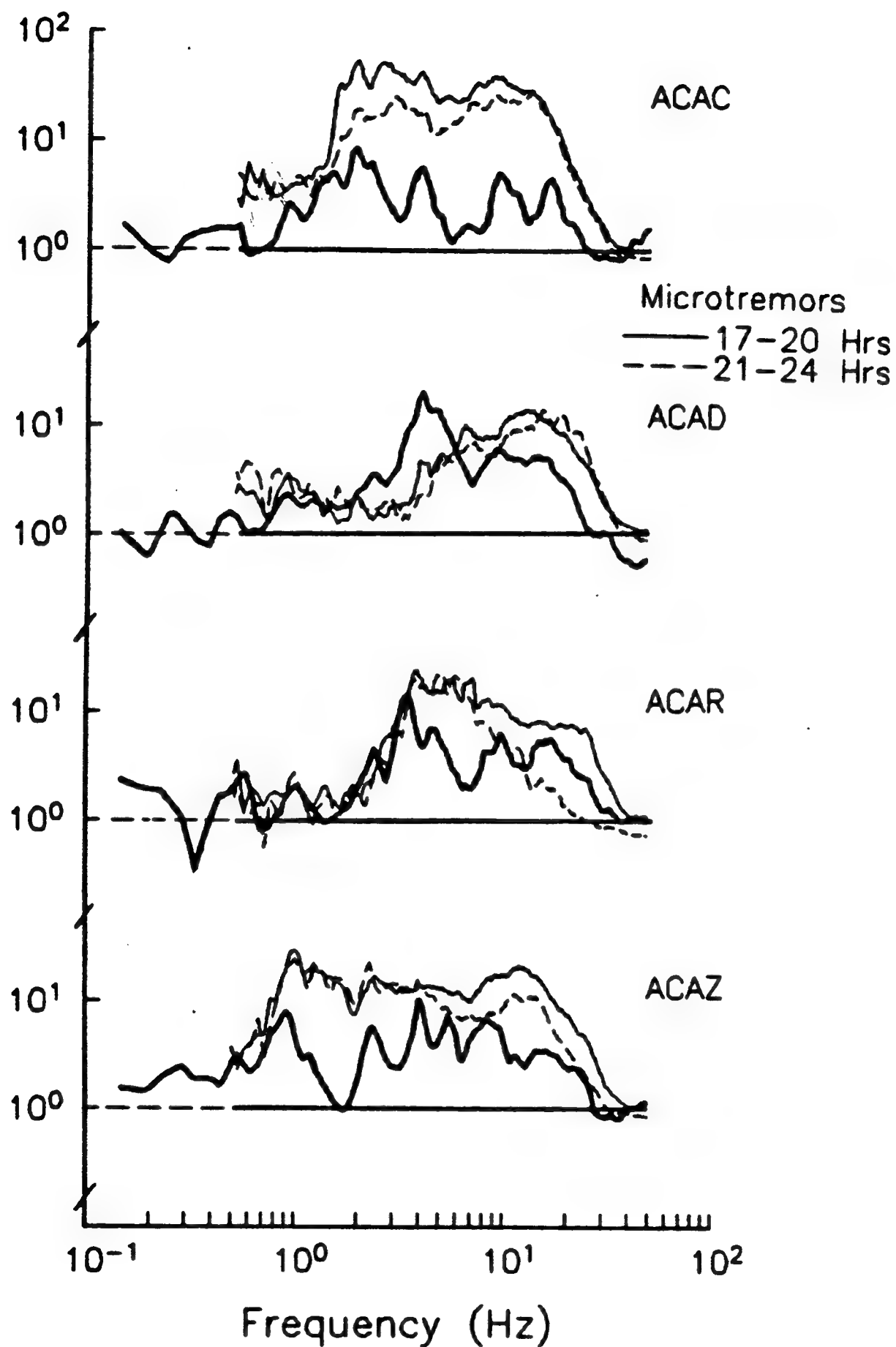


Figure 2.26 Spectral ratio from Gutierrez et al (1992).

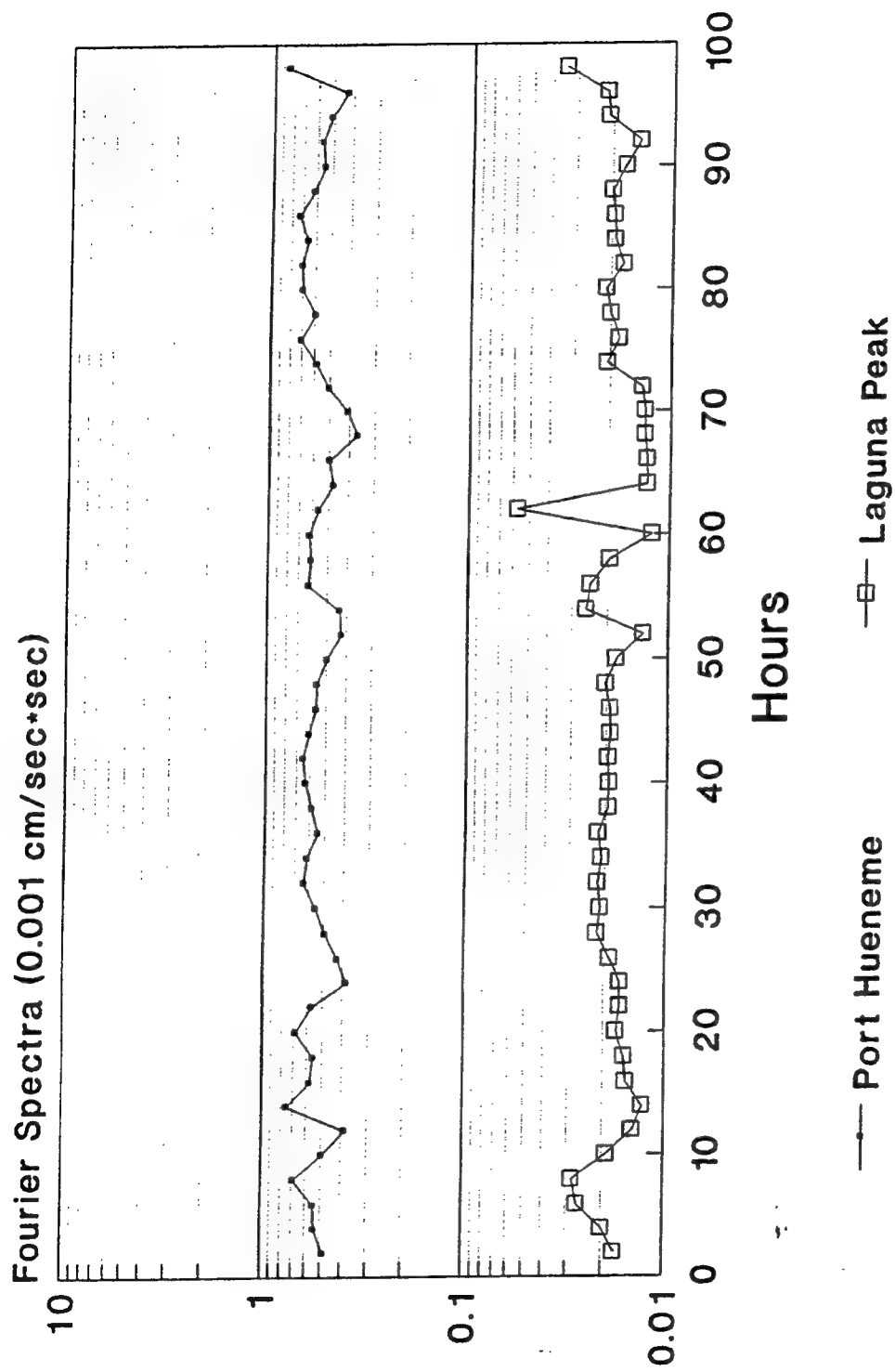


Figure 2.27a Long term measurements, period range 0.5 to 0.7 seconds.

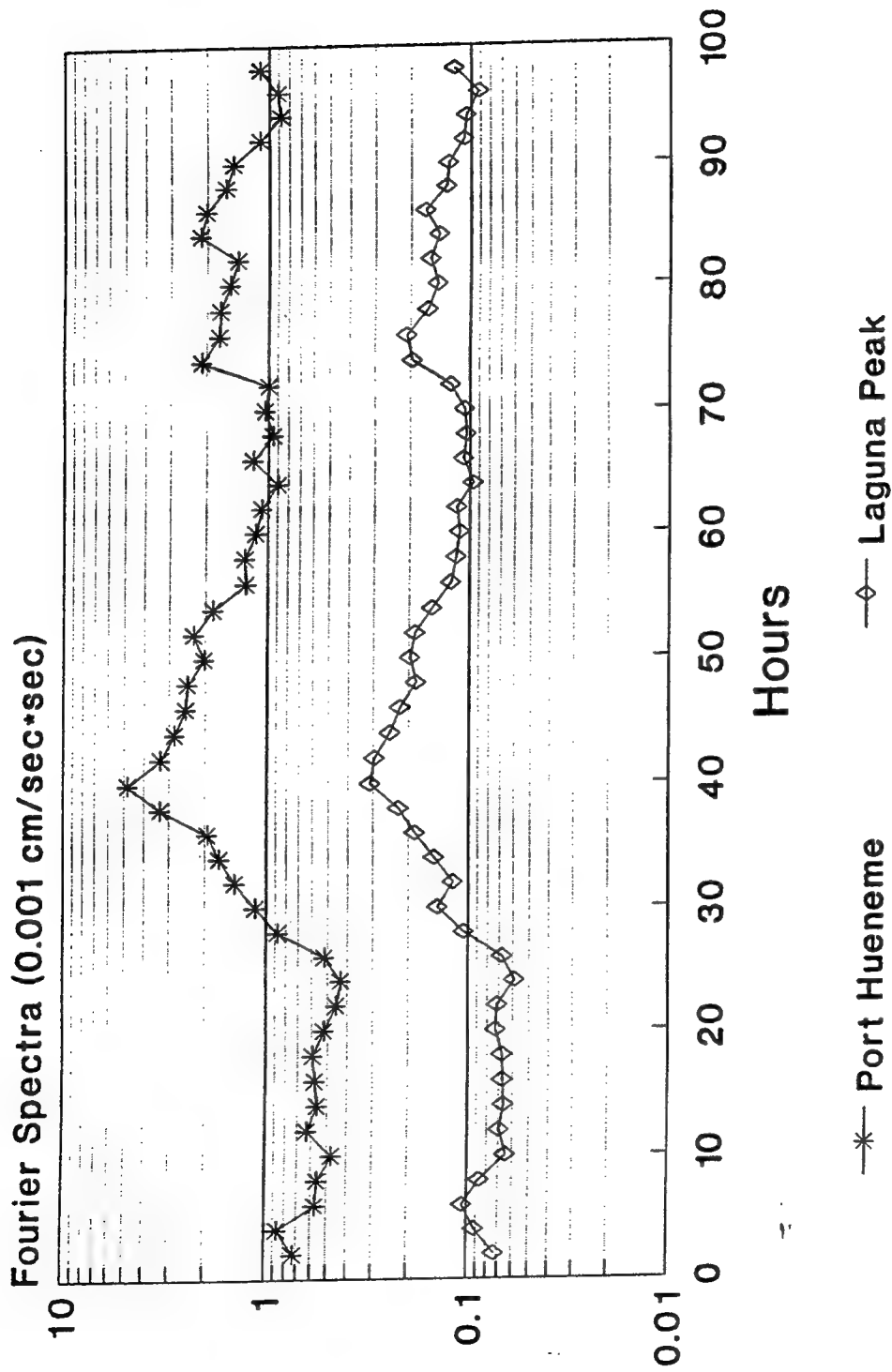


Figure 2.27b Long term measurements, period range 2.0 to 4.0 seconds.

CHAPTER 3: MICROSEISM MEASUREMENT RELIABILITY

Introduction

Previous chapters and a previous report (Ferritto, 1994) discussed the use of microtremors as a tool to assist in prediction of ground motion amplification and microzonation. This chapter will discuss tests conducted in the Port Hueneme area to investigate the convergence of the measurements and their repeatability. Understanding the regional geology is fundamental to selection of an appropriate reference site and correct interpretation of the microseism results. The following sections will briefly discuss the region and then present the series of microseism measurements performed.

The following section is based directly on California Mines and Geology Open File report 76-5 and Majors Engineering (1993). The Oxnard Plain is in the southwest portion of the Ventura Basin, a part of the Transverse Range Geomorphic Province. The area is a structural feature formed by tectonic compression and consists of a synclinal basin with a substantial depth of recent alluvium overlying older rock. It extends inland from the coast along the northwestern edge of the Santa Monica Mountains, merging into the Las Posas and Pleasant valleys, and abuts the Camarillo Hills and South Mountain. It is a flat alluvial area rising in elevation from sea level to about 100 feet (30 m). "The geology underlying the Oxnard Plain are nearly 45,000 feet (14,000 m) thick consisting of Upper Cretaceous, Tertiary and Quaternary age components which have been deposited on a pre-Upper Cretaceous base of igneous and/or metamorphic rocks. The sedimentary measures are largely of marine origin with locally abundant volcanic and continental deposits." Figure 3.1 shows the geologic time scale, CDMG (1969). The Oxnard Plain represents an ancient delta of the Santa Clara River and was formed at the end of the last glacial epoch which resulted in the surface sediments being interlayered sands, silts and clays. The San Pedro Formation of Lower Pleistocene age is encountered at a depth of approximately 400 feet (120 m). Igneous and metamorphic rock are believed to be at depths of 6,000 feet (1800 m) or more.

The Quaternary sediments underlying the Oxnard Plain are about 3,400 feet (1,000 m) thick in the area near the Naval Construction Battalion Center (NCBC), Port Hueneme. The youngest of the Quaternary sediments are composed of loosely to poorly consolidated Holocene (recent less than 10,000 years old) materials deposited during the post-glacial period of rising sea level and include marine, lagoonal, lacustrine, fluvial-flood plain, deltaic and eolian environments. These materials consist of sand, gravel silt, clay, mudstone, local regions of cobbles and boulders, and occasional regions of lenses of peat, carbonaceous material and sea shells. Figure 3.2 shows the southern end of the Oxnard Plain showing contours of depth of Holocene sediments and areas where peat or similar vegetal material may exist. Figure 3.3 shows the Port Hueneme area geologic description and Figure 3.4 shows surface soil classification. Figure 3.5 shows the geologic cross section through Port Hueneme.

As a sedimentary rock becomes older and more deeply buried it becomes more dense and less subject to ground motion amplification. Figure 3.6 shows the local geology for the closest rock outcrop area. The CDMG (1976) categorized the geology in terms of age of deposit. Category A consists of landslides, Category B represents younger alluvium, Category C older alluvium, Category D includes poorly lithified and slightly older formations, Category E includes moderately lithified slightly older formations and Category F represents the firmest or most dense rock. Within this region it includes volcanic rocks, igneous-metamorphic rock and usually the oldest and firmest and densest sedimentary rocks.

CDMG (1976) developed boring logs shown in Figure 3.7. The soils in the region are composed of fill over mostly sand with clay interbeds and is interpreted as alluvium of Holocene age deposited at sea level in a stream channel or lagoonal setting. The water table is at a depth of about 6 feet. Figure 3.8 shows the NFESC site and Figure 3.9 presents a typical boring log from T.K Engineering (1986).

Array Measurements NFESC Site

This study repeats measurements made in a previous study (Ferritto, 1994) to investigate the error bounds and measurement stability. The same soil and rock locations were used herein. As stated above, the rock reference site used for this study was Laguna Peak which is a mountain top location shown in Figure 3.6 having middle Miocene Topanga Formation sandstone siltstone and conglomerate overlain by a thin layer of alluvial deposit. The site is classified a DE transition zone with the composition similar to the San Pedro Formation beneath the Oxnard Plain. A number of soil sites shown in Figure 3.8 were selected in the NFESC compound for array measurements. Building 3007 close to the boring log location was selected as a soil reference site. To determine the spatial variation of amplification at the NFESC site, a series of sequential measurements were made at stations A1 through C4. Measurements were made for 5 minute duration at each station and all measurements were completed in about 3 hours. The measurements were made simultaneously at the soil site, the soil reference site and the rock reference site. Based on conclusions shown in Chapter 2 concerning delays in recording site and reference signals, the data recording software was modified to permit the unattended simultaneous recordings at the reference sites and is a significant difference from the procedures used previously (Ferritto, 1994) which recorded reference measurements at 30 minute intervals.

The data were recorded for 5 minutes at a 20 Hz sampling rate and the seismometer amplifiers were set to attenuate signals outside the band of 0.1 Hz to 2.5 Hz. Fourier spectra were computed based on the average of 20 overlapping samples. Spectral ratio were computed by dividing the soil spectra by the rock reference spectra using a 7 point triangular smoothing algorithm. The spectral ratios were then divided into period segments of interest for comparison. The process of measurements was repeated and a series of data assembled. Contour plots showing individual measurements and a 3 measurement average are shown in Figure 3.10. Individual measurement were seen to

vary as much as ± 30 percent.. Figure 3.11 presents the average of another set of 3 measurements and Figure 3.12 presents an average of 7 measurements. With the error level in mind, we note a general consistency in the data between group averages. The site is a relatively uniform site and thus there is not major variation in values as might be observed had other geology been present. A small variation in values can sometimes alter the contour shapes significantly; this is a limitation inherent in the contouring algorithms. A 3 to 5 sample average is thought to be capable of presenting a good representation of the site.. It should also be obvious that a single sample contour can be misleading.

It must be recognized that contour plots are an attempt to give a spatial representation of the variation of spectral ratio. The spectral ratio is a function of period and must be divided into bands for representation. There is subjectivity involved in the presentation of the data using contour plots. First the division of spectral ratio into bands is judgmental and second the representation of the data in each band varies in amplitude. One might choose to average the data within a band or perhaps to plot maxima for each period band. The reader should be aware that the contour plots have limitations and are only expressions of the data. Each spectral ratio is a unique complete transfer function which shows how one site responds relative to another. The spectral ratio contours are intended to facilitate location of soft spots where amplification is greatest.

From the contours it is noted that the NFESC site does have variation of about ± 20 percent. This is thought not to be a major variation and should be expected at a waterfront site. Figure 3.13 shows the error convergence using the seven sample average as the basis for comparison. The figure shows the average error and the upper bound error which might occur at any one station. Use of a five sample ensemble for this case would seem to keep error below 10 percent

Soil Reference Site

It is often not possible to find an accessible rock reference site near Navy bases; thus, the use of a soil reference site would be of major utility. A previous report, Ferritto (1994), presents an extensive discussion of Japanese research and their use of soil reference sites. The array measurement data discussed in the previous section was used to develop spectral ratios relative to the soil reference site near the boring logs shown in Figure 3.8.

It is important to keep in mind that all of the measurements and contours are relative to the soil response at the soil reference site. Figure 3.14 shows that relationship for a typical soil site of interest. Spectra for the soil site, the rock reference site and the soil site of interest are shown. Spectral ratios are then constructed using the rock and soil reference sites. Comparing the spectral ratios in Figure 3.14, we note they are substantially different not only in magnitude but also in shape. This is derived from the fundamental differences in rock and soil reference site response. The soil site of interest relative to the rock site shows high amplification (30 to 40s) at some period ranges and lower at others based on the relative frequency component amplification between rock and

soil. The soil site shows amplification of between 0.8 and 1.8 relative to the response of the soil reference site. Periods where amplification was high relative to the rock reference site do not necessarily have any relation to the same location relative to the response of the soil reference site. Thus in looking at contours of amplification from each measurement comparison of the soil site response relative to rock and the soil site response relative to the soil reference site can only indicate the same general shape of response but not have a fixed numerical relationship. For the soil reference site to be useable we would expect that the contours derived from the measurements relative to the soil reference site look like those of the contours of measurements relative to the rock reference site. To examine the results 3-dimensional surface plots were made of the average of 7 measurements made on the array shown in Figure 3.8 using the Laguna Peak rock reference site and the soil reference site near the boring log. Figure 3.15 presents the data for the rock reference site and Figure 3.16 the data for the soil reference site. There is a very good correlation of the general shape of the surfaces giving credence to the use of soil reference sites.

Eras	Approximate age (in millions of years)	Subdivisions	Approximate duration (in millions of years)
Quaternary	.01	Recent	.01
		Pleistocene	3
Tertiary	3	Pliocene	9
	12	Miocene	13
	25	Oligocene	15
	40	Eocene	20
	60	Paleocene	10
	70	Cretaceous	65
	135	Jurassic	45
Mesozoic	180	Triassic	45
	225	Permian	45
	270	Carboniferous	80
Paleozoic	350	Devonian	50
	400	Silurian	40
	440	Ordovician	60
	500	Cambrian	100
	600		
Precambrian		Worldwide subdivisions not well established	2800 +
Oldest rock dated 3.5 billion Age of the earth 4.5 billion			

Figure 3.1 Geologic Time, from CDMG (1969)

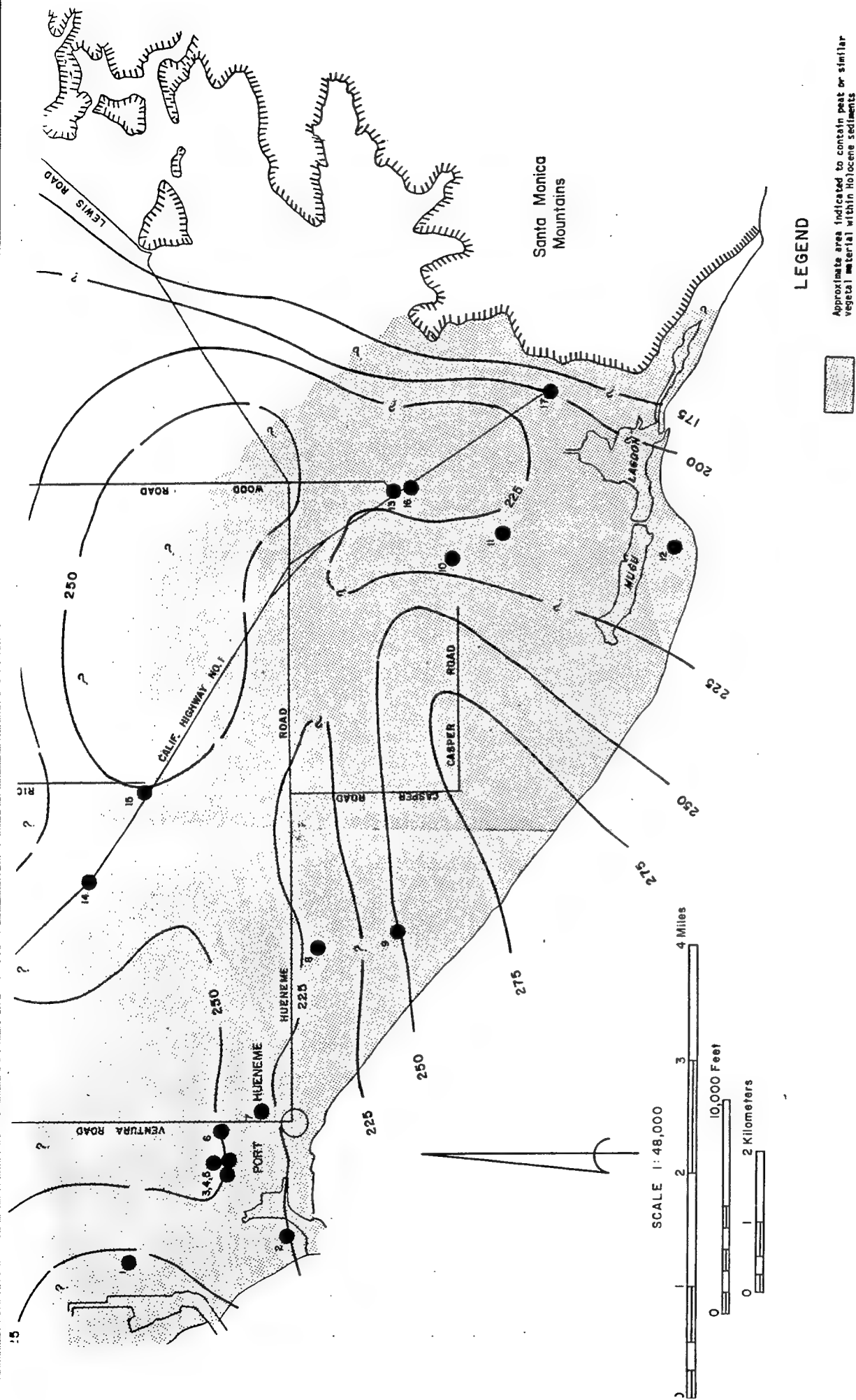


Figure 3.2 Contours of Holocene sediments from CDMG (1976)

LEGEND

- Approximate area indicated to contain peat or similar vegetative material within Holocene sediments
- Approximate location of water well or highway bridge boring in which description has been made of one or more of the following occurrences of vegetative or organic material within Holocene sediments: Peat, organic fragments or woody particles, wood or vegetable fibers, organic silty clay, organic debris, or carbonized plant remains. Number refers to well listed in text Appendix.
- Isopach of approximate thickness, in feet, of Holocene sediments.
- Areas of exposure of pre-Holocene rocks including Pleistocene sediments.

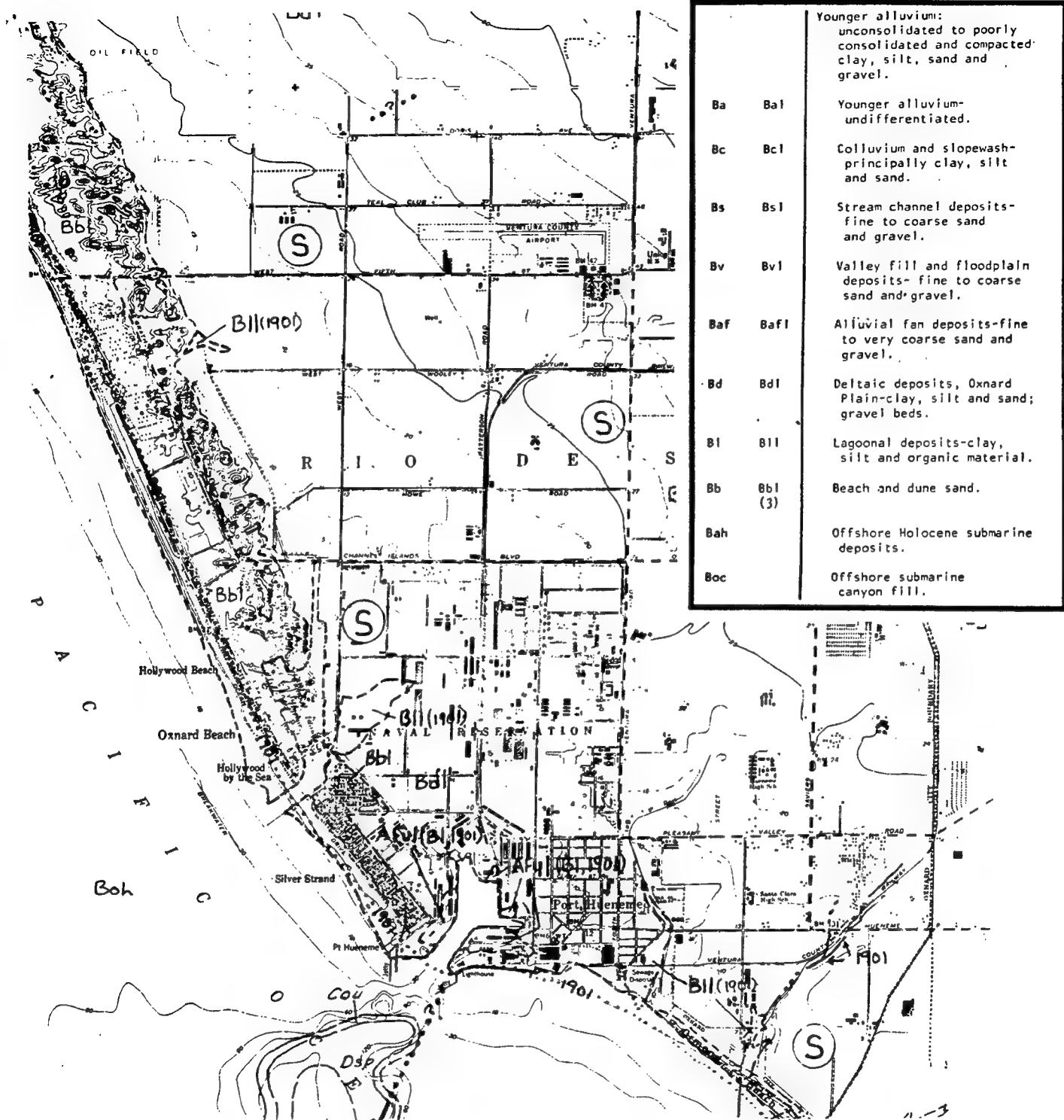


Figure 3.3Port Hueneme geology from CDMG (1976)

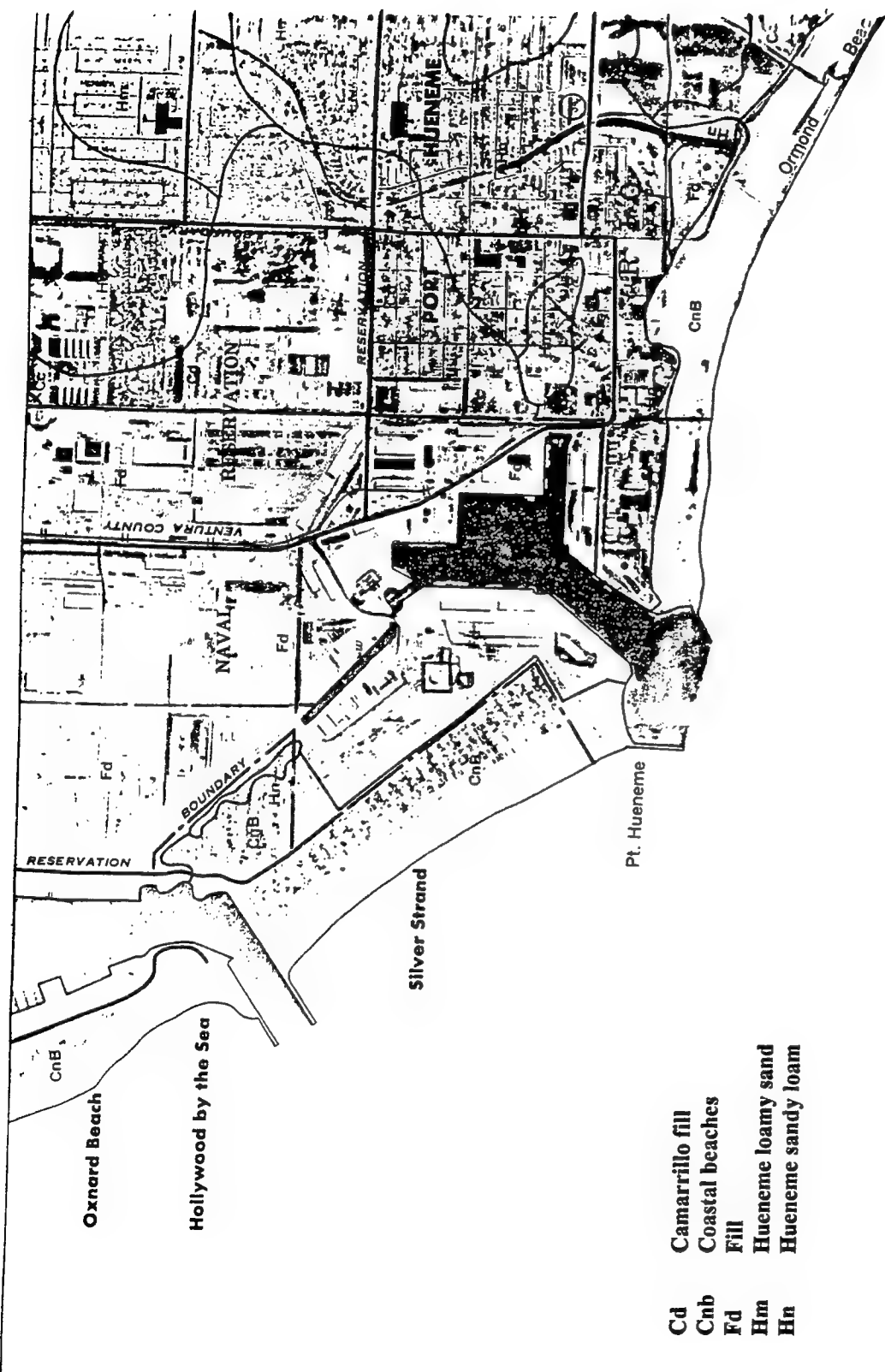
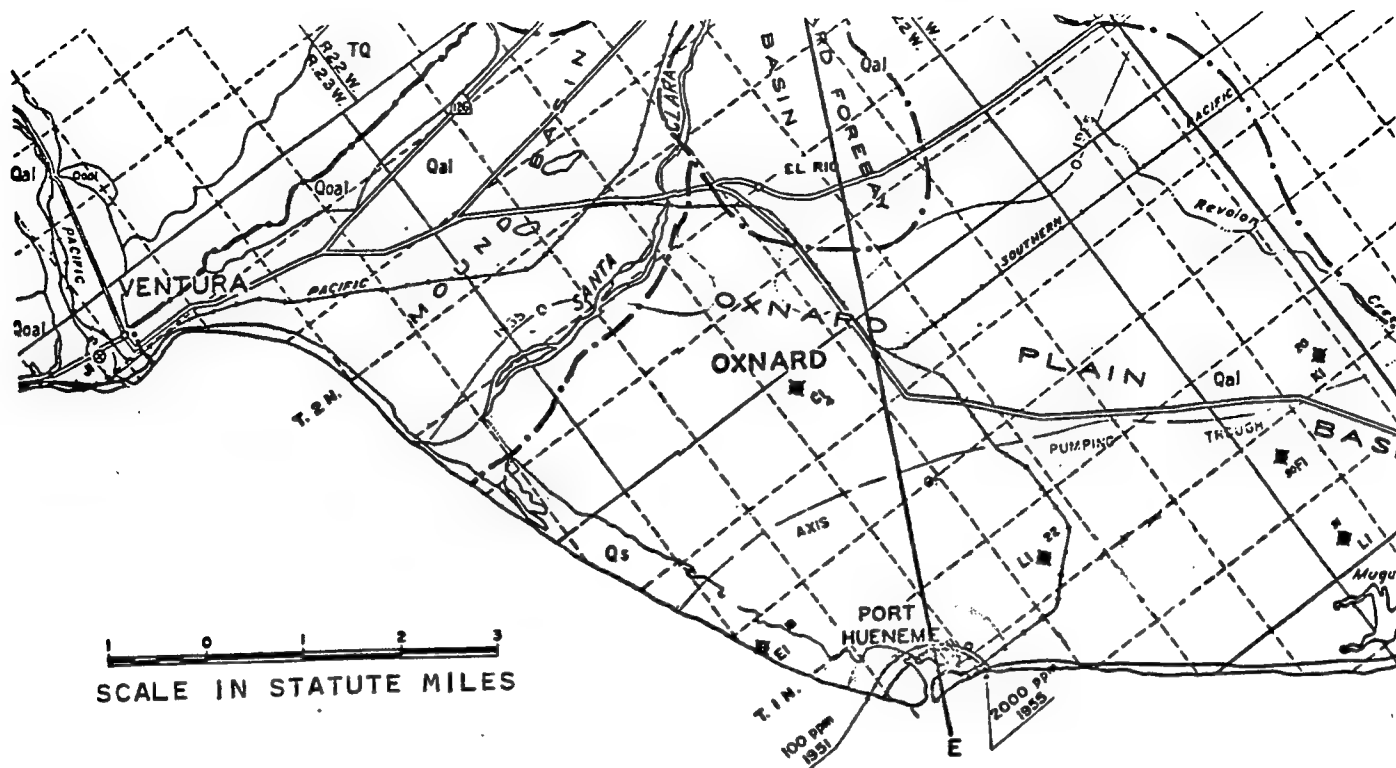


Figure 3.4 Port Hueneme surface soils from CDMG (1969)



Seawater Intrusion

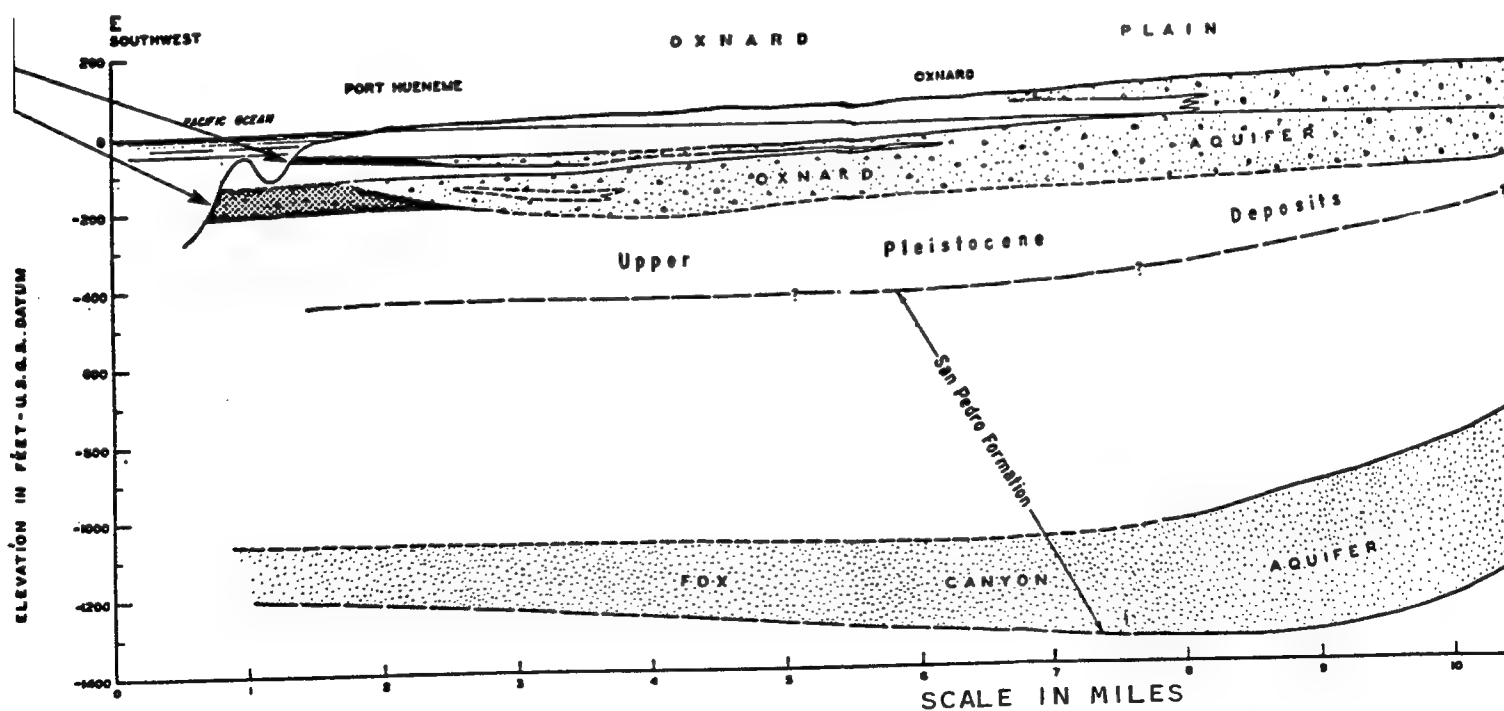


Figure 3.5 Geologic cross section.

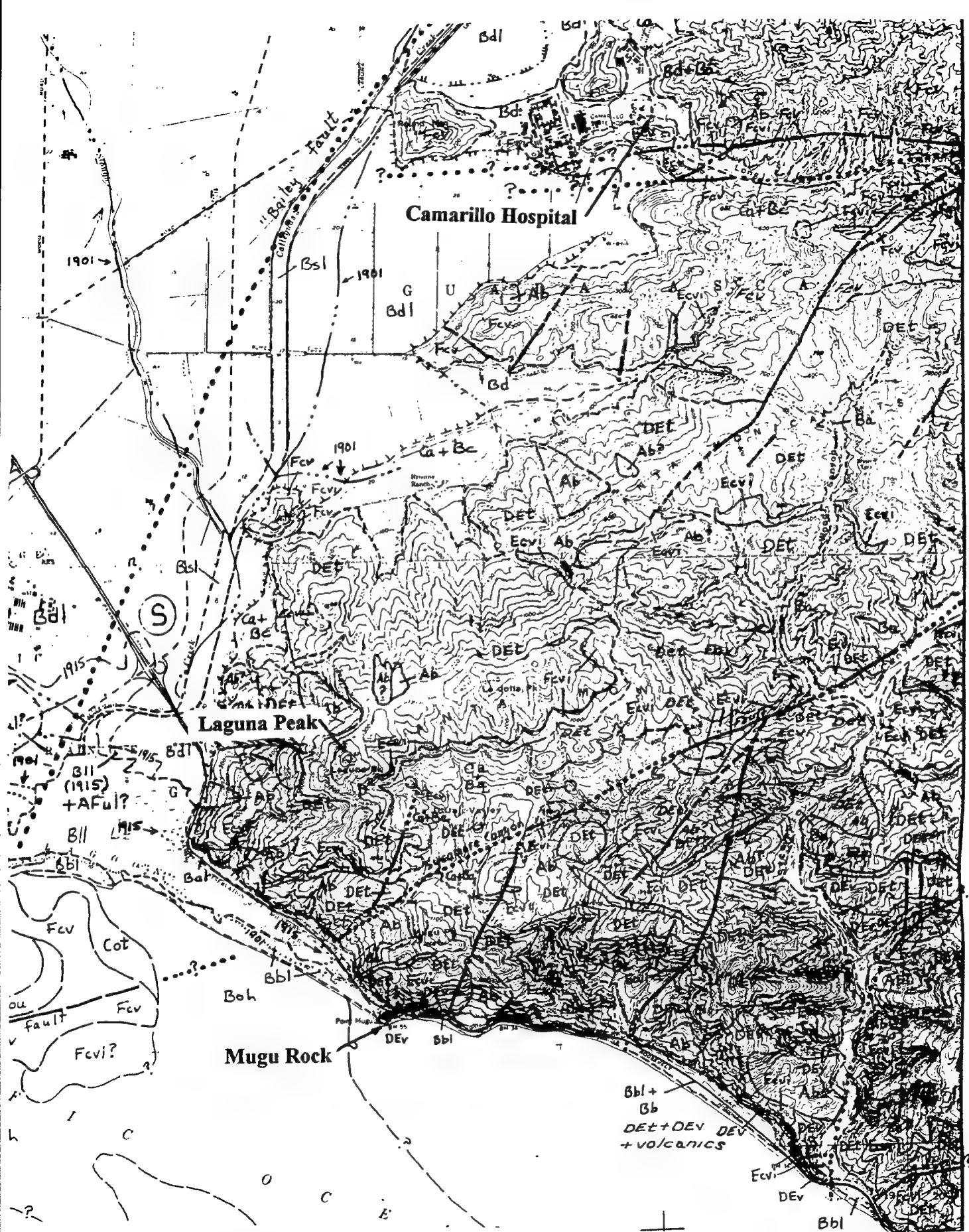


Figure 3.6 Reference site geology from CDMG (1976)

A	Ab	Landslides. "Bedrock" slides - with components of slump and block slide.	F	Fc	Well lithified formations: very well cemented and lithified sandstone and conglomerate; well indurated and lithified shale and siltstone; most volcanic rocks.
	Ad	Debris flows and other surficial slides.		Fcv	Coldwater Formation-sandstone.
	As	Offshore landslides.		Fcvi	Conejo Volcanics-resistant intrusive rocks.
D		Poorly lithified formations: very well consolidated to poorly cemented sand(friable) sandstone) and gravel (ravelly conglomerate); poorly to moderately indurated clay and silt (mudstone, shale and siltstone).		Fcva	Conejo Volcanics-andesite to dacite.
	Dd	Casitas Formation-conglomerate.		Fku	Upper Cretaceous sandstone and shale.
	Dp	Pico Formation(Western facies): sandstone, shale and mudstone.		Fm	Matilija Formation-sandstone.
	Ds	Saugus Formation-conglomerate, sandstone and siltstone.		Fsc	Santa Susana Formation (lower part): Simi conglomerate.
	Dsb	Santa Barbara Formation-mudstone, siltstone, sandstone and conglomerate.		AF	Man emplaced fill.
	Dsp	San Pedro Formation-sandstone, conglomerate and mudstone.		AFu AFul	Artificial fill-uncompacted.
DE		Transition zone-units contain major portions of rocks of both "D" and "E" zones.		AFc AFcl	Artificial fill-compacted, "engineered."
	DEm	Monterey/Modelo Formations (DEmb-"burnt shale"): clay to silicified shale, siltstone and sandstone.			
	DEp	Pico Formation(Eastern facies): sandstone and siltstone.			
	DEr	Rincon Formation-siltstone, mudstone and shale.			
	DEs	Sespe Formation-sandstone, siltstone and conglomerate.			
	DEsm	Santa Margarita Formation-mudstone, siltstone and sandstone.			
	DEt	Topanga Formation-sandstone, siltstone and conglomerate.			
	DEv	Vaqueros Formation-sandstone, claystone and siltstone.			
E		Moderately well lithified formations: well cemented sandstone and conglomerate; well indurated to silicified shale and siltstone; unweathered basalt.			
	Ed	Cozy Dell Formation-shale and siltstone.			
	Evb	Conejo Volcanics-layered basalt.			
	Ecvl	Conejo Volcanics-intrusive basalt.			
	Ej	Juncal Formation-shale and siltstone.			
	El	Lajas Formation-conglomerate, sandstone, siltstone and shale.			
	Ess	Santa Susana Formation (upper part): sandstone.			
	Et	Towsley Formation-sandstone and siltstone.			

Figure 3.6 Reference site
geology from CDMG (1976)
Continued

**Figure 3.7 Boring logs, see Figure 3.2 for location
From CDMG(1976)**

MAP INDEX NUMBER	STATE WELL NUMBER OR BRIDGE NUMBER	GROUND ELEVATION, IN FEET ABOVE SEA LEVEL	MEASURED WELL DEPTH IN FEET AND LITHOLOGIC DESCRIPTION
1	1N-22W-17H3	9'	<p>2' to 10', Fine to coarse sand with some carbonaceous matter.</p> <p>96' to 100', Medium to very coarse sand and gray clay with wood fragments.</p> <p>110' to 125', Medium to coarse sandy clay with a few wood fragments.</p> <p>145' to 172', Medium to coarse sandy clay with a few wood fragments.</p>
2	1N-22W-20N2	5'	<p>8' to 28', Interbedded brown clay with wood fragments, broken shells and fine to coarse sand.</p> <p>28' to 32', Coarse sand and gravel with some clay, wood and shell fragments.</p> <p>32' to 38', Fine sand and some coarse sand, clay and wood fragments.</p> <p>38' to 52', Brown clay with sand, gravel and wood fragments.</p> <p>72' to 85', Gray to black clay with some gravel and wood.</p> <p>100' to 120', Medium to very coarse sand and granules and dark gray organic silty clay.</p> <p>120' to 125', Sand and clay, as above, with 10 to 15 percent wood and peat seams.</p> <p>245' to 255', Gray to black clay and one-half inch gravel. Occasional thin beds of peat. (This interval probably in Upper Pleistocene - E.C.S.)</p>
3	1N-22W-20H1	10'	<p>106' to 117', Sandy silt: Gray-black color with fine sand, also black organic particles - wood?</p>
4	1N-22W-20H2	10'	<p>8' to 12', Organic debris with medium grained sand and silt.</p>
5	1N-22W-20H4	10'	<p>87' to 91', Medium to coarse, angular to subangular arkosic sand and gravel, 50 percent gray to green silty clay with some fibers of wood found throughout.</p>

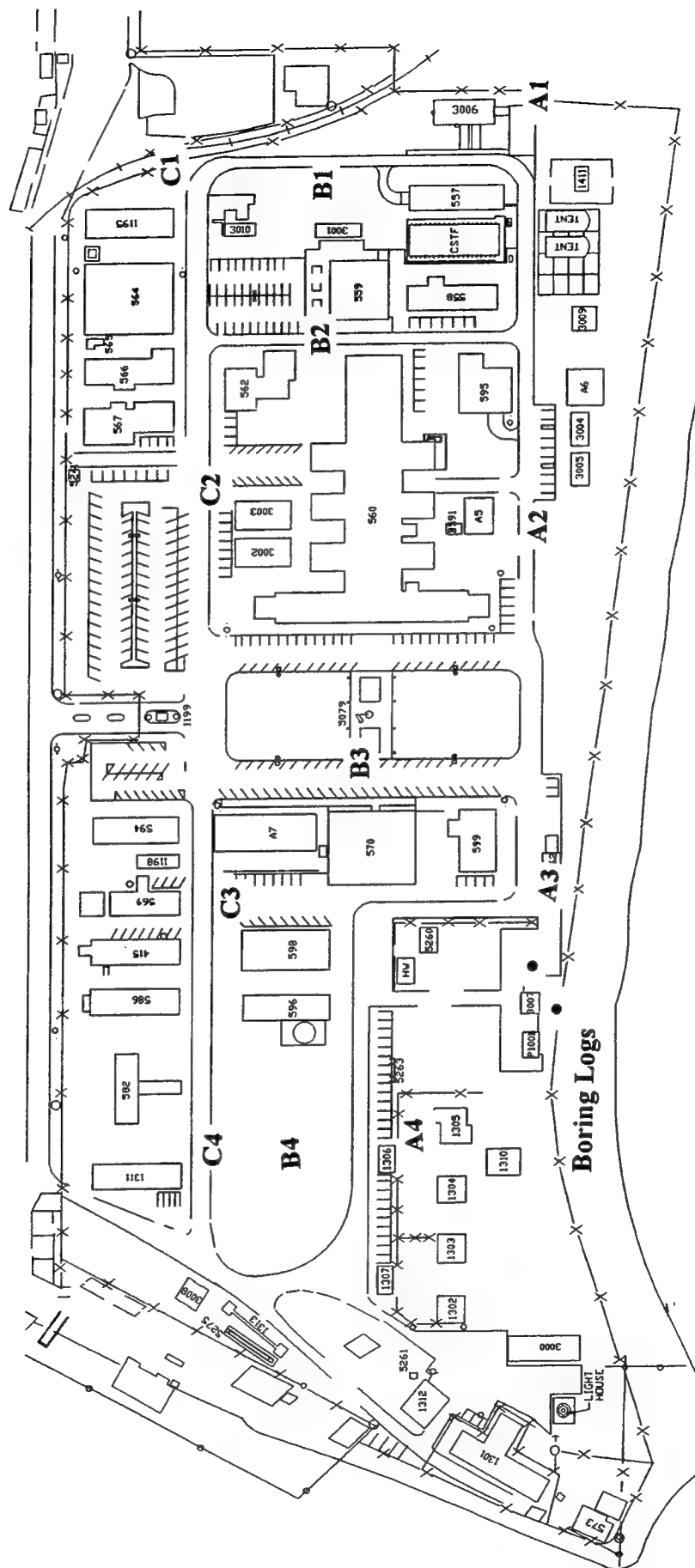


Figure 3.8. NFESC site showing measurement stations.


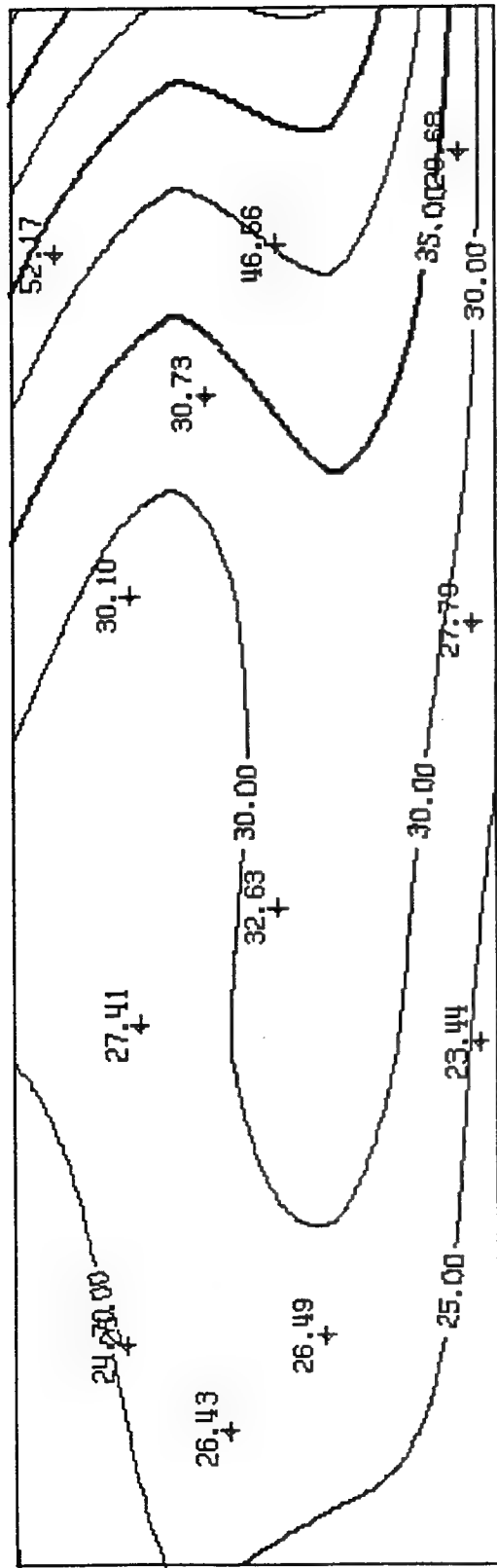
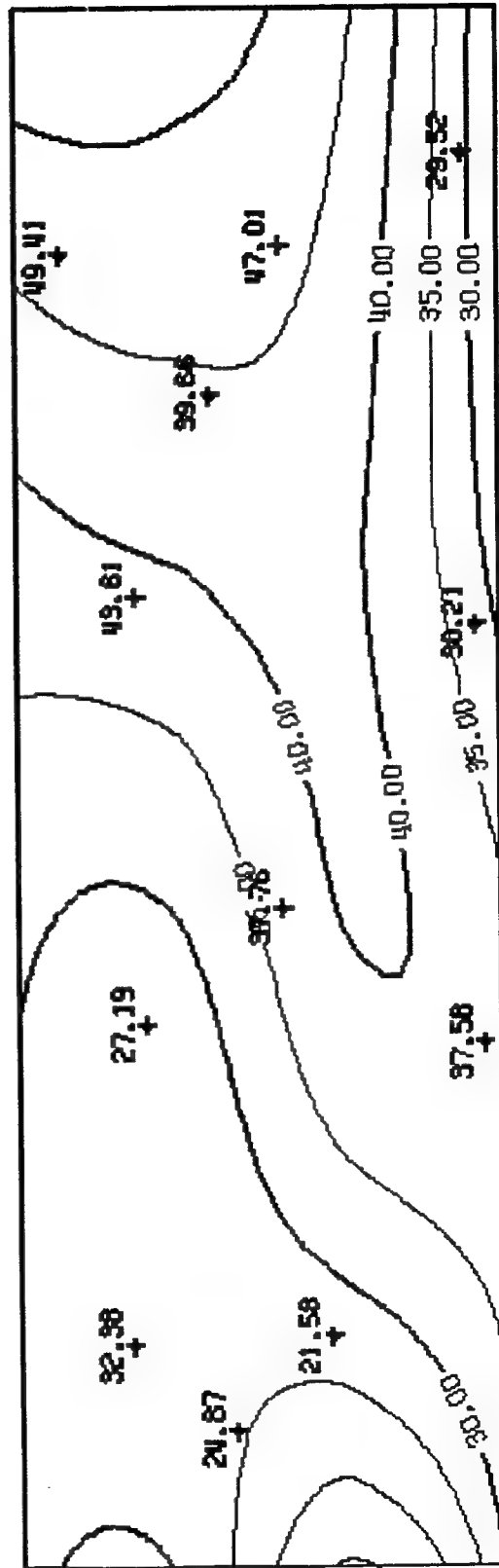
BORING LOG NO. 1					
Project Ventilation Improvements			Job No. 85-221F-2		
Driving Weight 140 lbs.			Height of drop: 30 inches		
Depth (feet)	Samples	Blows/foot	DESCRIPTION OF SOILS	Dry Density pcf	Moisture Content, %
1			2" A.C., 6" Base		
2			FILL: Silty & gravelly sand, brown to tan, moist & loose to moderate dense.		
3		19		106.3	8.7
4			SAND: Some gravel, brown, moist & medium dense to dense		
5					
6					
7					
8		21	Increase gravel & cobbles below 5'	104.8	4.7
9					
10					
11		40		116.9	11.0
12					
13					
14					
15					
16		34	End of Boring at 15'	105.3	22.0
17			Water Table at 12'		
18					
19					
20					
21					
22					
23					
24					
25					
26					
27					
28					
29					
30					
31					
32					
33					
34					
35					

Figure 3.9 Boring log, NFESC compound.

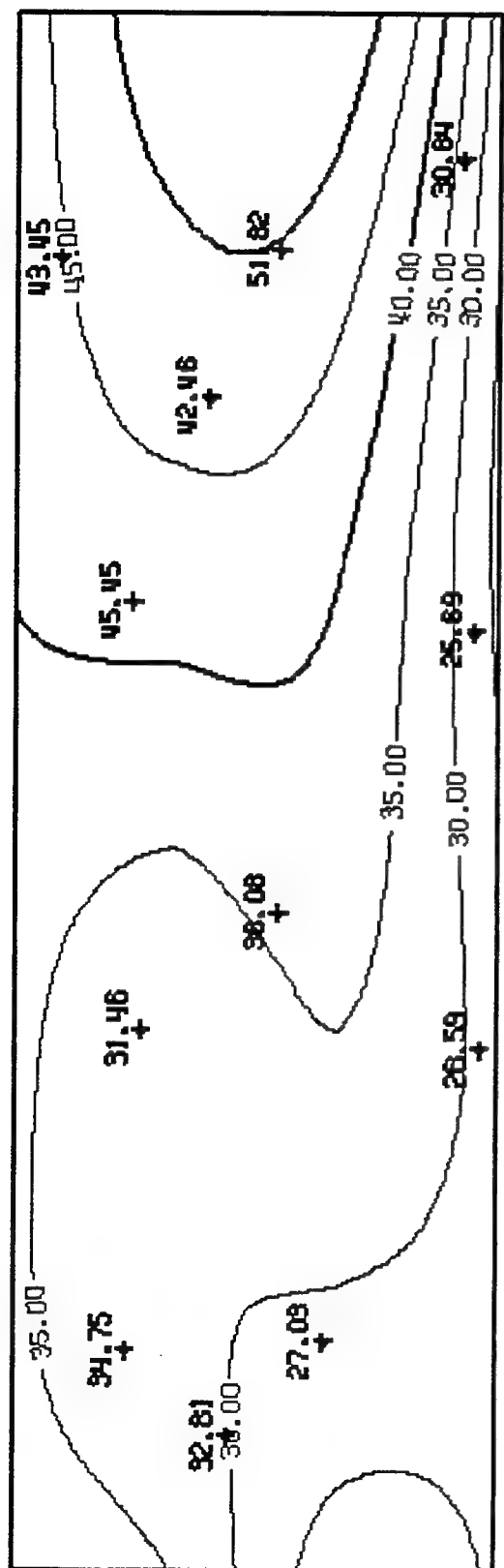


Trial 1

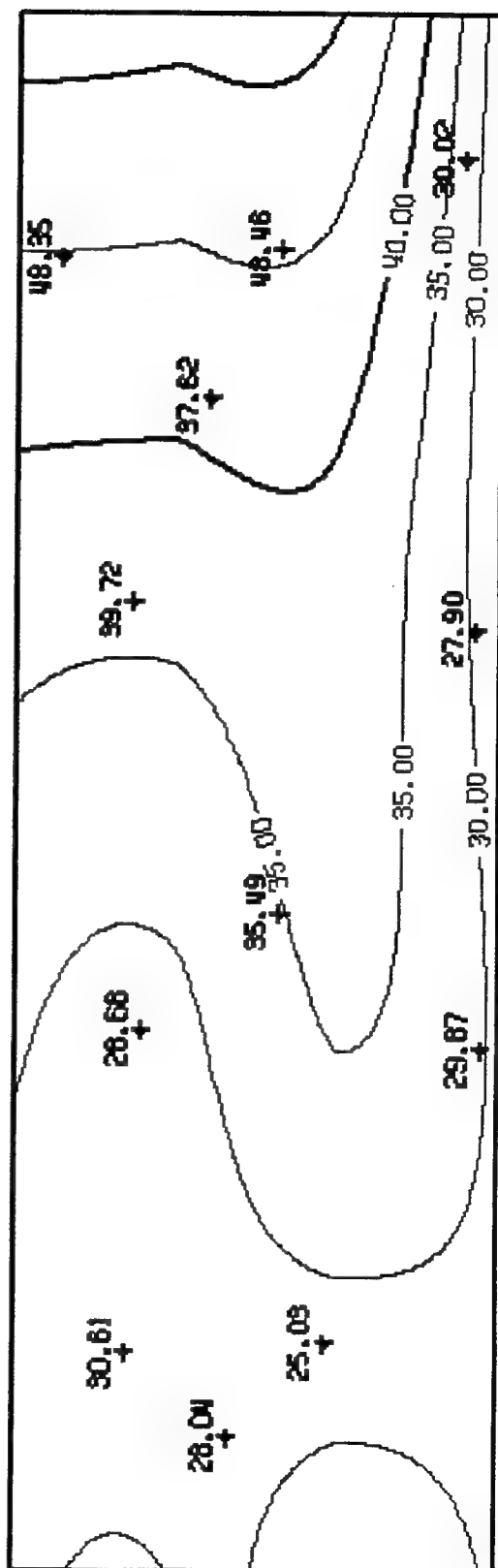


Trial 2

Figure 3.10a. Contours of amplification, period range 0.5 to 0.7 sec.

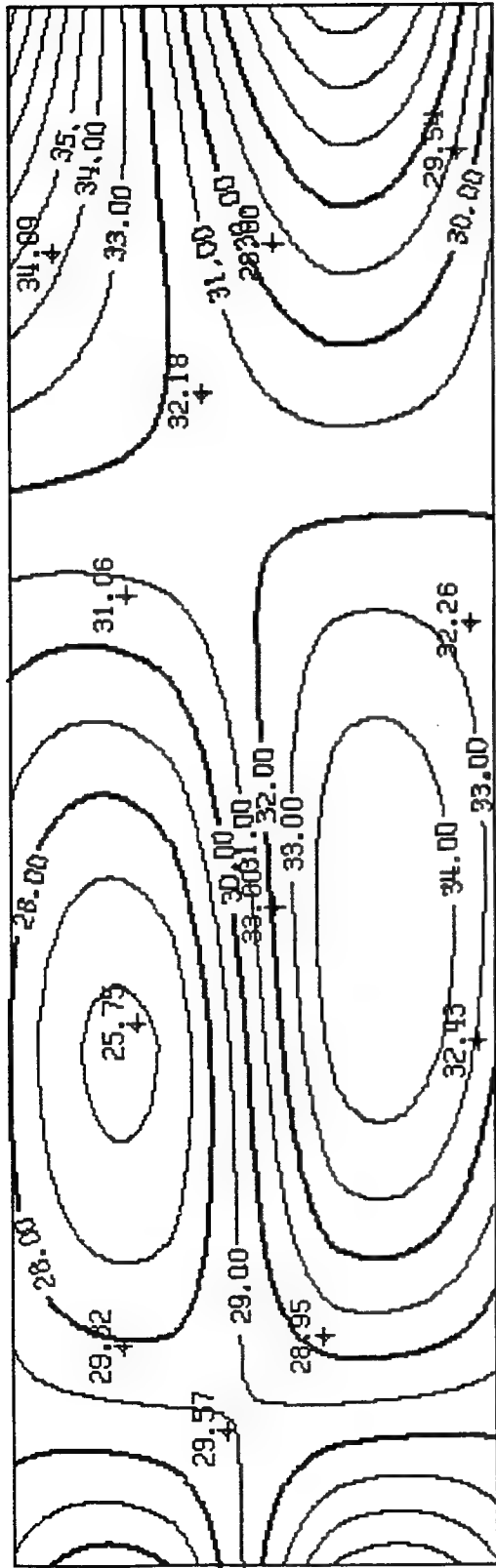


Trial 3

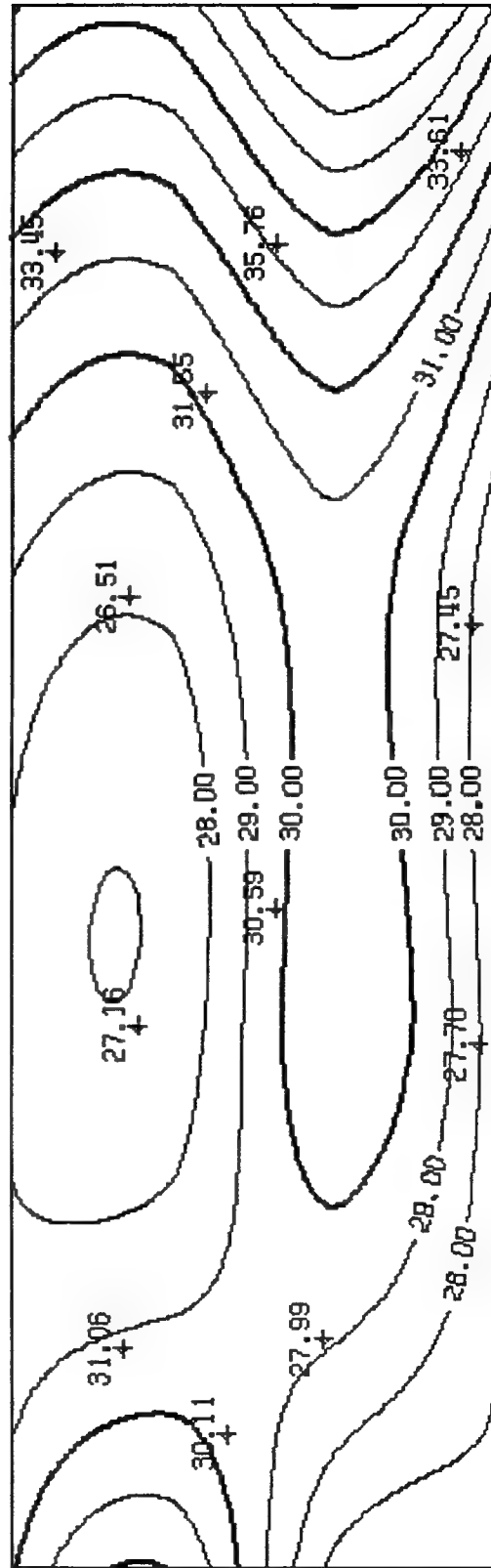


Average of 3 trials

Figure 3.10a. Continued

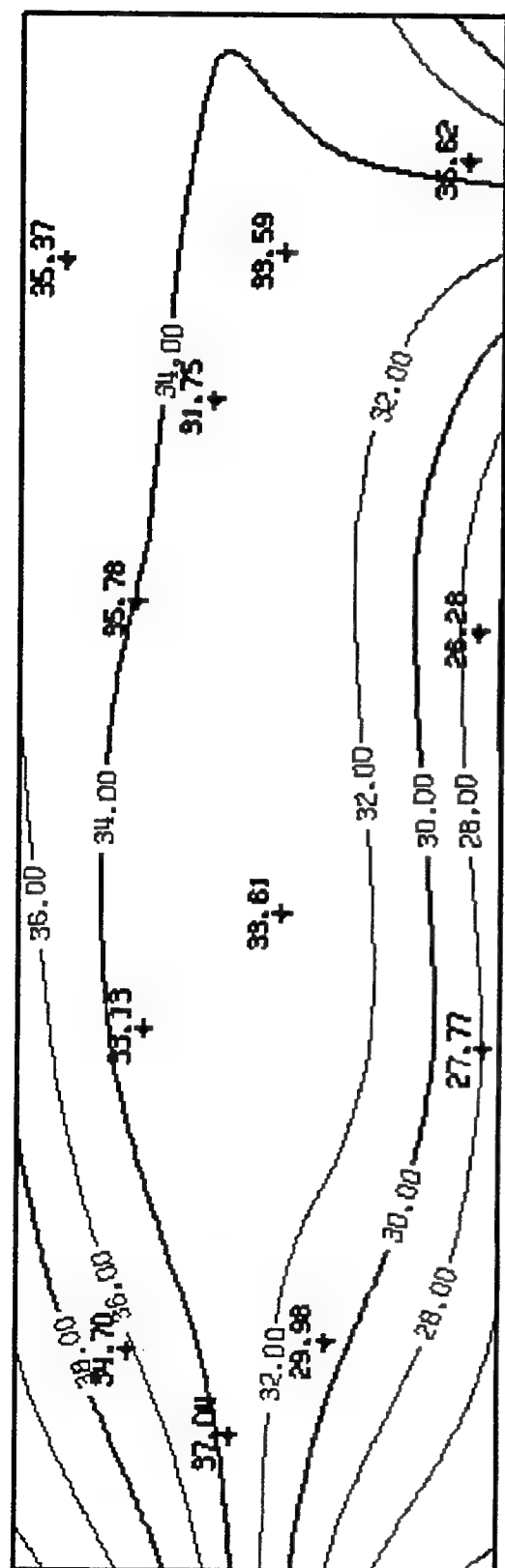


Trial 1

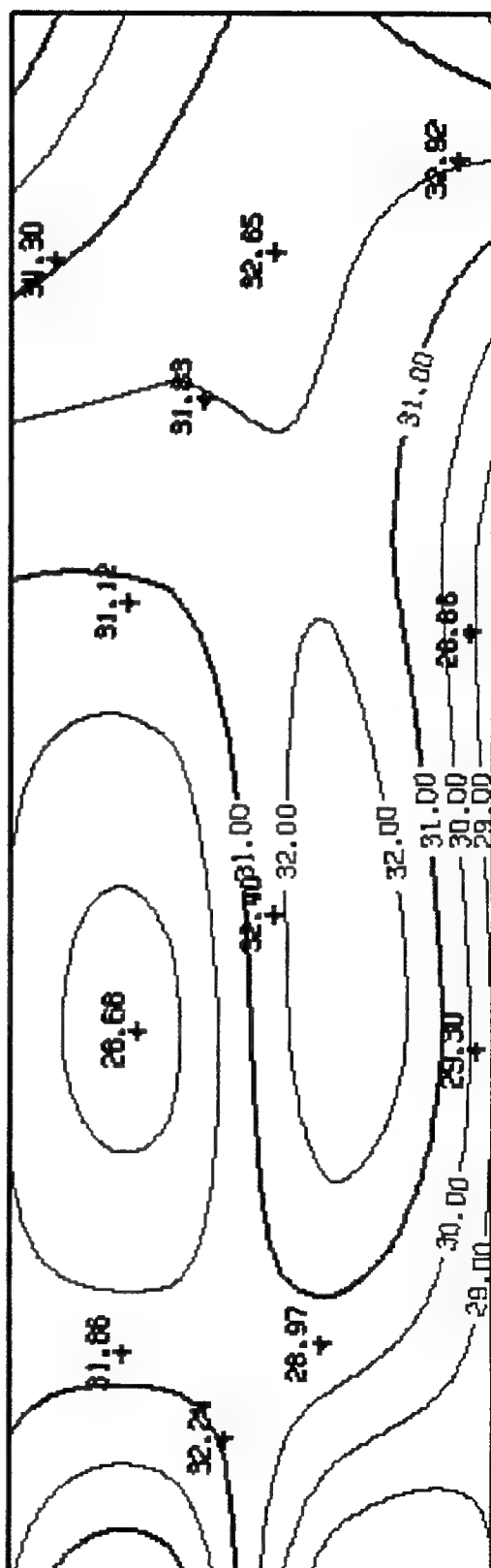


Trial 2

Figure 3.10b. Contours of amplification, period range 0.7 to 1.0 sec.

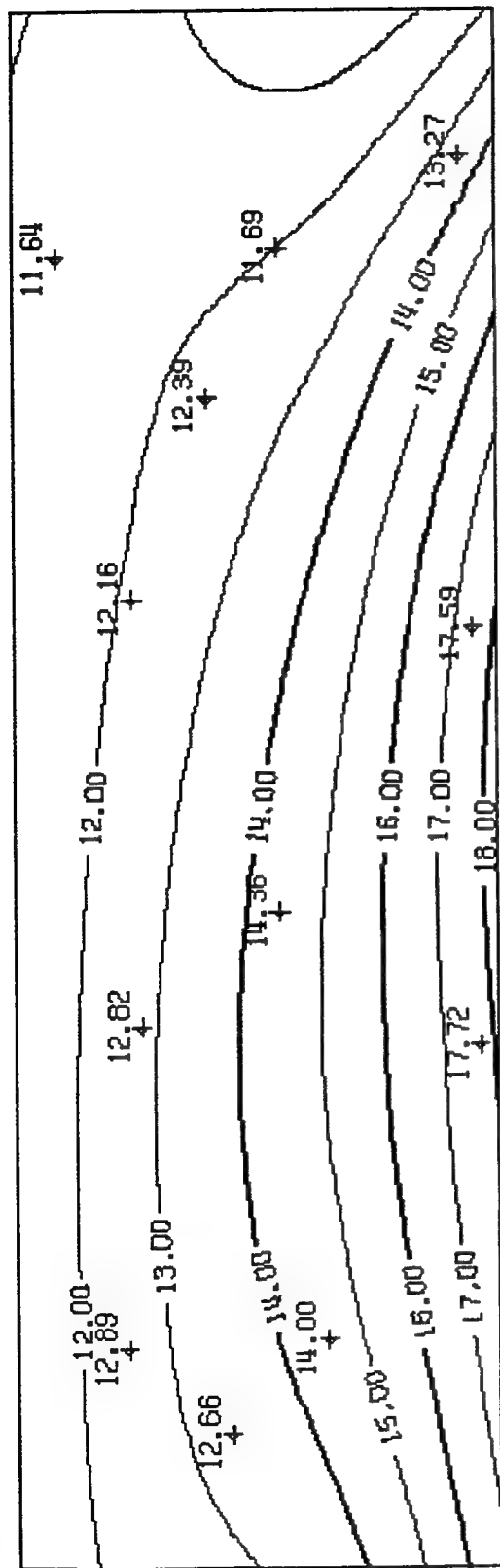


Trial 3

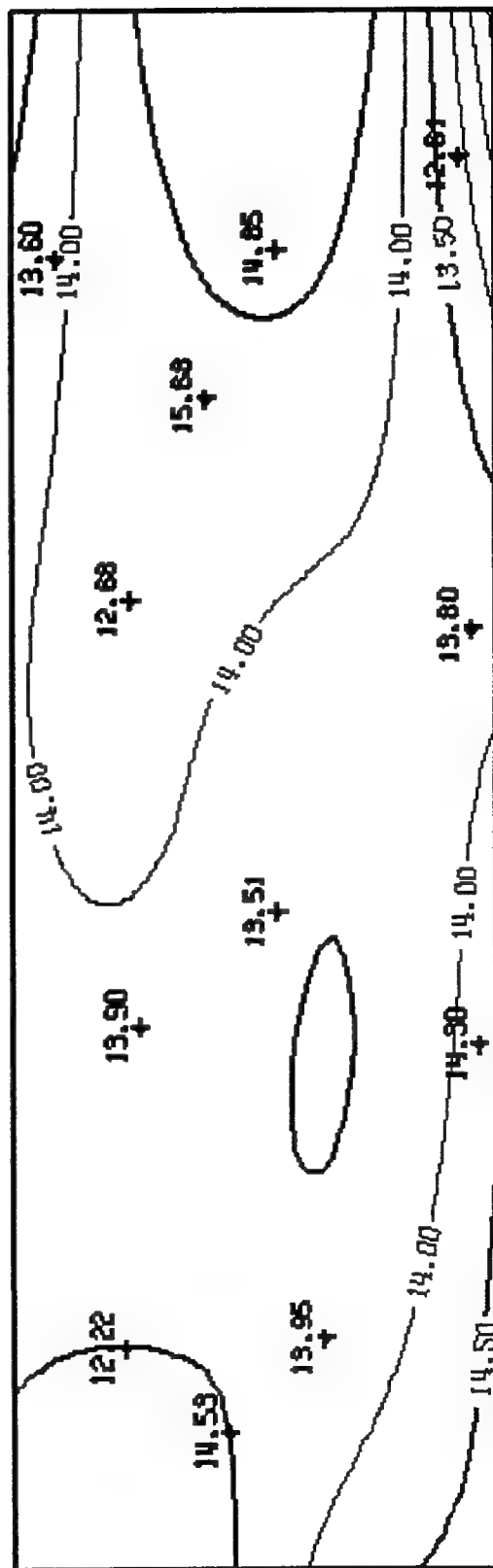


Average of 3 trials

Figure 3.10b. Continued

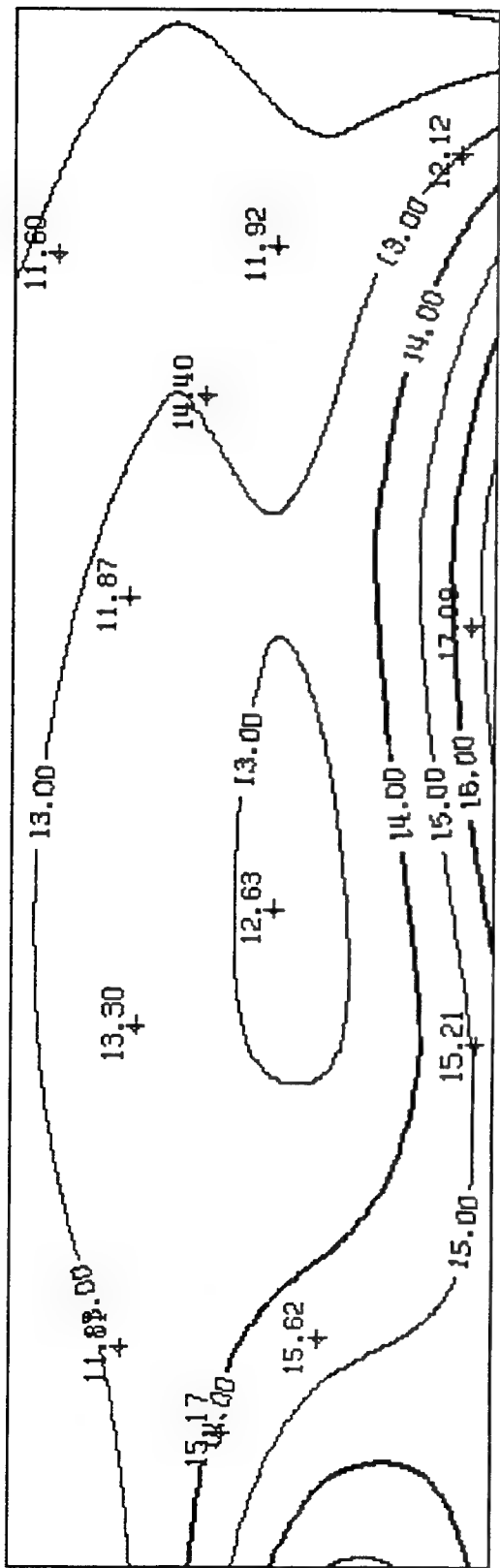


Trial 1

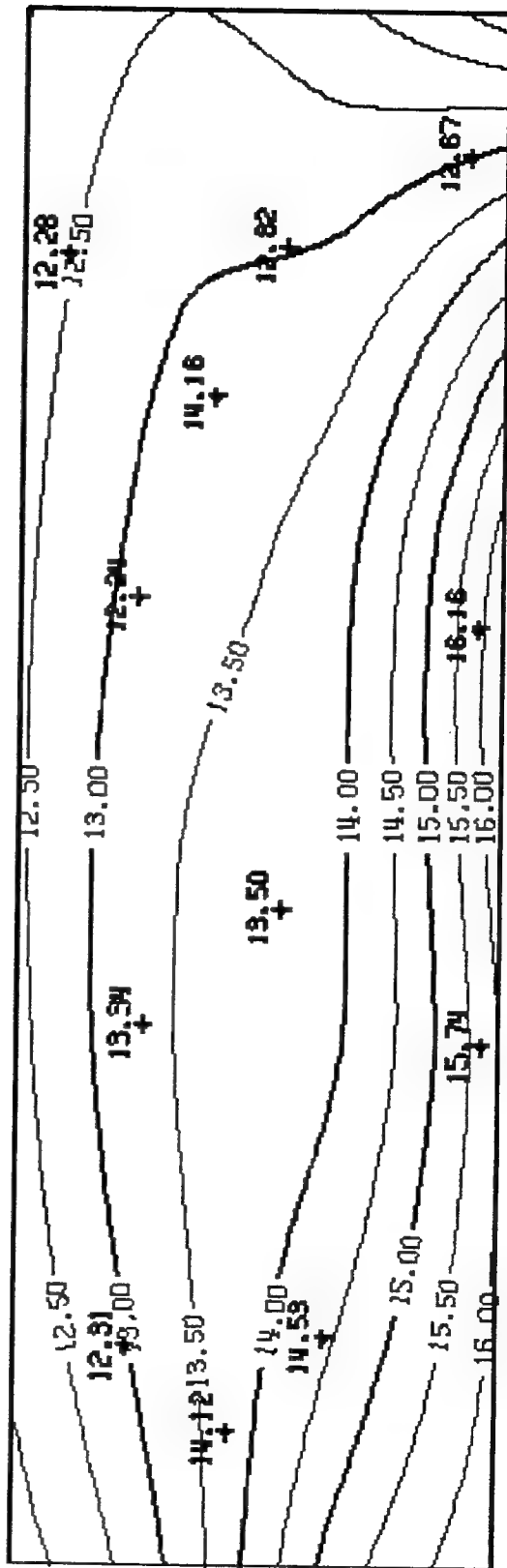


Trial 2

Figure 3.10c. Contours of amplification, period range 2.0 to 4.0 sec.

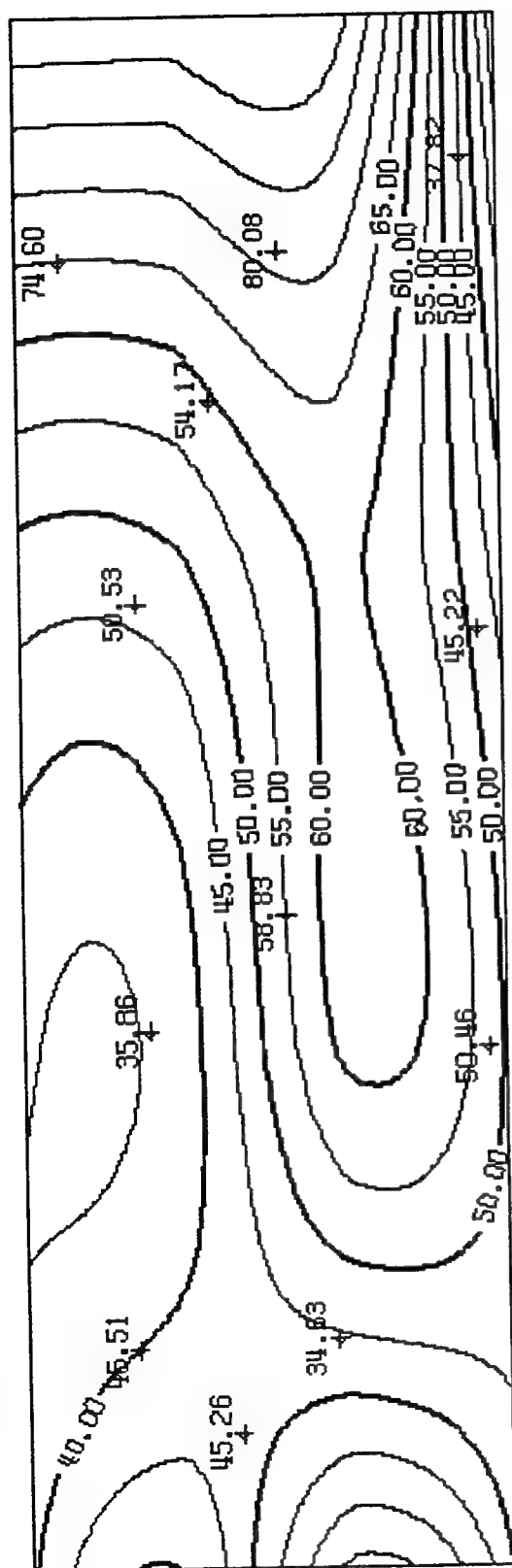


Trial 3

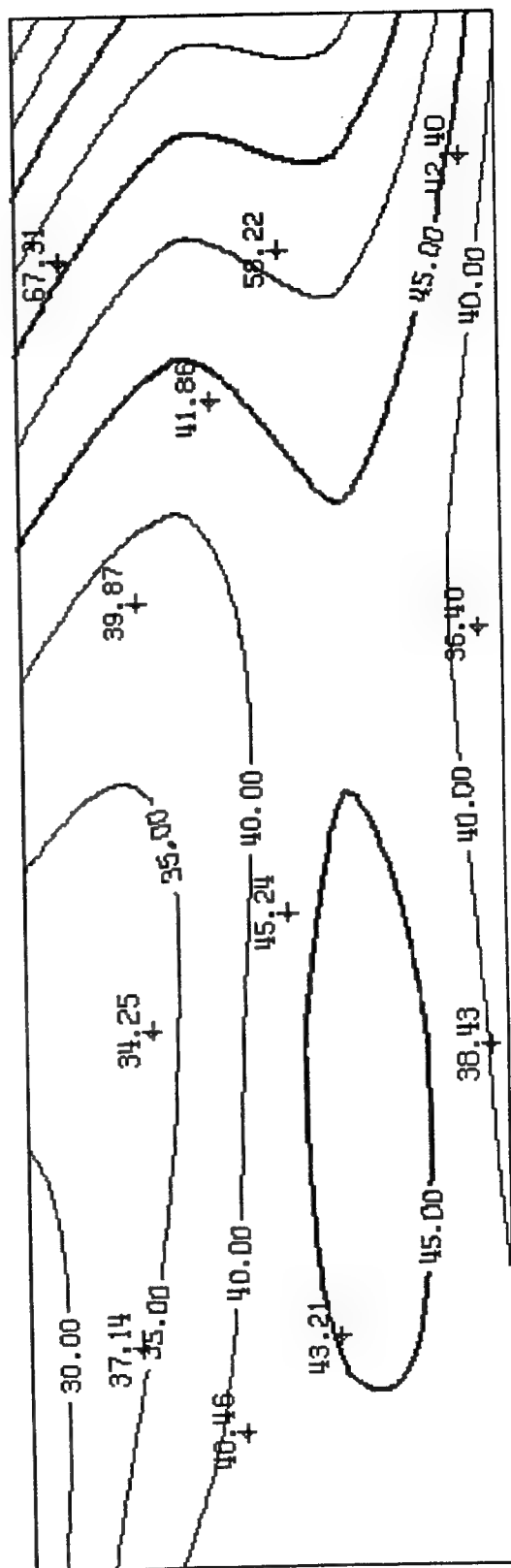


Average of 3 trials

Figure 3.10c. Continued

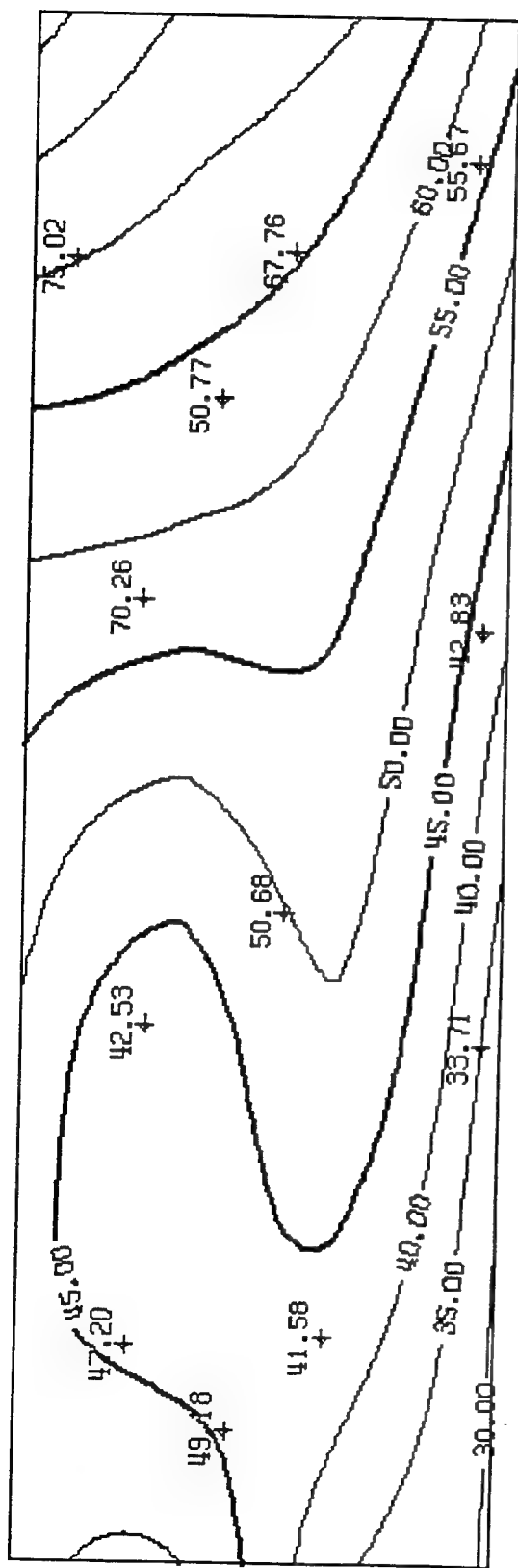


Trial 1

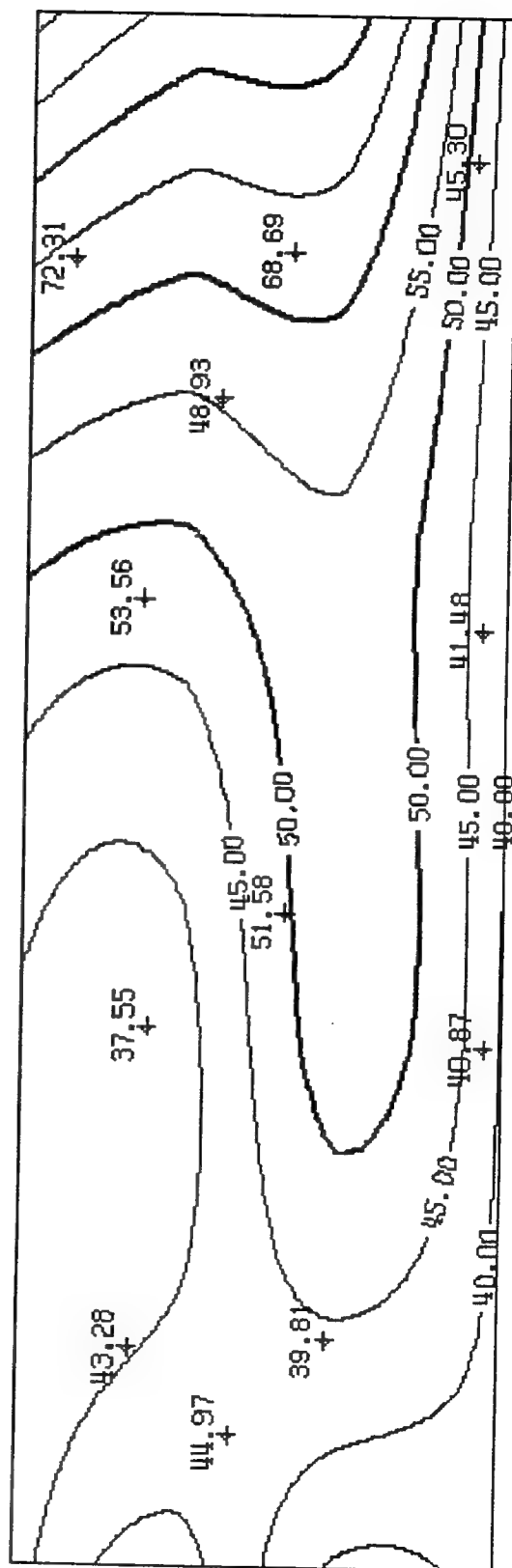


Trial 2

Figure 3.10d. Contours of peak amplification over period 0.5 to 10 sec.



Trial 3



Average of 3 trials

Figure 3.10d. Continued

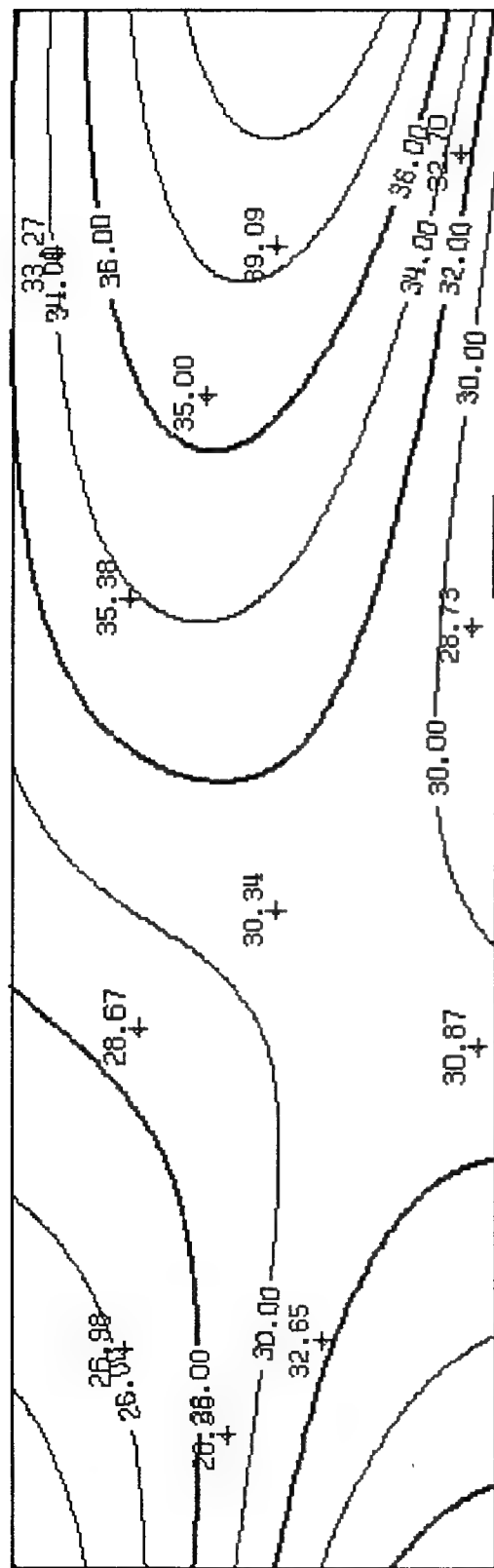


Figure 3.11a. Contours of another 3 trial average amplification, period range 0.5 to 0.7 sec.

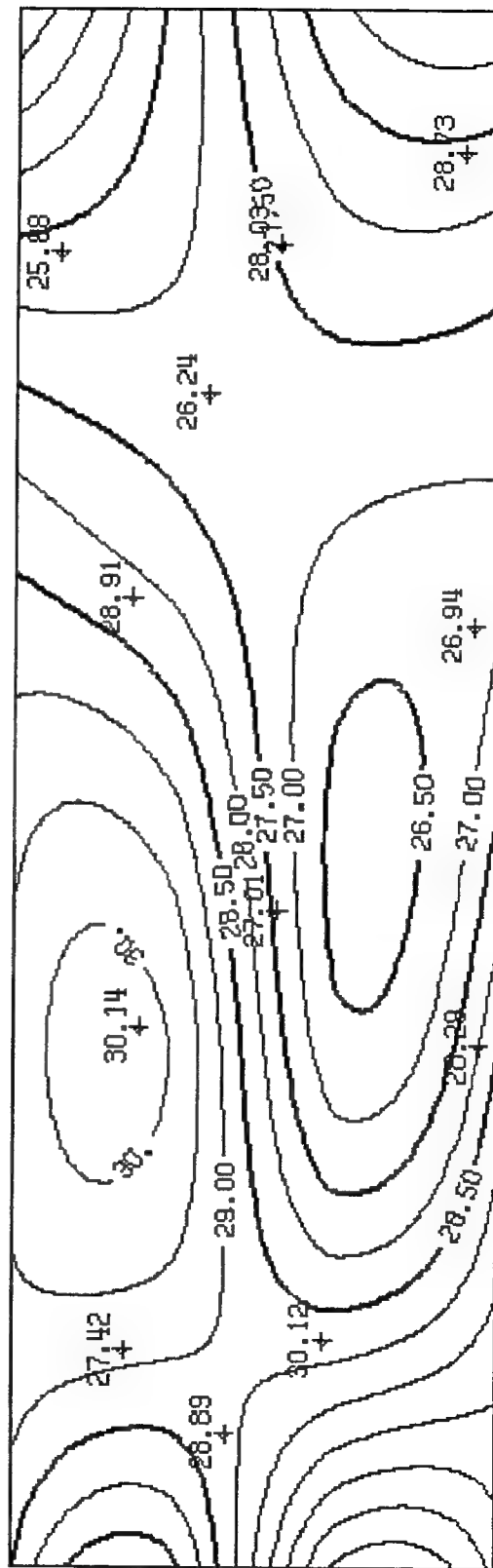


Figure 3.11b. Contours of another 3 trial average amplification, period range 0.7 to 1.0 sec.

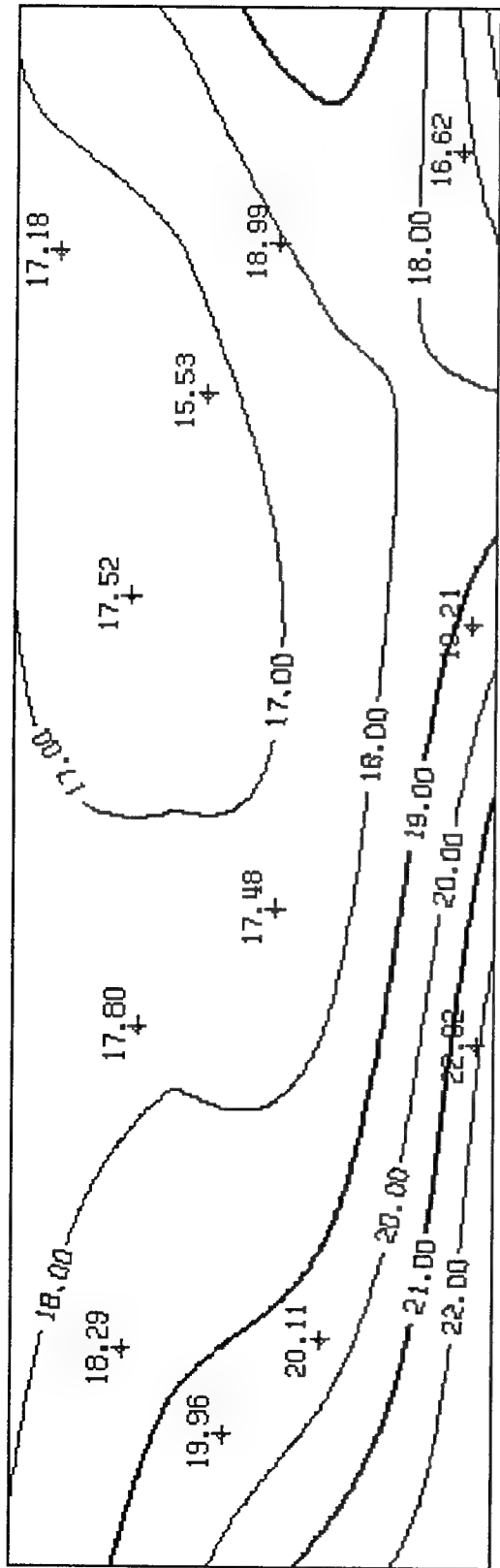


Figure 3.11c. Contours of another 3 trial average amplification, period range 2.0 to 4.0 sec.

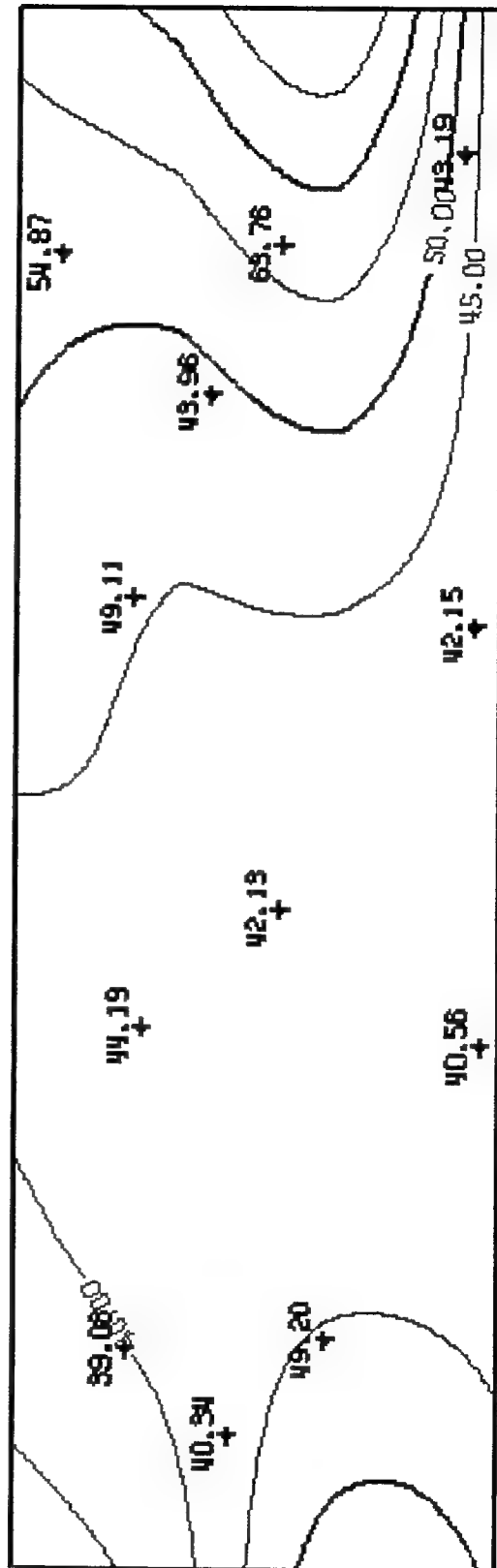


Figure 3.11d. Contours of 3 trial average peak amplification over period 0.5 to 10 sec.

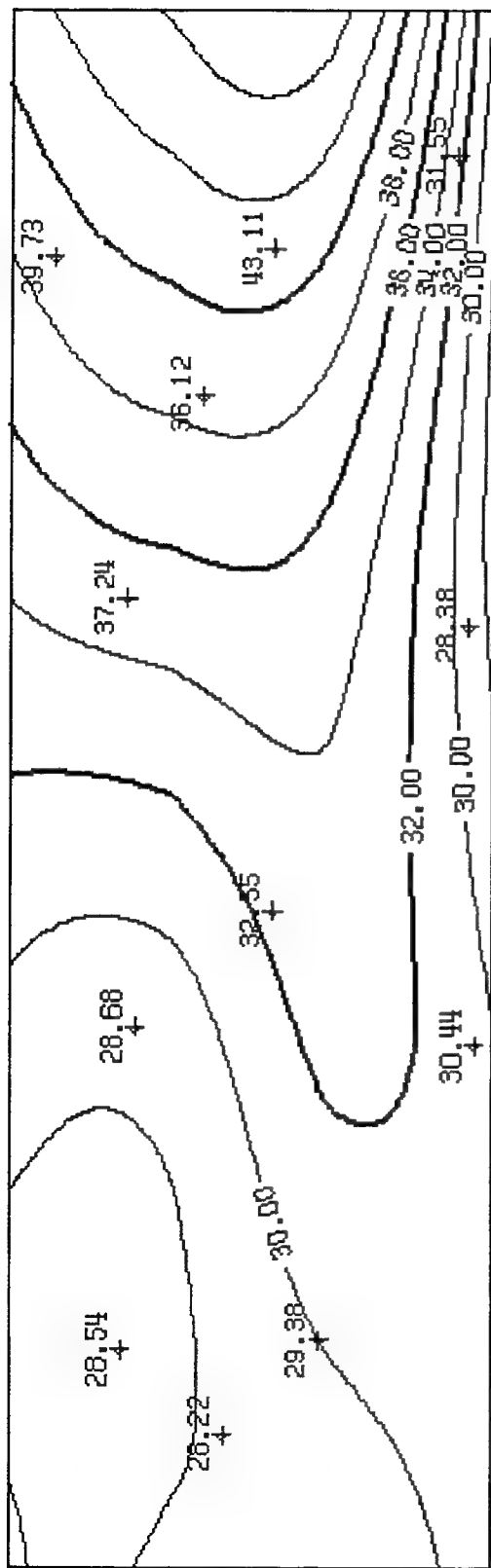


Figure 3.12a. Contours of 7 trial average amplification, period range 0.5 to 0.7 sec.

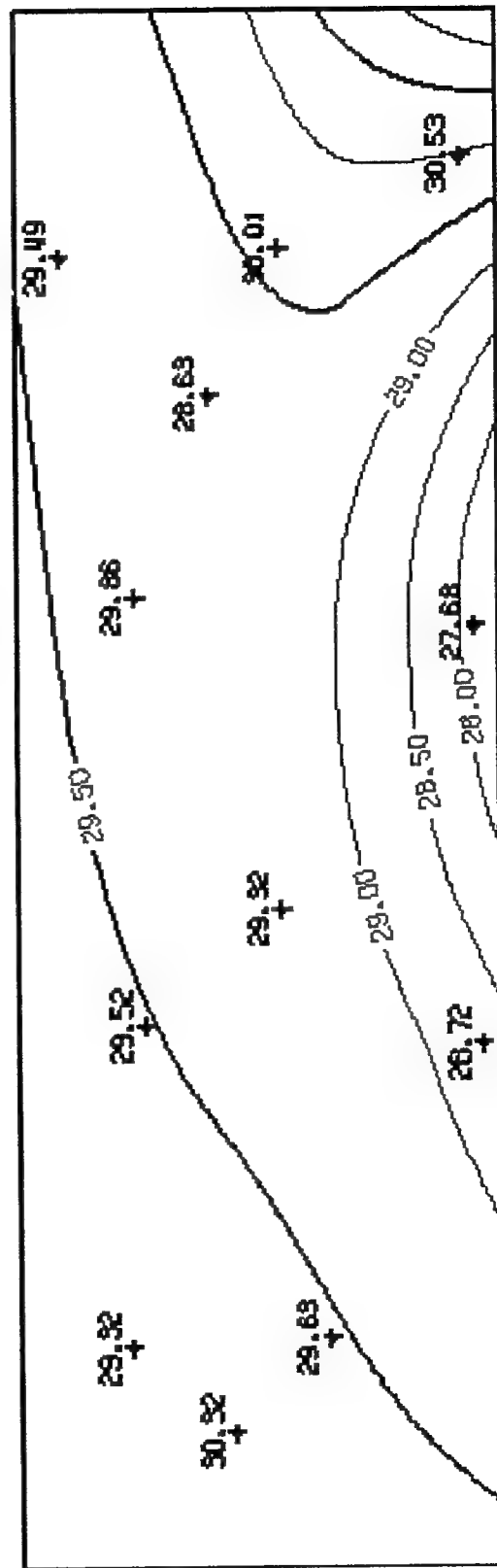


Figure 3.12b. Contours of 7 trial average amplification, period range 0.7 to 1.0 sec.

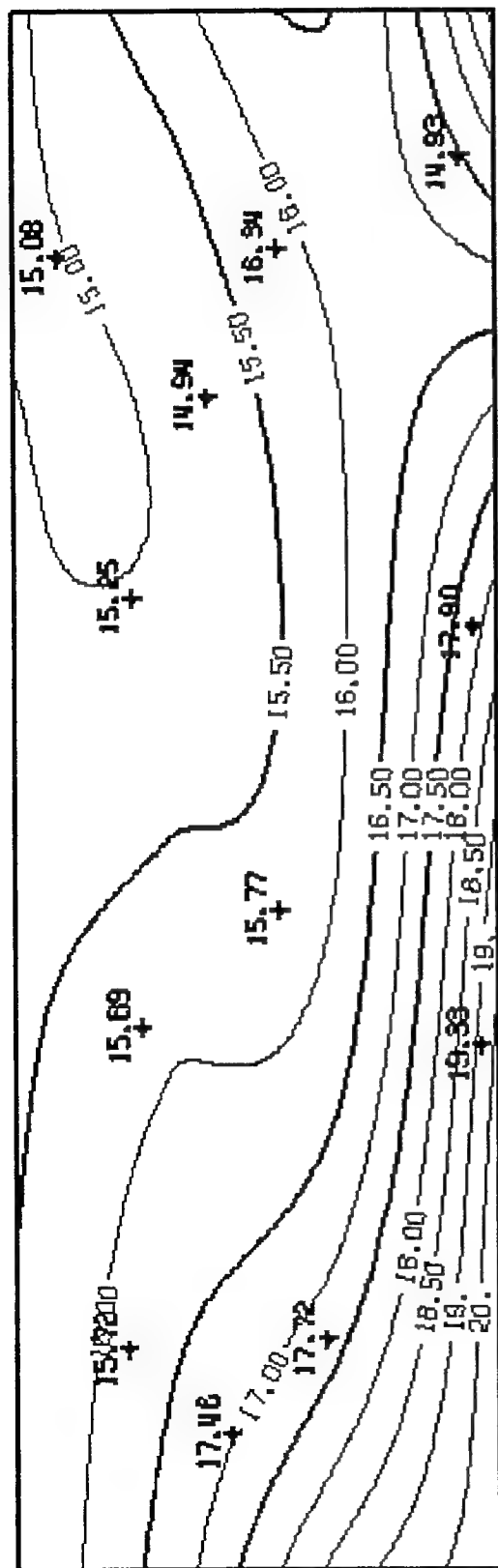


Figure 3.12c. Contours of 7 trial average amplification, period range 2.0 to 4.0 sec.

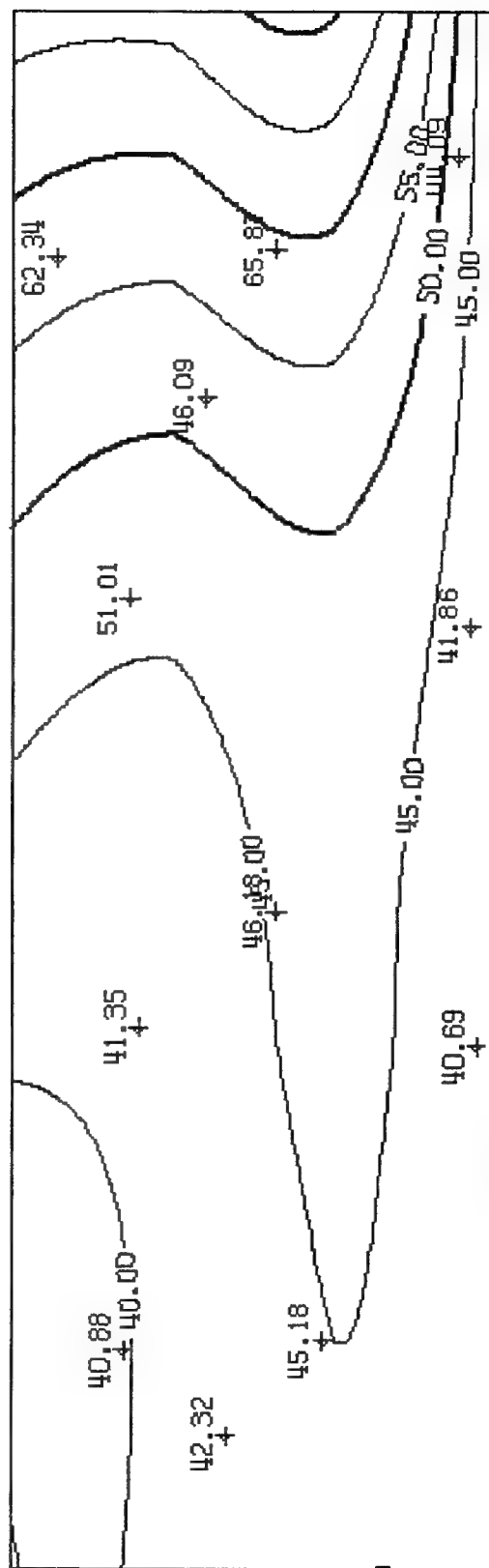


Figure 3.12d. Contours of 7 trial average peak amplification over period 0.5 to 10 sec.

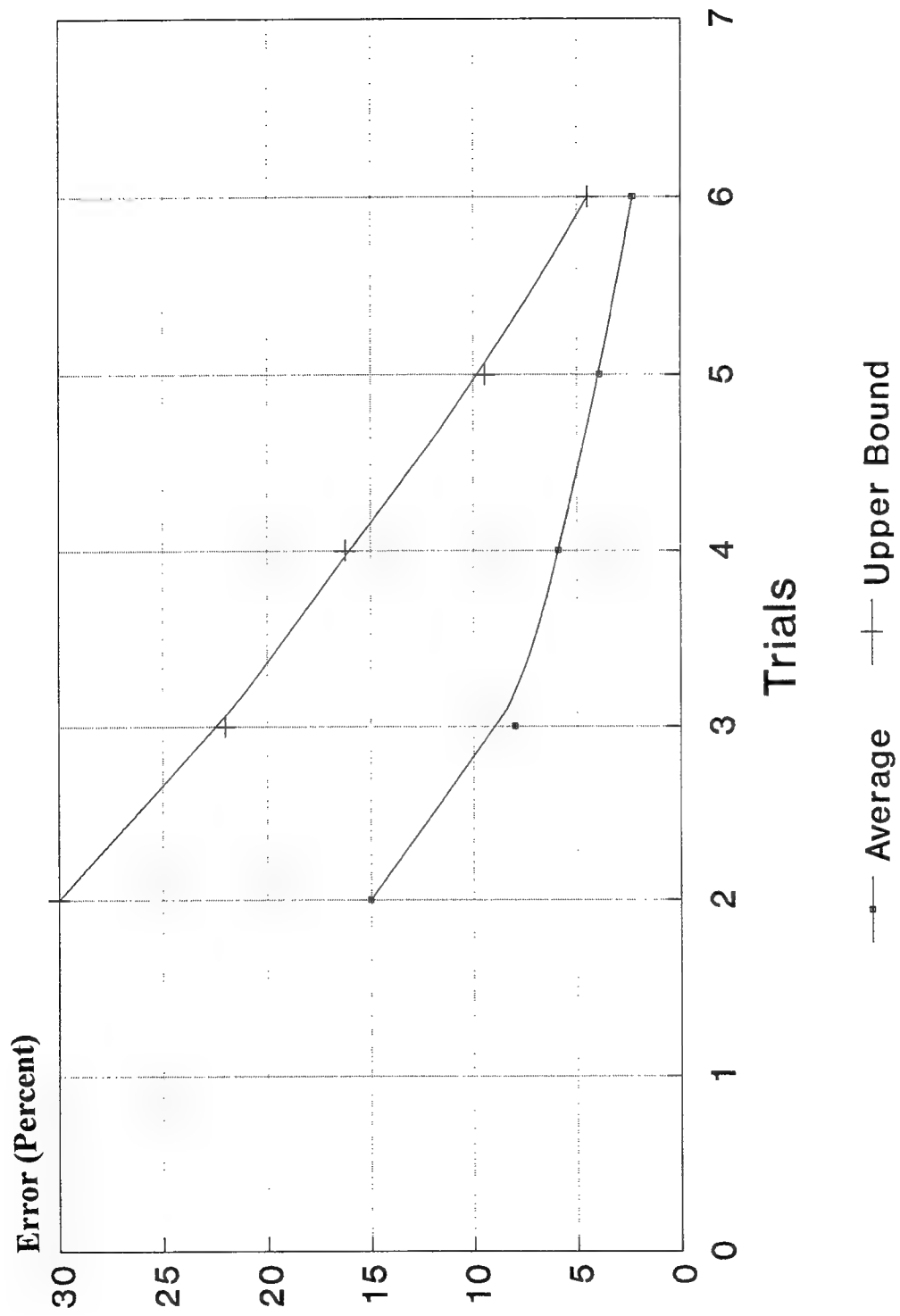


Figure 3.13 Microseism measurement convergence.

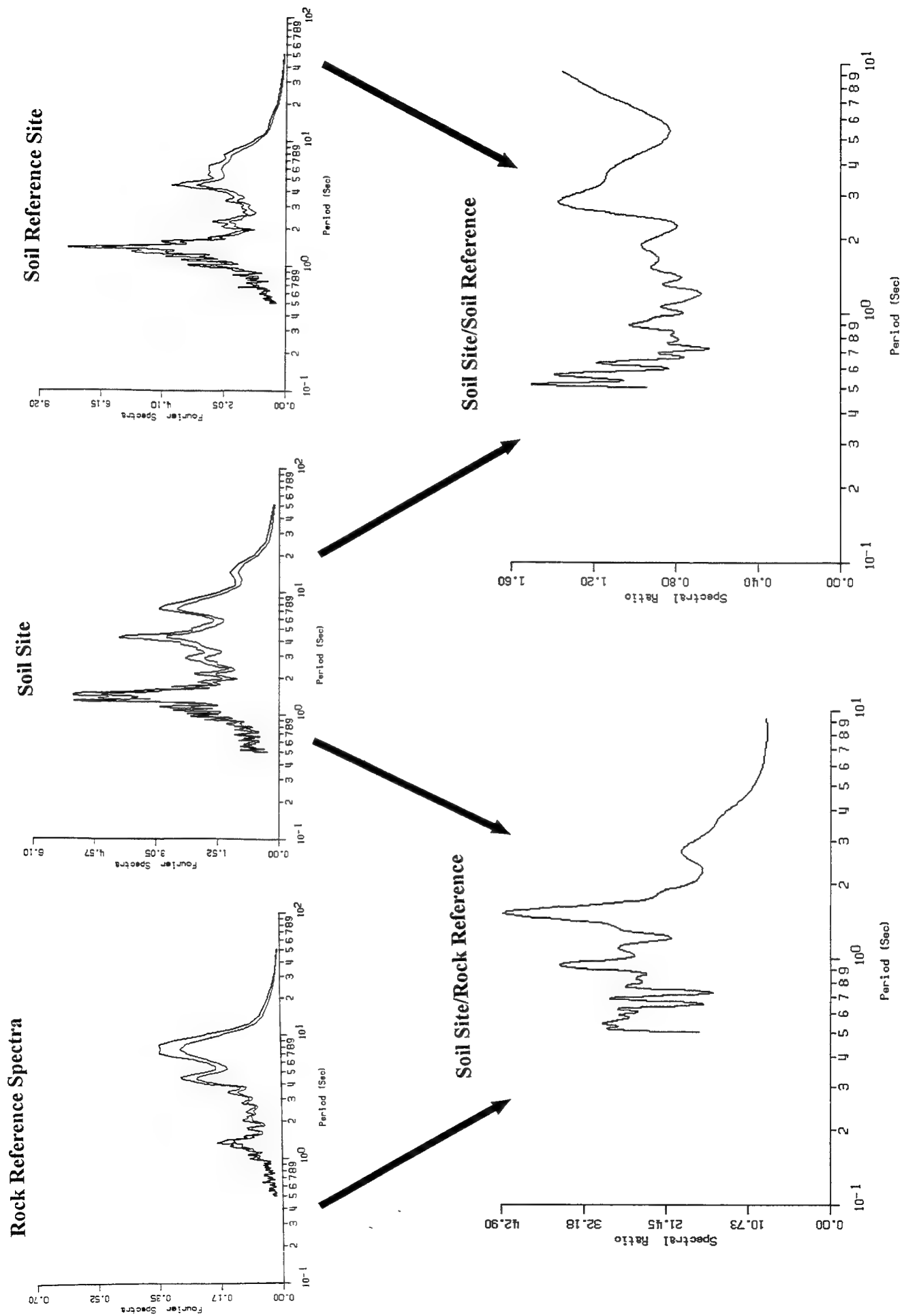
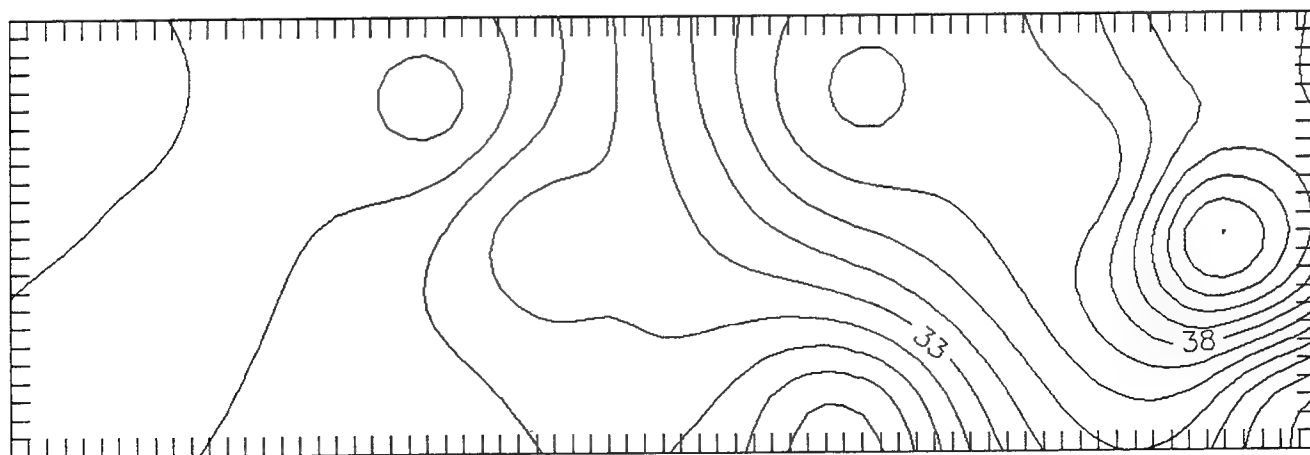
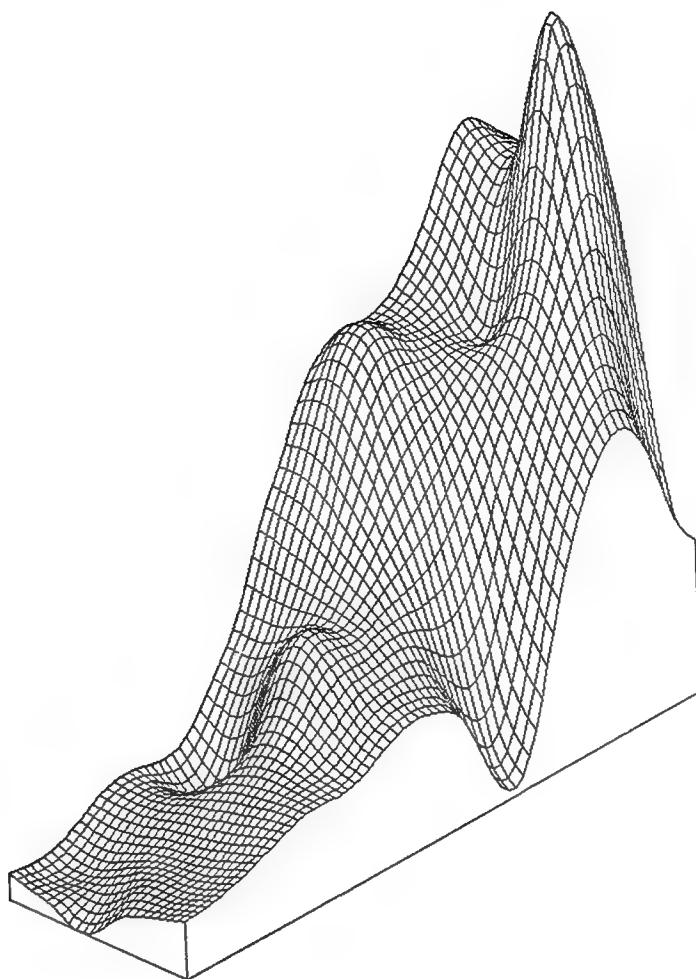
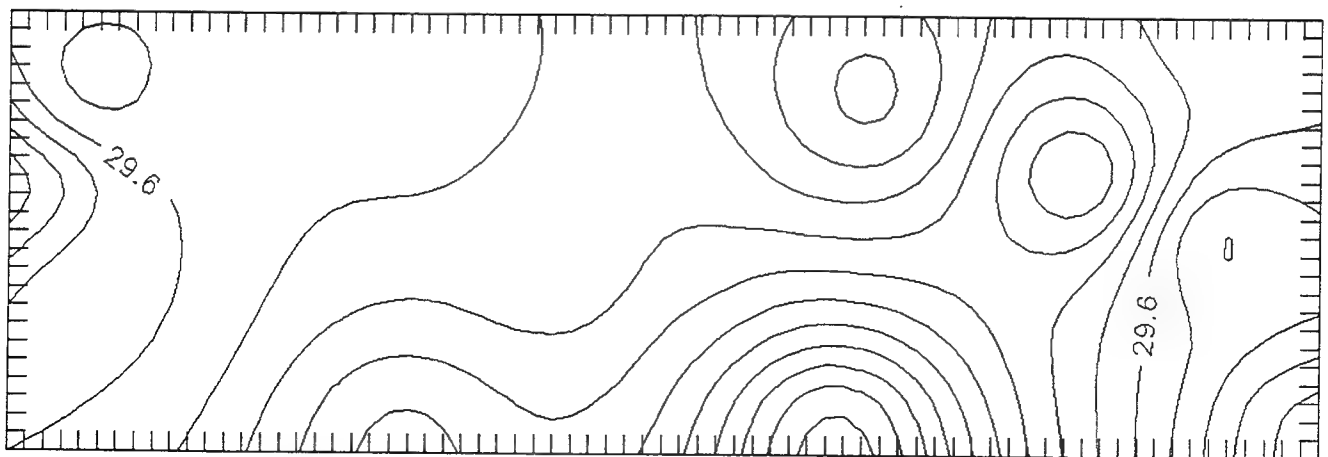
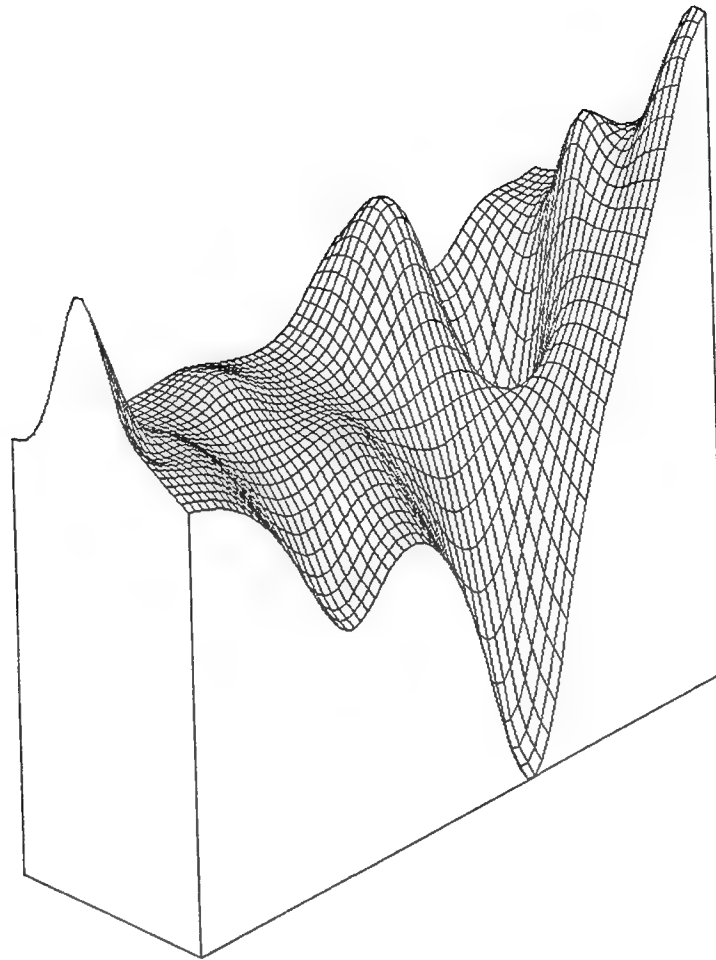


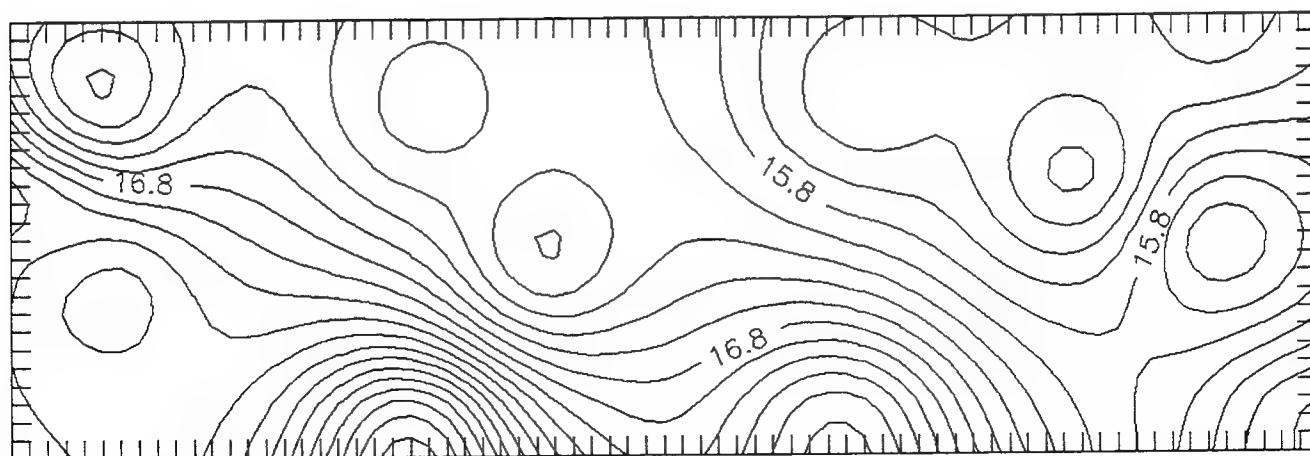
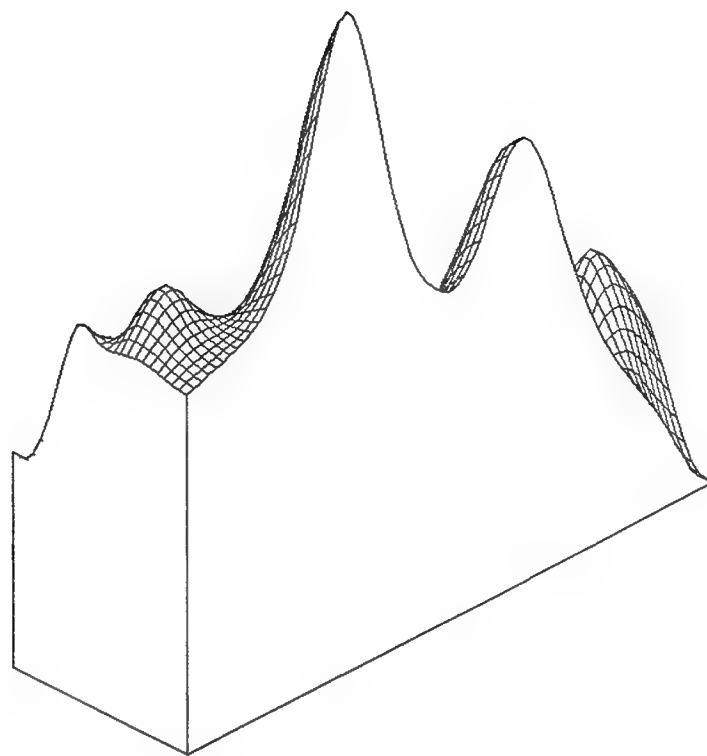
Figure 3.14 Illustration of soil and rock reference sites.



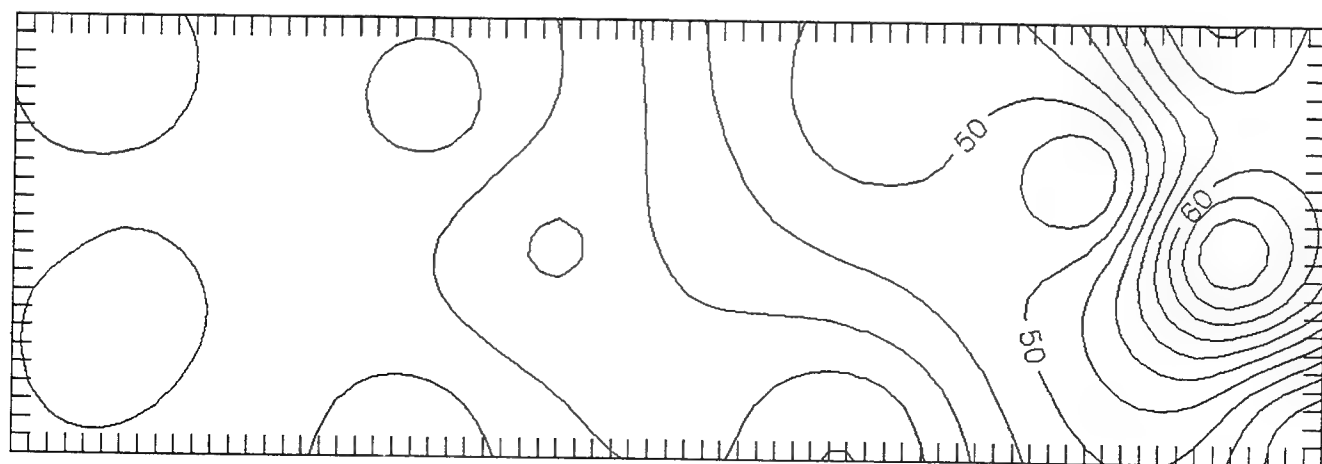
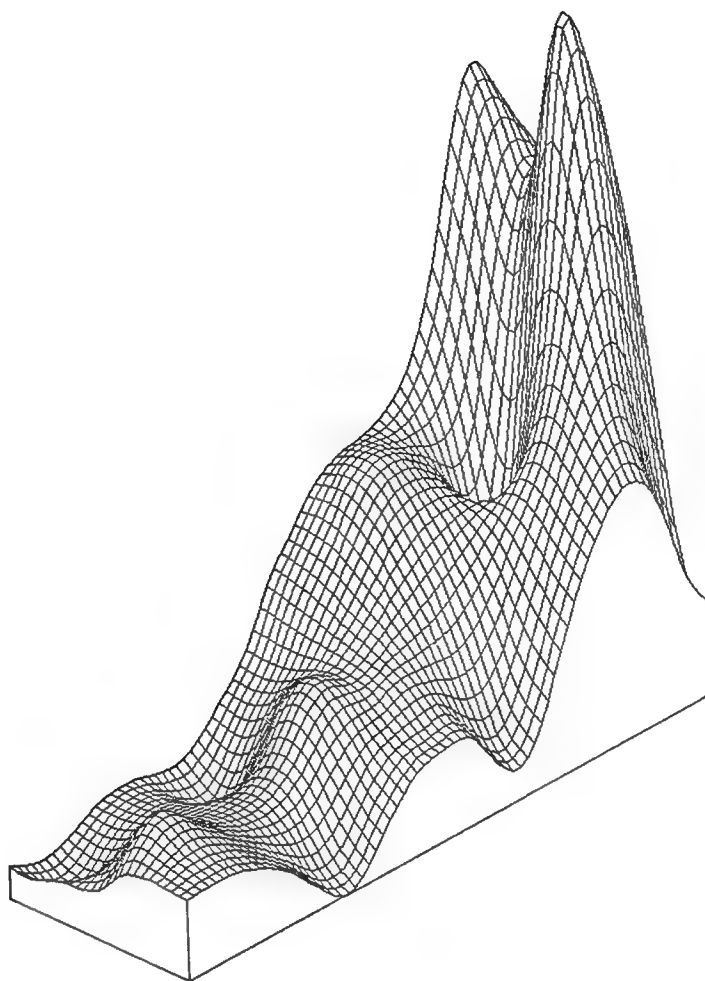
**Figure 3.15a. Surface plot based on rock reference site,
period range 0.5 to 0.7 seconds**



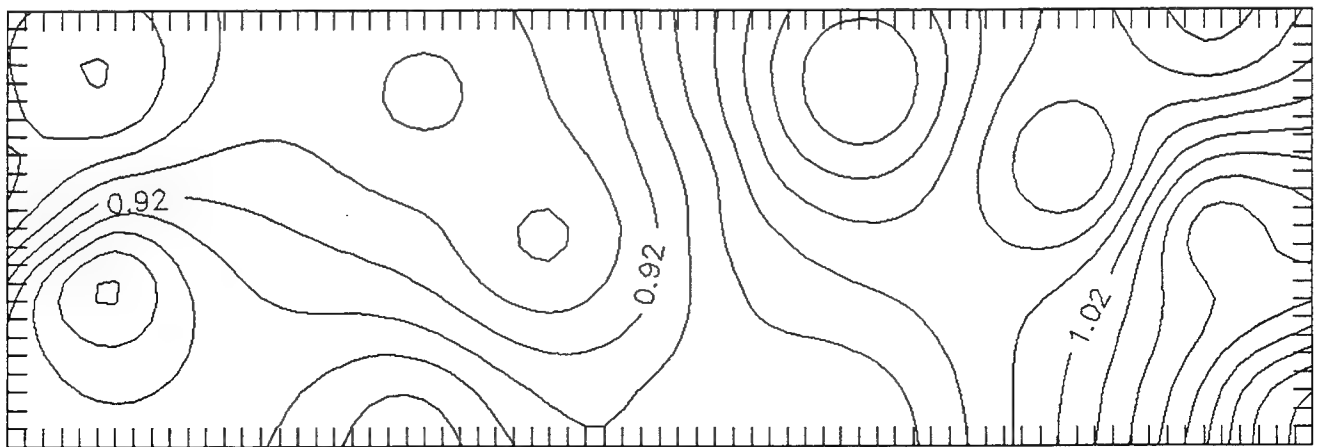
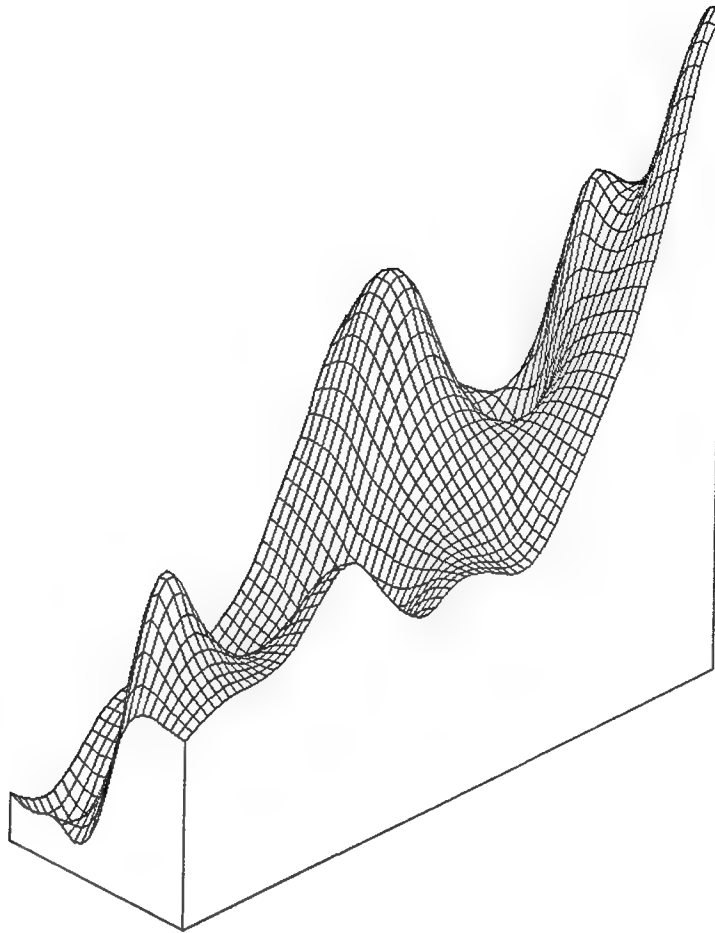
**Figure 3.15b. Surface plot based on rock reference site,
period range 0.7 to 1.0 seconds**



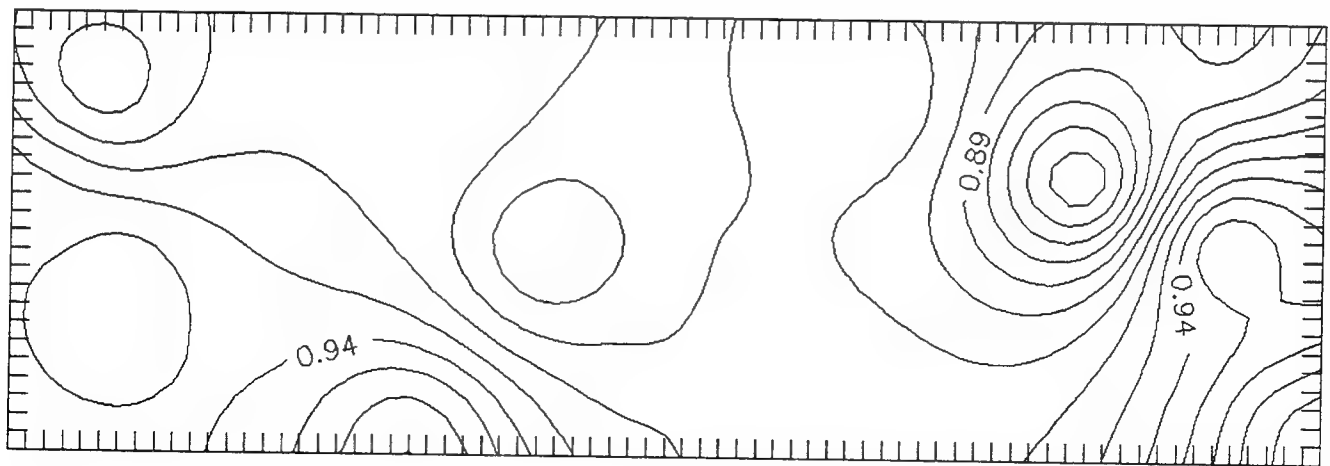
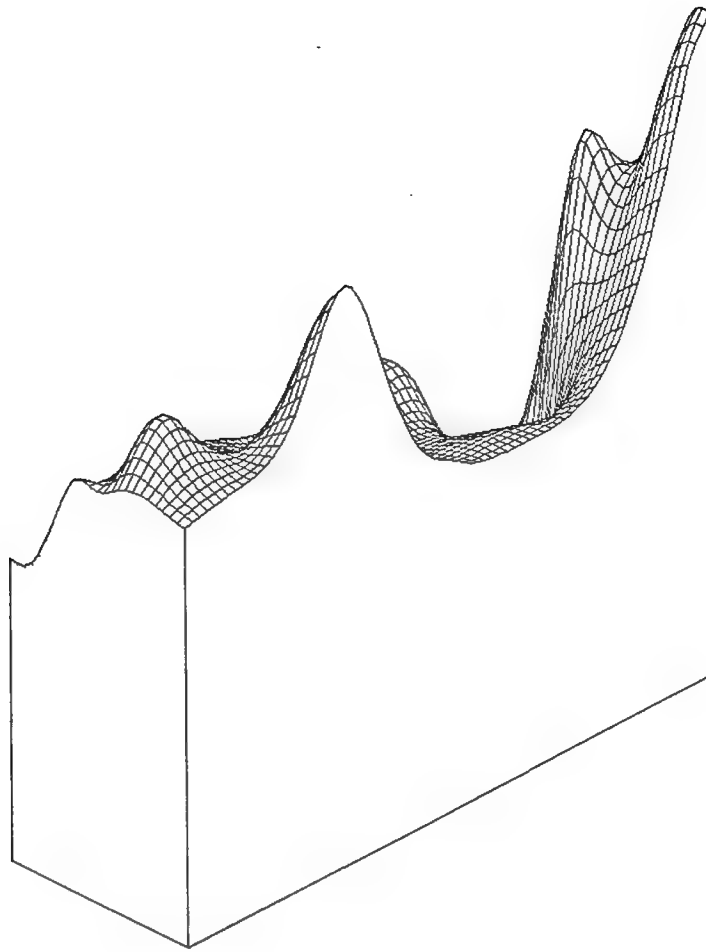
**Figure 3.15c. Surface plot based on rock reference site,
period range 2.0 to 4.0 seconds**



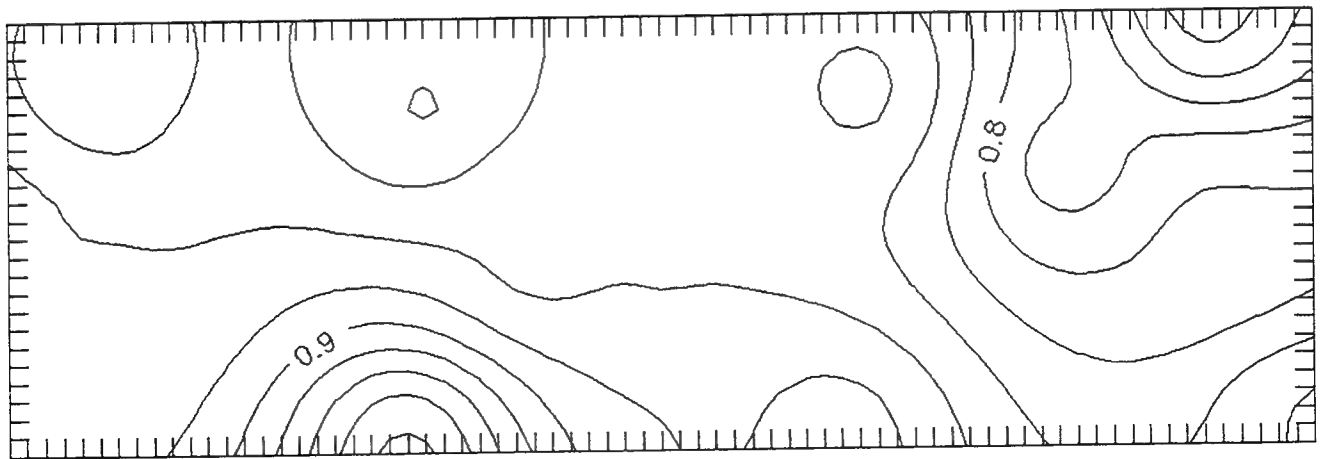
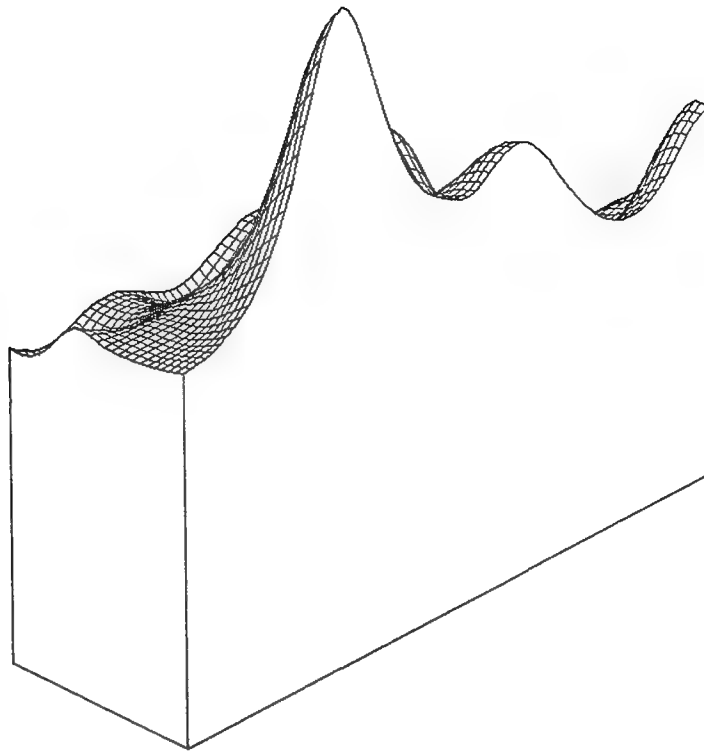
**Figure 3.15d. Surface plot based on rock reference site,
for peak over period range 0.5 to 10.0 seconds**



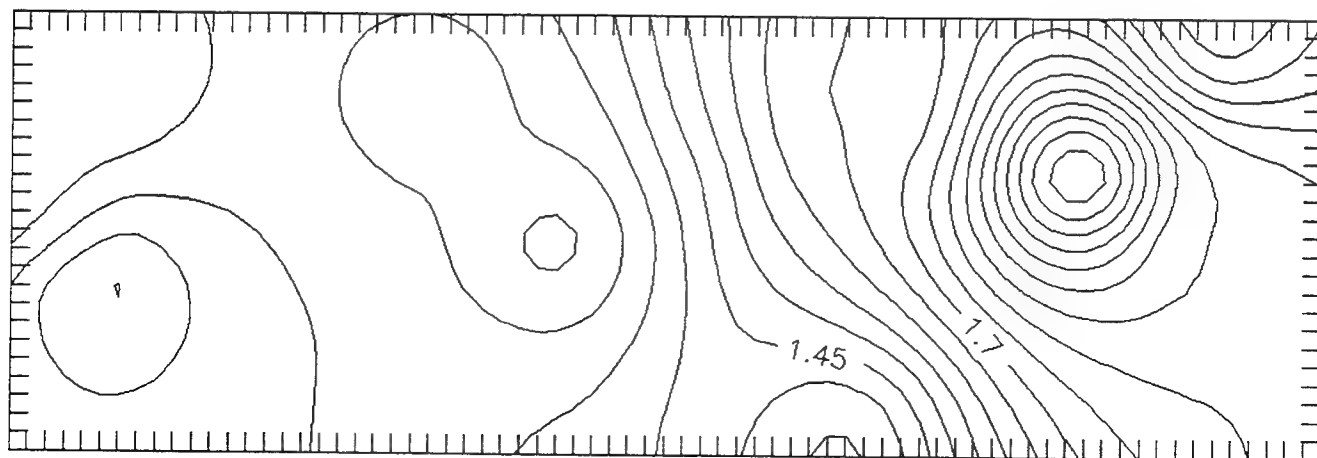
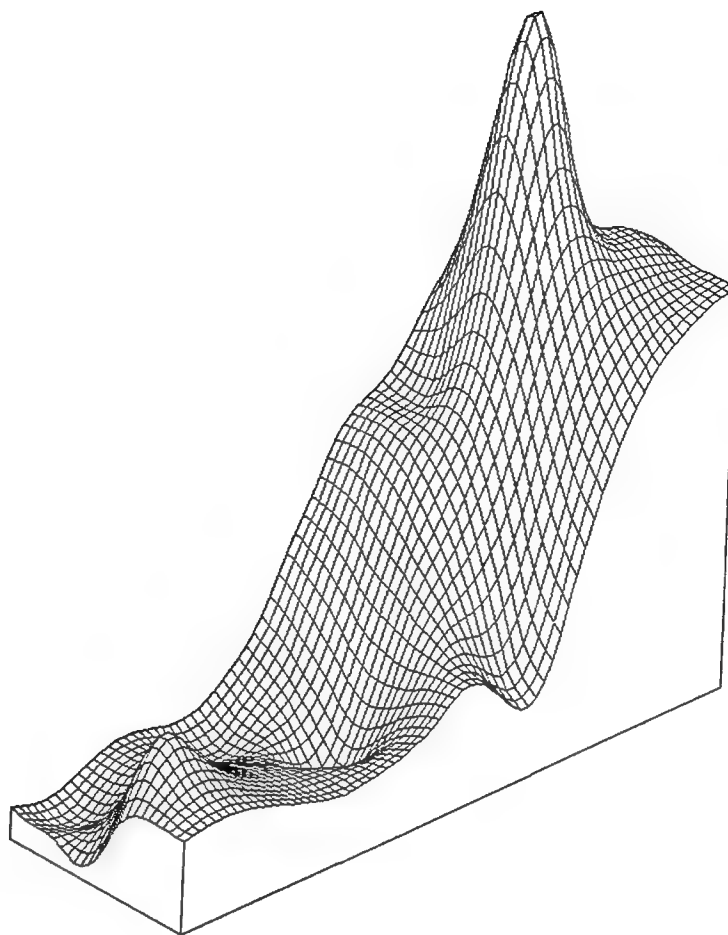
**Figure 3.16a. Surface plot based on soil reference site,
period range 0.5 to 0.7 seconds**



**Figure 3.16b. Surface plot based on soil reference site,
period range 0.7 to 1.0 seconds**



**Figure 3.16c. Surface plot based on soil reference site,
period range 2.0 to 4.0 seconds**



**Figure 3.16d. Surface plot based on soil reference site,
for peak over period range 0.5 to 10.0 seconds**

Chapter 4 Investigation of Nonlinear Amplification.

Introduction

The Port Hueneme site and the Treasure Island site are fairly typical Navy soft sites associated with waterfront construction. Both the Port Hueneme and Treasure Island studies showed that microseism measurements produce high levels of spectral ratio amplification. These levels are much higher than would be expected during the strong ground motion shaking associated with a large earthquake. It is of major importance to the understanding of microseism usage that the phenomenon of high amplification be explored. There appears to be an inverse relationship between amplification and level of excitation.

Earthquake Data Treasure Island

Data was compiled in an attempt to develop a trend to amplification at soft sites. Darragh and Shakal (1991) report data for Treasure Island and Figure 4.1 shows peak spectral ratios for the Treasure Island / Yerba Buena site pairs for the Loma Prieta earthquake and a number of aftershocks. Note that the Yerba Buena site serves as a rock reference site for the soft soil site at Treasure Island and the Y axis reflects the peak rock velocity at the reference site. Also plotted on Figure 4.1 is the microseism data recorded by the author and discussed in Chapter 6 of a previous report, Ferritto (1994). Note that the microseism data points are an extension of the strong motion data establishing a clear trend.

Earthquake Data Gilroy

Darragh and Shakal (1991) also report data for Gilroy and Figure 4.2 shows peak spectral ratios for the Gilroy #2 / Gilroy #1 site pairs for the Loma Prieta, Morgan Hill and Coyote Lake earthquakes. As part of this research, microseism measurements were made at the Gilroy sites and the microseism spectral ratios are given in Figure 4.3 and also plotted on Figure 4.2. Gilroy #1 is a rock site and Gilroy #2 is an alluvium site whose profile and shear wave velocity is given in Figure 4.4 according to Gibbs (1992). The microseism data when taken in conjunction with data shown Figure 4.1 confirm the trend shown.

Earthquake Data Coalinga

Borcherdt (1983) presents acceleration data for the Coalinga earthquake of 1983 and 18 aftershocks. The data is presented in terms of acceleration ratio of soil to rock sites rather than as spectral ratio as presented above. However the data is shown in Figure 4.5 to confirm the trend that as the peak rock velocity decreases an increase in amplification is seen on alluvial sites.

Earthquake Data Northridge, USC Data

The Northridge earthquake of January 17, 1994, Magnitude 6.7 presented the opportunity to obtain high quality data. As part of this task data recorded on the University of Southern California Network was digitized for the main shock and 5 aftershocks. Five site pairs were selected and the available events are shown as follows:

Rock Site	Soil Site	Events
USC 61	USC 63	Main Shock After Shock 1 After Shock 4 After Shock 5
USC 16	USC 18	Main Shock After Shock 1 After Shock 2 After Shock 5
USC 61	USC 60	Main Shock After Shock 1 After Shock 4 After Shock 5
USC 16	USC 49	Main Shock After Shock 1 After Shock 2 After Shock 5
USC 16	USC 13	Main Shock After Shock 1 After Shock 2 After Shock 3

The data recording stations are listed in Table 4.1 and the recorded events are given in Table 4.2. Figure 4.6 shows the locations of the recording stations and the events. Table 4.3 gives details of the recordings and Table 4.4 give available site characteristics. The following data reduction was performed at the University of Southern California. Each recorded acceleration was high pass-filtered so that both horizontal components have the same lower cut-off frequency. Motions in the radial and transverse direction were evaluated. From each time history three segments were defined such that Segment 1 is a 12 second segment of strong shaking for the main event and 4 seconds for the aftershocks. The beginning of segment 1 precedes the time of arrival of S-waves at the station. Segment 2 is a 9 second duration segment for the main shock and 3 second duration segment for the aftershocks. It is taken after the strong motion and represents weak motion following arrivals composed of late surface waves or strong motion coda waves. The third segment encompasses both segments 1 and 3. Fourier spectrum were calculated for each record segment and the ratio for soft site/hard site determined.

Using the University of Southern California data discussed in the paragraph above, maximum and average spectral ratios for frequencies below 10 Hz were determined for each of the segments described above. The data was plotted as a function of both magnitude of the event and peak particle velocity at the rock station for the event. Although the ratios varied somewhat for each of the segments the general trend could be represented by any of the three sets of plots. Figure 4.7 to 4.11 show the main shock and aftershock average spectral ratios for the five site location pairs as a function of the peak particle velocity measured at the rock site for the specific event. Figure 4.12 to 4.16 show main shock and aftershock peak spectral ratio for the 5 site pairs. Note that the sites are all characterized as stiff sites and do not exhibit the strong inverse dependence of amplification on peak rock velocity or level of excitation exhibited by the soft sites. To better illustrate this point Figures 4.17 to 4.21 show the spectra plots for the main shock and aftershocks plotted on the same graph. There does not appear to be any significant increase in aftershock amplification compared to the levels of the main shock.

Earthquake Data Northridge, CIT Data

Data for an additional 5 site pairs was obtained from the California Institute of Technology strong motion data base. The data consisted of the main shock and several aftershocks recorded at each site pair. Table 4.5 gives the station locations which are shown in Figure 4.22, and Table 4.6 gives the events recorded at each station which were used in this study and Table 4.7 give the recording site geology. Smoothed spectral ratios between soil and rock site pairs were determined and the maximum ratio between 0.5 and 2 Hz was plotted as a function of peak rock particle velocity recorded in each event, Figures 4.22 to 4.26. All the station pairs except pair 2 did not show an increase in amplification with decreasing levels of excitation. Station pair 2 composed of the rock site LA00 and the soil site LA02 (Century City) does show the inverse relationship between amplification and peak rock velocity. The LA02 site is a soil site noted to have terraced deposits. This site does seem to demonstrate a relationship between excitation level and amplification.

Discussion

The data presented in this chapter is intended to demonstrate the inverse relationship between spectra amplification and peak rock velocity for soft sites. Data on stiff sites seems to imply that the relationship does not apply to these sites. Microseism measurements on soft sites predict high amplification and seem to be a clear extension of the soft site data trend. The relationship supports the premise of strain dependent material properties such that as the strain levels increase an increase in damping and reduction in shear modulus is observed. Sugito (1991) presents a relationship for velocity amplification in terms of a beta factor which is a function of the site shear wave velocity and depth to bedrock.

While the microseism data noted here for soft sites confirms the general trend, additional microseism data is required on other sites to extend this relationship. The

Sugito approach does however provide a framework to extend the range of a possible relationship to include both strong motion and microseisms.

References

- Borcherdt, R. D. et. al. (1983) "Effects of local geologic conditions on strong-ground motions in the vicinity of Coalinga, California." USGS Open File Report 83-845
Workshop on Site Effects of Soil and Rock on Ground Motion and the Implications for Earthquake-Resistant Design, July 1983
- Darragh, R.B., and Shakal, A.F. (1991) "The site response of two rock and soil stations pairs to strong and weak ground motion", Bulletin Seismological Society America, 1885-1899
- Ferritto J. M. (1994) NFESC TR-2020-SHR "Feasibility For Use Of Microseisms As An Aid to Navy Base Microzonation" Port Hueneme CA August 1994
- Gibbs J et. al. (1992) USGS Open File Report 92-287 "Seismic velocities and geologic logs from borehole measurements at seven strong motion stations that recorded the 1989 Loma Prieta Earthquake", Menlo Park California 1992
- Sugito M et al (1991) "Nonlinear ground motion amplification factors based on local soil parameters" Proceedings Fourth International Conference on Seismic Microzonation, Stanford California

Table 4.1 USC Recording Station Locations

Stat. No.	Lat. (North)	Long. (West)	Address
USC# 13	34 7 54N, 118 26 22W		14145 MULHOLLAND DR., BEVERLY HILLS, CA
USC# 16	34 5 22N, 118 26 5N		700 N, FARING RD., LOS ANGELES, CA
USC# 18	34 5 15N, 118 21 55W		8023 WILLOUGHBY AV., HOLLYWOOD, CA
USC# 49	34 2 31N, 118 33 13W		17281 SUNSET BLVD., PACIFIC PALISADES, CA
USC# 60	34 14 16N, 118 15 13W		4747 NEW YORK AVE., LA CRESCENTA, CA
USC# 61	34 17 11N, 118 13 31W		BIG TUJUNGA STATION, ANGELES NATIONAL FOREST, CA
USC# 63	34 12 0N, 118 13 52W		3320 LAS PALMAS AVE., GLENDALE, CA

**Table 4.2 List of USC Events
Northridge Earthquake Sequence**

Earthquake Name	Date	Time (GMT)	Lat. (North)	Lon. (West)	MMI	Mag	Depth (km)
Main	01/17/1994	1230	34 12 48	118 32 13	8	6.7	18.4
Aft. (1)	01/17/1994	1231	34 16 43	118 28 22	-	5.9	0.0
Aft. (2)	01/17/1994	1239	34 15 40	118 32 02	-	4.5	14.8
Aft. (3)	01/17/1994	1306	34 15 16	118 32 42	-	4.6	0.0
Aft. (4)	01/19/1994	1409	34 12 52	118 30 34	-	4.5	17.2
Aft. (5)	03/20/1994	2120	34 13 53	118 28 30	-	5.3	13.1

Table 4.3 List of USC Records

Log #	Ref #	Eq	Station	Vol_2 File	t (sec)	L_1 (sec)	L_2 (sec)	H (km)	R (km)	Azim. (deg)
94.130.0	FE001	main	USC #13	v2x1300.dat	2.0	12.	9.	18.4	12.7	134
94.160.0	FE002	main	USC #16	v2x1600.dat	2.5	12.	9.	18.4	16.7	145
94.180.0	FE003	main	USC #18	v2x1800.dat	3.0	12.	9.	18.4	21.1	131
94.490.0	FE004	main	USC #49	v2x4900.dat	1.0	12.	9.	18.4	19.2	184
94.600.0	FE005	main	USC #60	v2x6000.dat	3.5	12.	9.	18.4	26.2	83
94.610.0	FE006	main	USC #61	v2x6100.dat	4.0	12.	9.	18.4	29.8	74
94.630.0	FE007	main	USC #63	v2x6300.dat	3.0	12.	9.	18.4	28.2	92
94.130.1	FE008	aft (1)	USC #13	v2x1301.dat	2.0	4.	3.	.0	16.6	169
94.160.1	FE009	aft (1)	USC #16	v2x1601.dat	2.5	4.	3.	.0	21.4	170
94.180.1	FE010	aft (1)	USC #18	v2x1801.dat	3.0	4.	3.	.0	23.4	154
94.490.1	FE011	aft (1)	USC #49	v2x4901.dat	0.0	4.	3.	.0	27.4	195
94.600.1	FE012	aft (1)	USC #60	v2x6001.dat	2.0	4.	3.	.0	20.6	102
94.610.1	FE013	aft (1)	USC #61	v2x6101.dat	2.5	4.	3.	.0	22.7	88
94.630.1	FE014	aft (1)	USC #63	v2x6301.dat	2.5	4.	3.	.0	23.8	111
94.130.4	FE015	aft (2)	USC #13	v2x1304.dat	2.0	4.	3.	14.8	16.8	148
94.160.2	FE016	aft (2)	USC #16	v2x1602.dat	2.5	4.	3.	14.8	21.2	154
94.180.2	FE017	aft (2)	USC #18	v2x1802.dat	2.5	4.	3.	14.8	24.7	141
94.490.2	FE018	aft (2)	USC #49	v2x4902.dat	3.0	4.	3.	14.8	24.5	184
94.131.0	FE019	aft (3)	USC #13	v2x1310.dat	2.0	4.	3.	.0	16.7	144
94.160.3	FE020	aft (3)	USC #16	v2x1603.dat	2.0	4.	3.	.0	21.0	151
94.600.9	FE021	aft (4)	USC #60	v2x6009.dat	3.0	4.	3.	17.2	23.7	83
94.610.7	FE022	aft (4)	USC #61	v2x6107.dat	3.0	4.	3.	17.2	27.3	72
94.631.2	FE023	aft (4)	USC #63	v2x6312.dat	3.0	4.	3.	17.2	25.6	93
94.160.9	FE024	aft (5)	USC #16	v2x1609.dat	2.0	4.	3.	13.1	16.2	166
94.180.9	FE025	aft (5)	USC #18	v2x1809.dat	2.0	4.	3.	13.1	18.8	147
94.491.2	FE026	aft (5)	USC #49	v2x4912.dat	2.5	4.	3.	13.1	22.3	199
94.601.2	FE027	aft (5)	USC #60	v2x6012.dat	2.5	4.	3.	13.1	20.3	87
94.611.0	FE028	aft (5)	USC #61	v2x6110.dat	3.0	4.	3.	13.1	23.6	75
94.631.6	FE029	aft (5)	USC #63	v2x6316.dat	2.5	4.	3.	13.1	22.6	98

t = time when Segment 1 starts (measured from the trigger time)

L_1 = duration of Segment 1

L_2 = duration of Segment 2

H = depth of hypocenter

R = epicentral distance

Azim. = azimuth of the station (measured clockwise from North)

Table 4.4 Site Characterization USC Recording Stations

USC Site #	Depth of Sediments (feet)	Geotechnical Site Characteristic s*	Soil Site Classification s _L *	Average Shear Wave Velocity** in top 30 m	Overall Classification
13	5,000	0	1	C	Stiff soil over sediments
16	0	2	0	B	Rock
18	9,000	0	1	B	Stiff soil over sediments
49	?	0	1	C	Stiff soil over sediments
60	0	1	1	C	Stiff soil over rock
61	0	2	0	B	Rock
63	0	2	1	C	Stiff soil over rock

* See Trifunac (1990) Earthqu. Engng & Struct. Dynam. Vol. 19, No. 6, 833--846

** A: $v > 760$ m/sec;

B: $360 \text{ m/sec} < v < 760 \text{ m/sec}$

C: $180 \text{ m/sec} < v < 360 \text{ m/sec}$

D: $v < 180 \text{ m/sec}$

Table 4.5 Location of sites in California Institute of Technology data base.

Code	Latitude	Longitude	Station Site location
	North	West	
LA00	34.1062	118.4542	Stone Canyon Reservoir Dam also SCY
LA02	34.0630	118.4180	LA Country Club Century City also LCN
LA03	34.0900	118.3390	Hollywood Storage Grounds also HSB
LA04	34.0700	118.1500	Freemont School Alhambra also ALHA
JFPP	34.3120	118.4960	Jenson Filtration Plant Generator Bldg.
NWHP	34.3880	118.5332	Newhall LA County Fire Dept
PAS	34.148	118.170	Kresge Lab
USC	34.019	118.285	Museum of Science and Technology Exposition Blvd.
DGR	33.650	117.009	Dominigoni Reservoir
SVD	34.104	117.097	Seven Oaks Dam inside tunnel

Table 4.6 Location of sites in California Institute of Technology data base.

Event Id	Latitude North	Longitude West	Local Magnitude	1	2	Magnitude		
94017123157	34:16.71	118:28.36	5.9	1	2	3	4	5
94017132644	34:19.03	118:27.29	4.7		2		4	
94017135602	34:17.09	118:37.43	4.4		2			
94017233330	34:19.58	118:41.90	5.6				4	
94017234925	34:20.55	118:39.93	4.0	1	2			
94018003935	34:22.72	118:33.79	4.4		2			
94018040126	34:21.45	118:37.34	4.3		2			
94018152346	34:22.72	118:33.64	4.8	1				
94019210928	34:22.71	118:42.64	5.1	1		3		
94021183915	34:18.06	118:27.97	4.6	1				
94021185244	34:17.90	118:27.14	4.1	1		3		
94021185344	34:17.62	118:27.68	4.2			3		
94023085508	34:17.95	118:25.69	4.1					5
94024041518	34:20.71	118:33.13	4.6					5
94027171958	34:16.41	118:33.75	4.6					5
94028200953	34:22.46	118:29.69	4.2					5
94029112035	34:18.32	118:34.76	5.1				4	
94029121656	34:16.69	118:36.65	4.3					5
94056125912	34:21.42	118:28.79	4.1				4	
94042140753	34:20.40	118:28.80	3.6				4	

Table 4.7 Geology of sites in California Institute of Technology data base.

Code	Latitude North	Longitude West	Site Conditions
LA00	34.1062	118.4542	Pre-Tertiary Jurassic marine bedrock at dam
LA02	34.0630	118.4180	Pleistocene nonmarine terrace Deposits
LA03	34.0900	118.3390	Pleistocene nonmarine deep alluvium 130m, sandstone and shale
LA04	34.0700	118.1500	Pleistocene nonmarine few hundred feet of alluvium, siltstone
JFPP	34.3120	118.4960	Quaternary sedimentary bedrock Saugus Formation.
NWHP	34.3880	118.5332	Alluvium
PAS	34.148	118.170	Weathered Mesozoic granitic rock tonalite diorite
USC	34.019	118.285	400 ft of alluvium over clay and shale
DGR	33.650	117.009	Rock, Dominigoni Reservoir
SVD	34.104	117.097	Alluvium, Seven Oaks Dam inside tunnel

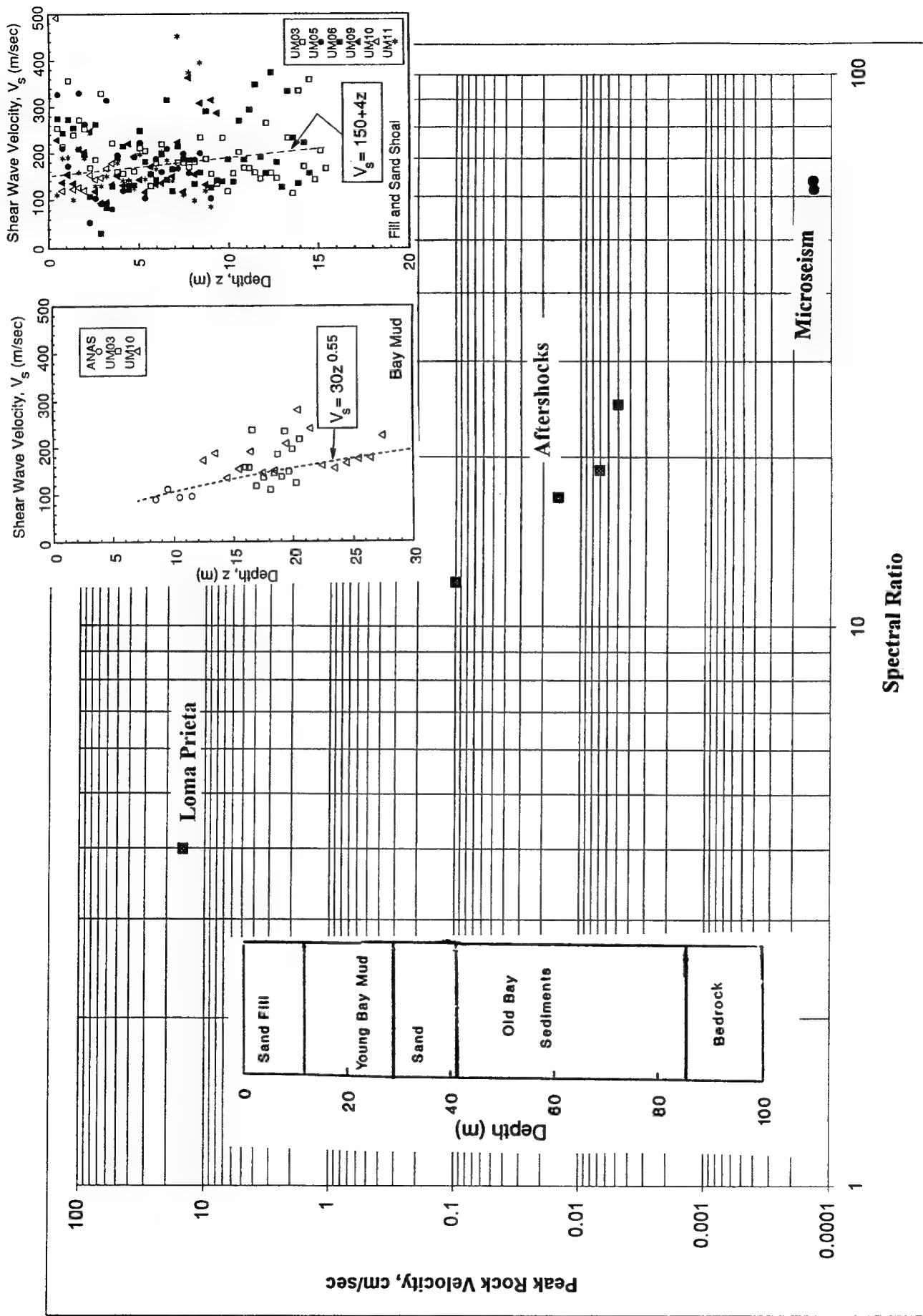


Figure 4.1. Spectral ratio for Treasure Island/Yerba Buena pairs

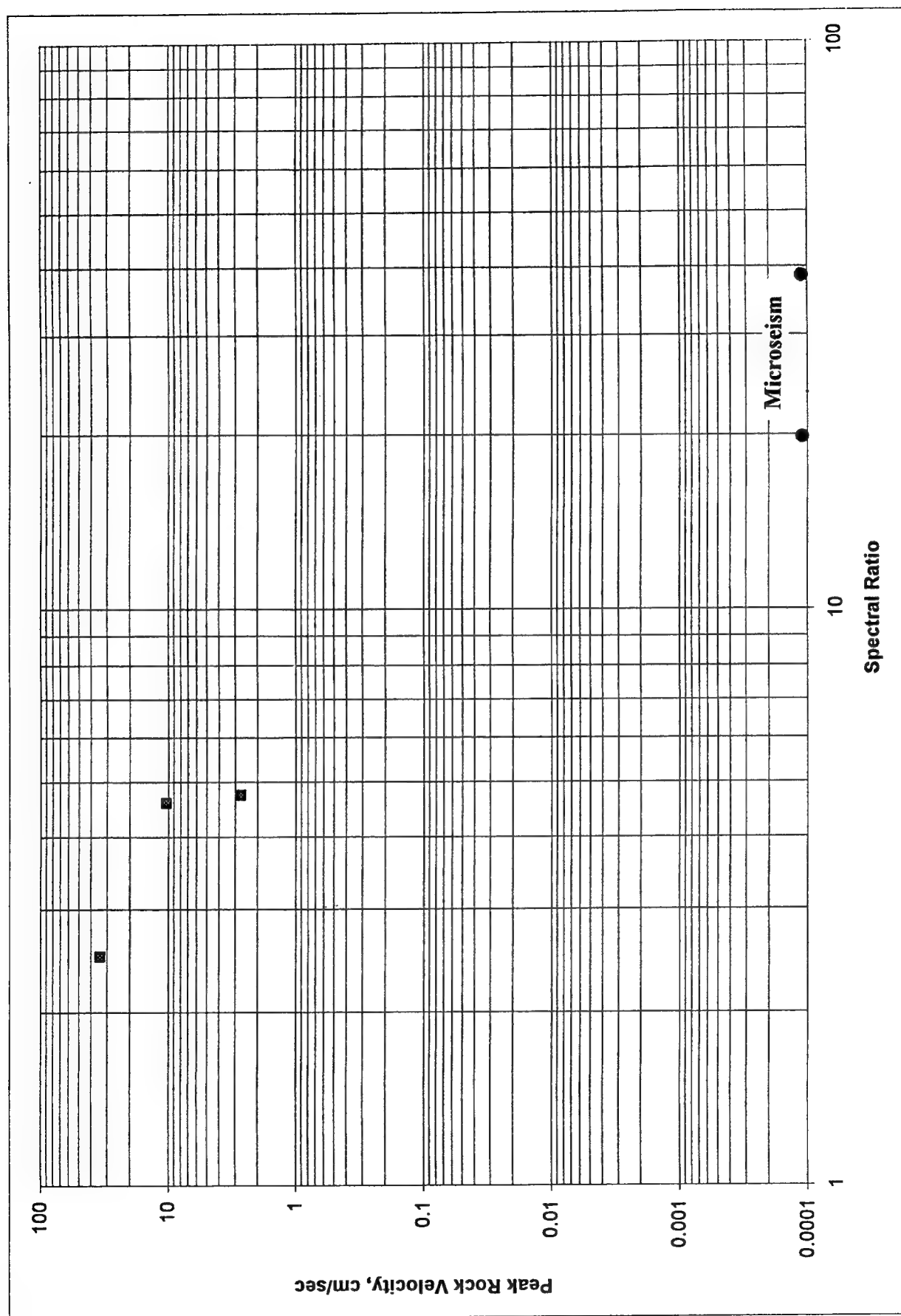


Figure 4.2. Spectral ratio for Gilroy #2/Gilroy#1 pairs

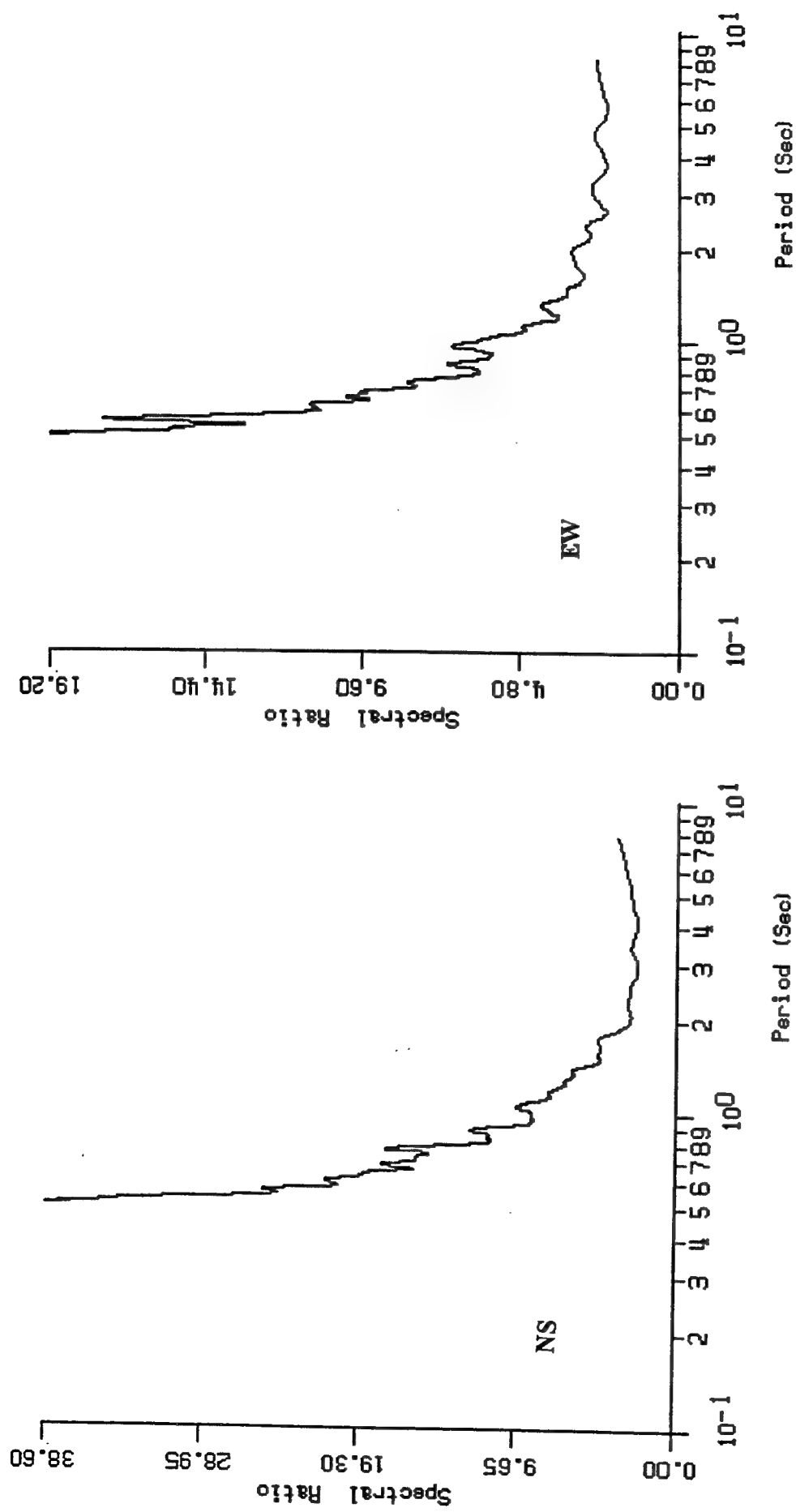


Figure 4.3. Gilroy #2/Gilroy #1 microseism spectral ratios

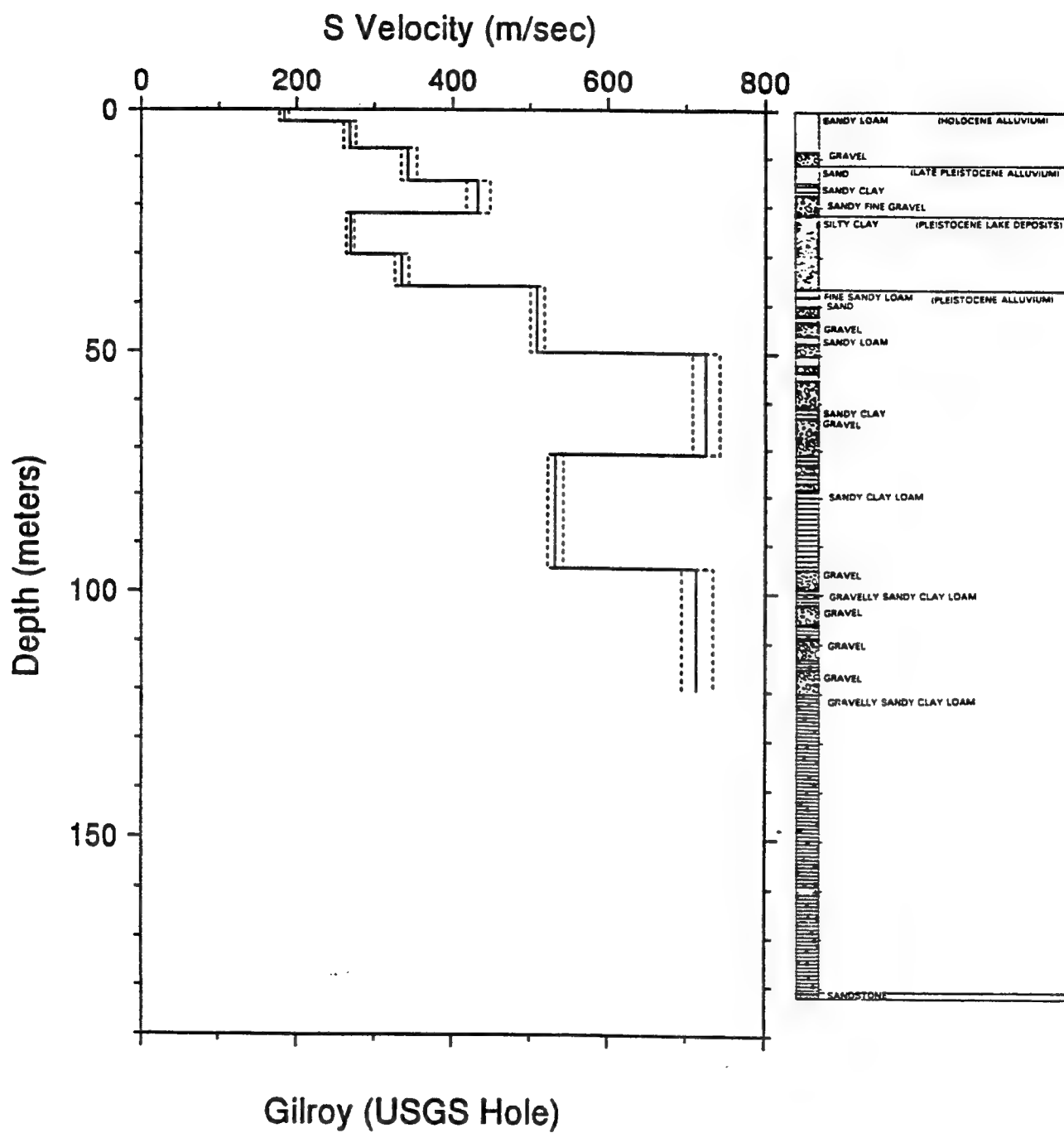


Figure 4.4. Gilroy #2 profile.

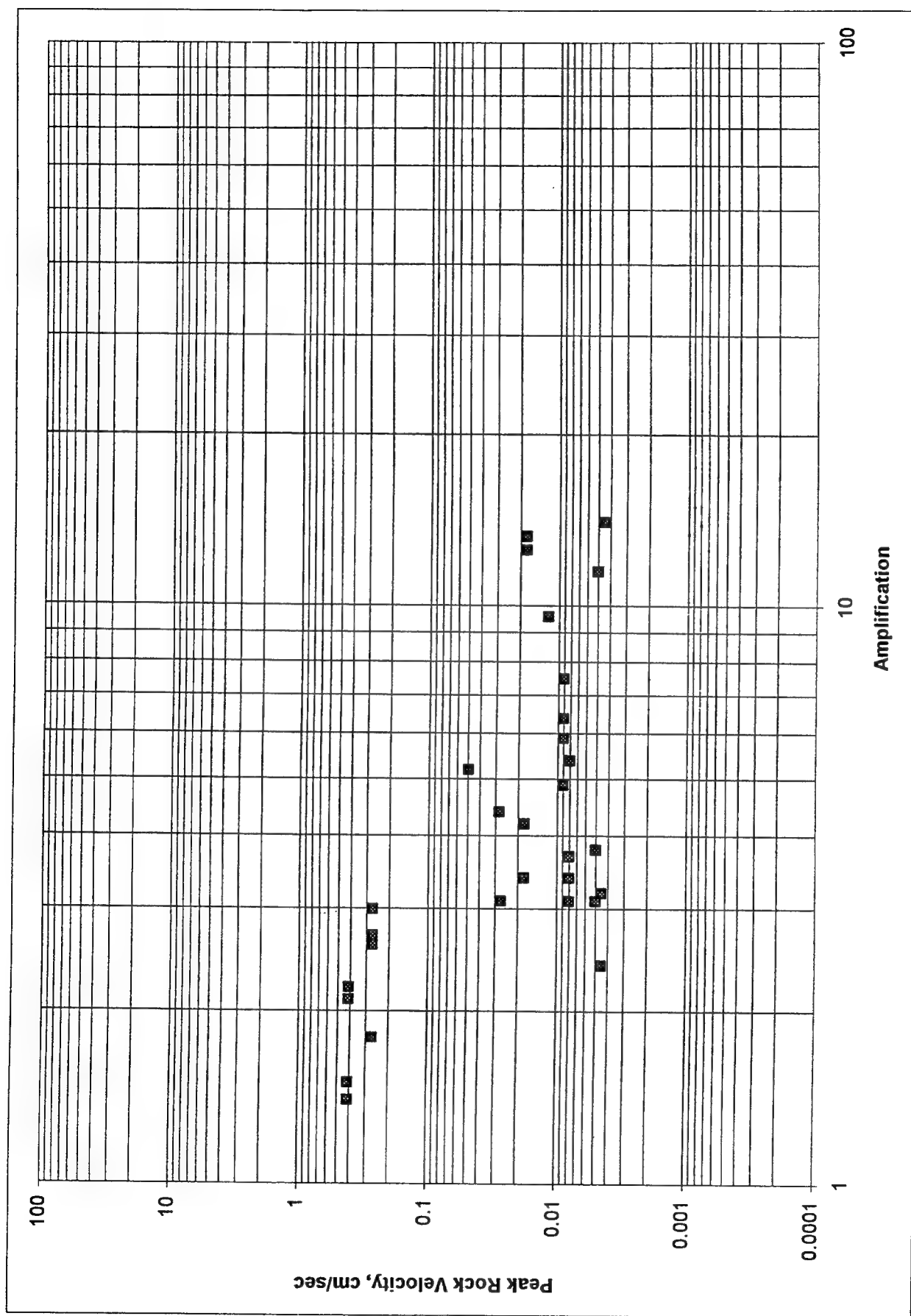


Figure 4.5. Amplification Coalinga pairs

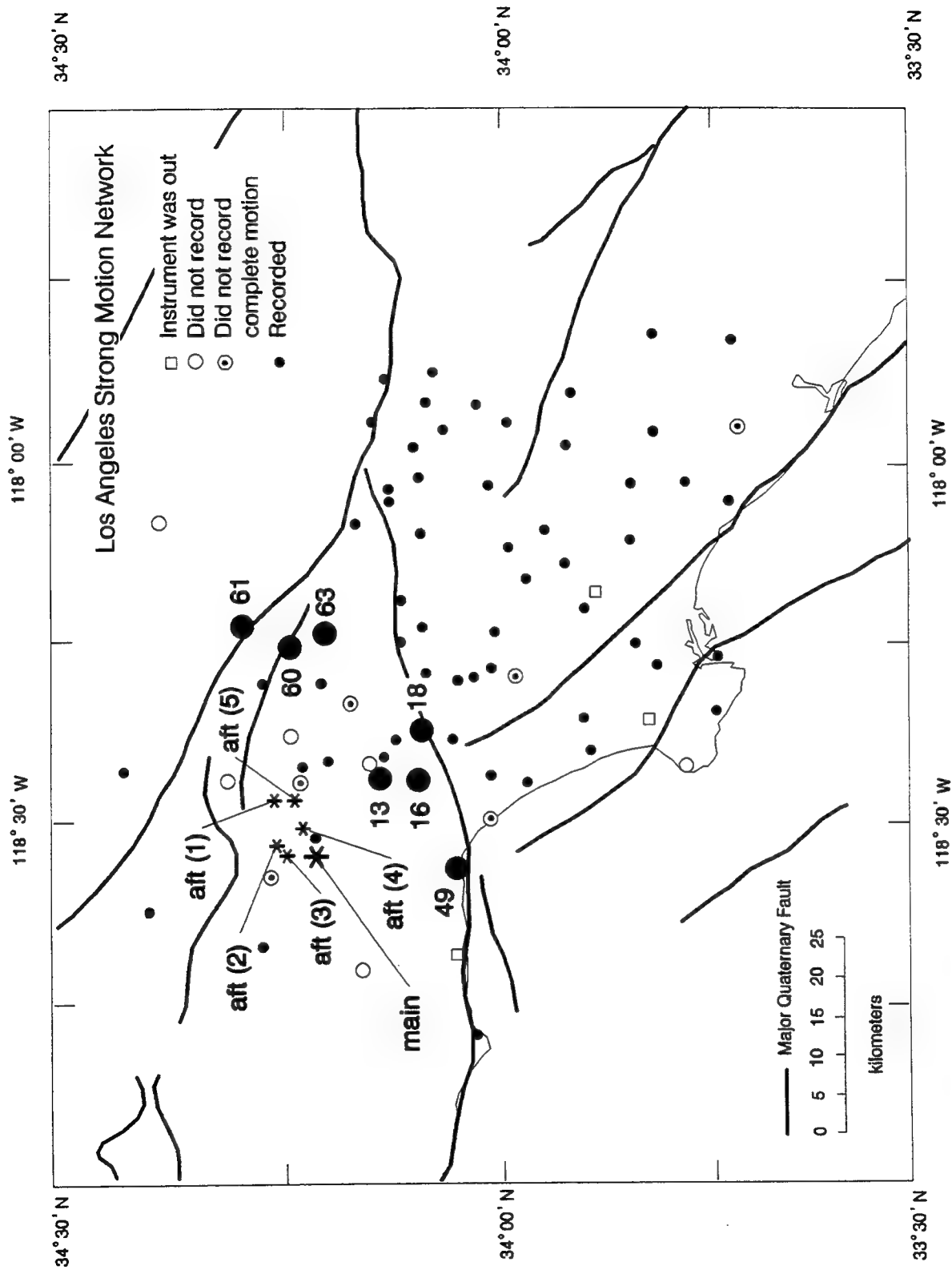


Figure 4.6 Location of USC recording stations and event epicenters.

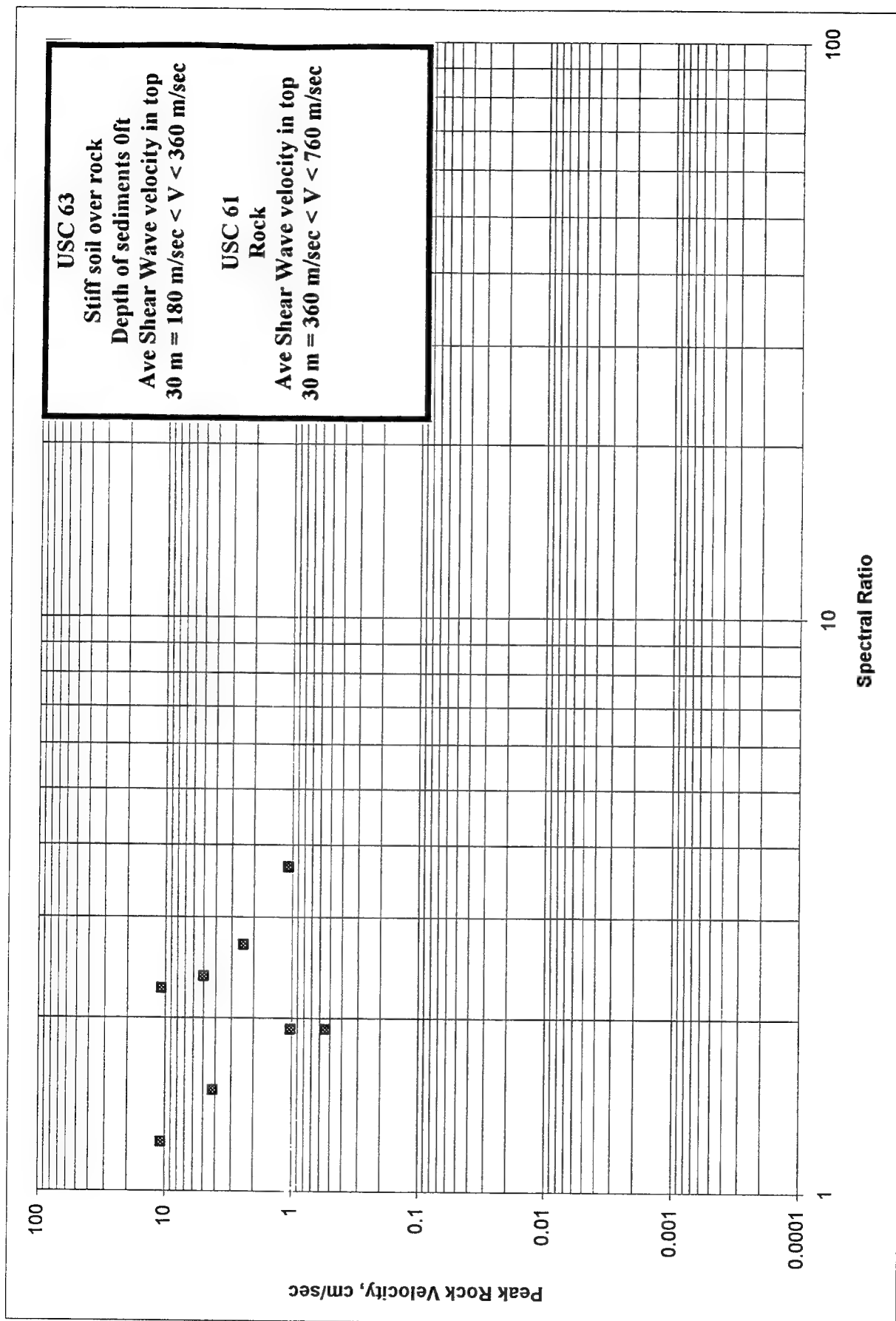


Figure 4.7. USC site pair 1 average spectral ratios, Northridge sequence.

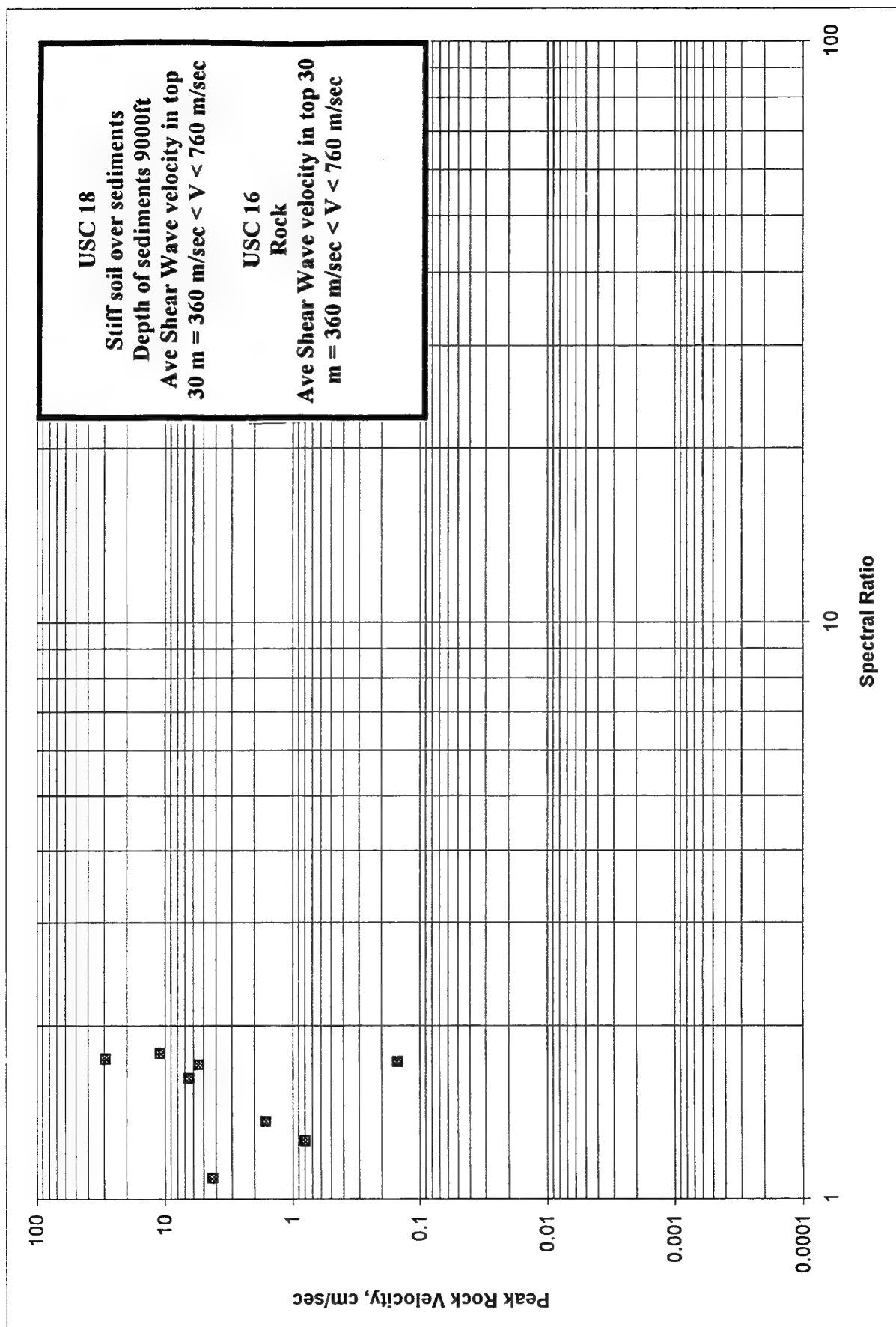


Figure 4.8. USC site pair 2 average spectral ratios, Northridge sequence.

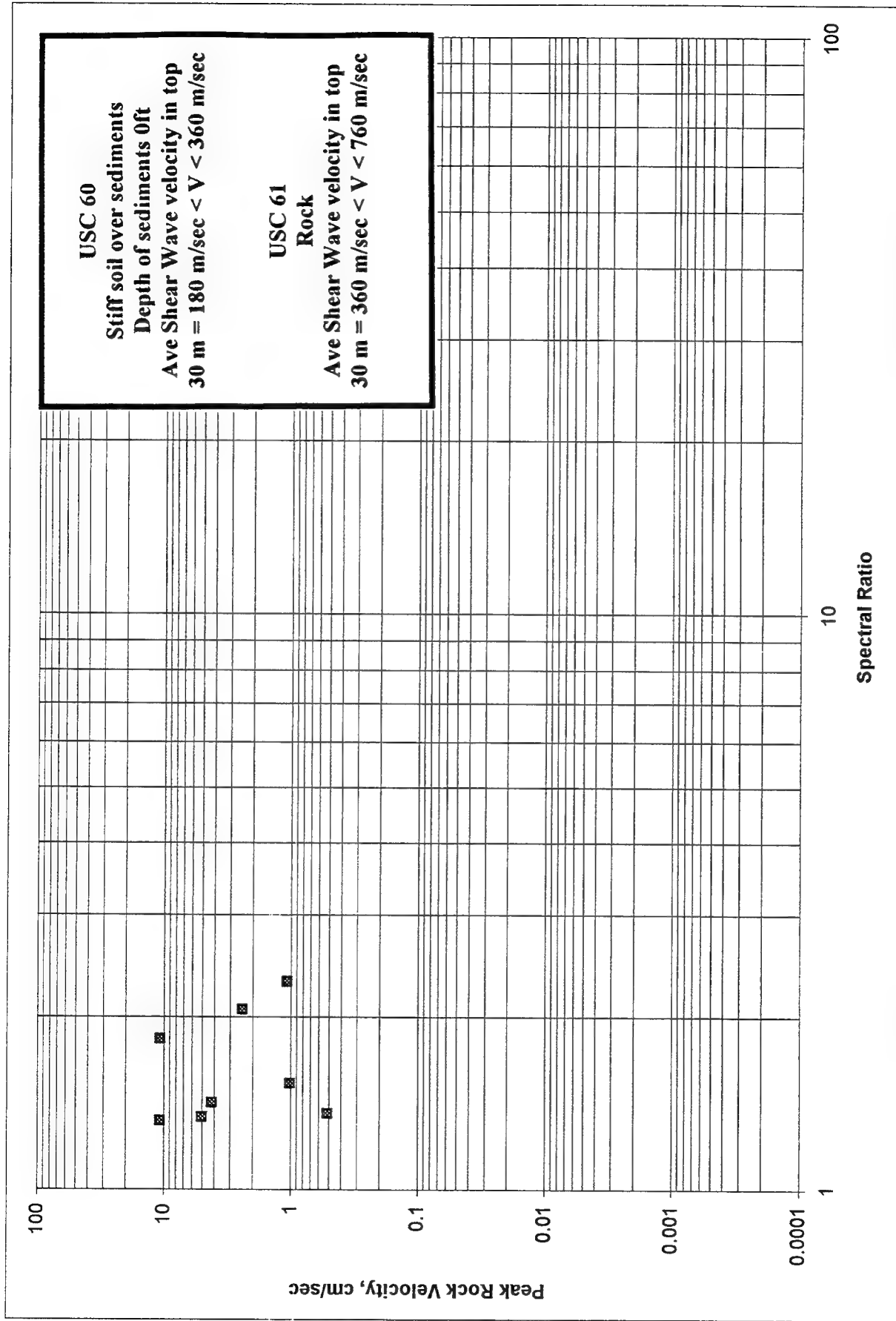


Figure 4.9. USC site pair 3 average spectral ratios, Northridge sequence.

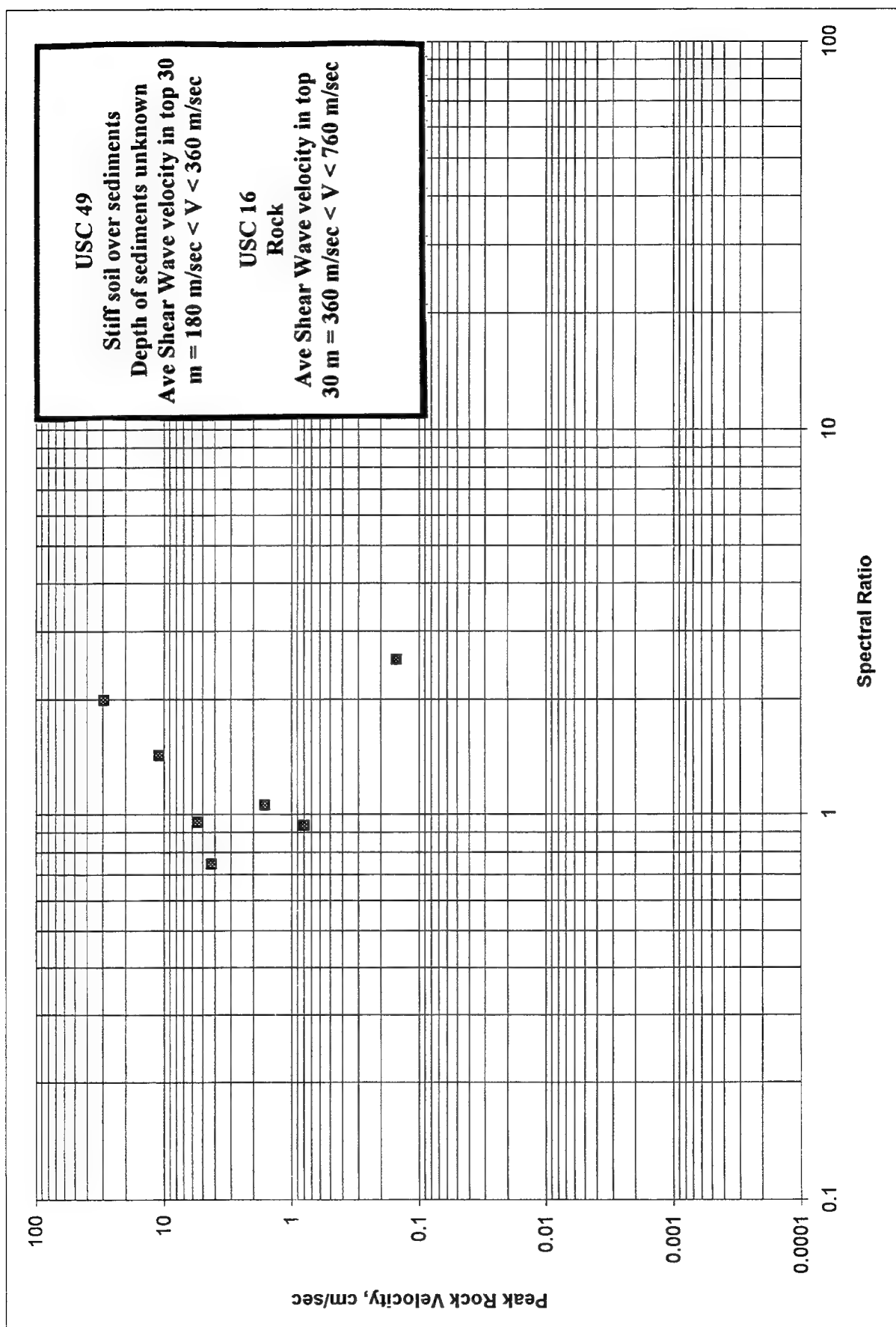


Figure 4.10. USC site pair 4 average spectral ratios, Northridge sequence.

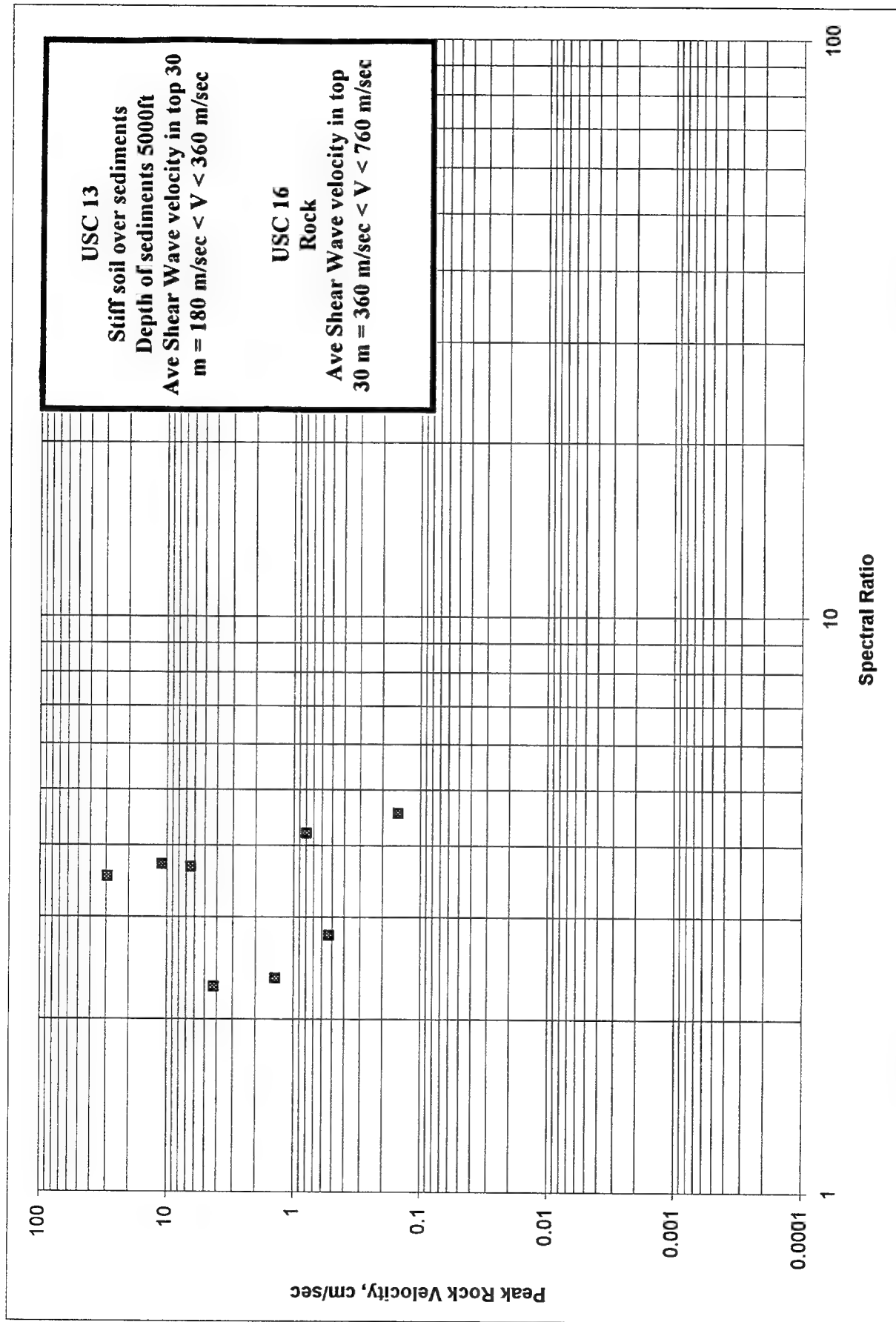


Figure 4.11. USC site pair 5 average spectral ratios, Northridge sequence.

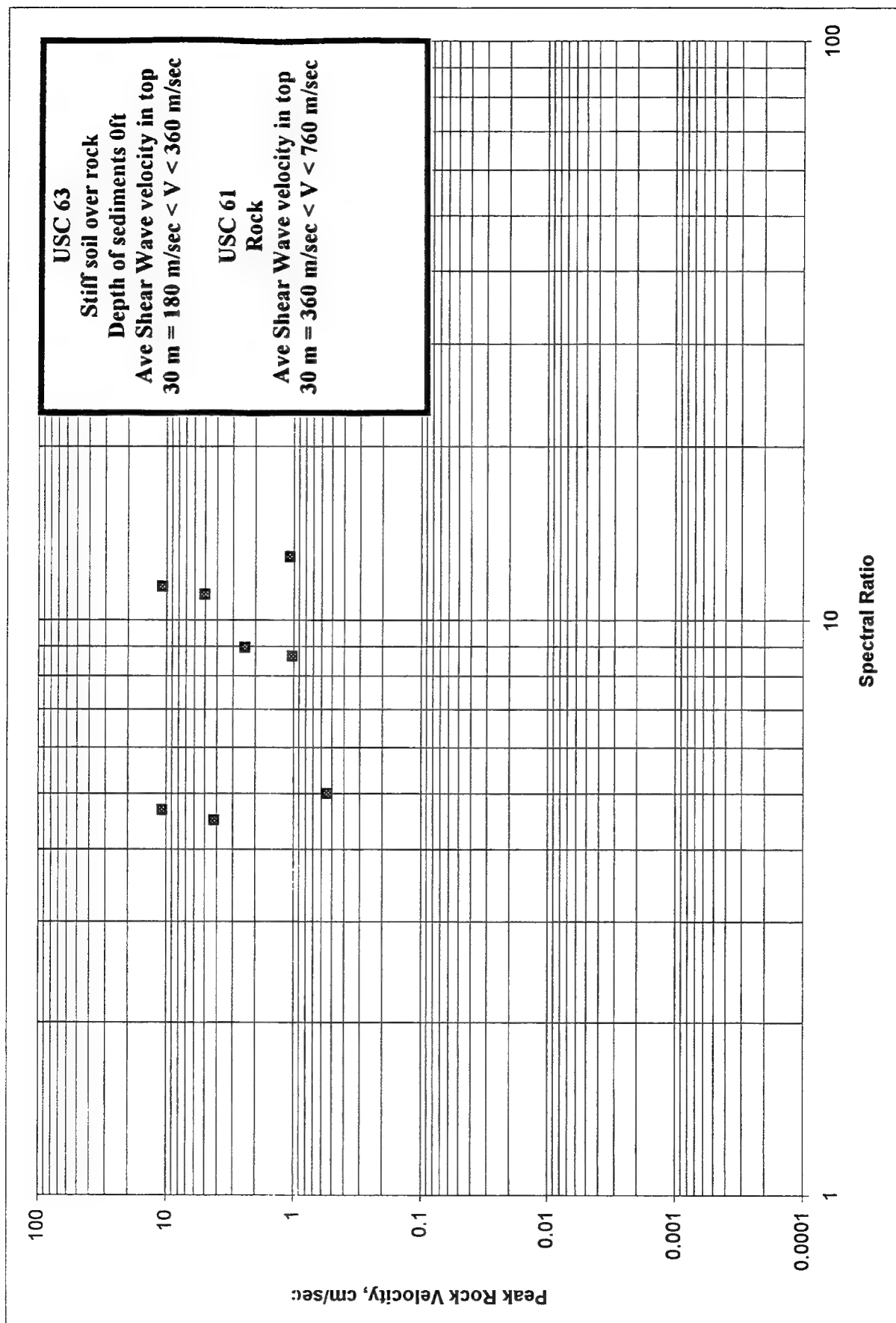


Figure 4.12. USC site pair 1 maximum spectral ratios, Northridge sequence.

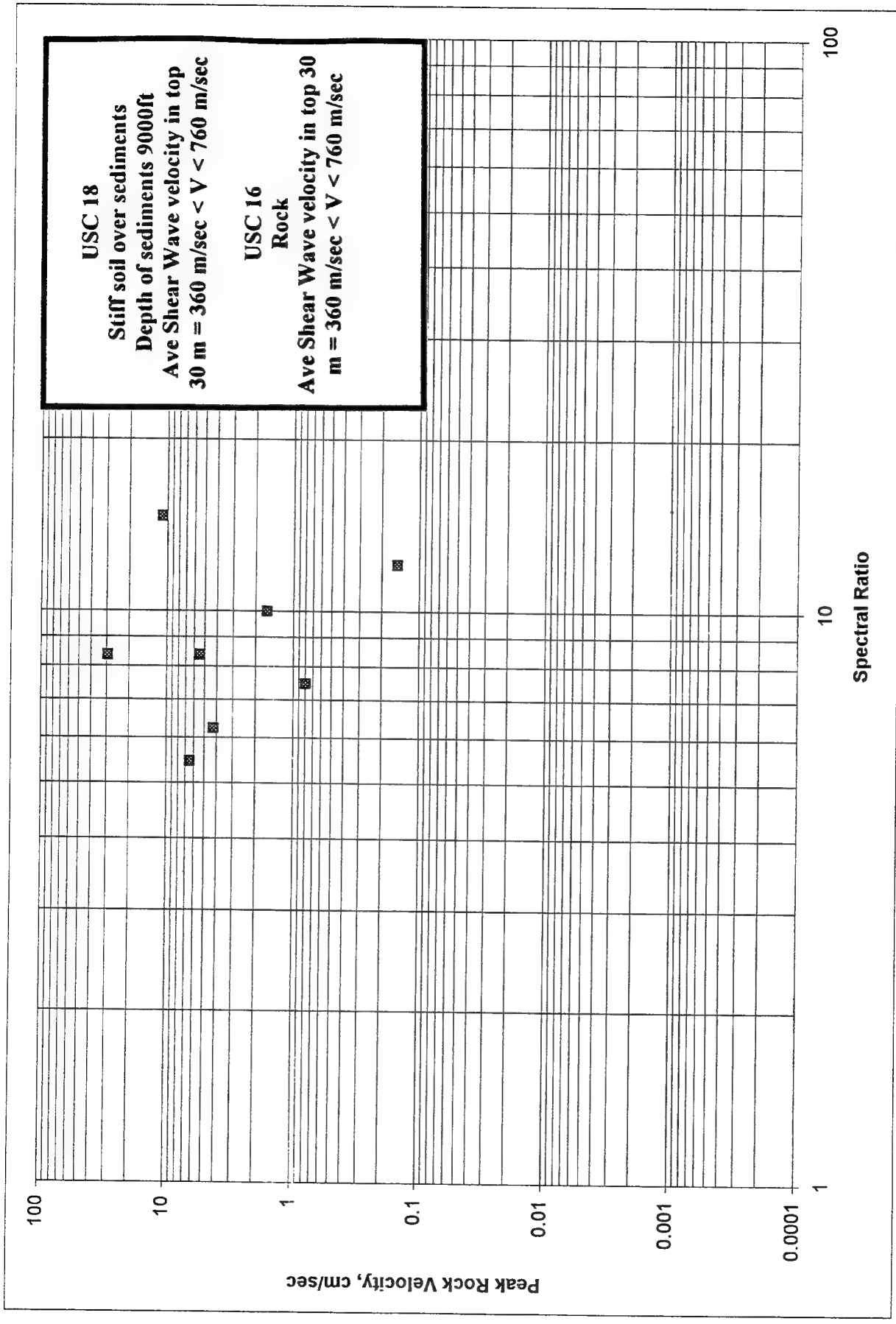


Figure 4.13. USC site pair 2 maximum spectral ratios, Northridge sequence.

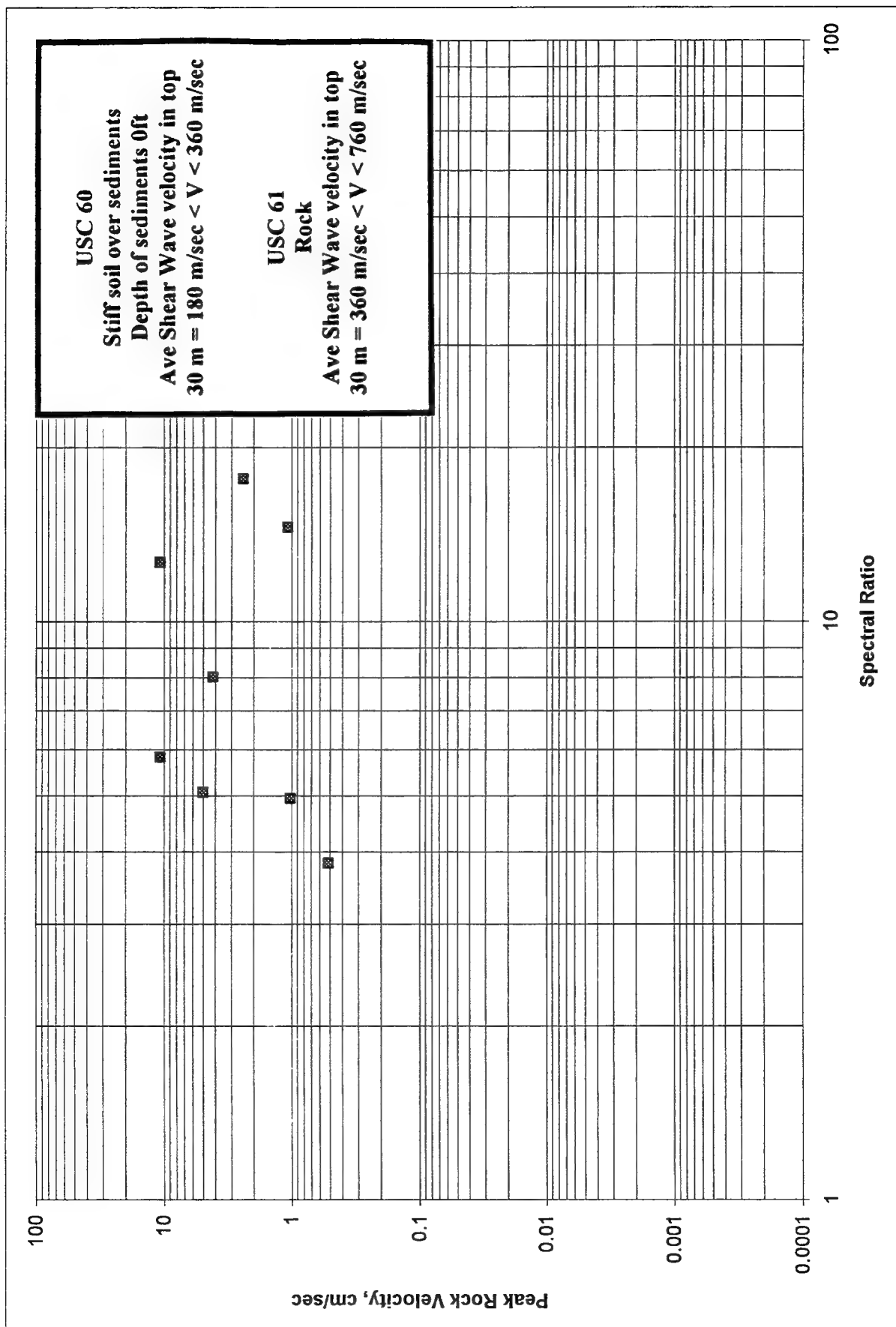


Figure 4.14. USC site pair 3 maximum spectral ratios, Northridge sequence.

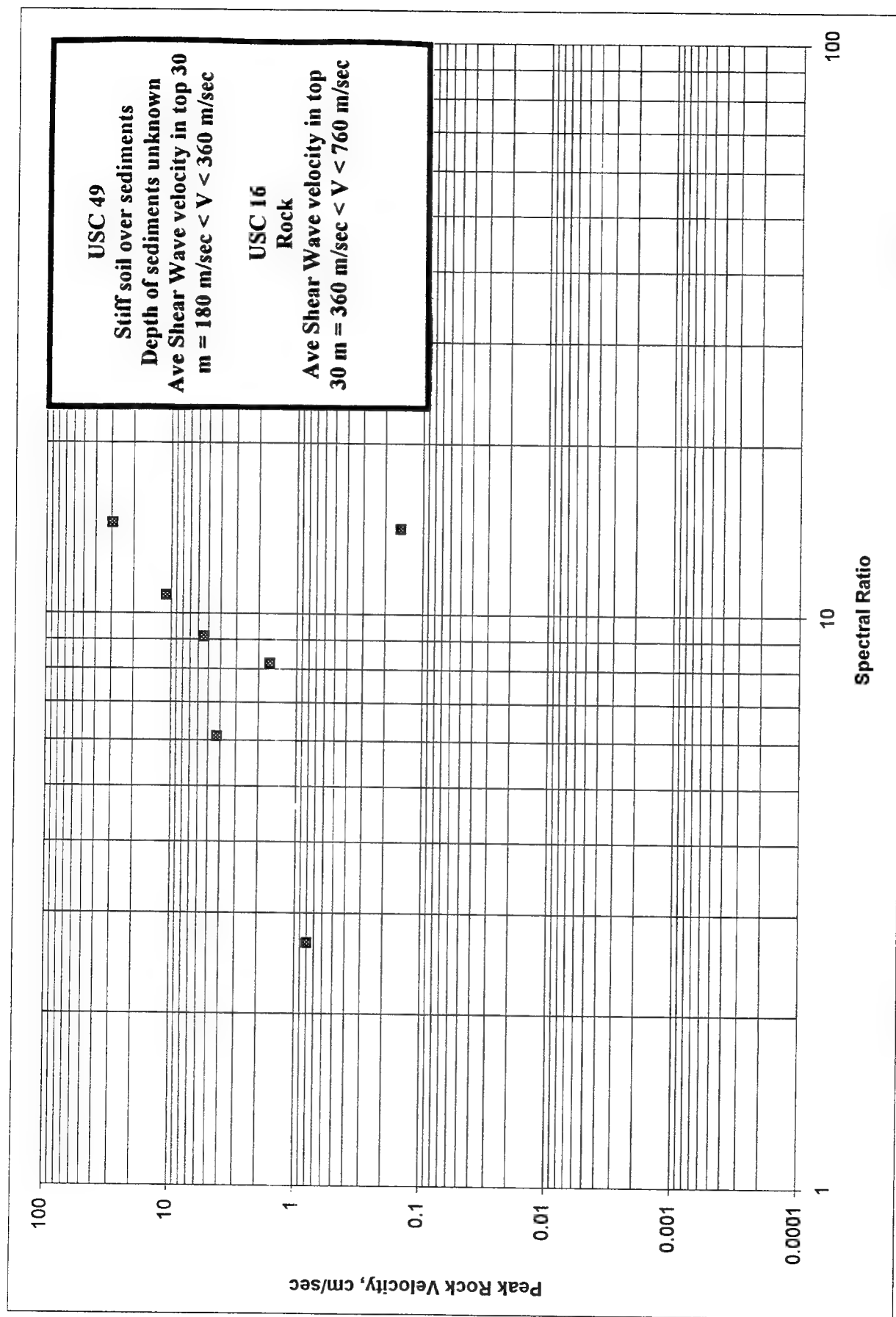


Figure 4.15. USC site pair 4 maximum spectral ratios, Northridge sequence.

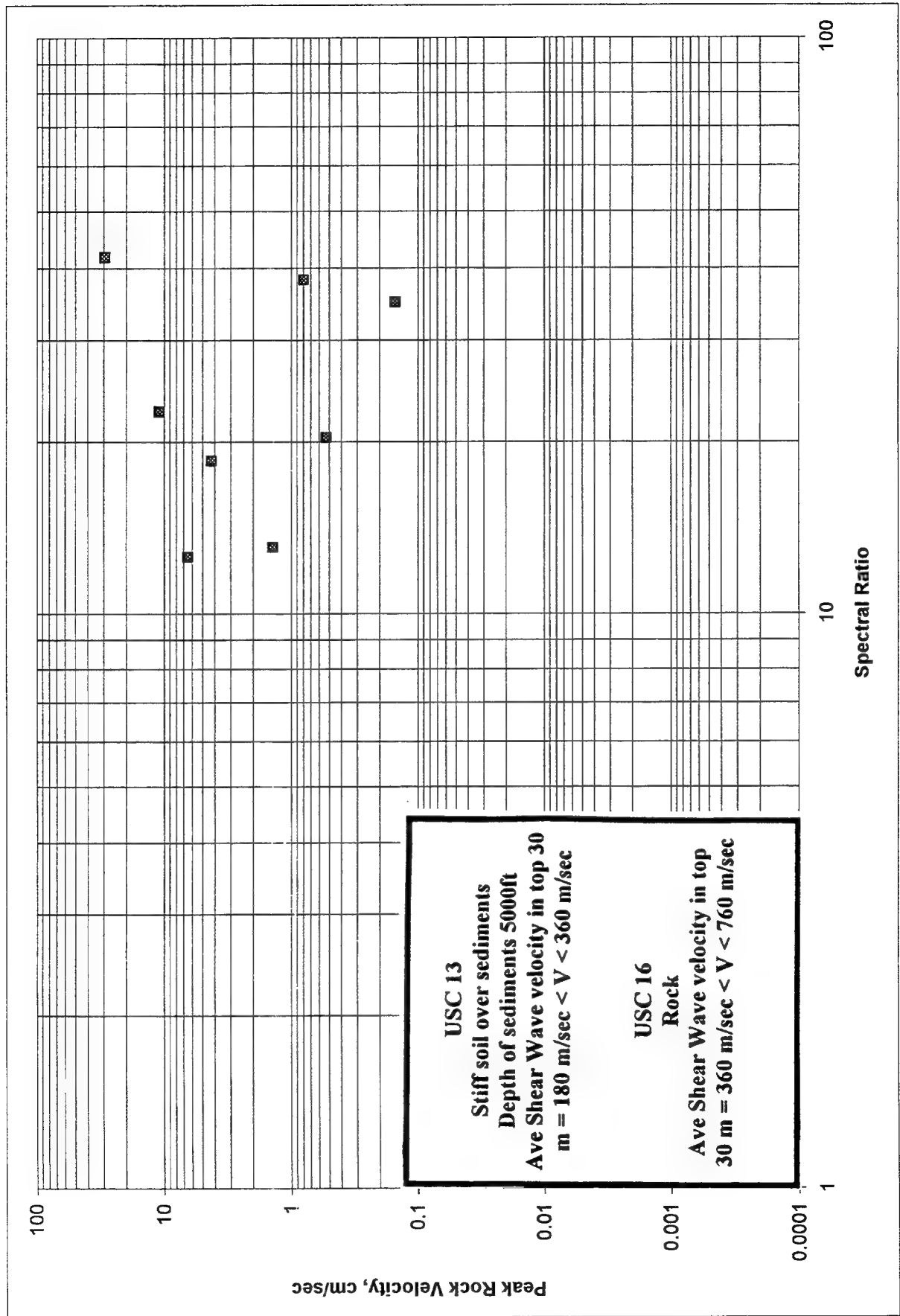


Figure 4.16. USC site pair 5 maximum spectral ratios, Northridge sequence.

Pair 1: USC #61, USC #63

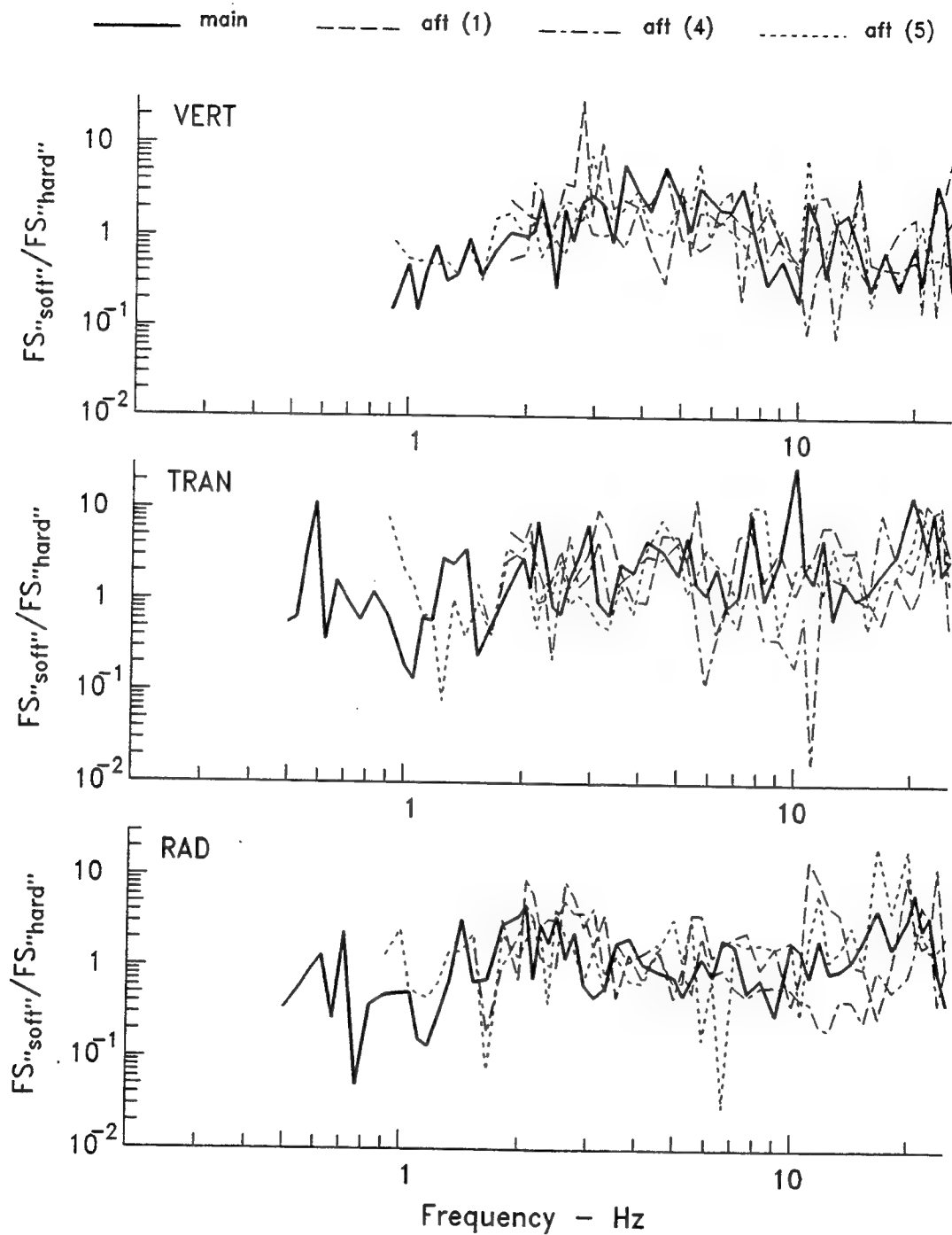


Figure 4.17 Spectra, main Nothridge shock and aftershocks, pair 1.

Pair 2: USC #16, USC #18

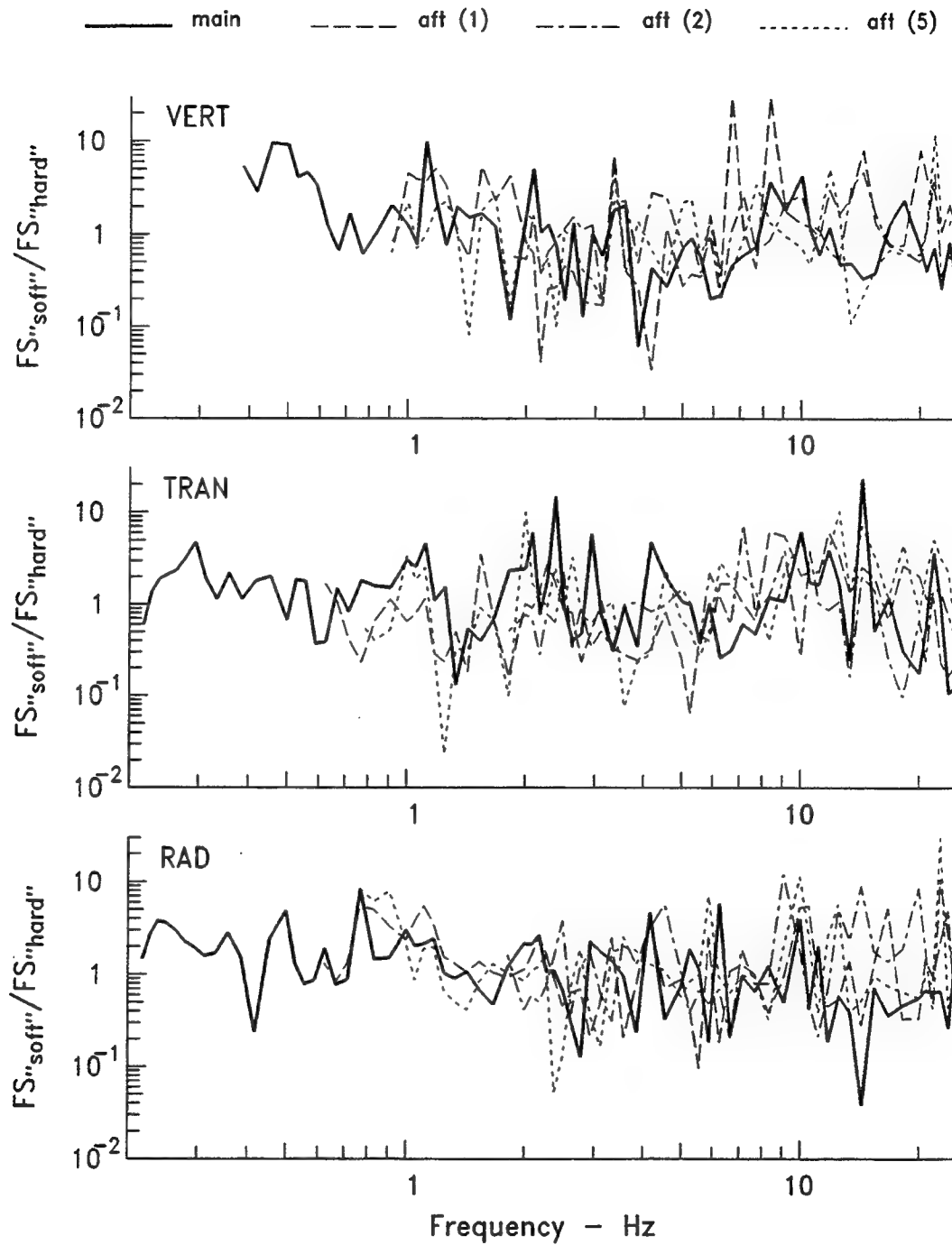


Figure 4.18 Spectra, main Nothridge shock and aftershocks, pair 2.

Pair 3: USC #61, USC #60

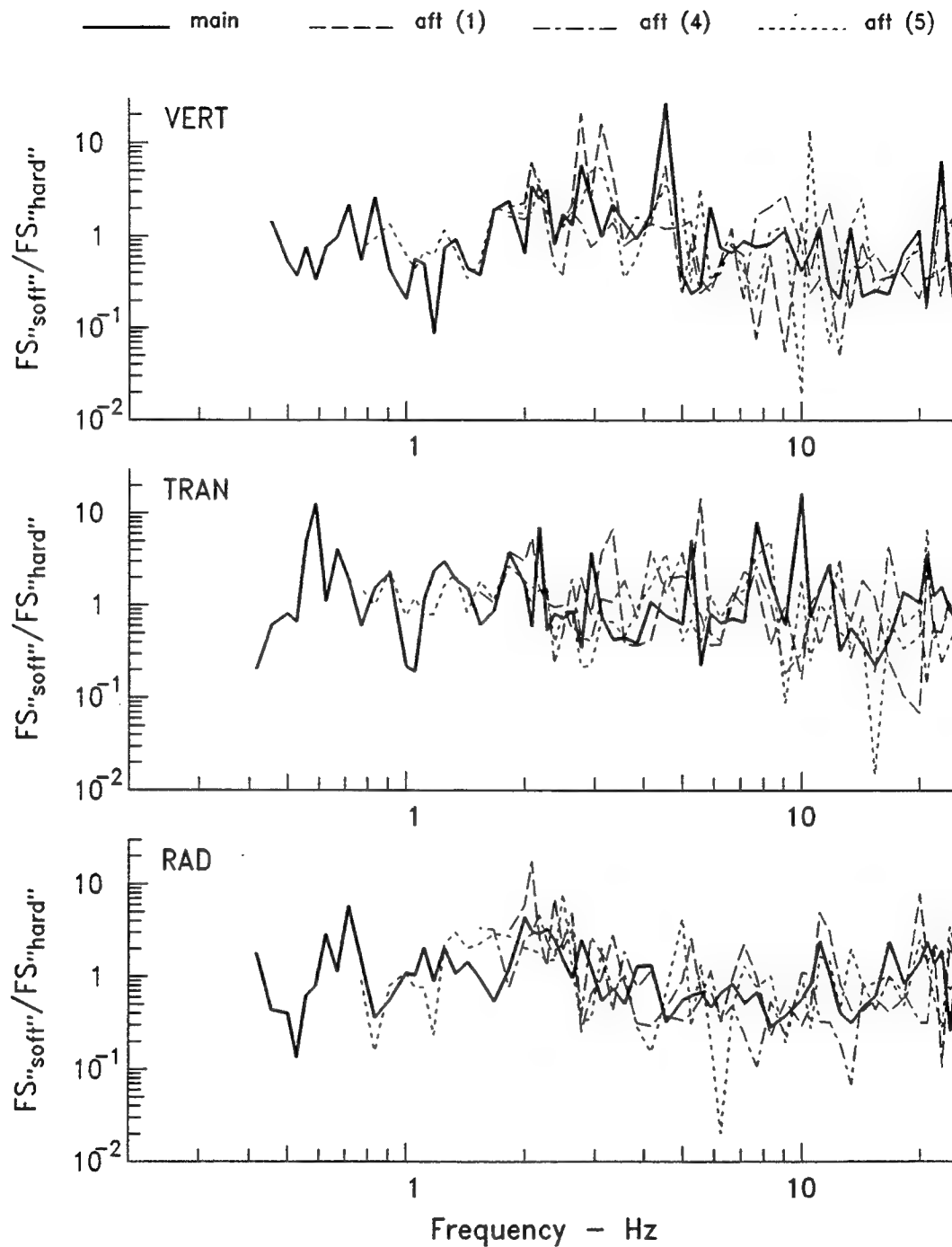


Figure 4.19 Spectra, main Nothridge shock and aftershocks, pair 3.

Pair 4: USC #16, USC #49

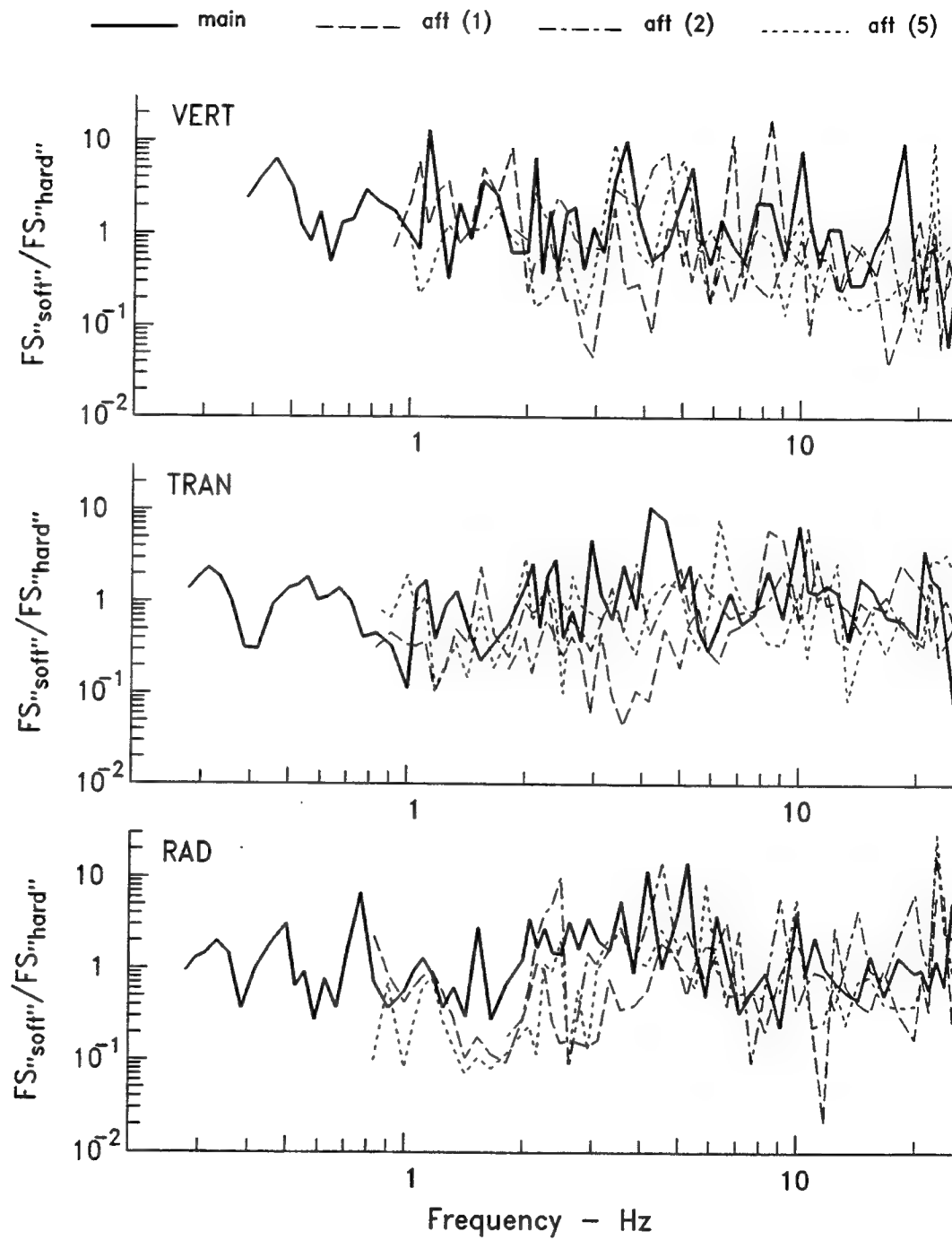


Figure 4.20 Spectra, main Nothridge shock and aftershocks, pair 4.

Pair 5: USC #16, USC #13

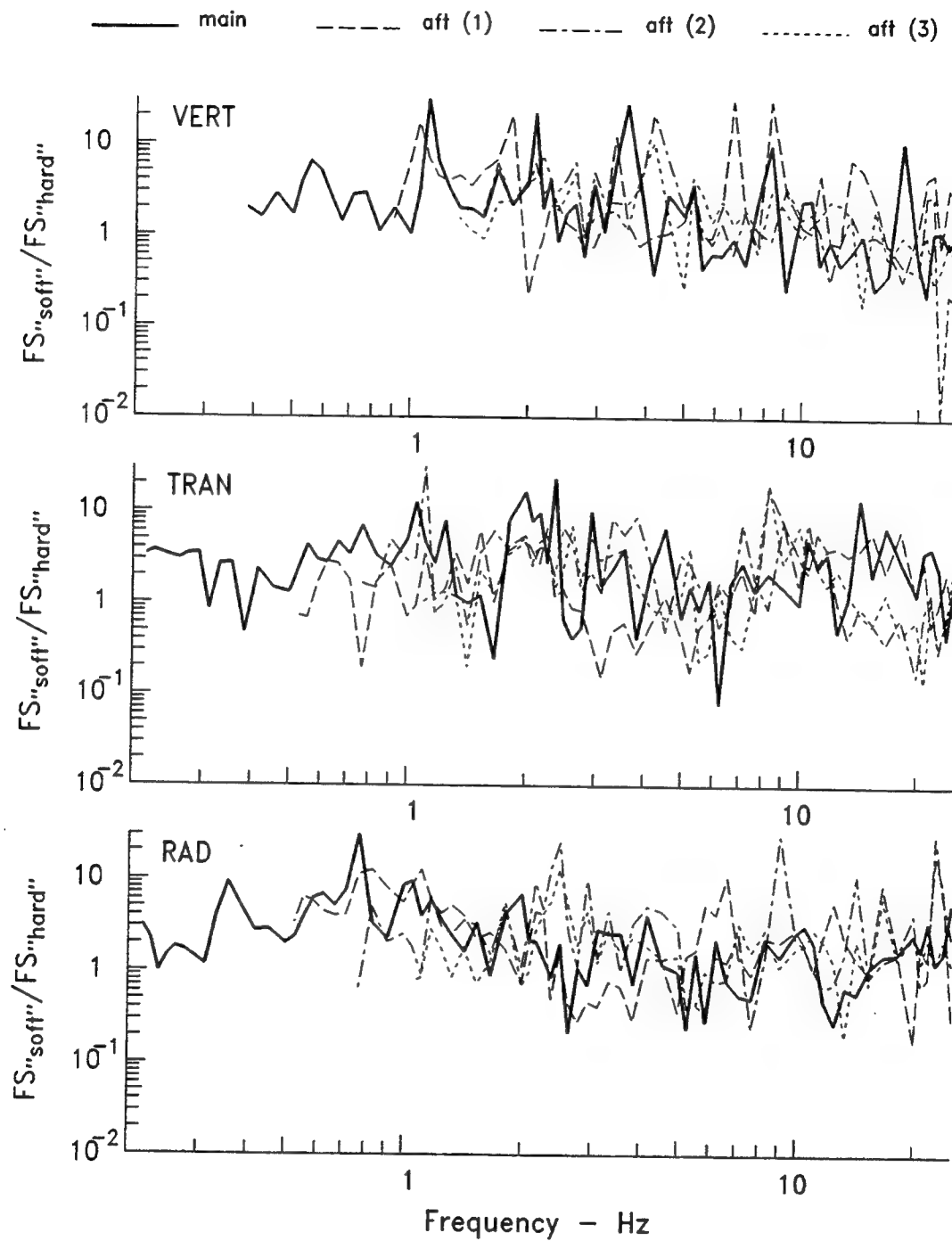


Figure 4.21 Spectra, main Nothridge shock and aftershocks, pair 5.

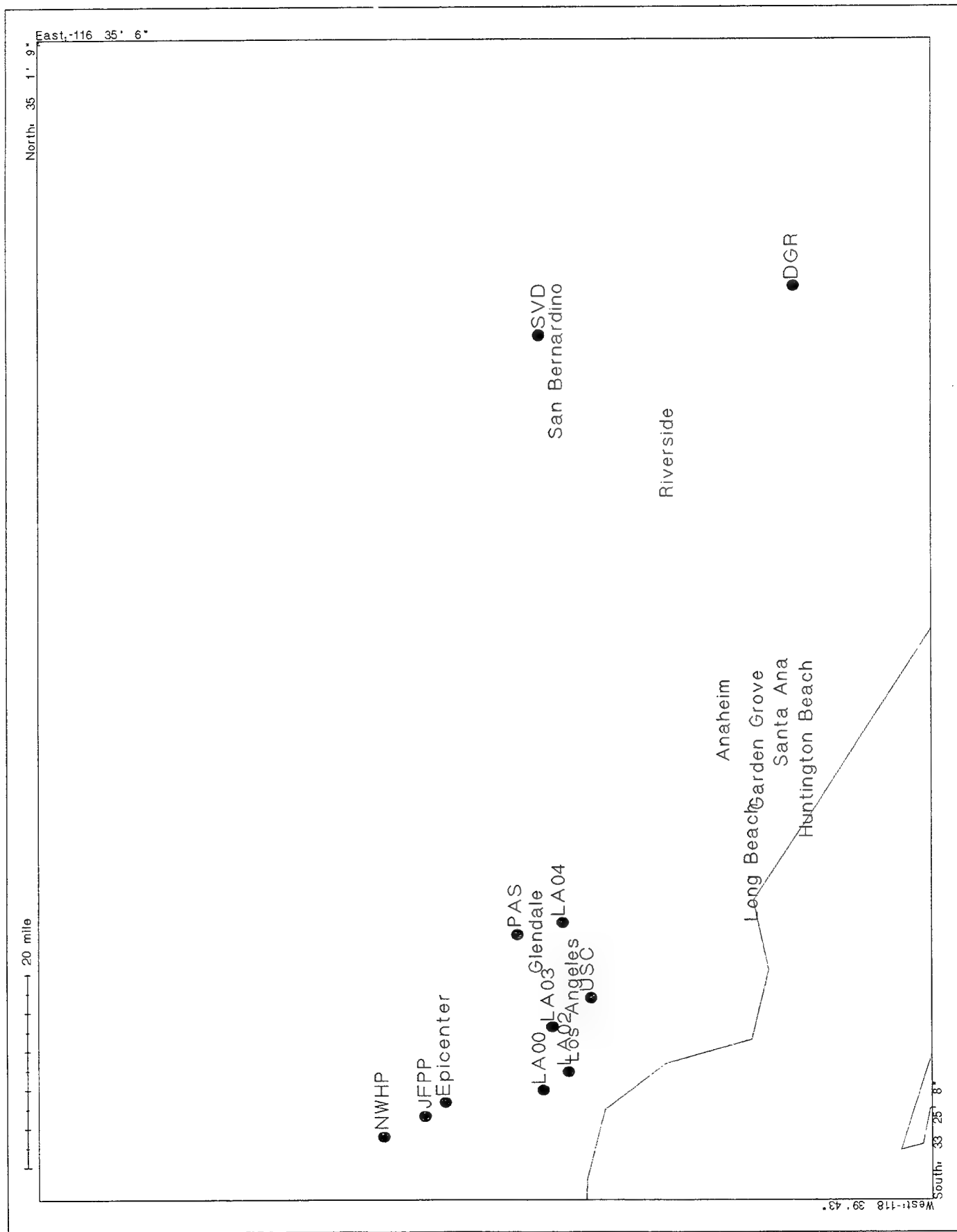


Figure 4.22 Map of CIT sites.

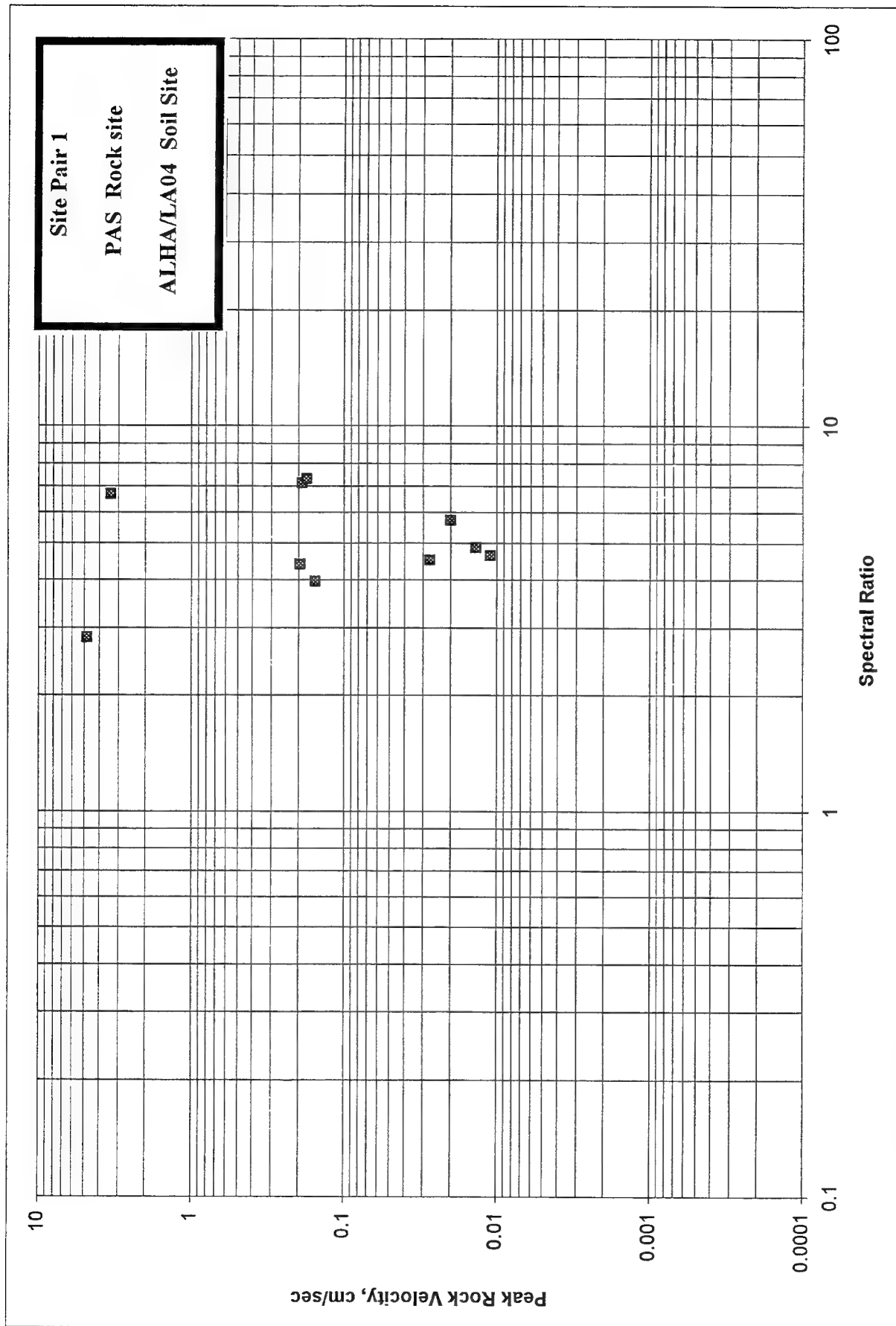


Figure 4.23. CIT Site Pair 1, maximum spectral ratio, Northridge sequence.

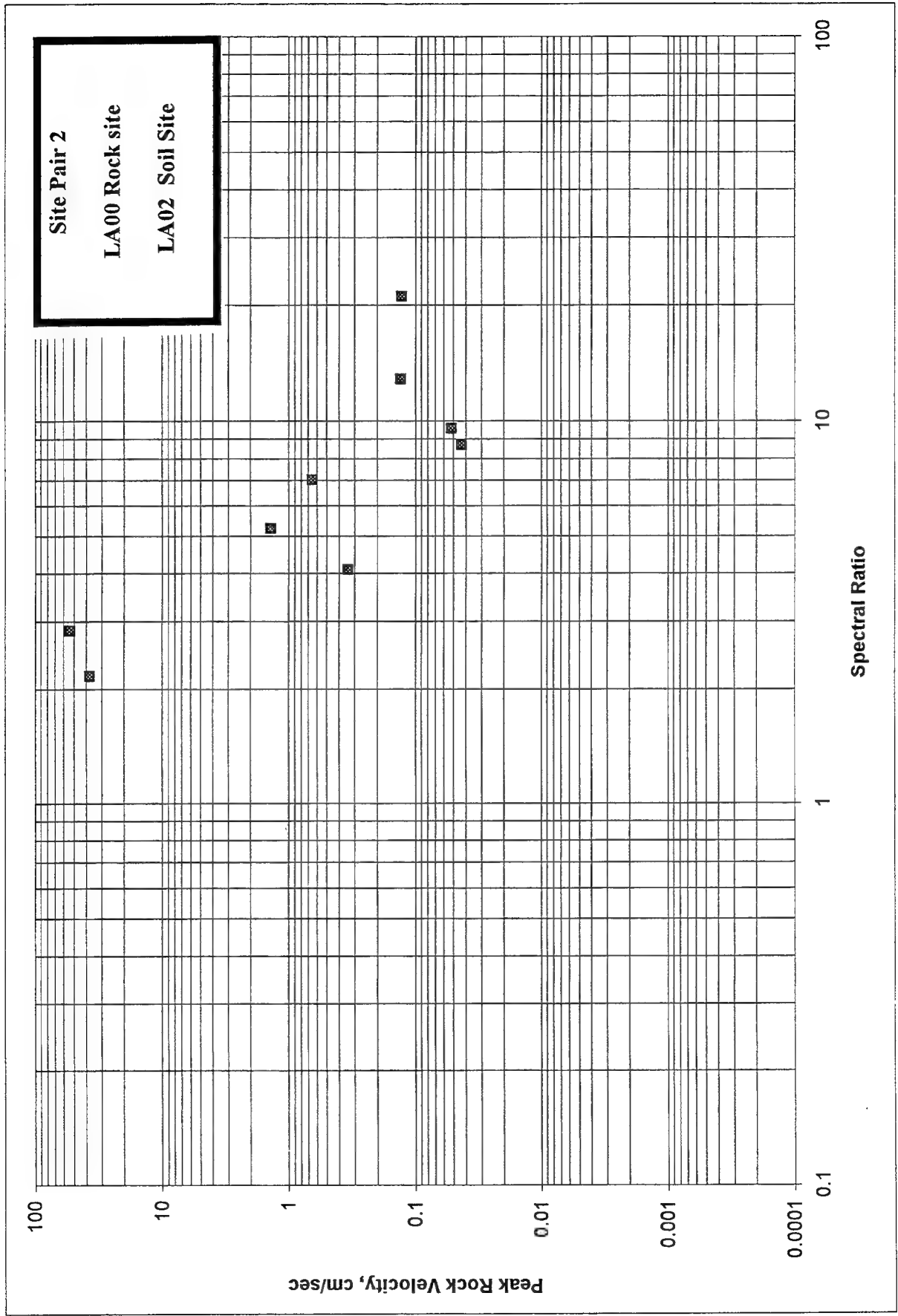


Figure 4.24. CIT Site Pair 2, maximum spectral ratio, Northridge sequence.

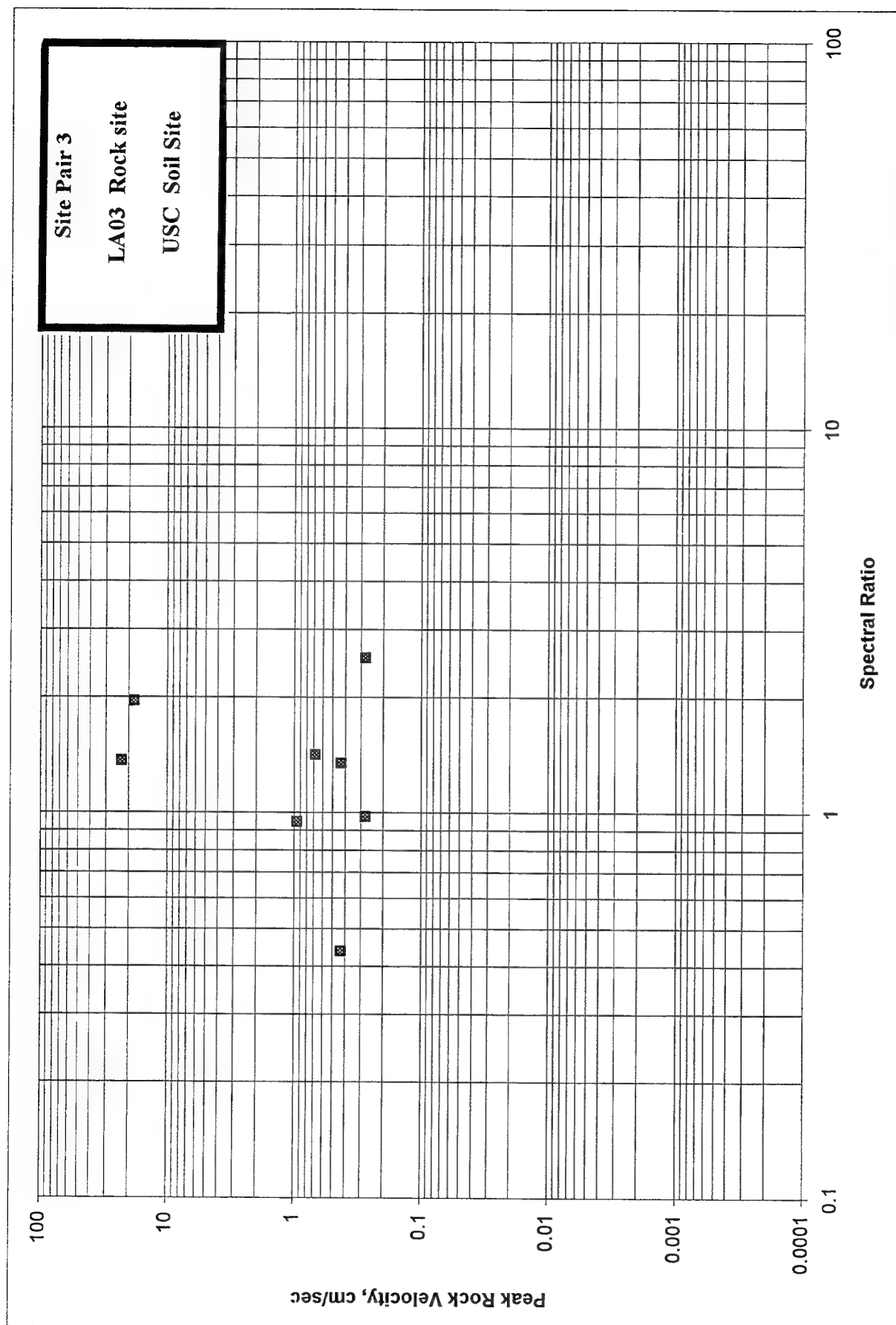


Figure 4.25. CIT Site Pair 3, maximum spectral ratio, Northridge sequence.

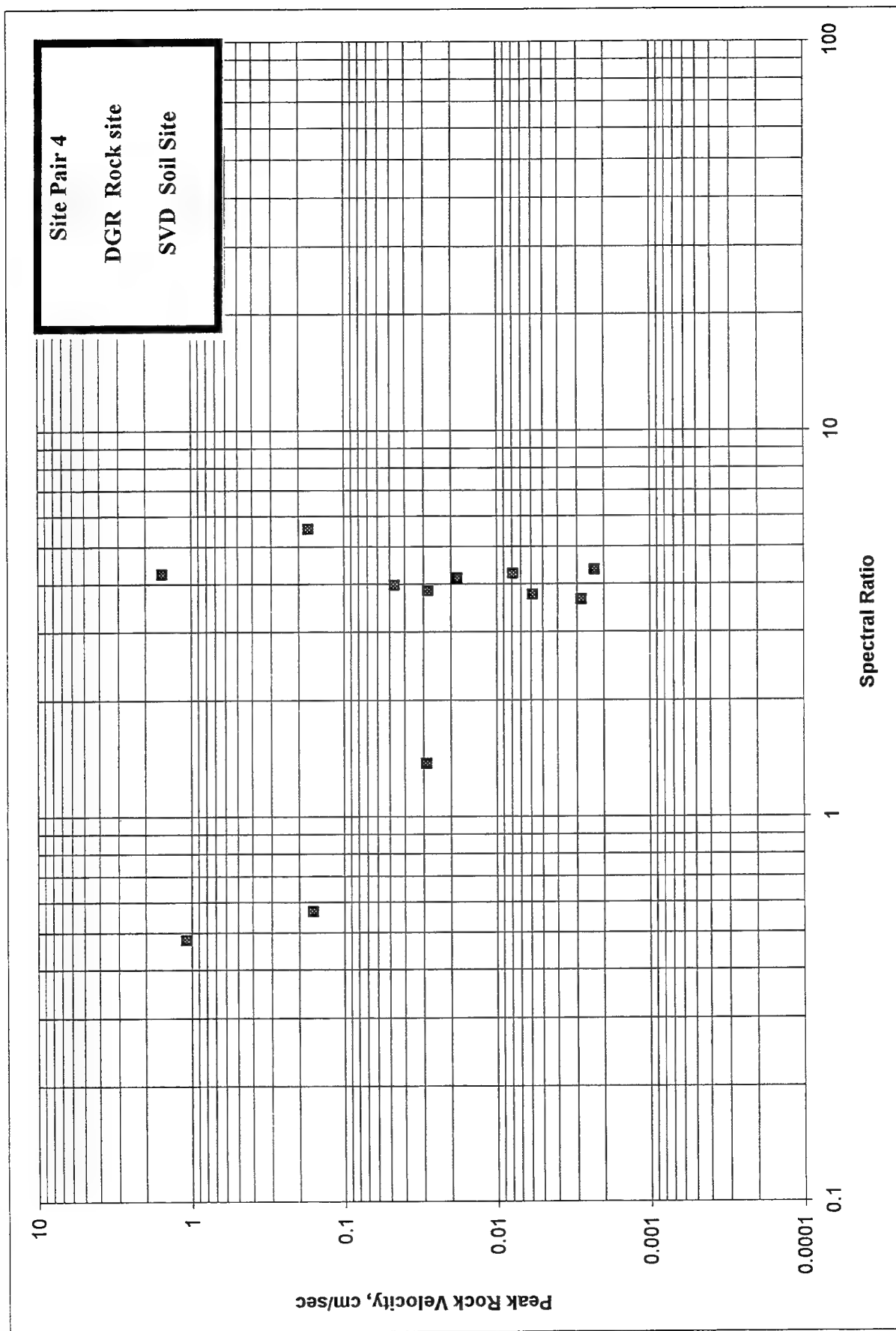


Figure 4.26. CIT Site Pair 4, maximum spectral ratio, Northridge sequence.

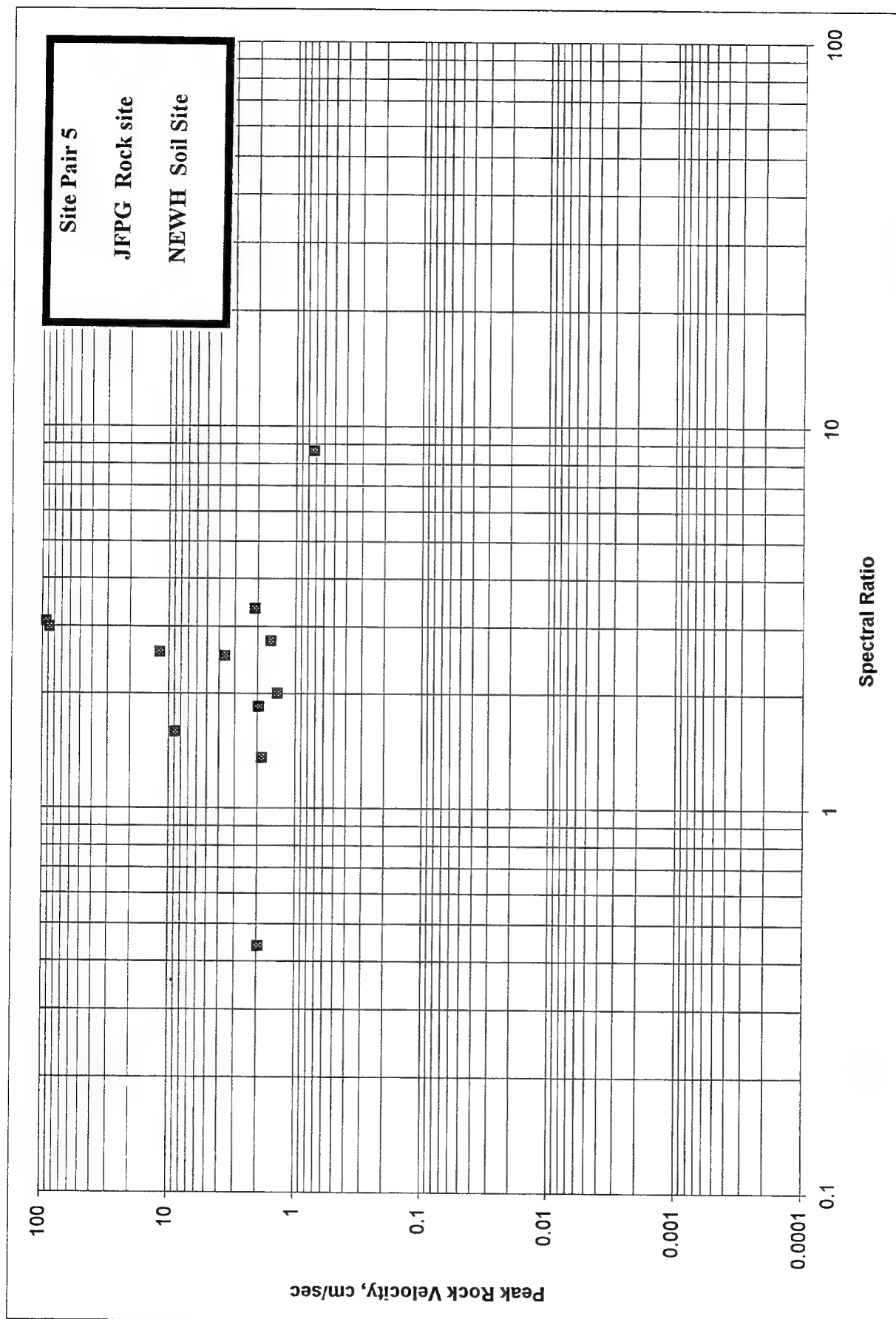


Figure 4.27. CIT Site Pair 5, maximum spectral ratio, Northridge sequence.

Chapter 5 Summary

Feasibility of Microseism Measurements

The purpose of this study was to explore the feasibility of using microseism measurements as an extension of geophysical site properties to improve the understanding of local site response. A typical Navy application would involve soft marginal soils at the waterfront. Existing boring logs may not be available over wide areas and may lack data at depth. Often shear wave velocity is not available and must be estimated from standard penetration blowcount data. Obtaining such data can be costly and is limited to projects of such size to warrant such a detailed investigation. Strain effects on damping and shear modulus require laboratory testing and are usually not performed; several standard type curves for sand and clay are routinely used as substitutes. There is a strong need for an inexpensive field test to quantify site behavior. Microseism measurements seem to offer that potential.

The report has presented microseism measurements which show high levels of amplification at the low levels of excitation. Data was presented showing such a response is expected and that a relationship exists such that spectral ratio amplification is inversely related to the level of excitation. Traditional wave propagation analysis techniques for local site response were seen to be applicable to microseism measurements. Because spectral ratio obtained from microseism measurements are higher than those of strong motion shaking, normalized results can be used to provide information of the spatial variation relative to a site of known response. Microseism measurements at a soil site can be used to estimate fundamental period and damping of the site and serve as a means for improving the reliability of material property data used in the wave propagation computation. A systems identification procedure was shown to lend insight to the process.

- It is concluded that microseism measurements can be used on a relative normalized basis to extend the information from a known local response to areas where additional data is lacking.
- A systems analysis procedure applied to the microseism data can be used to extend the knowledge of site material properties such as shear velocity and damping.
- Long term measurements describe overall site stability and are essential. Microseism measurements can be conducted during windows of stability

Development of Procedure

A generalized procedure should consist of the following steps:

1. Careful review of site geology
2. Investigation of rock reference site and its variability
3. Selection of a rock reference site
4. Selection of a soil reference site having extensive borehole data
5. Long term measurements between rock and soil reference site to establish stability

6. Selection of an array plan to cover region of interest
7. Conducting measurements at rock reference site, soil reference site and at each array site.
8. Reduction of data using appropriate spectral processing

It should be noted that it is recommended that closely spaced measurements be made both at the rock and soil reference site throughout the array measurements to monitor overall stability. Generally a window of several hours is available for array measurements. Having a soil reference site, one is able to track that variation.

Acknowledgment

Professor M. Trifunac, University of Southern California, provided some of the Northridge earthquake data under contract with the Navy. Dr. Hong Kie Thio, California Institute of Technology also provided Northridge data under Navy contract. Their assistance is appreciated. This task had been funded by the Office of Naval Research.

DISTRIBUTION LIST

A/FBO/BDE/ESB / LEMANAS, ARLINGTON, VA
ABRAHAMSON, NORMAN A. / SAN GABRIEL, CA
AF / 750 SPTS/DE, ONIZUKA AFB, CA
AFESC / AL/EQ-TIC (FL 7050), TYNDALL AFB, FL
AGBABIAN ASSOCIATES / NIGBOR, PASADENA, CA
ARMY / HQDA (DAEN-ZCM), WASHINGTON, DC
ARMY BELVOIR R&D CEN / STRBE-AALO, FORT BELVOIR, VA
ARMY CECOM R&D TECH LIBRARY / ASNC-ELC-I-T, FORT MONMOUTH, NJ
ARMY CERL / LIB, CHAMPAIGN, IL
ARMY ENGRG DIST / LIB, SEATTLE, WA
ARMY EWES / LIBRARY, VICKSBURG, MS
BRIGHAM YOUNG UNIV / ROLLINS, PROVO, UT
BRIGHAM YOUNG UNIV / YOUD, PROVO, UT
BRITISH EMBASSY / SCI & TECH DEPT (WILKINS), WASHINGTON, DC
BUREAU OF RECLAMATION / D-1512 (GS DEPUY), DENVER, CO
CALIF DIVISION MINES & GEOLOGY / SHAKAL, SACRAMENTO, CA
CALIFORNIA ENGINEERING FOUNDATION / SACRAMENTO, CA
CASE WESTERN RESERVE UNIV / CE DEPT (PERDIKARIS), CLEVELAND, OH
CHESNAVFACENGCOM / CODE 112.1, WASHINGTON, DC
CHESNAVFACENGCOM / CODE 402 (FRANCIS), WASHINGTON, DC
CHESNAVFACENGCOM / CODE 407, WASHINGTON, DC
CIUDAD UNIVERSITARIA / LERMO, COYOCAN,
CLARKSON UNIV / CEE DEPT, POTSDAM, NY
COLORADO SCHOOL OF MINES / DEPT OF ENGRG (CHUNG), GOLDEN, CO
COLORADO STATE UNIV / CE DEPT (W CHARLIE), FORT COLLINS, CO
COLUMBIA UNIVERSITY / JACOB, PALISADES, NY
COLUMBIA UNIVERSITY / LERNER-LAM, PALISADES, NY
COLUMBIA UNIVERSITY / SEEBER, PALISADES, NY
COM GEN FMF / LANT, SCE, NORFOLK, VA
COMNAVAIRSYSCOM / AIR-714, WASHINGTON, DC
COMNAVSURF / CODE N42A, NORFOLK, VA
DAMES & MOORE / DONOVAN, SAN FRANCISCO, CA
DAMES & MOORE / LIB, LOS ANGELES, CA
DARRAGH, ROBERT B / DAVIS, CA
DEPT OF STATE / FOREIGN BLDGS OPS, BDE-ESB, ARLINGTON, VA
DFSC-F / ALEXANDRIA, VA
DIA / DB-6E1, WASHINGTON, DC
DIA / OGA-4B2, WASHINGTON, DC
DIA / VP-TPO, WASHINGTON, DC
DIPARTIMENTO ING STRUTTURALE / FACCIOLI, MILANO,
DTRCEN / CODE 172, BETHESDA, MD
DTRCEN / CODE 1760, BETHESDA, MD
EERI / OAKLAND, CA
EQE ENGINEERING INC / JOHNSON, SAN FRANCISCO, CA
FLORIDA INST OF TECH / CE DEPT (KALAJIAN), MELBOURNE, FL
GEOMATRIX CONSULTANTS / COPPERSMITH, SAN FRANCISCO, CA
GEORGIA INST OF TECH / CE SCHL (KAHN), ATLANTA, GA
GEORGIA INST OF TECH / CE SCHL (SWANGER), ATLANTA, GA

GSA / HALL, WASHINGTON, DC
HJ DEGENKOLB ASSOC / W. MURDOUGH, SAN FRANCISCO, CA
HOUSNER, GEORGE W / LA CANADA, CA
HUGHES AIRCRAFT CO / TECH DOC CEN, EL SEGUNDO, CA
IOWA STATE UNIV / CE DEPT, AMES, IA
KAJIMA CORP / TUKEMURA, TOKYO 107,
KAJIMA CORP / YAMANAKA, TOKYO 107,
KAJIMU TECHNICAL RESEARCH INSTITUTE / ISHIDA, CHOFU-SHI TOKYO,
KINEMETRICE INC . SERECI, PASADENA, CA
LANTNAVFACENGCOM / CODE 15C, NORFOLK, VA
LAWRENCE LIVERMORE NATL LAB / PLANT ENGRG LIB, LIVERMORE, CA
LAWRENCE LIVERMORE NATL LAB / SOMMER, LIVERMORE, CA
LEIGHTON ASSOCIATES / MAYDYIAR, DIAMOND BAR, CA
LONG BEACH PORT / ALLEN, LONG BEACH, CA
LONG BEACH PORT / LUZZI, LONG BEACH, CA
LONG BEACH PORT / REUS, LONG BEACH, CA
LOS ANGELES COUNTY / PW DEPT (J. VICELJA), HARBOR CITY, CA
MATRECON, INC / H. HAXO, ALAMEDA, CA
MC CLELLAND ENGRS, INC / LIB, HOUSTON, TX
MCAS / CODE 1JE.50 (ISAACS), SANTA ANA, CA
MCAS / EL TORO, CODE 1JD, SANTA ANA, CA
MCKEE, ROBER / GLENDALE, CA
MOBIL R&D CORP / OFFSHORE ENGRG LIB, DALLAS, TX
NAS / CODE 18300, LEMOORE, CA
NAS / FAC MGMT OFFC, ALAMEDA, CA
NAS / MIRAMAR, SAN DIEGO, CA
NAS / NI, CODE 183, SAN DIEGO, CA
NAS / PWO, WILLOW GROVE, PA
NAS / PWO, KEY WEST, FL
NAS / SCE, BARBERS POINT, HI
NATL ACADEMY OF SCIENCES / NRC, DR. CHUNG, WASHINGTON, DC
NAVAIRWPNSTA / CODE 1018, POINT MUGU, CA
NAVCONSTRACEN / CO, PORT HUENEME, CA
NAVCONSTRACEN / CODE S24, GULFPORT, MS
NAVFACENGCOM / CODE 04A3C, HUBLER, ALEXANDRIA, VA
NAVFACENGCOM / DEL COLLO, ALEXANDRIA, VA
NAVMEDCOM / NWREG, FAC ENGR, PWD, OAKLAND, CA
NAVOCEANO / CODE 6200 (M PAIGE), NSTL, MS
NAVPGSCOL / CODE 61WL (O WILSON), MONTEREY, CA
NAVPGSCOL / PWO, MONTEREY, CA
NAVPHIBASE / SCE, SAN DIEGO, CA
NAVSCOLCECOFF / CODE C35, PORT HUENEME, CA
NAVSECGRUACT / PWO, CHESAPEAKE, VA
NAVSHIPYD / CODE 244.13, LONG BEACH, CA
NAVSHIPYD / CODE 420, LONG BEACH, CA
NAVSHIPYD / CODE 450-HD, PORTSMOUTH, VA
NAVWPNCEN / PWO (CODE 266), CHINA LAKE, CA
NAWS / ROICC NIEMI, POINT MUGU, CA
NCCOSC / CODE 541 (BACHMAN), SAN DIEGO, CA
NCCOSC / CODE 9642, SAN DIEGO, CA
NFESC ECDDET / NICKERSON, WASHINGTON, DC
NFESC ECDDET / WU, WASHINGTON, DC
NOAA / JOSEPH VADUS, ROCKVILLE, MD
NORDA / CODE 1121SP, NSTL, MS

NORDA / CODE 363, NSTL, MS
NORTHNAVFACENGCOM / CODE 408AF, LESTER, PA
NRL / CODE 2511, WASHINGTON, DC
NRL / CODE 4670, WASHINGTON, DC
PACNAVFACENGCOM / CODE 102, PEARL HARBOR, HI
PACNAVFACENGCOM / CODE 2011, PEARL HARBOR, HI
PMB ENGRG / LUNDBERG, SAN FRANCISCO, CA
PURDUE UNIV / CE SCOL (ALTSCHAEFFL), WEST LAFAYETTE, IN
PURDUE UNIV / CE SCOL (CHEN), WEST LAFAYETTE, IN
PURDUE UNIV / CE SCOL (LEONARDS), WEST LAFAYETTE, IN
PWC / CODE 1011, PEARL HARBOR, HI
PWC / CODE 102, OAKLAND, CA
PWC / CODE 123C, SAN DIEGO, CA
PWC / CODE 400, OAKLAND, CA
PWC / CODE 420, OAKLAND, CA
REFRACTION TECHNOLOGY INC / PASSMORE, DALLAS, TX
RENSSELAER POLYTECHNIC INSTITUTE / ELGAMAL, TROY, NY
RODGERS, PETER W / SANTA BARBARA, CA
SAN DIEGO PORT / AUSTIN, SAN DIEGO, CA
SAN DIEGO PORT / PORT FAC, PROJ ENGR, SAN DIEGO, CA
SAN DIEGO STATE UNIV / CE DEPT (KRISHNAMOORTHY), SAN DIEGO, CA
SANDIA NATL LABS / LIB, LIVERMORE, CA
SCRIPPS INSITITUTE OF OCEANOGRAPHY / BABCOCK, LA JOLLA, CA
SCRIPPS INSITITUTE OF OCEANOGRAPHY / KIRKENDALL, LA JOLLA, CA
SCRIPPS INSITITUTE OF OCEANOGRAPHY / ORCUTT, LA JOLLA, CA
SCRIPPS INST OF OCEANOGRAPHY / LIB, LA JOLLA, CA
SEATTLE PORT / DAVE VAN VLEET, SEATTLE, WA
SEATTLE PORT / DAVID TORSETH, SEATTLE, WA
SEATTLE UNIV / CE DEPT (SCHWAEGLER), SEATTLE, WA
SOUTHNAVFACENGCOM / CODE 04A, NORTH CHARLESTON, SC
SOUTHNAVFACENGCOM / CODE 102H, NORTH CHARLESTON, SC
SOUTHWEST RSCH INST / MARCHAND, SAN ANTONIO, TX
SOWESTNAVFACENGCOM / LANGSTRAAT, SAN DIEGO, CA
SOWESTNAVFACENGCOM / O'LEARY, SAN DIEGO, CA
SPCC / PWO, MECHANICSBURG, PA
STATE UNIV OF NEW YORK / CE DEPT, BUFFALO, NY
STATE UNIV OF NEW YORK / CE DEPT, BUFFALO, NY
TECHNOLOGY UTILIZATION / K WILLINGER, WASHINGTON, DC
TELEDYNE-BROWN ENGINEERING / TROSPER, GARLAND, TX
UCLA / VUCETIC, LOS ANGELES, CA
UCSB / ARCHULETA, SANTA BARBARA, CA
UNIV OF CALIFORNIA / CE DEPT (FENVES), BERKELEY, CA
UNIV OF CALIFORNIA / CE DEPT (FOURNEY), LOS ANGELES, CA
UNIV OF CALIFORNIA / CE DEPT (MITCHELL), BERKELEY, CA
UNIV OF CALIFORNIA / CE DEPT (TAYLOR), DAVIS, CA
UNIV OF CALIFORNIA / CE DEPT (WILLIAMSON), BERKELEY, CA
UNIV OF CALIFORNIA / IDRIS, DAVIS, CA
UNIV OF CALIFORNIA / INMAN, LA JOLLA, CA
UNIV OF HAWAII / CE DEPT (CHIU), HONOLULU, HI
UNIV OF HAWAII / MANOA, LIB, HONOLULU, HI
UNIV OF NEVADA / ANDERSON, RENO, NV
UNIV OF RHODE ISLAND / CE DEPT (KOVACS), KINGSTON, RI
UNIV OF TEXAS / CE DEPT (R. OLSON), AUSTIN, TX
UNIV OF TEXAS / ECJ 4.8 (BREEN), AUSTIN, TX

UNIV OF THE PACIFIC / CE DEPT (KANE), STOCKTON, CA
UNIV OF WASHINGTON / CE DEPT (HARTZ), SEATTLE, WA
UNIV OF WASHINGTON / CE DEPT (KRAMER), SEATTLE, WA
UNIV OF WASHINGTON / CE DEPT (MATTOCK), SEATTLE, WA
UNIV OF WASHINGTON / RL TERREL, EDMONDS, WA
US BUREAU OF MINES / WILLIAMS SPOKANE, WA
US DEPT OF STATE / ARMSTRONG, WASHINGTON, DC
US GEOLOGICAL SURVEY / BONILLA, MENLO PARK, CA
US GEOLOGICAL SURVEY / BOORE, MENLO PARK, CA
US GEOLOGICAL SURVEY / BORCHERDT, MENLO PARK, CA
US GEOLOGICAL SURVEY / BRADY, MENLO PARK, CA
US GEOLOGICAL SURVEY / GLASSMOYER, MENLO PARK, CA
US GEOLOGICAL SURVEY / HEATON, PASADENA, CA
US GEOLOGICAL SURVEY / SEEKINS, MENLO PARK, CA
US NUCLEAR REGULATORY COMMISSION / KIM, WASHINGTON, DC
USA CERL / WALASZEK, CHAMPAIGN, IL
USACOE / CESP-D-CO-EQ, SAN FRANCISCO, CA
USAE / CEWES-IM-MI-R, VICKSBURG, MS
USC / AKI, LOS ANGELES, CA
VENTURA COUNTY / DEPUTY PW DIR, VENTURA, CA
WESTERN GEOPHYSICAL COMPANY / WORKMAN, HOUSTON, TX
WESTNAVFACENGCOM / FARIS, SAN BRUNO, CA
WESTNAVFACENGCOM / VALDEMORO, SAN BRUNO, CA
WESTNAVFACENGCOM / ZIGANT, SAN BRUNO, CA
WOODWARD-CLYDE CONS / ARZAMENDI, SAN DIEGO, CA
WOODWARD-CLYDE CONSULTANTS / SCOTT, DENVER, CO
WOODWARD-CLYDE CONSULTANTS / WEST REG, LIB, OAKLAND, CA